HEAT FLOW NEAR MAJOR STRIKE-SLIP FAULTS IN CENTRAL AND SOUTHERN CALIFORNIA

Thesis by

Thomas Louis Henyey

In Partial Fulfillment of the Requirements

For the Degree of

Doctor of Philosophy

California Institute of Technology

Pasadena, California

1968

(Submitted May 16, 1968)

ACKNOWLEDGMENTS

It is a pleasure to acknowledge the advice and patience of Dr. Gerald Wasserburg, and to extend to Dr. Robert Roy my sincere thanks for his untiring help and understanding, which above all contributed to the successful completion of this project. The comments and suggestions of Drs. James Brune and Leon Silver on various phases of the work were also extremely valuable. I would like to express my appreciation to the California State Department of Water Resources, and in particular to Mr. Ronald Bisio of that organization, for making available drill holes, drill core, and drilling reports for use in this investigation. I would also like to thank the Southern Pacific Land Company and the Granite Rock Company for making drill holes available. Finally, special words are reserved for my wife, Sally, whose skill and patience as a typist was ultimately responsible for the presentation of this work. The research was supported by the National Science Foundation.

ABSTRACT

Seventeen heat flow measurements have been made near the San Andreas, San Jacinto, and Garlock faults of California in regions representative of several levels of seismic activity. Data from these measurements in conjunction with results of other heat flow investigations in central and southern California show no maxima directly attributable to the fault zones. This negative result along with stress-drop results from earthquakes suggests an upper bound of the order of 200 bars for the absolute stress in the vicinity of the San Andreas fault. In addition, the average heat flow in the four regions investigated (San Bernardino Mountains - Lake Hughes, Anza, Hollister, and Tehachapi Mountains) is the same; the mean value of 23 determinations is 1.7 $\mu cal/cm^2/sec \pm 0.1$ s.d.

In the region between Lake Hughes and San Bernardino, presently seismically inactive but in the zone of rupture from the ~8 magnitude Fort Tejon earthquake, six measurements show no correlation with distance from the San Andreas fault. Near the San Jacinto fault in an area characterized by frequent medium magnitude earthquakes, determinations at 1 and 4 km from the fault are equal but 20 per cent higher than a measurement 13 km to the west, but not appreciably different from a probable regional average 25 km to the east. Near Hollister where the San Andreas is actively creeping at a rate of several centimeters per year, a measurement 8 km east of the fault yields a flux twice as great as one 30 km to the west, but values at intermediate points suggest that this anomaly may reflect

more the regional geology than the San Andreas fault alone. Finally, measurements across the historically inactive Garlock fault exhibit high fluxes near the fault in comparison with a determination 8 km to the north, but do not differ significantly from determinations in the Mojave Block to the south.

In California, the major fault systems appear to lie in transition zones between blocks of crust characterized by Basin and Range heat flows -- Mojave Block and Salton Trough -- and blocks representative of normal continental heat flows -- Central Valley and the crustal strip between the San Jacinto-San Andreas fault system and the Pacific continental margin.

Photographic materials on pages 48, 50, 83, 104, 120, 149, and 155 are essential and will not reproduce clearly on Xerox copies. Photographic copies should be ordered.

TABLE OF CONTENTS

I. INTRODUCTION

Wasserburg, Knopoff, and Kovach proposed in 1964 (written communication, NSF Grant GP-3412) measuring heat flow in the vicinity of major strike-slip faults in California. It was suggested that near large, seismically active faults, a significant amount of strain energy released during active periods along the fault might be converted to heat. Furthermore, if this were the case, this energy conversion might be observed as an anomalous heat flow with fluxes significantly above the so-called "normal continental heat flow". Anomalies as high as 50-100% of this "normal value" were originally suggested based on the Gutenberg-Richter seismic energy-earthquake magnitude relation, assuming that at least as much strain energy was converted to heat as was radiated in the form of seismic waves during an earthquake. During the course of this study, many geologic investigations along the major faults in California have demonstrated the importance of creep as a fault mechanism, and it was immediately recognized that here would be an important source of heat depending, of course, how widespread, both in time and space, this creep was.

A program of field heat flow investigations was proposed to explore the possibilities of observing these anomalies. A series of holes were drilled along the San Andreas and San Jacinto fault zones in several regions characterized by different types of fault and seismic conditions as well as different geologic terranes. A group of holes drilled by the California State Department of Water Resources on tunnel alignments near the San Andreas and Garlock faults was

also used during the course of this investigation. A hole drilled by the Southern Pacific Land Company near Lucerne Valley was deepened and used as one of several base level values at distance from the San Andreas fault. Finally a group of holes have just been or are just being drilled in other parts of central and southern California for which only preliminary values exist, but constitute an important part of the entire heat flow picture and will thus be integrated into the general discussion.

The supervision of drilling, the field temperature measurements, and the laboratory thermal conductivity and radioactive heat productivity measurements were carried out by the author during the years 1965-1967, with the help of many different field and laboratory assistants.

II. DRILLING AND SITE SELECTIONS

Diamond core drilling techniques, similar to those used in mineral exploration were used to prepare the holes and extract continuous rock core samples. All holes were drilled to a depth of at least 200 meters, which appears to be a minimum depth at which reliable heat flow measurements can be generally made. Many of the holes were drilled 300 meters or deeper, but in most cases gave the same gradient at 300 meters as at 200 meters, thereby yielding the only advantage of a statistically better average gradient. Minimum hole depths are dependent on several factors: (1) the depth to the water table, (2) the depth of weathering and highly fractured rock, (3) the depth of penetration of long term climatic fluctuations, and (4) the severity of the local topography. It might also be added that the cost of drilling is not constant with depth, but rather follows what might be more akin to a second-order scheme. Careful site selection can often greatly reduce the effects of (1), (2), and (4), but (3) generally remains unknown; its effect can be either masked by or attributed to one of the other effects. Whereas annual temperature oscillations prevail to only several tens of meters (Carslaw and Jaeger, 1959, p. 66), centennial variations may involve significant disturbances to hundreds of meters. A semi-infinite medium of diffusivity $\varkappa$ subjected to an oscillatory surface temperature of frequency f propagates a temperature wave inward of wavelength λ given by

$$\lambda = \left(\frac{4\pi\varkappa}{f}\right)^{1/2}$$

which decays with depth z according to

$$e^{-2\pi z/\lambda}$$

Thus at a depth of one wavelength, the surface amplitude has been reduced by

$$e^{-2\pi} \simeq 0.002.$$

For example, if we consider a normal annual fluctuation for southern California with a probable amplitude of 10°C (20°C range) (Kendrew, 1953; U. S. Weather Bureau, 1964), we have that at a depth of one wavelength -- 20 meters for 1 cycle/year -- the temperature disturbance would be 0.02°C. At 100 meters, above which depth we have not used temperatures for gradient determinations, the effect for any reasonable annual surface fluctuation would be essentially non-existent (the surface amplitude would be diminished by $e^{-10\pi}$). Regular temperature fluctuations over a one-hundred year period are not likely to be as large as the annual variation. Oscillations in surface temperature of the order of 10°C per century might be expected to result from only such severe changes in surface conditions as forestation and deforestation or glacial advance and retreat. There is no reason to believe that any such effects have occurred in the regions under consideration in southern California. It also seems highly unlikely that relatively short term general or periodic climatic fluctuations would reach this magnitude. At most, a 10°C range for intermediate latitudes is suggested for all of Tertiary time (Bowen, 1966) with this figure also being a maximum for the difference in temperature between glacial and interglacial times. Weather Bureau

statistics, for example, suggest at least for the last century that mean annual temperatures have generally remained within one or two degrees of the long term average temperature, a suggestion which is consistent with paleoclimatological evidence from the distribution of flora and fauna and their rates of growth, the advance and retreat of glaciers and ice packs, and the measurements of ocean temperatures (Nairn, 1963; Brooks, 1949). A fluctuation with an amplitude of the order of 1°C per century would be diminished by $e^{-\pi}$ at 100 meters to about 0.04°C and by $e^{-2\pi}$ at 200 meters to about 0.002°C. This would introduce a maximum error of about 0.4°C/km in the gradient between 100 and 200 meters, while gradients below 200 meters would be almost totally unaffected.

The drilling was contracted out to two commercial drilling companies, E. J. Longyear Company of Phoenix, Arizona, and Joy Manufacturing Company of Tuscon, Arizona. Careful supervision of the drilling operation was often necessary to insure competent holes and good core recovery. As many technical problems often arise requiring the client's decision, close supervision also helps reduce costs due to delay time or improper decision on the part of the driller.

Holes were drilled either one of two standard sizes, BX wireline or NX wireline. NX wireline holes are about 3 inches in diameter and yield core 2 inches in diameter. BX wireline holes are about 2 inches in diameter and yield core about $1\frac{1}{2}$ inches in diameter. Costs are generally one-fourth to one-third more for NX drilling, and hence this size was used for near surface drilling; casing could then be set

in the weathered zone and the hole reduced to BX size for drilling in the fresh rock below. While the NX size gives a better statistical sampling of the rock, especially in coarse-grained material, it was found that in most instances BX core size was quite satisfactory. BX holes can be conveniently cased, and were in most cases, with $1\frac{1}{4}$ inch black iron pipe at nominal cost, thus guaranteeing access to the hole at later dates. It has been found throughout the course of this investigation that grouting holes upon completion of drilling is necessary in many cases to prevent water circulation in the hole due to ground water movement (see descriptions of holes HO-1 and LH-3). Since this problem is not known to exist until the first logging, it is recommended that the procedure of grouting be carried out systematically on each hole as it is completed. This is easily accomplished after the $1\frac{1}{4}$ inch pipe has been set by pumping the grouting compound, such as cement or AM-9*, through the pipe and utilizing a one-way check valve at the bottom to prevent return of the grout back into the pipe after it has been flushed with enough clean water to just completely fill it.

The selection of a suitable site can be the most important factor in a representative heat flow determination. The nature of the San Andreas problem limited our sites to a relatively narrow band along the fault, yet a certain amount of latitude was available within

---

*A product of American Cyanamid Company

a given region for locating a particular site. We might outline the criteria we used for selecting a given region and a particular location within this region. First, as was mentioned earlier, different regions were chosen on the basis of differing fault and seismic conditions. Second, regions were chosen for which adequate and relatively detailed geologic maps existed. Third, except for the Hollister region, to keep from introducing the additional complication of lateral heat transfer, areas were selected where crystalline basement cropped out on both sides of the fault. Particular sites were then chosen on the basis of the geologic mapping, a reconnaissance survey in the neighborhood of a potential site, and the local topography, consistent with vehicular access to the site. Care was taken to stay as far as possible from local faults, dikes, roof pendants, and major contacts. The holes were generally located where competent, fresh-looking rock cropped out. Finally, when possible, sites were chosen where the immediate topographic relief, within one-half km, was relatively subdued. Such a choice will help minimize the uncertainty of the topographic correction and help eliminate possible ground water problems often associated with severe topography, as will be noted later. Temperature effects due to annual and secular changes in the level of the ground water table have been neglected. These effects can be shown to be small in crystalline terrane for the actual changes in level which are observed. By making the temperature measurements well below the water-air interface, the effects are further reduced. In this work, temperature logging was not begun until the

probe was below the water table as determined by the point at which rapid equilibration of the probe was first observed.

The importance of having a good understanding of the local geology cannot be overemphasized; this will become more apparent as we proceed with the discussion and interpretation of the data.

III. DESCRIPTION OF MEASURING APPARATUS

A determination of the heat flow involves the measurement of two quantities, $\frac{\Delta T}{\Delta z}$, the vertical component of the geothermal gradient and k, the thermal conductivity. $\frac{\Delta T}{\Delta z}$ is measured in the field and k in the laboratory.

A. Temperature Logging Gear

Temperatures were measured in the drill holes using thermally sensitive resistors (thermistors) enclosed in a waterproof housing lowered down the hole at the end of a four-conductor cable. The thermistors used were sintered manganese and nickel oxides which approximately obey the usual semiconductor temperature-resistance law

$$R_T = Ae^{B/T} \qquad (1)$$

where R_T is the resistance at temperature T (°K), and A and B are constants depending upon the materials used. The individual thermistors were arranged in a parallel-series array, consisting of four units in series, each unit containing four thermistor beads in parallel. Beads were chosen with a resistance of approximately 10K ohms at the ice point (3K at 25°C) and having about a 1 Ω/0.01°C resistance-temperature coefficient at 25°C. Such arrays, as opposed to individual beads, have the advantage of dissipating the i^2R losses over a larger volume, thereby minimizing self-heating errors.

The thermistors and electrical connections are encased in a stainless steel housing (see Figure 1) to which is attached a waterproof neoprene-coated electrical connector. A thin sleeve of neoprene is then vulcanized from the connector down over the major part of the stainless steel housing, forming a waterproof unit. The thermistors are pushed down into the long (about 250 mm) stainless steel tubes which are partially filled with a thermally conducting grease (Wakefield 128) for rapid equilibration of the sensors with the environment. The electrical connections between the thermistor elements are made in the main body of the probe and potted in a high resistance (electrical), hard-setting epoxy resin. The probes are designed to function without loss of precision or physical integrity in the temperature range, 0°C to 70°C.

The probes were calibrated at 10°C intervals from 0°C to 60°C, and a second-order polynomial of the form

$$\ell n\, R_T = a + \frac{b}{T} + \frac{c}{T^2} \qquad (a, b, c \text{ constants}) \qquad (2)$$

was fit to the points, using a least-squares technique programmed for the IBM 7094. Tables were then printed out on the computer, giving probe resistances in 0.001°C temperature steps between 0°C and 70°C. We can write (2) as

$$\ell n\, R_T = a + \frac{b}{T}\left(1 + \frac{c}{b}\,\frac{1}{T}\right)$$

and using (2) instead of (1) has the effect of imposing a temperature dependence on the constant B in (1), given by the term

Figure 1. Thermistor Probe Construction (Explanation)

A: Four 2.5 mm diameter stainless steel tubes silver brazed to housing.

B: Sensor portion of probe. Each tube contains one Fenwal K 396A thermistor assembly which consists of four thermistors spaced 5 mm apart, wired in parallel, with a total resistance of 3500 ohms at 0° C.

C: Four pole underwater connector, Mecca 1728-4.

D: Neoprene jacket vulcanized to connector cable and bonded to stainless steel housing with Hughson Chemlock 305, 320.

E: Split ring cable clamp tightened by set screws.

F: Leads from the four thermistor assemblies connected in series (as shown in diagram) and the remaining two leads soldered to conductors from connector. All connections covered with polyolefin heat shrinkable tubing. Total resistance of the probe is 10K-11K ohms at 0°C.

G: Cavity filled with epoxy-resin, Tra-Con 2109.

H: Thermistor beads.

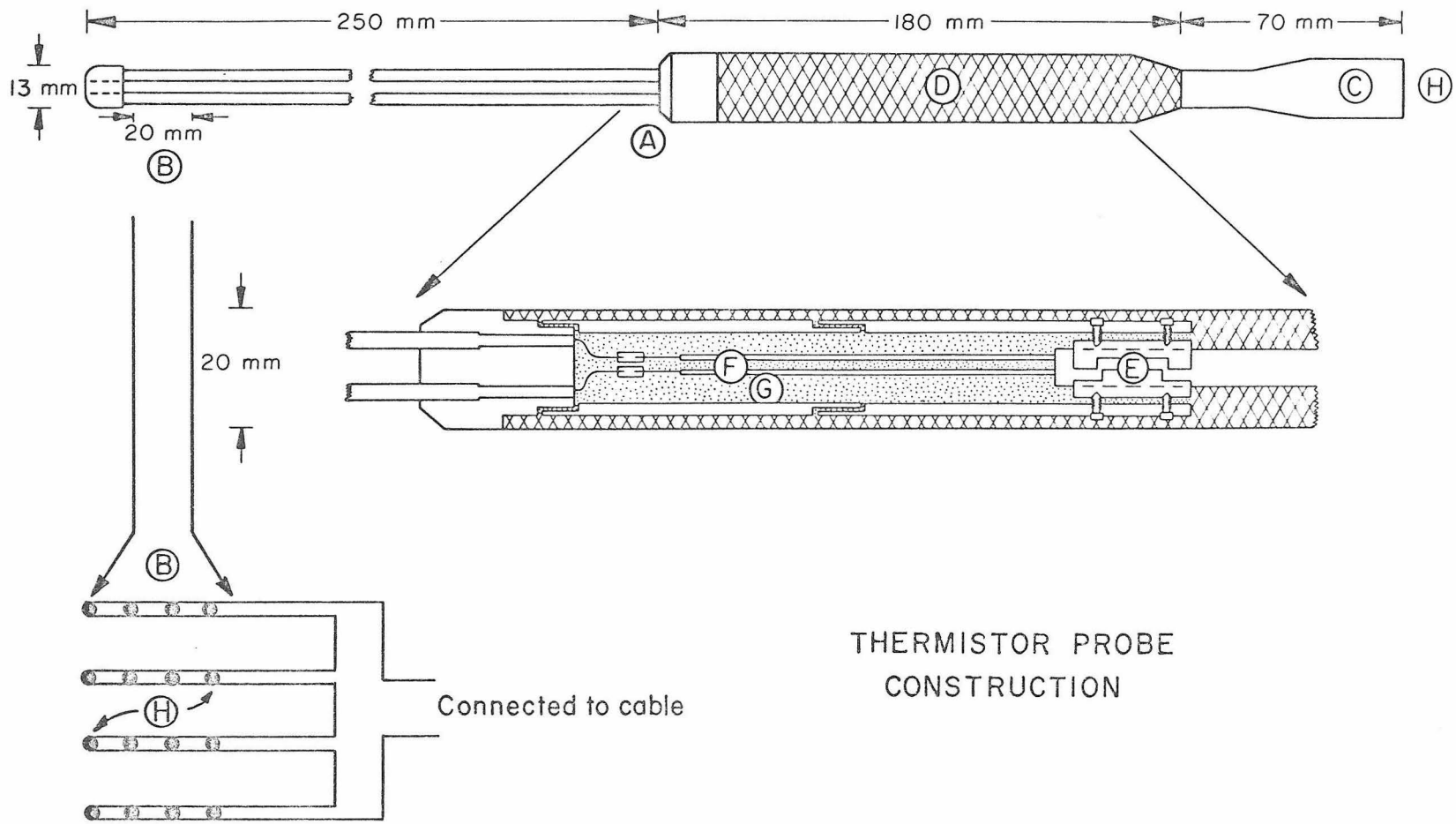

THERMISTOR PROBE CONSTRUCTION

Figure 1

$$\frac{c}{b}\frac{1}{T}$$

This term runs from 0.112 at 0°C to 0.092 at 60°C.

Calibration was performed in our laboratory against a Leeds and Northrup 25 Ω platinum resistance thermometer in a total-emersion, constant-temperature bath. The resistance of the platinum thermometer was determined using a Leeds and Northrup K-3 potentiometer and a 10 Ω standard resistor using the circuit shown in Figure 2. The total absolute accuracy of calibration is believed to be good to ±0.05°C. The possible errors in calibration are due to dial reading errors on the potentiometer (±1 μV), accuracy of the K-3 potentiometer (±0.015% of reading ±2 μV on the range used, according to Leeds and Northrup specifications on the limits of error), accuracy of standard resistor (±0.002%), and the error in primary calibration, estimated to be ±0.01°C from the calibration certificate issued by Leeds and Northrup. If we assume that all errors accumulate unfavorably, we would have from the relation in Figure 2, the maximum fractional error in R_{Pt}

$$\frac{\Delta R_{Pt}}{R_{Pt}} = \Sigma \frac{\Delta V_{Pt}}{V_{Pt}} + \Sigma \frac{\Delta V_S}{V_S} + \frac{\Delta R_S}{R_S}$$

where the summations indicate the sum of the dial reading and potentiometer errors. Under the assumption that all the errors in the resistance measurements accumulate unfavorably, we have that the maximum fractional error in R_{Pt} contributing to the absolute accuracy is given by

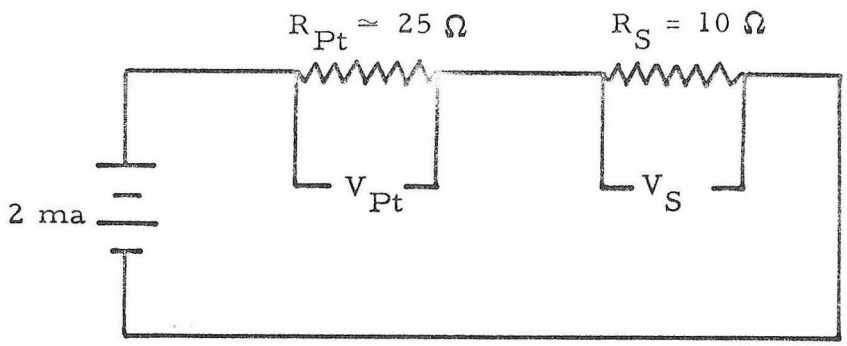

$$R_{Pt} = \frac{V_{Pt}}{V_S} R_S$$

Circuit Used for Temperature Calibration.

V_{Pt}: voltage drop across platinum thermometer as determined from K-3

V_S : voltage drop across standard resistor as determined from K-3

R_{Pt}: resistance of platinum thermometer

R_S : resistance of standard resistor

2 ma: D.C. current supplied

Figure 2

$$\left(\frac{\Delta R_{Pt}}{R_{Pt}}\right)_{acc} = \pm 0.00053$$

while the fractional error in precision (due to the dial reading errors) is given by

$$\left(\frac{\Delta R_{Pt}}{R_{Pt}}\right)_{prec} = \pm 0.00007$$

For

$$R_{Pt} \simeq 25\ \Omega$$

and a resistance-temperature coefficient for the platinum thermometer of 0.001 Ω/0.01°C between 0°C and 100°C, we have

$$\left(\frac{\Delta R_{Pt}}{R_{Pt}}\right)_{acc} \rightarrow \pm 0.13°C$$

corresponding to a standard error of 0.06°C, and

$$\left(\frac{\Delta R_{Pt}}{R_{Pt}}\right)_{prec} \rightarrow \pm 0.02°C \qquad (3)$$

corresponding to a standard error of 0.01°C. The least-squares residuals at the calibration points were in <u>all</u> cases less than 0.01°C; furthermore, the probes were calibrated at several intermediate points and agreed in all cases to better than 0.01°C with the values determined by the least-squares fit, consistent with the estimate of precision. In addition, the ice point value for the platinum thermometer was checked in our laboratory and agreed to 0.01°C with the value determined by Leeds and Northrup, suggesting that the accuracy of our calibration was significantly better than ±0.13°C. The discrepancy between the precision and accuracy can be explained

if one considers where the maximum contribution to the error arose, namely, from the reported accuracy of the K-3 potentiometer (±0.015% ±2 μV). The bulk of this error is likely to be systematic for a given set of measurements because they are all made on the same voltage range of the potentiometer. Deviations from linearity (contributing to random errors) are probably an order of magnitude smaller than 0.015%. From the relation in Figure 2, we see that systematic errors in V_{Pt} and V_S tend to cancel. If we consider the deviations from linearity to be ±0.002% with a systematic error of ±1 μV, we would have

$$\left(\frac{\Delta R_{Pt}}{R_{Pt}}\right)_{acc} = \pm 0.00016$$

$$\rightarrow \pm 0.04°C$$

corresponding to a standard error of ±0.02°C. If we allow for a maximum systematic error in primary calibration of ±0.01°C, we get the figure, mentioned earlier, of ±0.05°C for the error in absolute accuracy. ±0.05°C corresponds to a standard error of ±0.03°C. Further checks on the accuracy of calibration were made by using newly calibrated probes to log thermally stable holes which had been previously logged with probes calibrated independently by both Harvard University and the United States Geological Survey. In the several instances this was done, temperatures at similar depths in the holes agreed, for the most part, to 0.02°C with the Harvard probes and to 0.04°C with the U.S.G.S. probe (see Table 1, and also bottom hole temperatures for two logs of SB-10, Appendix VI). Finally, systematic thermistor drift errors were found to be negligible during

Temperature Comparisons, Butte, Montana DDH B-3

	CIT 11/27/67		HU 8/9/67		USGS 5/30/67	
Depth(m)	T(°C)	ΔT(°C)	T(°C)	ΔT(°C)	T(°C)	ΔT(°C)
240	13.73		13.75		13.77	
		.64		.63		.64
260	14.37		14.38		14.41	
		.67		.66		.67
280	15.04		15.04		15.08	
		.68		.68		.68
300	15.72		15.72		15.76	
		.69		.70		.67
320	16.41		16.42		16.43	
		.65		.65		.66
340	17.06		17.07		17.09	
		.66		.66		.66
360	17.72		17.73		17.75	
		.64		.64		.64
380	18.36		18.37		18.39	
		.63		.63		.63
400	18.99		19.00		19.02	
		.65		.65		.66
420	19.64		19.65		19.68	
		.67		.66		.66
440	20.31		20.31		20.34	
		.66		.66		.67
460	20.97		20.97		21.01	
		.65		.66		.67
480	21.62		21.63		21.68	
		.67		.66		.65
500	22.29		22.29		21.33	
		.63		.63		.62
520	22.91		22.92		22.95	
		.66		.64		.66
540	23.57		23.56		23.61	
		.64		.63		.65
560	24.21		24.19		24.26	
		.68		.67		.66
580	24.89		24.86		24.92	
		.61		.61		.62
600	25.50		25.47		25.54	

Table 1 (from Roy, et al., 1968)

the period of probe use. In no cases were apparent drifts of greater than 0.02°C found upon recalibration, which is well within the maximum calibration error.

The contribution from calibration errors to the error of a gradient determination (which is what we are really concerned about) can be estimated from the precision of the calibrated temperatures. From (3), the maximum error should not exceed ±0.04°C in 10°C or 0.4%. After smoothing with the least-squares fit, this error will be considerably reduced, and the error in a gradient, with temperatures in the range of calibration, should not exceed a couple of tenths of one per cent.

The field apparatus for determining probe resistance consisted of a 4000-foot, four-conductor cable (Vector N3 CW1-4-280), together with a portable half-symmetrical Wheatstone bridge modified for lead-wire compensation (Mueller type) as shown in Figure 3. The ratio arm resistance values of 10K Ω were chosen to provide maximum sensitivity at the null detector with minimum power dissipation in the thermistor. A transistorized null detector (Hewlett-Packard 419A) was used to detect bridge null. Stray emf's were eliminated by using a battery reversing switch. The current supplied to the thermistor was kept such that the temperature rise due to the power dissipation was less than .003°C under normal conditions (bridge current of 200 μa). Again, this is a systematic error and has negligible effect on temperature gradients. Temperature errors due to the bridge can occur from errors in the resistance values of ratio-arm resistors and

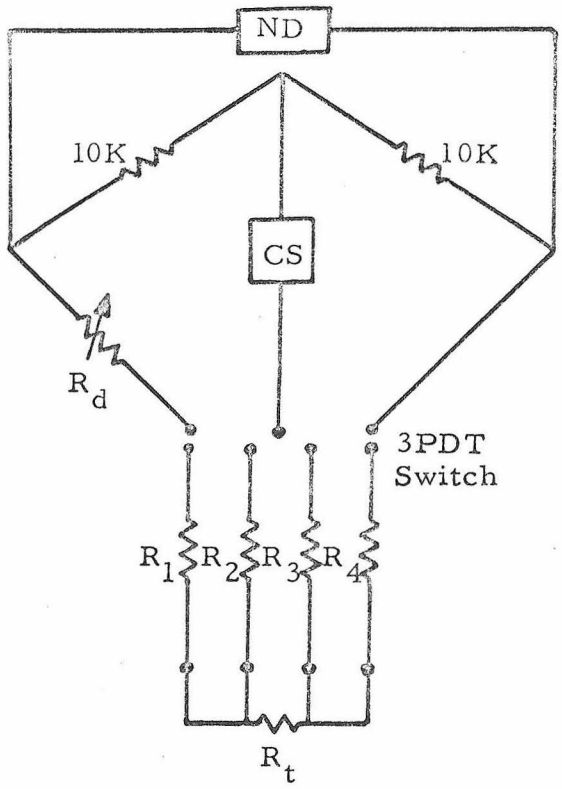

Mueller Bridge Circuit Used for Temperature Measurements.

ND: Battery operated D.C. null detector. CS: Current supply for bridge, two mercury cells in series (2.7 volts), with on-off and polarity reversing switches, voltage divider, and current meter. Bridge usually operated with 100 to 200 μ amp. R_d: 6 decade variable resistor. R_t: Thermistor. R_1, R_2, R_3, R_4: Lead wire resistances.

At null in first switch position, $R_{t1} = R_{d1} + (R_1 - R_4)$; in second switch position $R_{t2} = R_{d2} + (R_4 - R_1)$; thus the actual value $R_t = (R_{d1} + R_{d2})/2$.

Figure 3

on the decade. We have at bridge null the relation

$$R_{Th} = \frac{R_1}{R_2} R_D$$

where R_{Th} is the resistance of the thermistor, R_D, the decade resistance, and R_1 and R_2, the ratio arm resistances. Thus

$$\frac{\Delta R_{Th}}{R_{Th}} = \frac{\Delta R_1}{R_1} + \frac{\Delta R_2}{R_2} + \frac{\Delta R_D}{R_D}$$

for most unfavorable accumulation of errors. The tolerances on the ratio-arm resistances are 0.001% and on the decade 0.01%. Thus

$$\frac{\Delta R_{Th}}{R_{Th}} \simeq 0.0001$$

or at 3000 Ω (the mean of a normal operating range)

$$\Delta R_{Th} \simeq 0.3\ \Omega$$

which for a resistance-temperature coefficient of 1 Ω/0.01°C gives a possible error of 0.003°C, almost negligible. It might be noted that R_1 and R_2 had matched temperature coefficients to eliminate an additional source of error.

The one final source of error in temperature could conceivably come from a lead wire leakage resistance, effectively putting a finite yet high impedance resistor in parallel with the thermistor. Leakage resistance of the cable was checked periodically and found to be in the multi-megohm range which would contribute a maximum error in absolute temperature of perhaps 0.005°C. This error is approximately

the same for all measurements and, if this small, will yield essentially no error in the gradient.

If we now sum up all possible errors, we see that at most we could have a 0.06°C error in absolute temperature or a standard error of ±0.03°C, which should contribute a maximum of only a couple of tenths of one per cent error to a determination of the geothermal gradient.

In addition to the temperature calibration of the probe, two other sources of error could conceivably contribute to an error in geothermal gradient; the error in the determination of the depth interval Δz, and the resolution of the Wheatstone bridge. The cable was pre-stretched for ~12 hours in the deepest drill hole (LV-1) prior to the marking of it in 10-meter intervals. The cable was then rewound and marked under tension by lowering it 10 meters at a time down the drill hole. A 10-meter rod was used to measure the interval. If we reasonably assume that these markings are good to ±1 cm, the error in Δz for a 10-meter interval will be 0.1%, and for intervals >10 meters, the error becomes progressively smaller. For short interval (~1 meter) logging, a meter stick can be used at the hole site and the same precision obtained. The resolution of the bridge used (with the six decade variable resistor having a 0.01 Ω minimum step size and the Hewlett-Packard 419A) was ±0.0001°C. For a 10-meter interval in a 20°C/km gradient, this corresponds to a maximum error of 0.1%; for a 1-meter interval, the error would be 1%. The errors are diminished for averages over more than one interval. Thus the

total error in gradient for a single 10-meter interval should not exceed a few tenths of one per cent and for a single 1-meter interval about one per cent. We thus conclude that any variability in gradients above these levels of error found under field circumstances will be due to external conditions such as variations in thermal conductivity, water movement in the drill hole, etc.

Temperatures in this work will be reported to the nearest one-hundredth of a degree C, except in several instances where hole conditions necessitated small-interval logging. Generally speaking, thermal instability in the holes usually prevented making measurements to better than ±0.01°C, and reproducibility in a given hole for different sets of measurements was also of the order of ±0.01°C.

B. Thermal Conductivity Apparatus

The thermal conductivity of individual core samples was measured with the divided bar apparatus described by Birch (1950), Beck (1957), and more recently, with modifications to help reduce side heat losses and thermal contact resistance, by Roy, Decker, Blackwell, and Birch (1968). Figure 4 shows the geometry and component parts of the apparatus as it was used for this work.

Measurement of thermal conductivity with a divided bar is basically a substitution technique which gives the ratio of conductivity of an unknown sample to that of a standard whose value is known from absolute measurements. The standards which were used are natural quartz (heat flow normal to optic axis -- that is, the disks were

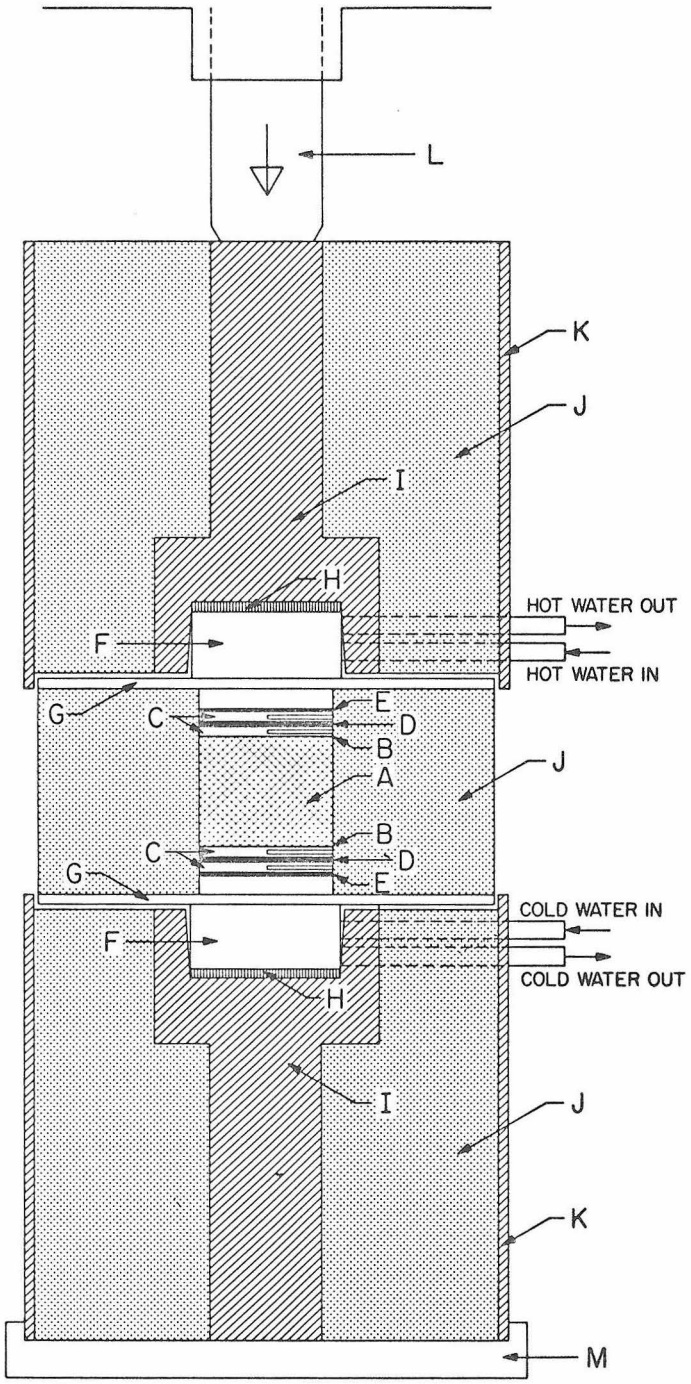

CONDUCTIVITY APPARATUS (to scale)

0 1 2 3 4

Scale (inches)

LIST OF COMPONENTS

A. 1.500" thick sample
B. 0.010" thick stainless steel disks
C. 0.125" thick copper disks with 0.062" I.D. thermocouple wells
D. 0.100" thick lexan disks
E. 0.030" thick lexan disks
F. Constant temperature copper heads
G. 0.125" thick copper disks press fitted over tops of copper heads
H. 0.125" thick neoprene disk to compensate for misalignment
I. Leucite holders for constant temperature heads
J. High density styrofoam insulation
K. Leucite cylindrical shell
L. Hydraulically operated piston
M. Aluminum base attached to frame

Figure 4

ground with their faces containing the optic axis) and silica glass (G.E. 101). The status of absolute measurements of quartz and silica glass has recently been reviewed by Roy, Decker, Blackwell, and Birch (1968), and it is clear that the discrepancies among the better determinations remain uncomfortably large, approximately 3%. The experimental results of Ratcliffe (1959) have been used. Table 2 shows the analytic relations derived experimentally by Ratcliffe and lists a few calculated values. If better absolute values become available in the future, our results can easily be adjusted.

Plastic disks (Lexan) were used as references above and below the sample; they have about 1/15 the conductivity of average rock. Thus the temperature drop across a 2.5 mm reference disk is equivalent to that across a 38 mm ($1\frac{1}{2}$ inch) sample having an average rock conductivity; keeping the ratio of these two temperature drops near unity helps minimize systematic errors in the measurement of thermocouple emf's. The use of thin reference disks helped reduce side heat loss along the divided bar. The Lexan disks were cemented, with a semiviscous epoxy (Tra-Con 3132), to the copper disks and heating elements to eliminate variations in contact resistance and allow for ease of interchange of samples. Most samples measured were 38 mm long; Vaseline was applied at their contact surfaces to minimize the contact resistance.

The temperature difference across the entire stack (between heating elements) was kept at about 20°C, with an attempt to have the mean sample temperature within a few degrees of the in-situ

THERMAL CONDUCTIVITY OF SILICA GLASS AND NATURAL QUARTZ AFTER RATCLIFFE

Analytic Relations Derived Experimentally by Ratcliffe:

$$K_{SiGl} = 0.00316 + 46 \times 10^{-7}\, T - 0.16 \times 10^{-7}\, T^2 \quad \frac{cal}{cm \cdot sec \cdot °C}$$

$$-150°C \leq T \leq 50°C$$

$$K_{NatQtz} = (60.7 + 0.242\, T)^{-1} \quad \frac{cal}{cm \cdot sec \cdot °C} \qquad 0°C \leq T \leq 100°C$$

(in direction normal to optic axis)

Table of Values Calculated from Relations Given Above:

T°C	K_{SiGl}	K_{NatQtz} ($\perp$ to optic axis)
0	3.16×10^{-3} cal/cm·sec·°C	16.5×10^{-3} cal/cm·sec·°C
10	3.20	15.8
20	3.25	15.3
30	3.28	14.7
40	3.32	14.2
50	3.35	13.7

Table 2

temperature. Temperature coefficients of conductivity were determined in several cases and are applied to the data where necessary. The effective conductivity across the Lexan reference disks was calibrated with a 38 mm combination of quartz and silica glass disks with a mean resistivity of about 180 $\frac{\text{cm}\cdot\text{sec}\cdot^\circ\text{C}}{\text{cal}}$, approximately equivalent to an average rock. Recalibrations were performed on a daily basis and were reproducible to better than ±1%. Natural quartz and silica glass were also run independently, and it was found that their calibration of the Lexan did not differ by more than 3%. Thus it is assumed that the calibration of the divided bar is consistent with Ratcliffe's standards to ±1% for rock resistivities between 110 $\frac{\text{cm}\cdot\text{sec}\cdot^\circ\text{C}}{\text{cal}}$ and 250 $\frac{\text{cm}\cdot\text{sec}\cdot^\circ\text{C}}{\text{cal}}$. This range includes most of the rocks measured in this study. Six-inch diameter cylinders of styrofoam were machined to fit the divided bar, as indicated in Figure 4, to help reduce side losses. Calibrating with standards of similar geometry and conductivity as the average rock sample also helped minimize the effects of side losses.

Copper-Constantan (Omega) precision thermocouples in insulating ceramic tubing were inserted in small holes in the copper disks to measure the temperature differences. A K-3 (Leeds and Northrup) potentiometer with an electronic null detector (Astrodata 121 Z) was used to measure the thermocouple emf's. Systematic plus random errors due to the accuracy of the K-3 potentiometer (±0.015% ±0.5 μV on range used) and reading of the instrument (±0.1 μV) do not exceed 1%. Because of the cancellation of systematic errors,

this figure is probably less than 0.5%.

In all instances, samples were water saturated by evacuating the sample for at least 24 hours under a vacuum of several mm of mercury and then introducing boiled water around the sample at about 2500 psi for at least two hours. The disks were then stored in water until measured and coated with silicone grease while being measured to preserve the saturated condition. Repeated measurements of saturated samples were reproducible to 1% or better. Most of the samples were prepared by making two rough cuts with a diamond saw and finishing the surfaces with a diamond lap. A number of samples prepared this way were resurfaced by an optical grinding company to a flat and parallel tolerance of ±0.0005 inch; remeasurement of these samples gave values of conductivity equivalent to the original values within the limits of reproducibility (±1%).

A correction factor (based on the assumption of continuity of flux in the divided bar) was applied to the sample conductivity due to the fact that sample diameters and thicknesses varied by up to a millimeter from the diameters and thicknesses of the standards used for calibration of the divided bar. Application of the correction factor given below will introduce errors within the limits of sample reproducibility for diameters differing by up to ±5% of the standard diameters (Jaeger and Beck, 1955), and will be valid for any difference in thickness insofar as the effects of side heat loss can be neglected. The way in which the correction C is applied is shown in equation (4), which gives the sample conductivity K_s in terms of the effective

conductivity of the Lexan K_ℓ, and the ratio of the temperature drops across the sample E_s and the Lexan $\overline{E}_\ell$ (average of drops across disks on both sides of divided bar).

$$K_s = CK_\ell \frac{\overline{E}_\ell}{E_s} \tag{4}$$

where

$$C = \frac{\ell_s d_{st}^2}{\ell_{st} d_s^2}$$

ℓ_{st} and d_{st} being the standard length ($1\frac{1}{2}$ inch) and standard diameter, respectively, and ℓ_s and d_s, the sample thickness and diameter.

Axial pressures of 100 bars (equivalent to the lithostatic load at 300-meter depth) were applied to the core to ensure good surface to surface contact with the divided bar. Pressure coefficients of saturated samples have been found to be insignificant by other investigators (Walsh and Decker, 1966) and have been neglected in this study. Finally, hot and cold temperature baths with temperature control to 0.02°C were used, and errors from thermal instability within the divided bar was negligible.

Thus systematic and random errors should in no case contribute more than a 5% error to the conductivity determination of a single disk. This figure is less than the variation from disk to disk for most rocks.

IV. DETERMINATION OF RADIOACTIVE HEAT PRODUCTION

A. General Statement

Birch, Roy, and Blackwell (in prep.) have shown that a significant portion of the heat flow at any given locality can be attributed to the radioactive heat production in the near surface rocks. They have suggested that within a geologic province, variations in heat flow can be explained entirely in terms of a regional heat flow with superposed variations due to the local radioactive heat productivity. Thus if one is to study variations in heat flow due to faults, for example, or differences in the lower curst and upper mantle from region to region, the effect of the local radioactivity on the heat flow must be removed if possible. Although the omnipresent lack of knowledge of geologic structure and lithology at depth precludes our being able to give a definitive answer to what the absolute effect of the local radioactivity is, using the approach of Birch, Roy, and Blackwell, as well as what we know about the local and regional geology and geophysics, in most instances relatively cogent arguments can be given for making a good approximation as to what its effect is on the heat flow.

The data will be discussed and interpreted later. Only the method used to determine the radioactive heat production is described here.

B. Determination of U-Th and K Content

Uranium-thorium and potassium analyses were made on core samples from most of the holes involved in the heat flow study.

Samples 38 mm long ($1\frac{1}{2}$ inch) were taken every 25 or 50 feet in the hole and put into one, two, or three composite groups.

The contribution to the radioactivity from the uranium and thorium series was determined by measuring the rate of α-particle emission, from thick sample powders, with an α-particle ZnS scintillation detector. The sample emission rates were compared to the emission rate of similar samples of known (from isotope dilution analyses) uranium-thorium content. The powder was prepared by breaking the pieces of core into pea-sized pieces with a diamond mortar and then pulverizing these pieces down to a size small enough to pass through a 200-mesh screen. The sample was then prepared by packing 7 grams of the powder into a 2 inch by 3/32 inch deep aluminum pan with a glass slide. Variability of repacked samples was within the statistical error of the measurement. Attention was given to the possibility that a significant portion of the radon may be lost during the pulverizing process. Calculations given in Appendix II suggest that if all the radon is lost, the α-activity would be immediately reduced by about 21%. However, after one to two weeks equilibrium will be effectively re-established. U-Th values used in this work were determined from samples which were allowed to stand at least two weeks before they were measured.

The method of counting α-particles is especially suitable for finding the heat productivity due to the decay of uranium and thorium, since the average energy per α-particle (total energy of entire decay scheme divided by the number of α-particles) is about the same for

each of the three decay series. Hence the energy calculated by this method will depend very little on the U-Th ratio, and the assumption of a 1:4 U-Th ratio should not introduce an error of more than ±5% even for cases with extreme U-Th ratios. However, due to the fact that in average rock the mean range of α-particles from the U^{238} series ($\sim 2.0 \times 10^{-3}$ cm) is about 20% less than the mean range of α-particles from the Th^{232} series ($\sim 2.4 \times 10^{-3}$ cm), the thorium is effectively sampled over a 20% larger volume, and a thick sample of pure ordinary uranium should count about 20% lower than a thick sample of pure thorium having an equal equivalent-uranium (eU)* content. Measurements on pure uranium and thorium confirmed this analysis. Because the activities of samples were compared to the activities of similar rock samples (analyzed by isotope dilution) with approximately a 1:4 U-Th ratio, this effect is assumed to contribute errors no larger than ±5% to the determination of equivalent-uranium, provided it can be assumed that the sample U-Th ratios remained between 1:1 and 1:10 (see Clark, Peterman, and Heier, 1966, for examples of common ratios). We conclude that the two sources of error just discussed will in most cases contribute no more than a ±10% error to the determination of heat production from the U-Th content. It should be emphasized that radioactive equilibrium is

---

*When counting α-particles, one does not know from which decay series they originate. For this reason the concept of equivalent-uranium (abbreviated eU) is used. A sample with 1 ppm eU would have the α-activity of 1 ppm of ordinary uranium. It takes 4.14 ppm Th to give 1 ppm eU (see Appendix I).

assumed and necessary for the general applicability of this method.

The per cent K_2O was determined by X-ray fluorescence. The potassium K-shell fluorescence intensity from hard packed powder pills was compared with intensities from a number of similar standards whose K_2O contents had been chemically analyzed.

C. Conversion of Radioactive Content to Heat Generation

The conversion from equivalent-uranium and per cent potassium to heat production was done using the values of Birch (1954), as given in Table 3. A complete outline of this procedure and the final conversion factors are given in Appendix I. Total heat production values determined from these conversion factors by the methods outlined above are believed to be accurate to ±20%, corresponding to a standard error of ±10%. The errors are attributed to ±5% from sample α-counting statistics and ±2% from the standard sample's counting statistics; ±8% from the assumption regarding the U-Th ratio; ±2% due to the ±10% accuracy to which the K_2O values were determined; ±1% from the accuracy of the determination of the U-Th content of the standard sample from isotope dilution; and ±2% from the uncertainty of Birch's estimation of energy production (Birch, 1954). It should be emphasized that the ±20% does not include sampling errors, only measurement errors. Since the samples were crushed and α counted in only one, two, or three composites, no meaningful sampling errors could be determined. The possible ±4% and ±2% errors from the α-counting statistics represent

PARENT	END PRODUCTS	E Mev/atom	Q cal/gm·yr
$_{92}U^{238}$	$_{82}Pb^{206} + 8\,_2He^4$	47.4	0.71
$_{92}U^{235}$	$_{82}Pb^{207} + 7\,_2He^4$	45.2	4.30
$_{90}Th^{232}$	$_{82}Pb^{208} + 6\,_2He^4$	39.8	0.20
$_{19}K^{40}$	$_{18}A^{40}$ (11%); $_{20}Ca^{40}$ (89%)	0.71	0.22
U (ordinary)	----	--	0.73
K (ordinary)	----	--	2.7×10^{-5}

Table 3 (from Birch, 1954)

$$\frac{\pm 2\sqrt{N}}{N}$$

where N is the total number of counts above background (sample counting was generally terminated at 2000 counts). $\sigma = \sqrt{N}$ is the standard deviation of the measurement for a radioactive decay process where the measurement time, $t << t_{1/2}$, the species half-life, and the 95% C.L. is given by $\sim 2\sigma = 2\sqrt{N}$. Generally speaking, however, $\sqrt{N}$ is an upper bound on the standard deviation, since we have in the decay series some $t_{1/2} \simeq t$, and thus the 95% C.L. used overestimates the true 95% C.L.

The results of the equivalent-uranium and potassium analyses are given in Appendix V. The values of heat production for each hole are given in the hole summary tables. The value represents an average in the cases where more than one composite was run. Where weathered rock was encountered in the upper part of a hole in which the rock was fresh at depth, the determinations from the weathered zone were not included in the average.

Figure 5 shows a plot of eU versus %K on which each of the composites run has been plotted. The samples deviating significantly from the approximate best fit straight line have been labeled. The line has a slope of $\frac{1}{3} \times 10^4 \frac{\text{ppm K}}{\text{ppm eU}}$, or if a $\sim$4:1 U-Th ratio is assumed, the slope can be written as $\frac{2}{3} \times 10^4 \frac{\text{ppm K}}{\text{ppm U}}$. This value agrees well with the ratio of Wasserburg, MacDonald, Hoyle, and Fowler (1964) of $K/U = 10^4$. The rocks plotted cover a wide range of compositions from granite to hornblende diorite.

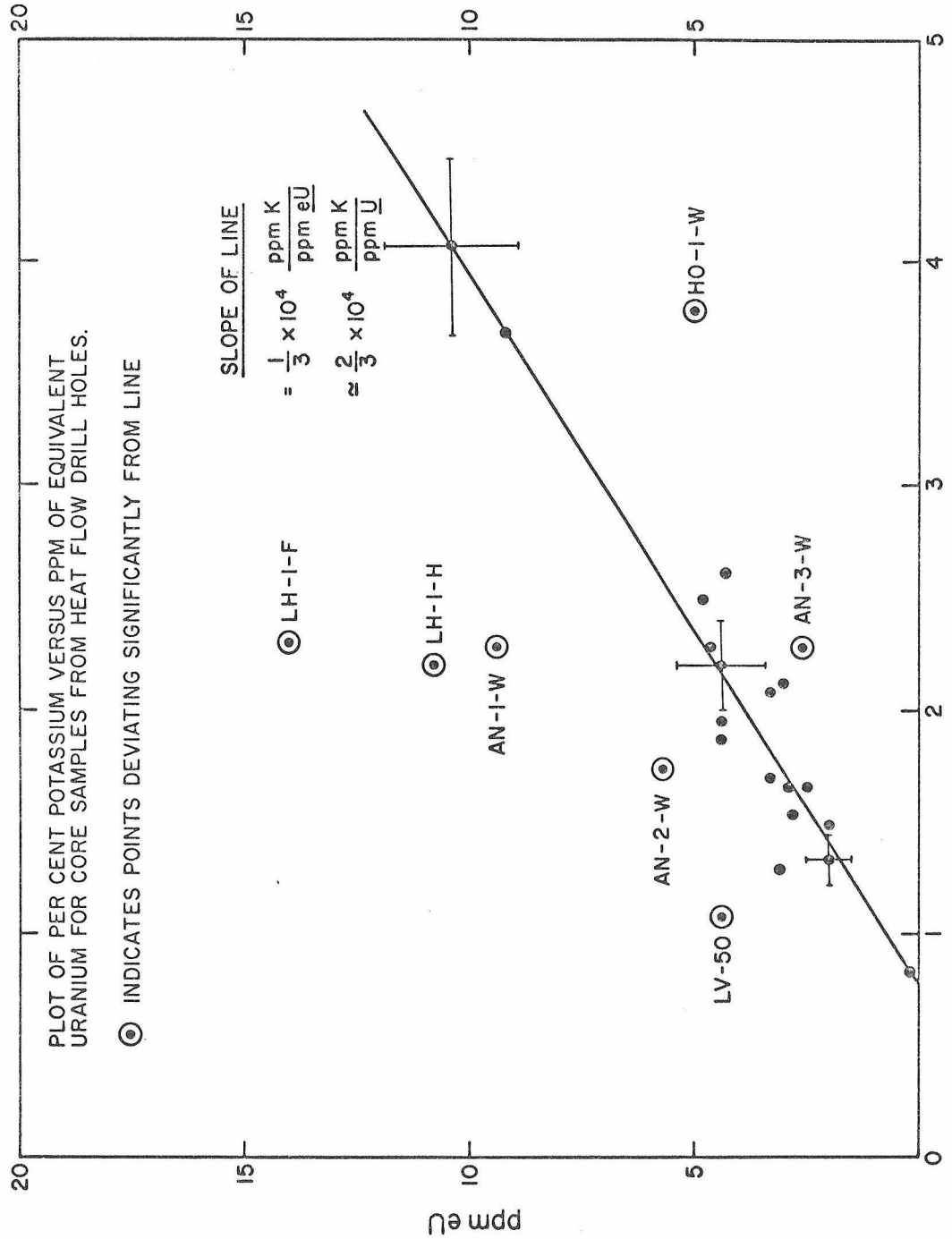
PLOT OF PER CENT POTASSIUM VERSUS PPM OF EQUIVALENT URANIUM FOR CORE SAMPLES FROM HEAT FLOW DRILL HOLES.
⊙ INDICATES POINTS DEVIATING SIGNIFICANTLY FROM LINE
SLOPE OF LINE
= 1/3 × 10⁴ ppm K / ppm eU
≃ 2/3 × 10⁴ ppm K / ppm U
LH-1-F
LH-1-H
AN-1-W
AN-2-W
LV-50
AN-3-W
HO-1-W
ppm eU
% K
0
5
10
15
20
1
2
3
4

Figure 5

The fact that is most remarkably apparent from Figure 5 is that those analyses deviating significantly from the line are all either severely weathered samples (LH-1-F, LH-1-H, AN-1-W, AN-2-W, and AN-3-W) or from near the surface (LV-50 and H-1-W). The only weathered sample that falls on the line is LH-2-CO, which is probably fortuitous. The plot suggested a criterion for helping to determine whether or not a radioactivity determination by the method used here was anomalous or not. Analyses falling significantly off the line, such as weathered samples, may reflect radioactive non-equilibrium where there has been enrichment or depletion of one or more radioactive species, and hence should not be averaged with consistent analyses from fresh samples. Thus, in our case the plot demonstrates the dangers which might be encountered if one generally assumes that radioactive determinations of near surface samples are representative of the rocks at depth.

V. BASIC EQUATION OF HEAT FLOW AND METHOD OF DATA REDUCTION

The basic equation used in heat flow analysis is the one-dimensional, steady-state heat conduction equation

$$f_z = -k \frac{dT}{dz} \tag{5}$$

where f_z is the vertical component of heat flow (expressed in $\mu cal/cm^2 \cdot sec$), k is the thermal conductivity (in cal/cm·sec·°C), and $\frac{dT}{dz}$ is the vertical temperature gradient (in °C/km). In practice the two quantities k and $\frac{dT}{dz}$ are determined separately, the former in the laboratory and the latter in the field; corrections are then generally applied to each and the quantities combined to give the value of the heat flow.

Three methods of combination are commonly used (see Blackwell, 1967). The first and simplest may be called the product method, whereby a mean harmonic conductivity* and a mean gradient,

---

*Determining the effective conductivity from a set of conductivity measurements for a particular drill hole is like averaging resistances in parallel.

$$\therefore k_{eff} \neq \frac{1}{n} \sum_n k_i$$

but rather we define the mean resistivity

$$R_m = \frac{1}{n} \sum_n \frac{1}{k_i}$$

and the mean harmonic conductivity

$$k_m = \frac{1}{R_m}$$

normally a least-squares first-order fit to the temperature-depth data, are multiplied to give an average heat flow. A second approach might be called the resistance integral method (first proposed by Bullard, 1939) and involves integration of equation (5) to give for some depth z

$$T_z = T_{z_o} - f_z \int_{z_o}^{z} \frac{dz}{k} \tag{6}$$

where T_z and T_{z_o} are the temperatures at z and z_o and

$$\int_{z_o}^{z} \frac{dz}{k} \tag{7}$$

is defined as the resistance integral since its value is the total thermal resistance between the depths z_o and z. In practice (Roy, 1963) (7) may be approximated by

$$\sum_{i=1}^{n} \frac{\Delta z_i}{k_i} \tag{8}$$

where k_i is the conductivity of the zone Δz_i and n is the total number of samples in the interval (z_o, z). It can be seen from (6) that a plot of resistance integral versus temperature gives a line with slope equal to the vertical heat flow. Normally a least-squares analysis is applied to the temperature-resistance integral points. The third method (Roy, 1963; Gough, 1963) has been called the interval method. Substituting the finite approximation (8) into (6) for an arbitrary depth interval (z_1, z_2) and solving for the flux f_z, we have for this interval

$$f_z = -(T_2 - T_1) \Big/ \left(\sum_{i=1}^{n} \frac{\Delta z_i}{k_i} \right) \tag{9}$$

or

$$f_z = -\left(\frac{T_2 - T_1}{z_2 - z_1}\right)\left(\frac{z_2 - z_1}{\sum_{i=1}^{n} \frac{\Delta z_i}{k_i}}\right) \qquad (10)$$

The first term in (10) is the average temperature gradient in the interval (z_1, z_2) and the second term is the mean harmonic conductivity. Thus the heat flow is calculated for a number of intervals in the hole and the arithmetic mean is taken as the best value. In each of the above methods, the residuals between the empirical values and the values determined from the mean or best fit should be examined and explanations given for any systematic deviations.

For the case of a completely homogeneous and uniform medium, all three methods give the same values for the flux. Variations between the methods occur when vertical variations in thermal conductivity are present in the interval which has been logged. When it can be shown that variations in thermal conductivity can be correlated with variations in the temperature gradient as in horizontally stratified media of differing rock type (one gets a "mirror image effect"; since the flux must be the same in any interval, a lower gradient means a higher conductivity and vice versa), the resistance integral and separate interval methods must be used to give the correct results. However, if no correlation can be demonstrated and the mean conductivity is the same for all temperature intervals, which is generally the case for measurements in granitic rocks, any of the three methods should be satisfactory. Blackwell's results (1967) show that when the gradient-conductivity correlation is poor,

even though large random variations in conductivity occur, the resulting heat flows determined from each of the three methods generally agree to within ±1-2%, which is well within the total uncertainty of any given heat flow determination. Invariably, however, the "goodness of fit", as represented by the standard errors, favors first the resistance integral, second the separate interval, and third the product method. Because of the simplicity of the product method, especially when applying the topographic correction, and because no apparent accuracy is lost with this method, and since the majority of the determinations were made in granitic rocks, the product method was used for data reduction. The separate interval method has also been used on the data from AN-1, SB-10, and DH-65 for comparison with the product method.

VI. TOPOGRAPHIC CORRECTION

The temperature gradient, which is measured essentially at the earth-atmosphere boundary, must be corrected for the irregularity of this surface. The general tendency is for gradients to be too low at locations which are positive with respect to the average surrounding topography and too high in regions which are negative, but in both cases approaching the true gradient with increase in depth. In addition, a correction should be applied to the gradient for possible changes in the elevation and configuration of this surface during geologic time. Uplift and erosion change, with time, the temperature conditions on either side of this boundary.

Methods of correcting for the effects which have just been discussed, have been investigated by Jeffreys (1940), Birch (1950), and Clark (1957). The most complete analysis as applied to heat flow studies has been developed by Birch and is used in this study. It was necessary to modify Birch's treatment for tunnel temperature measurements to the case applicable to drill holes. As was pointed out earlier, the product method of obtaining heat flow was used, in part, because of the simplicity in applying the topographic correction; a minimum amount of manipulation of the data is necessary. The topographic correction is developed in Appendix III with the modifications necessary for application to drill hole gradients. The final equation can be written as

$$T(z) - \alpha'[azL - azd + \overline{h}] = T_s - \alpha'[L - d] + \alpha[z + azd - \overline{h}] \qquad (11)$$

where

$$a = \frac{2}{\sqrt{\pi \varkappa t}}$$

$$\overline{h} = \sum_{\text{rings}} \overline{h}_r \overline{E}_r \frac{\Delta\Omega_r}{2\pi}$$

T(z) and z are the present uncorrected temperature at depth z and the depth, respectively; L and δ are the uplift and erosion at the collar (top) of the drill hole, respectively; α' is the change of surface or soil temperature with elevation; and $\overline{h}_r$ is the difference in elevation between the collar of the drill hole and the average elevation of the r^{th} ring (see Appendix III). These are the pertinent data which had to be determined for each hole in order to make the topographic correction. All other symbols are defined in Appendix III. If one plots the quantity $[z + az\delta - \overline{h}]$ versus the quantity $T(z) - \alpha'[azL - az\delta + \overline{h}]$ for a set of temperature-depth data, a straight line will result with slope α, the undisturbed geothermal gradient, and intercept $T_s - \alpha'[L - \delta]$, the surface temperature at the top of the drill hole. Equation (11) can be simplified in the steady-state case (topography has persisted as is indefinitely) to

$$T(z) - \alpha' \overline{h}(\infty) = T_s + \alpha[z - \overline{h}(\infty)] \qquad (12)$$

where

$$\overline{h}(\infty) = \sum_{\text{rings}} \overline{h}_r \frac{\Delta\Omega_r}{2\pi}$$

Relations (11) and (12) were programmed for the IBM 7094 and a least-squares straight line fit to the data.

It is only necessary to estimate L and δ for the time dependent correction, while α' must be estimated for both the time dependent and steady-state cases. Birch (1950) found a change of soil temperature with elevation of 4.5°C/km, decreasing upward, for the Colorado Front Range. Many investigators have systematically used this value for topographic corrections. Undoubtedly, however, this quantity is quite variable from region to region. The arguments Birch used to arrive at this figure are not really applicable to southern California. His value was based on soil temperatures in mountainous regions whose surface was covered with snow for a significant portion of the year at higher elevations.

As might be suspected, the atmospheric lapse rate can be used to give a first approximation to the rate of change of soil temperature. Lapse rates can be determined from weather station data at various elevations. The measurements of temperatures by these stations are usually made at about 6 feet above the ground surface, in the region of the so-called "macroclimate" (Geiger, 1950). While temperatures below 6 feet (microclimate) are controlled almost exclusively by the local ground conditions and the energy balance at this surface, temperatures in the macroclimatic region reflect the average ground conditions and energy regime over a large area. We might suspect then that there should be a certain correlation between these air temperatures and the soil temperatures and hence a correlation in rate of change of these temperatures with elevation. However, as Birch suggests, the lapse rate might be greater than the rate of

change of soil temperature by perhaps several degrees per km, which he attributes to periodic snow cover. Even in the case of no snow cover this might be expected (Geiger, 1950), due to the great increase in solar radiation with altitude, with only a slight increase in outward going radiation, and a simultaneous decrease of air temperature. Solar radiation increases 50% between 100 and 500 meters, and 100% between 100 and 4000 meters. Systematic measurements and quantitative discussions in these directions are lacking.

Figure 6 shows Weather Bureau temperature data and surface temperatures from drill hole data extrapolated to zero depth near Anza, California, plotted versus station elevation. An approximate linear fit to the data gives a lapse rate of about 5.8°C/km. We can, on the basis of our previous arguments, consider this an upper bound on the rate of change of soil temperature with elevation. Thus if we use Birch's value of 4.5°C/km, we probably would not be in error by more than ±1°C. Finally, if it can be assumed that in southern California the mean value of the lapse rate or change of soil temperature with altitude is approximately the same from one locality to another, using the wrong value will only introduce a small absolute error, the relative differences remaining the same. We might add that variations from linearity in the lapse rate may contribute errors every bit as large as the uncertainty which we have just discussed.

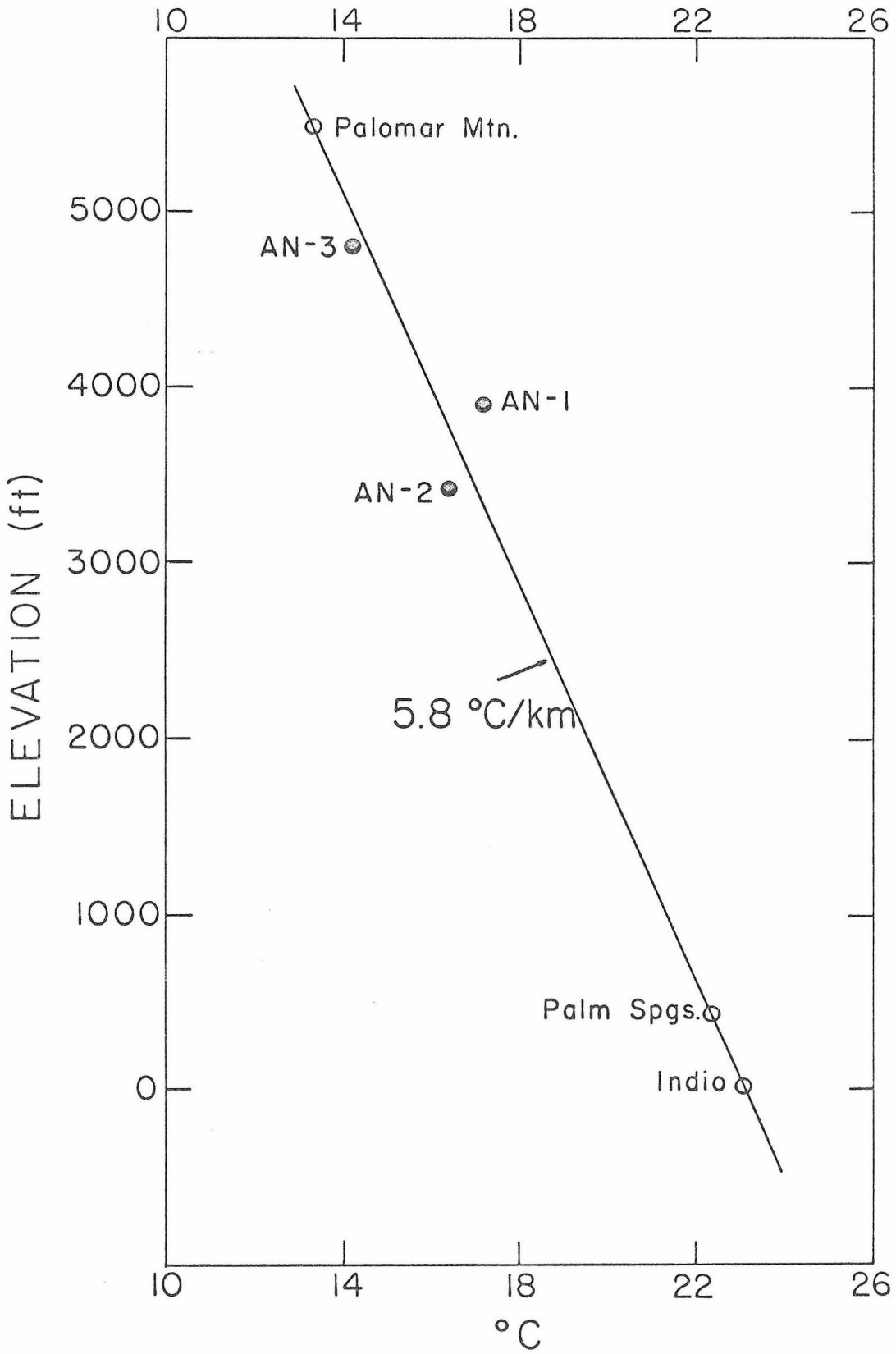
10
14
18
22
26
Palomar Mtn.
AN-3
AN-1
AN-2
5.8 °C/km
Palm Spgs.
Indio
5000
4000
3000
2000
1000
0
ELEVATION (ft)
°C

Figure 6

VII. PRESENTATION OF DATA

A. General Statement

The heat flow determinations reported in this study, in the vicinity of the San Andreas-Garlock-San Jacinto fault systems in southern California, all lie essentially on the boundary of two major physiographic provinces (see Fenneman, 1931), which have been called the Pacific Border and Basin and Range Provinces. The determinations near Hollister in central California all lie within the Pacific Border Province which extends to the eastern boundary of the Sierra Nevada. For the purpose of this discussion, however, the Pacific Border Province will be divided into five subprovinces (see Figure 7), the Coast Range, Great Valley, Sierra Nevada, Transverse Range, and Peninsular Range Provinces. The Basin and Range Province in southern California will be discussed in terms of two subprovinces, the Mojave Desert and Gulf of California (Salton Trough).

The seventeen completed determinations occur and will be discussed in five groups; the Anza, San Bernardino, Lake Hughes, Tehachapi Mountains, and Hollister groups. Each region is characterized by a particular type of seismic activity, the importance of which will be discussed later.

For each region, a brief resumé of the local geology is given, followed by presentation of the data for each of the holes. A short discussion of the geologic history pertaining to possible time dependent effects on the heat flow values is also included. Temperature-depth

curves from the most recent loggings are shown for all the drill holes.

A tabulated summary of the pertinent data is given for each hole (e.g. see Table 4). Both uncorrected and corrected values of the gradients are given in the tables, having been derived from least-squares, linear fits to the temperature-depth points. The number in parentheses before the mean resistivity indicates the number of samples influencing the value given. The numbers in parentheses before the uncorrected gradient indicate the depth interval used for determination of the heat flow. The limit of topographic influence indicates the radial extent, in km from the drill hole, to which the topographic correction was carried out. Finally, the errors after the resistivities, gradients, and heat flows are 95% confidence limits based on a normal distribution. The Student's t multiplier has been applied to the standard error according to the number of degrees of freedom (n-1 for sample means, and n-2 for least-squares linear fits). Thus, for example, the error in the mean resistivity would be given by

$$95\%\ \text{C.L.} = t_{n-1} \sqrt{\frac{\Sigma d_i^2}{n(n-1)}}$$

where t_{n-1} is Student's multiplier for n-1 degrees of freedom, and d_i is the deviation from the mean of the i^{th} sample (see Appendix VIII for other error formulas). The errors following the heat production values represent the ±20% maximum measurement error discussed before, plus a sampling error as determined from the ratio of the maximum difference between composite values and their average. Where only one composite has been used, the sampling error is

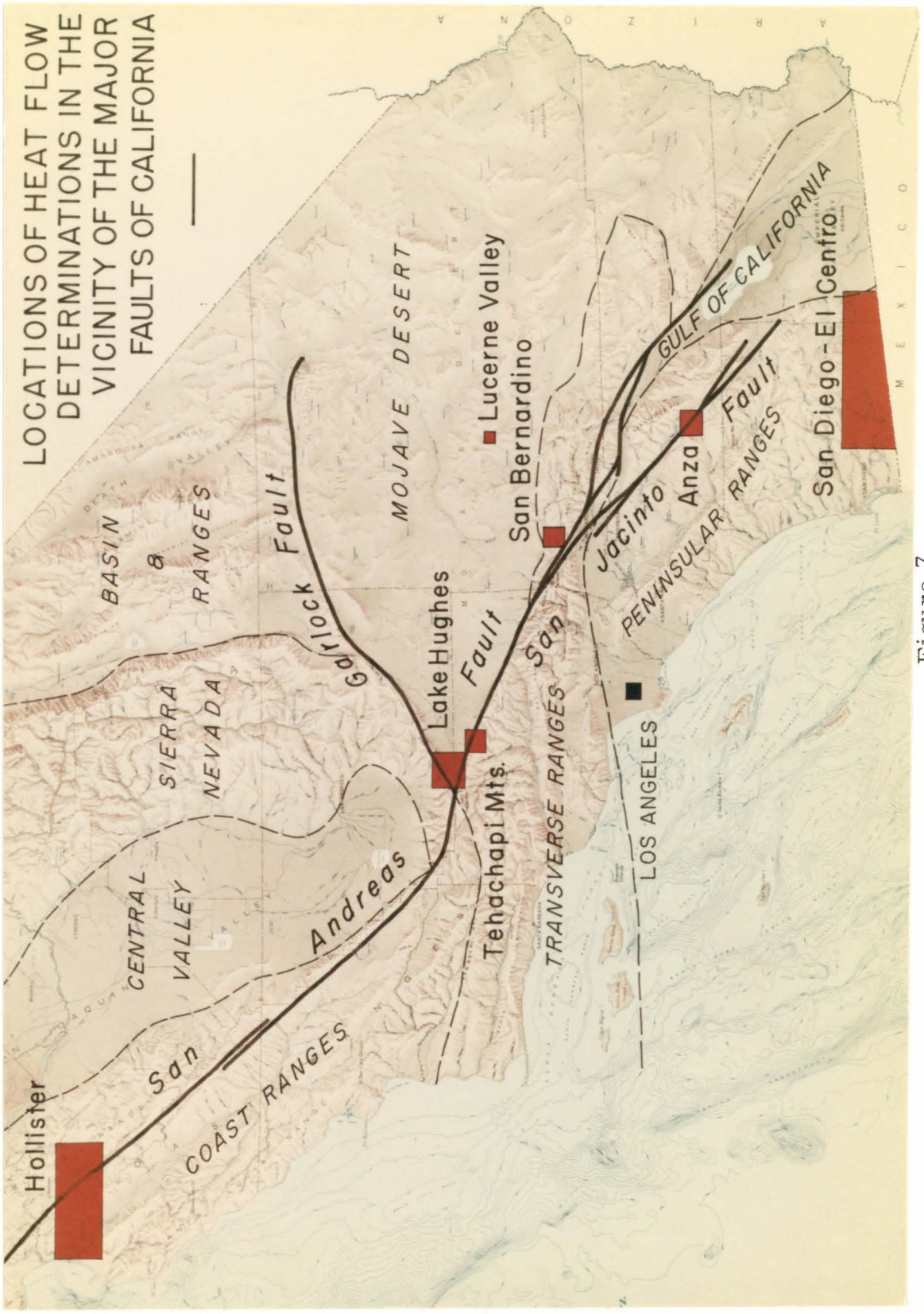
LOCATIONS OF HEAT FLOW DETERMINATIONS IN THE VICINITY OF THE MAJOR FAULTS OF CALIFORNIA
Hollister
San Andreas Fault
CENTRAL VALLEY
SIERRA NEVADA
BASIN & RANGES
COAST RANGES
Garlock Fault
MOJAVE DESERT
Lake Hughes
Tehachapi Mts.
San Andreas Fault
TRANSVERSE RANGES
Lucerne Valley
San Bernardino
LOS ANGELES
San Jacinto Fault
Anza
PENINSULAR RANGES
GULF OF CALIFORNIA
San Diego-El Centro
MEXICO

Figure 7

arbitrarily chosen to be ±10%.

All measured temperatures and their respective depths along with the measured conductivities and their depths for all holes are given in Appendices VI and VII.

B. Heat Flow near Anza, California

The first three holes in this investigation, AN-1, AN-2, and AN-3, were drilled near the town of Anza, California (see Figure 7). These holes are located in the pre-upper Cretaceous crystalline complex of the extreme northeastern part of the Peninsular Range Province near the San Jacinto fault. Figure 8 shows the relation of the drill sites to the local geology. Note that AN-1, AN-2, and AN-3 are designated as San Andreas #1, #2, and #3, respectively, in Figure 8. The geology of the San Jacinto fault zone has been described in detail by Sharp (1965), while the regional geology of the province has been discussed more generally by Larsen (1948), Jahns (1954), and others.

The Peninsular Range Province is a well-defined geologic and physiographic unit of southwestern California and the entire part of Baja California. The province is perhaps 1000 miles long and averages 50 miles wide. It is terminated at the north end by the Transverse Ranges. A physiographic cross section, east-west through the northern part of the Peninsular Ranges, reveals that it is much like the southern portion of the Sierra Nevada (Miller, 1935). Both are characterized by a gently seaward-sloping western flank, a spectacularly abrupt eastern escarpment, and an interior comprised

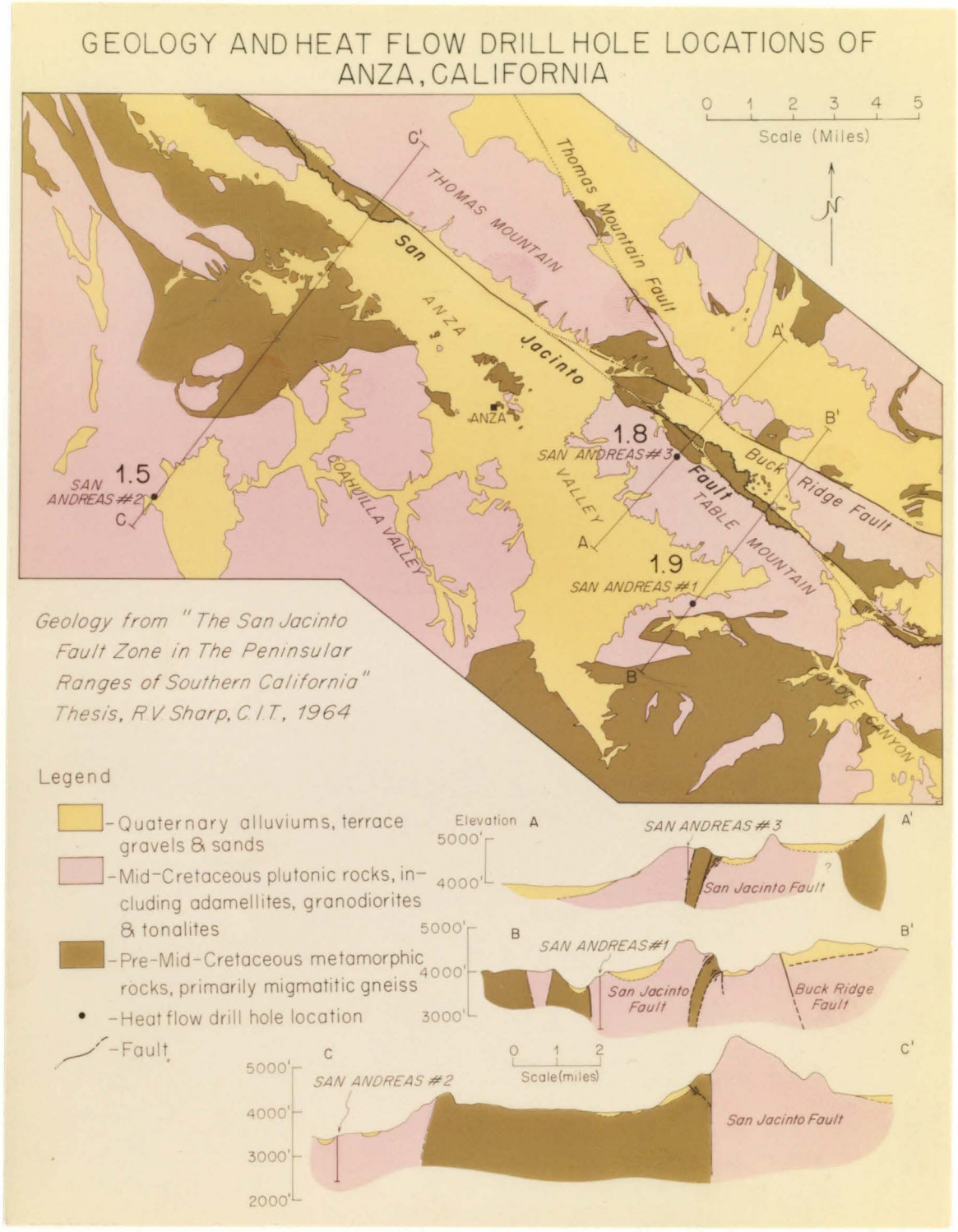
GEOLOGY AND HEAT FLOW DRILL HOLE LOCATIONS OF ANZA, CALIFORNIA
0 1 2 3 4 5
Scale (Miles)
N
C'
THOMAS MOUNTAIN
Thomas Mountain Fault
San
ANZA
Jacinto
ANZA
A'
B'
1.8
SAN ANDREAS #3
Buck
Ridge Fault
Fault
TABLE
MOUNTAIN
VALLEY
1.5
SAN
ANDREAS #2
C
COAHUILLA VALLEY
A
1.9
SAN ANDREAS #1
B
TOYON
CANYON
Geology from "The San Jacinto Fault Zone in The Peninsular Ranges of Southern California" Thesis, R.V. Sharp, C.I.T., 1964
Legend
-Quaternary alluviums, terrace gravels & sands
-Mid-Cretaceous plutonic rocks, including adamellites, granodiorites & tonalites
-Pre-Mid-Cretaceous metamorphic rocks, primarily migmatitic gneiss
-Heat flow drill hole location
-Fault
Elevation
A
A'
5000'
4000'
SAN ANDREAS #3
San Jacinto Fault
B
B'
5000'
4000'
3000'
SAN ANDREAS #1
San Jacinto Fault
Buck Ridge Fault
C
C'
0 1 2
Scale (miles)
5000'
4000'
3000'
2000'
SAN ANDREAS #2
San Jacinto Fault

Figure 8

of numerous subdued upland surfaces. The region, in contrast to the Sierra Nevada, is complicated by numerous through-going active faults with near-vertical dip, striking northwest-southeast and thus giving the province its characteristic structural grain.

The exposed rocks of the mountainous eastern portion of the province are chiefly igneous intrusive, metasedimentary, and metavolcanic types, and constitute what is called the southern California batholith. Gabbroic to granitic rocks with an overall average composition of quartz-diorite (tonalite) constitute the bulk of the crystalline terrane. U-Pb isotopic ages (Banks and Silver, 1964) suggest a mid-Cretaceous age for the batholith. Stratigraphic relations (Larsen, 1948) suggest unroofing of the batholith occurred in upper Cretaceous time. The pre-batholith metamorphic rocks form a widely distributed but subordinate part of the crystalline exposure. Tertiary and Quaternary sediments are generally confined to the westernmost part of the province. Although Tertiary and Quaternary volcanic deposits are widespread in adjacent provinces, evidence for significant volcanic activity within the Peninsular Ranges is lacking.

The San Jacinto is one of the main branches of the San Andreas fault system in southern California. The high degree of seismicity associated with it, and the fact that it continues on strike with the San Andreas fault coming from the northwest, suggest that it may also be, at present, the most active member. Arguments have been presented for up to 36 km right-lateral slip and 13 km of vertical movement by Sharp (1965) for the San Jacinto fault. The geologic mapping indicates

a rate of movement along the fault since Pleistocene time of at least 0.3 cm/year, and triangulation surveys have established current rates of at least 3 cm/year across the San Jacinto and related faults to the south of Anza, with perhaps up to three times this rate across the southern portion of the Imperial Valley (Whitten, 1955).

The predominant rock type in the Anza region, as described by Sharp, is a hornblende-biotite tonalite known as the Cahuilla Valley pluton. The evidence for the pluton being a single unit is not entirely clear; however, the variability appears confined chiefly to the hornblende-biotite ratio.

AN-1, AN-2, and AN-3 were all drilled within the boundaries of the Cahuilla Valley pluton on the southwest side of the fault. Although crystalline outcrop is continuous across the fault, no drilling was done northeast of the fault because of the severe topographic relief.

Temperature profiles for AN-1, 2, and 3 are shown in Figures 9, 10, and 11, and summaries of the pertinent hole data are given in Tables 4, 5, and 6. The core from all three holes was quite homogeneous and for the most part unfoliated, and hence deviations in conductivity from the mean harmonic value for each hole are quite small. However, weathering persisted to about 100 meters in AN-1 and 2, and to some degree, for most of the depth of AN-3. The greater depth of weathering at AN-3 is probably due to this hole's proximity to the fault zone.

AN-1 ANZA, CALIFORNIA

LOCATION and ELEVATION		DRILLING HISTORY	
Latitude	33° 29.5' N	Started	2/3/65
Longitude	116° 35.8' W	Stopped	4/16/65
Collar Elevation	3900 feet	Total Depth	1200 feet
Distance from Fault Trace	4 km	Hole Size	BX-Wireline Uncased

DEPTH	GEOLOGIC LOG
0 - 300 feet	Hornblende Tonalite (weathered)
300 - 1200 feet	Hornblende Tonalite (fresh)

CONDUCTIVITY, GRADIENT, HEAT FLOW, RADIOACTIVITY

Mean Resistivity	(29)	$135.8 \pm 2.3 \frac{cm \cdot sec \cdot °C}{cal}$
Mean Harmonic Conductivity		$7.36 \pm 0.1 \frac{mcal}{cm \cdot sec \cdot °C}$
Uncorrected Gradient	(160-360 m)	25.04 ± 0.21 °C/km
Corrected Gradient — Steady State		25.39 ± 0.24 °C/km
Corrected Gradient — Topographic Evolution		25.24 ± 0.24 °C/km
Uncorrected Heat Flow		1.84 ± 0.04 HFU
Corrected Heat Flow — Steady State		1.87 ± 0.04 HFU
Corrected Heat Flow — Topographic Evolution		1.86 ± 0.04 HFU
Limit of Topographic Influence		30 km
Radioactive Heat Production		$3.6 \pm 0.9 \frac{\times 10^{-13} cal}{cm^3 \cdot sec}$

Table 4

AN-2 ANZA, CALIFORNIA

LOCATION and ELEVATION		DRILLING HISTORY	
Latitude	33° 31.6' N	Started	4/21/65
Longitude	116° 48.4' W	Stopped	6/14/65
Collar Elevation	3420 feet	Total Depth	1000 feet
Distance from Fault Trace	13 km	Hole Size	BX-Wireline Uncased

DEPTH	GEOLOGIC LOG
0 - 250 feet	Hornblende Tonalite (weathered)
250 - 1000 feet	Hornblende Tonalite (fresh)

CONDUCTIVITY, GRADIENT, HEAT FLOW, RADIOACTIVITY

Mean Resistivity	(32)	$151.7 \pm 3.1 \frac{cm \cdot sec \cdot °C}{cal}$
Mean Harmonic Conductivity		$6.60 \pm 0.1 \frac{mcal}{cm \cdot sec \cdot °C}$
Uncorrected Gradient	(100-300 m)	22.63 ± 0.26 °C/km
Corrected Gradient — Steady State		22.18 ± 0.23 °C/km
Corrected Gradient — Topographic Evolution		22.03 ± 0.23 °C/km
Uncorrected Heat Flow		1.49 ± 0.04 HFU
Corrected Heat Flow — Steady State		1.46 ± 0.03 HFU
Corrected Heat Flow — Topographic Evolution		1.45 ± 0.03 HFU
Limit of Topographic Influence		30 km
Radioactive Heat Production		$2.2 \pm 0.8 \frac{x10^{-13} cal}{cm^3 \cdot sec}$

Table 5

AN-3 ANZA, CALIFORNIA

LOCATION and ELEVATION		DRILLING HISTORY	
Latitude	33° 32.3' N	Started	6/18/65
Longitude	116° 36.2' W	Stopped	7/15/65
Collar Elevation	4800 feet	Total Depth	700 feet
Distance from Fault Trace	1 km	Hole Size	BX-Wireline Cased $1\frac{1}{4}$" pipe

DEPTH	GEOLOGIC LOG
0 - 700 feet	Hornblende Tonalite (weathered)

CONDUCTIVITY, GRADIENT, HEAT FLOW, RADIOACTIVITY

Mean Resistivity	(31)	$146.6 \pm 4.9 \frac{cm \cdot sec \cdot °C}{cal}$
Mean Harmonic Conductivity		$6.82 \pm 0.2 \frac{mcal}{cm \cdot sec \cdot °C}$
Uncorrected Gradient	(110-210 m)	23.94 ± 0.20 °C/km
Corrected Gradient	Steady State	25.79 ± 0.20 °C/km
	Topographic Evolution	25.55 ± 0.20 °C/km
Uncorrected Heat Flow		1.63 ± 0.06 HFU
Corrected Heat Flow	Steady State	1.76 ± 0.06 HFU
	Topographic Evolution	1.74 ± 0.06 HFU
Limit of Topographic Influence		30 km
Radioactive Heat Production		$2.8 \pm 1.6 \frac{x10^{-13} cal}{cm^3 \cdot sec}$

Table 6

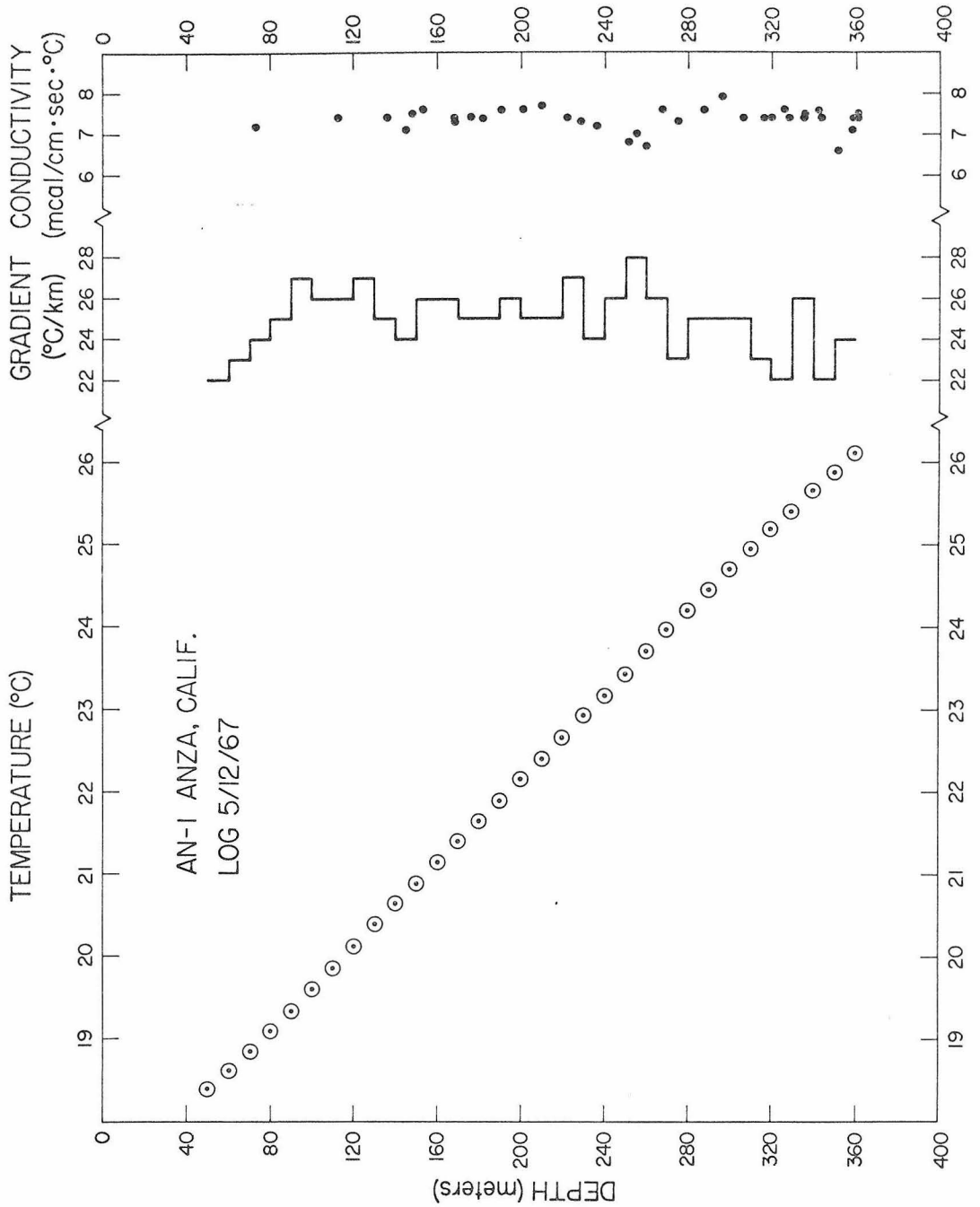
TEMPERATURE (°C)
GRADIENT (°C/km)
CONDUCTIVITY (mcal/cm·sec·°C)
AN-1 ANZA, CALIF.
LOG 5/12/67
DEPTH (meters)

Figure 9

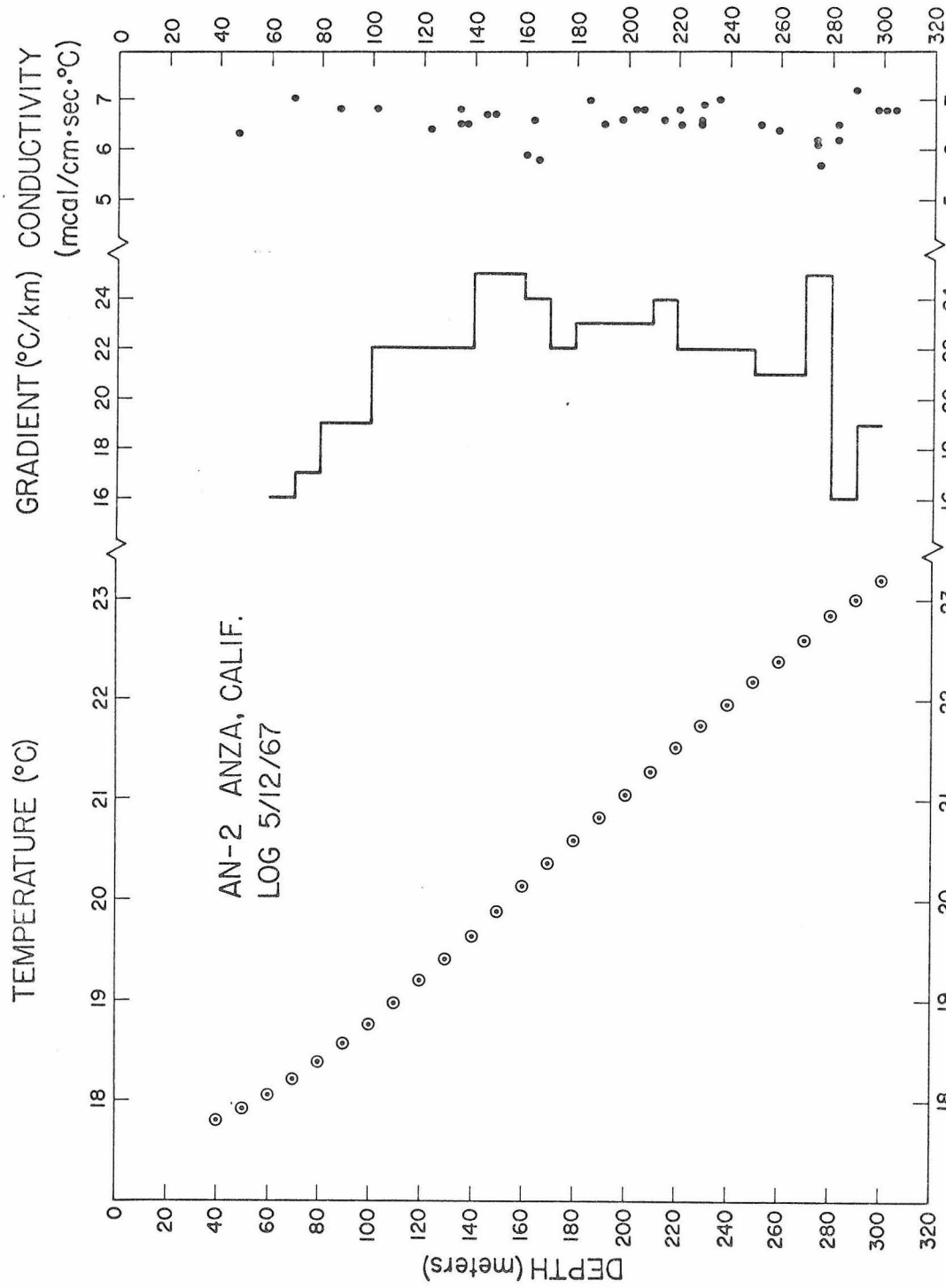
TEMPERATURE (°C)
GRADIENT (°C/km)
CONDUCTIVITY (mcal/cm·sec·°C)
AN-2 ANZA, CALIF.
LOG 5/12/67
DEPTH (meters)

Figure 10

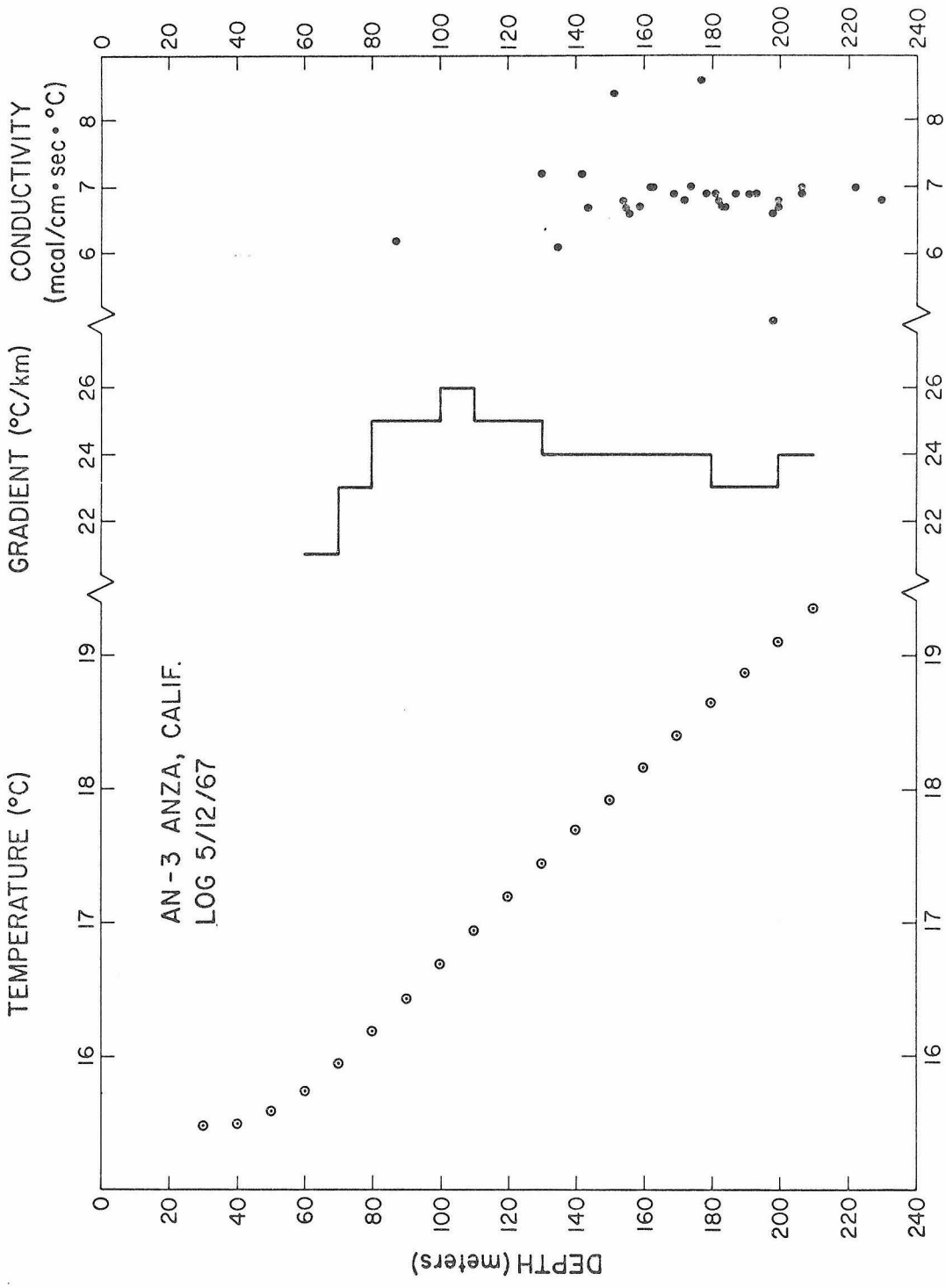
TEMPERATURE (°C)
GRADIENT (°C/km)
CONDUCTIVITY (mcal/cm • sec • °C)
AN-3 ANZA, CALIF.
LOG 5/12/67
DEPTH (meters)
0
20
40
60
80
100
120
140
160
180
200
220
240
16
17
18
19
22
24
26
6
7
8

Figure 11

The heat flow values (steady-state topographic conditions) of AN-1 and AN-3 are 1.9 and 1.8 μcal/cm^2·sec, respectively. (Hereafter 1 μcal/cm^2·sec will be designated 1 heat flow unit, abbreviated 1 HFU after the usage of White, 1957.) The value at AN-2, at a considerably greater distance from the San Jacinto fault than either of the other two holes, is significantly lower -- 1.5 HFU.

The radioactive heat production was determined from three groups of core samples for each hole. One group consisted of a 38 mm ($1\frac{1}{2}$ inch) sample every 50 feet for the first 250 feet, a similar sample every 100 feet from 300 feet deep to the bottom, and a third group, every 100 feet from 350 feet deep to the bottom. These groups are designated (for AN-1, for example) as AN-1-W, AN-1-H, and AN-1-F, respectively, in Appendix V. The groups from the weathered zones were not used in the averages, since their values of U-Th content varied significantly from the values of the other two groups in all cases.

Separate interval heat flows (with steady-state topographic correction) were calculated for 10, 20, and 30 meter intervals for AN-1. The results are shown in Figure 12. The total number of conductivity samples was 30 for both the 10 and 20 meter intervals and 25 for the 30 meter intervals. Thus there were 1.5 samples per 10 meter interval; 3 samples per 20 meter interval; and 4 samples per 30 meter interval. It can be seen that as the intervals get larger and the number of conductivity determinations per interval increases, the interval heat flow becomes more consistent. The averages of the

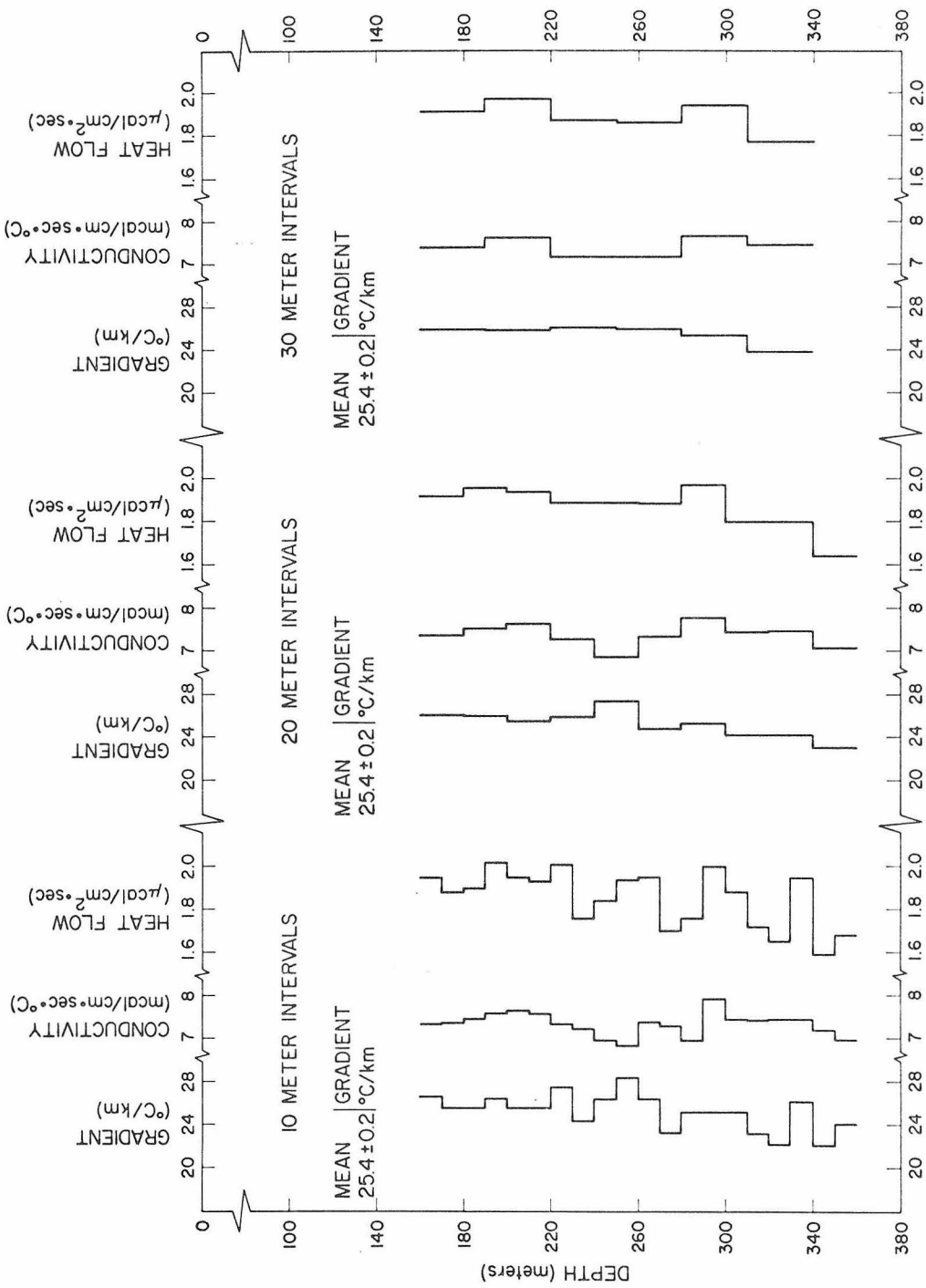

AN-I ANZA, CALIFORNIA INTERVAL HEAT FLOW

Figure 12

interval heat flows from the 10, 20, and 30 meter intervals are 1.85, 1.86, and 1.89 HFU, respectively. The value for the 30 meter intervals is slightly larger because the last interval stops short of the bottom part of the hole where the gradient decreases slightly and is apparently (from the measurements made) not entirely compensated for by the conductivity in that region.

The post-drilling temperature equilibration of AN-3 was studied from the four loggings made one week, one month, six months, and one year after drilling was completed to investigate the "age" time of a newly drilled hole. The results of the temperature measurements and gradients for each of the loggings is shown in Figure 13. The problem of drill hole equilibration was first discussed by Bullard (1947) and has more recently been considered in detail by Lachenbruch and Brewer (1959) and also Jaeger (1961); it is based on the theory of line sources. We will consider here only the basic aspects.

We have for the temperature disturbance v(t) in a medium of diffusivity $\varkappa$ due to an instantaneous line source of strength Q released at time $t = \tau$ along the z axis (Carslaw and Jaeger, 1959, p. 258)

$$v(t) = \frac{Q}{4\pi\varkappa(t-\tau)} e^{-(x^2+y^2)/4\varkappa t}, \qquad t > \tau \tag{13}$$

Now we have that the quantity of heat liberated per unit length of the line is $q = Q\rho c$, where ρ and c are the density and specific heat capacity, respectively, of the medium. Thus (13) can be written

$$v(t) = \frac{q}{4\pi k(t-\tau)} e^{-(x^2+y^2)/4\varkappa t}, \qquad t > \tau$$

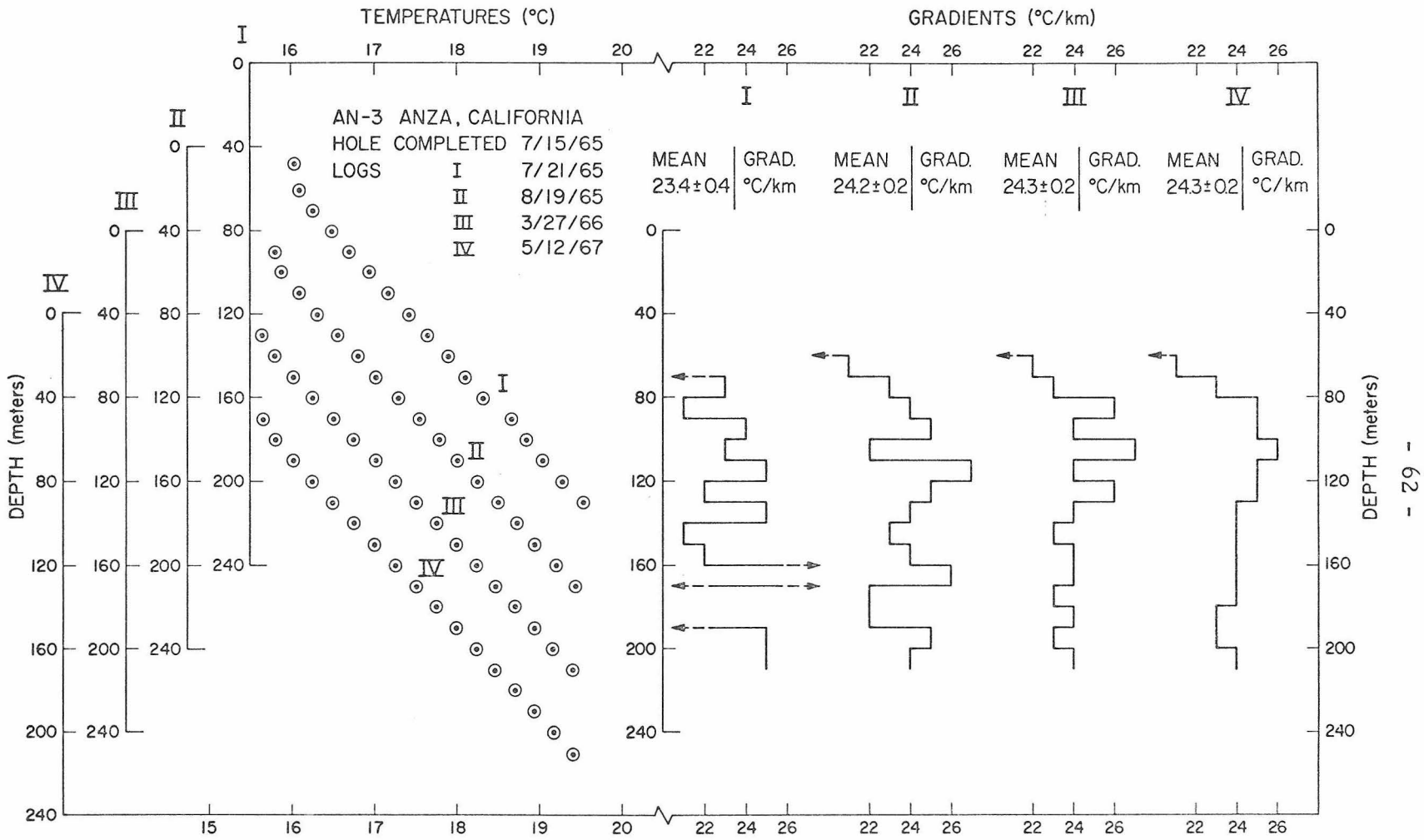
TEMPERATURES (°C)
GRADIENTS (°C/km)
AN-3 ANZA, CALIFORNIA
HOLE COMPLETED 7/15/65
LOGS I 7/21/65
II 8/19/65
III 3/27/66
IV 5/12/67
MEAN 23.4±0.4 GRAD. °C/km
MEAN 24.2±0.2 GRAD. °C/km
MEAN 24.3±0.2 GRAD. °C/km
MEAN 24.3±0.2 GRAD. °C/km
DEPTH (meters)

Figure 13

since $\varkappa = \frac{k}{\rho c}$, where k is the thermal conductivity. Now if we want to know the temperature near the line source we let

$$x \to 0$$

$$y \to 0$$

and thus

$$e^{-(x^2+y^2)/4\varkappa t} \to 1$$

We then have the axial temperature due to an instantaneous line source given by

$$v(t) = \frac{q}{4\pi k(t-\tau)} \tag{14}$$

Next we need to know the axial temperature V(t), due to a continuous line source of q(t) units of heat per unit time per unit length which persisted from time t = 0 to t = s; this is gotten by integration of (14) with respect to τ for $0 < \tau < s$, and holds for times $t \geq s$; assuming $q(t) = \overline{q}$ (a constant), we have

$$V(t) = \frac{\overline{q}}{4\pi k} \int_0^s \frac{1}{(t-\tau)} d\tau, \qquad t \geq s$$

$$= \frac{\overline{q}}{4\pi k} \ell n \frac{t}{t-s}, \qquad t \geq s \tag{15}$$

Equation (15) can be thought of as representing the cooling of a well in which the drilling operation acted as a constant linear source persisting throughout the time of drilling ($0 < t < s$), and where t is the time elapsed since the drill bit first reached the depth in question. In general, the time interval ($0 < t < s$) is different for each depth and represents the time elapsed from the moment the drill bit reached

the depth in question to the moment drilling ceased. Obviously the interval is a maximum for zero depth and goes to zero when the bottom of the hole is under consideration. It should be noted here that we could have assumed a time dependent source strength q(t). Lachenbruch and Brewer (1959) consider cases

$$q(t) \propto \frac{1}{t^{1/n}}, \qquad n = \text{some integer}$$

and conclude that the errors introduced by assuming q = constant are small when compared to some reasonable time varying cases. Furthermore variations in the source strength with depth in a homogeneous medium can probably be neglected if they obey the reasonable functional form

$$q(z) = \overline{q}_z + f(z - z')$$

for several tens of meters above and below the point in question. It must be remarked that "homogeneous" here means the thermal properties are truly uniform or they vary sufficiently rapidly (over very small depth intervals) such that their effects would average out after the passage of sufficient time, and that thereafter the medium would cool as if uniform throughout, with thermal properties intermediate between those of the extremes. Lachenbruch and Brewer also suggest that errors due to neglecting the finite radius of the hole and the presence of the surface at depths greater than 60 meters will likewise be negligible.

Now equation (15) represents the drilling disturbance. We can write

$$V(t) = \Theta(t) - \Theta(0)$$

where $\Theta(t)$ is the temperature with the drilling disturbance and $\Theta(0)$ is the undisturbed temperature. Thus (15) becomes

$$\Theta(t) = \Theta(0) + \frac{\overline{q}}{4\pi k} \ell n \frac{t}{t-s}, \qquad t \geq s \qquad (16)$$

A plot of $\ell n \frac{t}{t-s}$ versus $\Theta(t)$ for a particular depth gives a straight line of slope $\frac{\overline{q}}{4\pi k}$ and intercept $\Theta(0)$, and hole temperatures from a series of loggings at different times when plotted in this way will yield the undisturbed temperatures. One can then reconstruct the undisturbed temperature with depth profile.

In practice, newly drilled holes are usually left to "age" for a period of time until the drilling effects become negligible. Loggings at times $\approx$10s and greater were found by Lachenbruch and Brewer to yield temperatures which were in good agreement with the extrapolated (to infinite time) values. For a normal 1000 foot hole, 10s is commonly about six months to a year for near surface depths.

It should be pointed out that s represents in theory only actual drilling time, that is the length of time the source was "turned on", and not simply the time the drill rig is at the site. In most instances drilling time is contained in either one or two eight-hour shifts per day. In such cases, equation (16) has to be modified to allow for the turning on and off of the source. To do this, we consider for a particular depth, times, t_1, $t_2 \ldots t_n$ and s_1, $s_2 \ldots s_n$; the t's corresponding to the times from the starts of different drilling shifts (once the given depth has been reached) to the time of measurement; and the

s's representing the lengths of each shift, the n^{th} shift being the completion of the hole. We then have temperature disturbances v_1, $v_2 \ldots v_n$ due to each shift at the time of measurement given by (assuming $\bar{q}$ remains constant)

$$v_1 = \frac{q}{4\pi k} \ell n \left(\frac{t_1}{t_1 - s_1} \right)$$

$$v_2 = \frac{q}{4\pi k} \ell n \left(\frac{t_2}{t_2 - s_2} \right)$$

$$\vdots \qquad \vdots$$

$$v_n = \frac{q}{4\pi k} \ell n \left(\frac{t_n}{t_n - s_n} \right)$$

or the total disturbance V is given by

$$V = v_1 + v_2 + \ldots + v_n = \frac{q}{4\pi k} \left[\ell n \left(\frac{t_1}{t_1 - s_1} \right) + \ell n \left(\frac{t_2}{t_2 - s_2} \right) + \ldots + \ell n \left(\frac{t_n}{t_n - s_n} \right) \right]$$

or

$$V(t) = \frac{q}{4\pi k} \ell n \left[\frac{t_1 t_2 \ldots t_n}{(t_1 - s_1)(t_2 - s_2) \ldots (t_n - s_n)} \right] \tag{17}$$

where

$$t_j = t - \sum_{i=0}^{j=1} s_i - \sum_{i=0}^{j=1} p_i , \qquad s_o = p_o = 0$$

s_i being the i^{th} drilling shift time interval as indicated before, and p_i the time interval between the end of the i^{th} shift and the start of the $i + 1^{st}$ shift, t being the same as originally defined. Writing 17 in the same way as (16) we have

$$\Theta(t) = \Theta(0) + \frac{q}{4\pi k} \ell n \left[\frac{t_1 t_2 \ldots t_n}{(t_1 - s_1)(t_2 - s_2) \ldots (t_n - s_n)} \right] \tag{18}$$

If we now plot $\ell n[\ ]$ versus $\Theta(t)$ as before, the intercept again yields the undisturbed temperature $\Theta(0)$.

Jaeger (1961) has analyzed the effect of drilling fluids on drill hole temperature gradients in terms of a counterflow heat exchanger. He concludes that for normal diamond core fluid circulation rates, the temperature of the fluid accommodates itself to the rock temperature so that little heat exchange can take place except near the top and bottom of the hole; and thus the gradient in the central portion of the hole remains relatively undisturbed. Thus Jaeger suggests that gradients determined only hours after completion of drilling will be within perhaps 5% of the undisturbed gradient. His analysis, however, depends upon having an ideal hole with uniform lithology and complete water return. More often than not, a large percentage of the drilling fluid is lost into fractures in the formation which is being drilled. Good agreement with this theory was found for the case of a drill hole in Australia (Jaeger, 1961).

Returning to Figure 13, the first two logs were made with the same probe, while the third and fourth were made with two different ones. The absolute temperature calibrations were different for the various probes, and so they were normalized to the bottom hole temperature of AN-2. They could not be normalized to the bottom hole temperature of AN-3 since the last 30 meters in AN-3 were lost during cementing after drilling. The 210 meter point in Figure 13 does not then represent a bottom hole temperature and is seen to be equilibrating with time as the temperatures at shallower depths although,

as is to be expected, more slowly. It is quite clear that the gradient smoothes out considerably with time although the magnitude of the average gradient, as determined by a least-squares fit to the temperature-depth points, is not significantly different a year later from that measured one week after drilling. The change is seen to be only about 5%. Lachenbruch and Brewer found a similar behavior for the gradient in their hole. Although we do not have measurements in AN-3 a matter of hours after completion of drilling, it is interesting to note that the small absolute change in gradient from one week to one year later is in agreement with the results of Jaeger (1961). The raggedness in the gradient for early times is probably due to a combination of changes in drilling rates, changes in thermal properties with depth, and fracture zones. Of course, if any one of these factors are dominant in a hole (such as water loss into fractures), Jaeger's theory breaks down.

Figures 14 and 15 show the application of equations (16) and (18) to the temperature equilibration at the 50 meter and 150 meter depths of AN-3. Only the temperature values one week and one month after completion of drilling have been plotted. Essentially no change is observed between the six-month and one-year logs, and thus these temperatures are assumed to represent the equilibrium temperatures. It can be seen that the intercepts for both equations predict the equilibrium temperatures to within the limits of error. We recall that the difference between the two equations is that (16) does not allow for the "turning off" of the source while (18) does. The implication is then

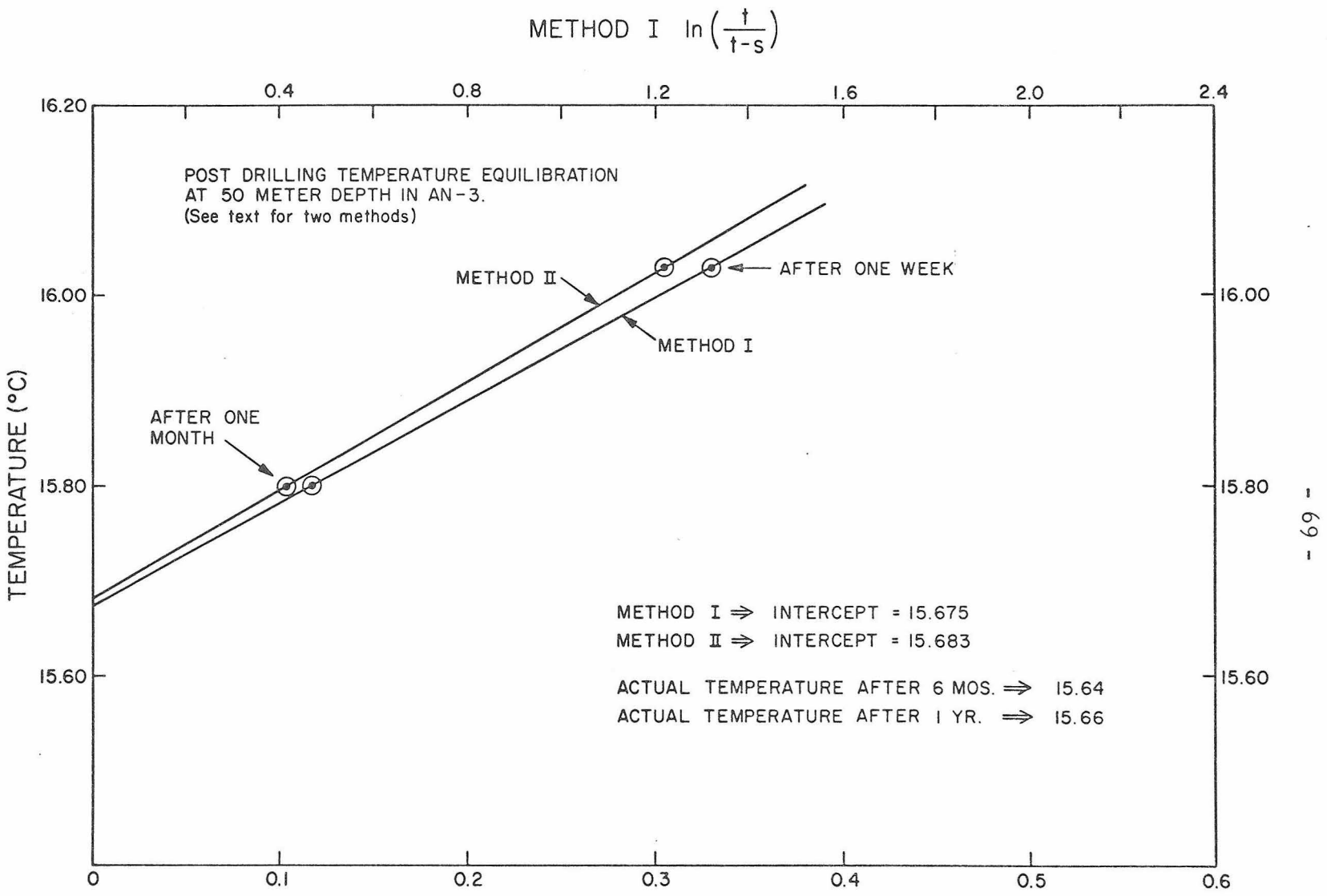

Figure 14 METHOD II $\ln\left[\frac{t_1\ t_2 \cdots\cdots t_n}{(t_1 - s_1)(t_2 - s_2)\cdots(t_n - s_n)}\right]$

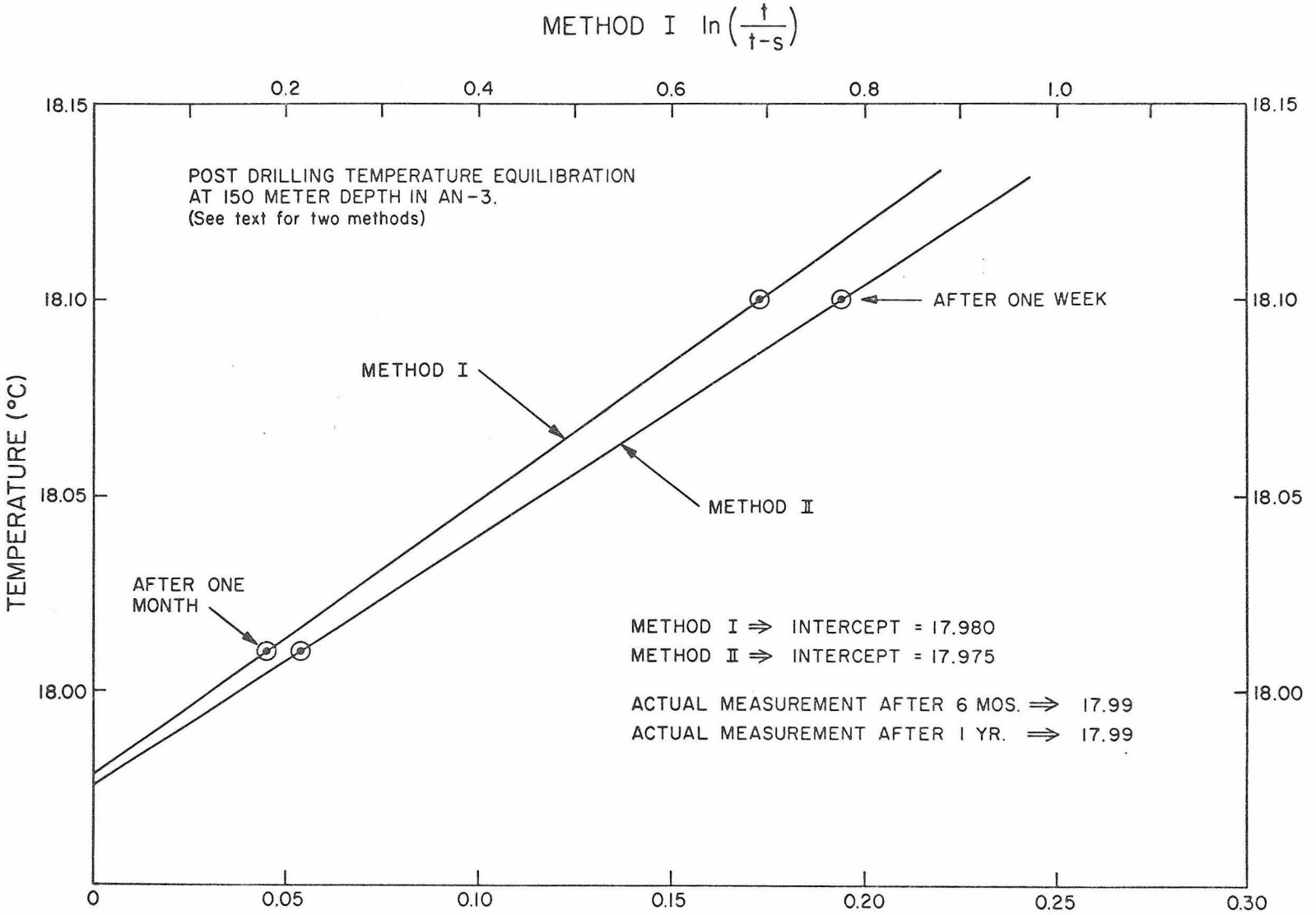

Figure 15 METHOD II $\ln\left[\frac{t_1\ t_2 \cdots\cdots t_n}{(t_1 - s_1)(t_2 - s_2)\cdots(t_n - s_n)}\right]$

that equation (16) can probably be used for times $t \geq ns$, where n is the number of drilling shifts, and the effect of neglecting the times between drilling shifts will yield an effectively lower source strength as given by the slope of the equilibration curve, while preserving the correct intercept or equilibrium temperature. For times $t < ns$, however, the effect of the non-continuous source may begin to show up and only equation (18) would be applicable.

Final loggings of all holes in this study were made at least one year after drilling was completed. In no cases did actual drilling time exceed one month.

Heat flow values based on an assumed topographic evolution, as suggested by the general physiographic history of the Peninsular Range Province, are also presented in Tables 4 to 6 . Physiographically, the three holes near Anza are located on the periphery of the broad Anza surface (Jahns, 1954, p. 48), AN-1 and AN-3 to the east and AN-2 to the west. This surface, as indicated before, is characteristic of the interior highland portion of the Peninsular Ranges. These surfaces are developed on crystalline terrane and generally contain discontinuous yet locally thick mantles of soil and weathered rock. Their evolution in relation to the evolution of the entire province has been interpreted in several different ways (Miller, 1935; Sauer, 1929; Dudley, 1935). Miller believes these surfaces (adjacent ones often being at quite different mean elevations) represent the dislocation of a regional peneplain by block faulting during Quaternary time. Thus little or no erosion would be necessary to explain the

present configuration. However, Miller would suggest as much as 1.1 - 1.2 km of uplift (mean elevation) at Anza in the last m.y.

Sauer argues that these typical surfaces of low relief and different (from surface to surface) mean elevation reflect a pattern of individual formation and differential erosion occurring throughout the history of topographic evolution. One might suppose that adjacent surfaces, such as the Anza and Hemet surfaces, which differ in mean elevation by about 400 feet, might have once been coplanar, but stronger erosion on the Anza surface has lowered it with respect to the Hemet surface. An equally plausible explanation, in this case, for the discordance of these surfaces, might be dip-slip motion on the San Jacinto fault. Thus evolution of these surfaces would follow the general evolution of the Peninsular Range Province.

Dudley suggests that these surfaces can be explained by erosion producing one surface, with subsequent burial of this surface, and the formation of a second surface at a higher elevation determined by the depth of burial of the first surface; then with renewed or continued uplift, we would have the first surface exhumed. This mechanism would suggest that in some instances a couple hundred meters of debris might have been removed from these surfaces, as well as the removal of the original material to produce the surface initially.

Larsen (1941), correlating surfaces of similar elevation throughout the Peninsular Ranges, says there is no reason to believe that lower surfaces are older than higher ones and have been exhumed at a later date, but rather these surfaces represent periods of

quiescence during the regional uplift (beginning say with the onset of the Pliocene) of a buried sunken crystalline surface of high relief yet low mean elevation; subsequent deposition then partially buried these surfaces. Again, this theory would involve the stripping of perhaps a couple of hundred meters of debris, plus the initial erosion to form the surface -- another couple of hundred meters.

We might consider for a moment possible evidence of more recent uplift and erosion in the Peninsular Ranges. Marine terraces of Late Pleistocene are reported (Jahns, 1954) to lie at elevations of about 400 meters above sea level in southern California and as high as 600 meters in Baja California. Large sections on non-marine Pleistocene silts, sands, and clastics (Bautista Beds) are extensively exposed throughout the northern part of the batholith; there has been subsequent stripping and eroding of these deposits as well (Sharp, 1965). Finally, terminated, altered, rejuvenated, and superposed stream courses are also prevalent in parts of the batholith. It is likely that many of these phenomena reflect the shuffling of fault blocks past one another, rather than a general period of uplift and rapid erosion; however, we cannot rule out this possibility.

On the basis of the foregoing discussion, we might suggest the following generalized physiographic history of the Anza region. During mid-Cretaceous time (120-100 m.y. ago) magmatic intrusions invaded the metamorphic complex, perhaps at a depth of 10 km or so, (see Bateman and Wharhaftig, 1966, concerning the Sierra Nevada) in the Peninsular Range region. Regional uplift began and continued into

upper-Cretaceous time, forming a region of relatively great relief. This was the period of unroofing of the batholith; significant erosion took place during this time and during the remainder of the upper-Cretaceous. The first sediments to be laid down on the crystalline basement were upper-Cretaceous; so that by Tertiary time (60 m.y. ago) the area had been reduced to a region of generally low relief with perhaps isolated monadnocks of more resistant lithology having elevations of several thousand feet above the surrounding country. The region was probably relatively stable during Early Tertiary time (60 m.y. to 36 m.y.) with continuing minor erosion and deposition. The period from the end of the Eocene to mid-Miocene (36 m.y. to 16 m.y.) was probably a period of gradual emergence of the region from below sea level. During upper-Miocene and Early Pliocene, the region became involved in the general orogeny which affected all of coastal California at this time. Dibblee (1954) has found continuous sedimentation from mid-Miocene to Recent in the adjacent Imperial Valley Province. General uplift about a coastal hinge line was concurrent with the onset of normal and lateral faulting. The region was broken into a number of positive blocks, regionally coupled, yet each capable of independent development. Part of one block which might be a depositional environment for debris from an adjacent block at one time, might later be a positive feature with respect to the same or another block. Thus physiographic features on any one block are a result of the history of that block. The major surface on any one block might represent the original regional erosion surface, while the

secondary surfaces represent the subsequent history of that block. Uplift continued through the Pleistocene, at which time it may have been accelerated, and is probably occurring at present. Strike-slip and normal faulting has occurred through recent time.

Extreme erosion has probably been confined to the steep fault scarps, as for example, the eastern escarpment and the interior rift valleys. The crystalline configuration of the major erosion surfaces has probably changed very little; periodic stripping and deposition of alluvial type sedimentation has occurred on these surfaces. Minor erosion surfaces, such as Table Mountain near Anza, may have been formed when sedimentation covered the Anza surface with a thickness of several hundred feet of debris. Minor erosion on the Anza surface would explain the deep weathering of the rocks in this area as discussed previously.

For the purposes of making a time-dependent terrain correction, we might now propose the following summary for the geologic and physiographic history in the Peninsular Ranges:

1) 120 m.y.-100 m.y.	Intrusion of batholith
2) 100 m.y.-60 m.y.	Up to 10 km of uplift and erosion; formation of peneplainal surface
3) 60 m.y. - 36 m.y.	Stable platform; continued minor erosion and deposition
4) 36 m.y. - 16 m.y.	Gradual emergence
5) 16 m.y. - Recent	Uplift to present level (uplift at Anza = 1.3 km, mean elevation; erosion = 0.1 km)

We will consider briefly the effects of 1) and 2) on the heat flow. The subject has been discussed by other people (see Larsen, 1945; Jaeger, 1964). It is obvious we can only make very general statements regarding the nature of the intrusion and the amount of material that had to be eroded to unroof the batholith. These same problems exist for all of the western United States, and so no matter in what pluton the heat flow is measured, essentially the same effects might be present and, therefore, constitute an additive constant to the heat flow throughout the western United States.

From before, we have assumed that the unroofing of the batholith (stripping of 10 km) occurred between perhaps 100 m.y. and 60 m.y. (unroofing or uplift could have started with the first intrusions, 120 m.y. ago). Under the assumption that this uplift and erosion progressed at approximately a constant rate, we might approximate its effect, for theoretical considerations, by a step function in time at 80 m.y. ago. If we consider an infinite half space of diffusivity $\varkappa$, this is equivalent to decreasing the surface temperature by αz_o where α is the geothermal grandient and z_o is the thickness of material eroded (10 km). The solution for the temperature v at a later time t is given by (Carslaw and Jaeger, 1959, p. 61)

$$v = \alpha z_o \operatorname{erf} \frac{z}{2\sqrt{\varkappa t}} + \alpha z$$

or the gradient at a later time would be given by

$$\frac{dv}{dz} = \frac{\alpha z_o}{\sqrt{\pi \varkappa t}} e^{-z^2/4\varkappa t} + \alpha$$

and the disturbance in the gradient at the surface would then be

$$\Delta \frac{dv}{dz}\Big|_{z=o} = \frac{\alpha z_o}{\sqrt{\pi \varkappa t}}$$

Putting α = 25°C/km, z_o = 10 km, $\varkappa \simeq 0.015$ c.g.s. units, and t = 80 m.y., we get

$$\Delta \frac{dv}{dz}\Big|_{z=o} \simeq 2.3°C/km$$

or a 10% effect. If we had put the step function change 100 m.y. ago, we would have gotten

$$\Delta \frac{dv}{dz}\Big|_{z=o} \simeq 2.0°C/km \qquad (19)$$

essentially the same; but if we had assumed the erosion occurred at a constant rate from t = 0 (100 m.y. ago) to present, the effect would be just twice that given by (19), namely 4.0°C/km (Birch, 1950, p.587). The cooling of the batholith can be approximated by the cooling of an infinitely long horizontal rectangular parallelepiped with initial temperature V_o in an infinite medium at zero initial temperature with the plane x = 0 kept at zero degrees.

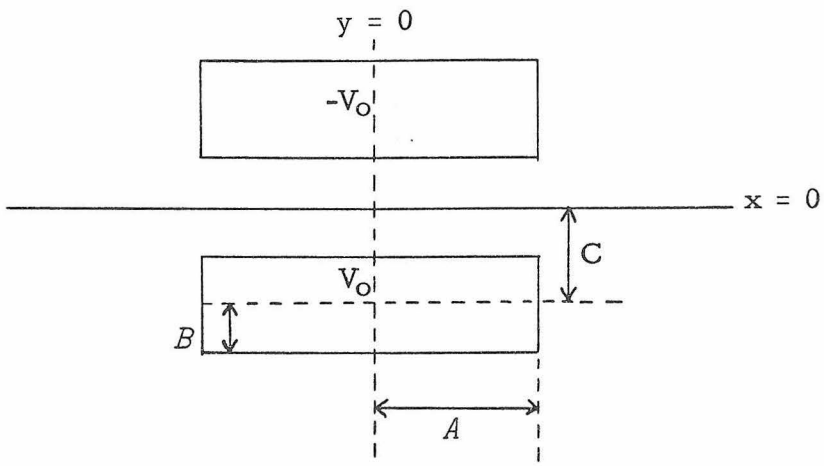

Figure 16

The plane x = 0 is kept at zero degrees by means of an image source of initial temperature $-V_o$ of similar geometry an equal distance away from the boundary in the direction $x < 0$. If we use the notation given in Figure 16, the temperature v at some later time is given by (Carslaw and Jaeger, 1959, p. 56)

$$v = \frac{V_o}{4\pi\varkappa t} \int_{C-B}^{C+B} \exp\left[\frac{-(x-x')^2}{4\varkappa t}\right] dx' \int_{-A}^{A} \exp\left[\frac{-(y-y')^2}{4\varkappa t}\right] dy'$$

$$- \frac{V_o}{4\pi\varkappa t} \int_{-(C+B)}^{-(C-B)} \exp\left[\frac{-(x-x')^2}{4\varkappa t}\right] dx' \int_{-A}^{A} \exp\left[\frac{-(y-y')^2}{4\varkappa t}\right] dy'$$

the solution of which is given by

$$v = \frac{V_o}{4} \left\{\operatorname{erf}\frac{A-y}{\sqrt{4\varkappa t}} + \operatorname{erf}\frac{A+y}{\sqrt{4\varkappa t}}\right\} \left\{\operatorname{erf}\frac{B+C-x}{\sqrt{4\varkappa t}} + \operatorname{erf}\frac{B-C+x}{\sqrt{4\varkappa t}}\right.$$

$$\left. - \operatorname{erf}\frac{B-C-x}{\sqrt{4\varkappa t}} - \operatorname{erf}\frac{B+C+x}{\sqrt{4\varkappa t}}\right\}$$

where $\varkappa$ is the thermal diffusivity and $\operatorname{erf}\xi = 2\pi^{-1/2} \int_o^{\xi} \exp(-x^2) dx$.

The gradient at x = 0, y = 0 is given by

$$\left.\frac{dv}{dx}\right|_{\substack{x=o \\ y=o}} = \frac{V_o}{\sqrt{\pi\varkappa t}} \operatorname{erf}\frac{A}{\sqrt{4\varkappa t}} \left\{\exp\left[-\left(\frac{B-C}{\sqrt{4\varkappa t}}\right)\right] - \exp\left[-\left(\frac{B+C}{\sqrt{4\varkappa t}}\right)\right]\right\} \qquad (20)$$

If we want to approximate the batholith by an infinite sheet, we let $A \to \infty$ and $\operatorname{erf}\frac{A}{\sqrt{4\varkappa t}} \to \operatorname{erf}\infty \to 1$. To include the effect of the latent heat of crystallization, we would set $V_o' = V_o + L/c$ where L is the latent heat and c the heat capacity. If we consider the batholith to have been a tabular body 100 km wide, 20 km thick and buried 10 km while it was cooling, and at an initial temperature of 500°C above ambient, we

would have from Figure 16

$$A = 50 \text{ km}$$

$$B = 10 \text{ km}$$

$$C = 20 \text{ km}$$

and from (20), the residual gradient after 100 m.y.

$$\frac{dv}{dx}\Big|_{\substack{x=o \\ y=o}} \simeq 0.4°C/km \qquad (21)$$

Had we considered the batholith to be an infinite sheet, we would have gotten

$$\frac{dv}{dx}\Big|_{\substack{x=o \\ y=o}} \simeq 1.1°C/km \qquad (22)$$

If the batholith had been closer to the surface or was being unroofed during the time it was cooling, the residual gradients, (21) and (22), would be still smaller. Only if the batholith were considerably thicker or the initial temperature above ambient higher, which seems unlikely from present geological and geophysical evidence, would we have expected an appreciable residual gradient after 100 m.y.

On the basis of the foregoing discussion, it is not unreasonable to assume that perhaps 10% of the present geothermal gradient at Anza can be accounted for by unroofing of the southern California batholith during Cretaceous time.

Returning to our summary of the geologic history, we see that from 60 m.y. to 16 m.y. the region was relatively stable. Uplift and erosion commenced about 16 m.y. ago, and the topography we see

today has thus evolved, for the most part, during the last 16 m.y. The corrected gradients and heat flows (topographic evolution) in Tables 4 , 5 , and 6 represent the case for a 16 m.y. topographic evolution with a 1.3 km of uplift and 0.1 km of erosion at each of the drill holes. It can be seen that the heat flow values at Anza, corrected for this model of topographic evolution, do not differ appreciably from the heat flow values determined under the assumption of steady-state topography.

Table 7 also gives, for interest and comparison, the additional cases of 1.5 km of uplift and 0.3 km of erosion; 1.7 km uplift, 0.5 km erosion; and 2.2 km uplift and 1.0 km erosion. These models are given for evolution times of 1, 4, and 9 m.y., in addition to the 16 m.y. case. It is important to note that the topographic correction is much more sensitive to erosion than to uplift since the erosion works against the geothermal gradient α, and uplift, against the atmospheric gradient α' where $\alpha >> \alpha'$. Also, both effects affect the gradient in the same sense -- increasing the observed heat flow.

Corrected Heat Flow for Models of Topographic Evolution at AN-1 for Comparison with Most Probable Model*

	1 m.y.	4 m.y.	9 m.y.	16 m.y.
1.3 km uplift 0.1 km erosion	1.78 HFU	1.82 HFU	1.84 HFU	*1.86 HFU
1.5 km uplift 0.3 km erosion	1.73	1.80	1.82	1.85
1.7 km uplift 0.5 km erosion	1.68	1.77	1.80	1.84
2.2 km uplift 1.0 km erosion	1.56	1.70	1.75	1.82

Table 7

Finally, the effect on the heat flow of an increased rate of erosion and uplift during Pleistocene time, which we alluded to earlier, can be shown to be negligible. If we liberally assume that the Bautista formation covers one-tenth of the outcrop area at an average thickness of 1 km in the Anza area, and further assume that it was stripped off uniformly from the entire region, we would have 0.1 km of erosion at each of the drill sites. If 0.1 km of erosion and 0.3 km of uplift occurred instantaneously one million years ago, the residual gradient would be approximately 0.3°C/km. If it occurred uniformly from then until the present, the figure would be 0.6°C/km, or at most a 2% effect.

C. Heat Flow in the San Bernardino Mountains and near Lucerne Valley, California

Three holes (SB-2, SB-5, and SB-10) drilled by the California State Department of Water Resources for geologic investigation along proposed tunnel alignments were used for the determination of heat flow in the San Bernardino Mountains, just north of San Bernardino, California (see location map, Figure 7). The three holes are located in Cretaceous (?) crystalline gneisses, varying in composition from quartz diorite to quartz monzonite (Bartlett, Calif. State Dept. of Water Resources, 1965), in the eastern portion of the Transverse Range Province 5 km northeast of the San Andreas fault. A single hole, LV-1, drilled by the Southern Pacific Land Company for mineral investigation near Lucerne Valley, California (see Figure 7) was

deepened as part of the San Andreas study and subsequently used for making a heat flow measurement. LV-1 is located about 50 km northeast of SB-2, 5, and 10 in a hornblende diorite of the pre-Tertiary crystalline complex of the Mojave Desert.

Detailed mapping in this part of the San Bernardino Mountains does not exist. The general geology of the Transverse Range Province is described by Bailey and Jahns (1954). Figure 17 shows the relation of SB-2, 5, and 10 to the generalized local geology. The San Bernardino Mountains are the most massive unit of the Transverse Range Province. The Transverse Ranges, so called because they transect the general northwest-southeast structural trend of adjacent provinces, extend in a relatively narrow belt from the western end of the Santa Ynez Mountains at Point Arguello, northwest of Santa Barbara, to the eastern end of the Little San Bernardino Mountains north of Indio and the Imperial Valley. Recent geologic investigations (L. T. Silver, personal communication) suggest that the structural trend of this province may extend considerably farther east, crossing most of southeastern California. The province is dissected by several northwest-southeast trending strike-slip faults, notably the San Gabriel, San Jacinto, and San Andreas. Cross sections, north-south through the eastern portion of the ranges reveal that they are characterized by steep flanks or escarpments on both sides, dropping to a mean elevation in the Mojave Desert to the north of about 3500 feet and to a mean elevation of 0-1000 feet to the south in the Imperial Valley and Los Angeles Basin. Moderately subdued relief

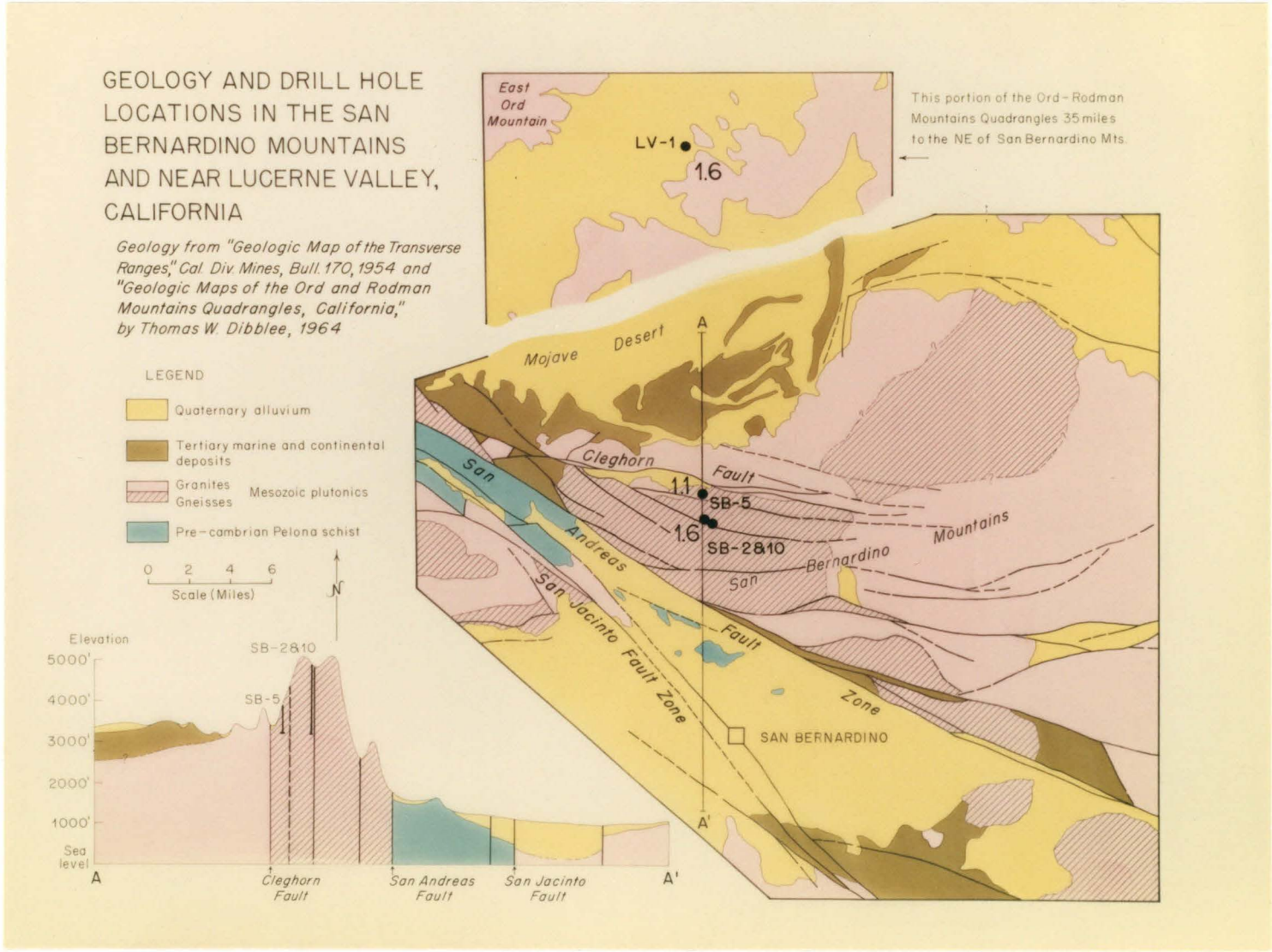
GEOLOGY AND DRILL HOLE LOCATIONS IN THE SAN BERNARDINO MOUNTAINS AND NEAR LUCERNE VALLEY, CALIFORNIA
Geology from "Geologic Map of the Transverse Ranges," Cal. Div. Mines, Bull. 170, 1954 and "Geologic Maps of the Ord and Rodman Mountains Quadrangles, California," by Thomas W. Dibblee, 1964
LEGEND
Quaternary alluvium
Tertiary marine and continental deposits
Granites Gneisses Mesozoic plutonics
Pre-cambrian Pelona schist
0 2 4 6
Scale (Miles)
N
East Ord Mountain
LV-1
1.6
This portion of the Ord-Rodman Mountains Quadrangles 35 miles to the NE of San Bernardino Mts.
Mojave Desert
A
Cleghorn Fault
1.1
SB-5
1.6
SB-2810
San Andreas Fault
San Bernardino Mountains
San Jacinto Fault Zone
SAN BERNARDINO
A'
Elevation
5000'
4000'
3000'
2000'
1000'
Sea level
SB-2810
SB-5
A
Cleghorn Fault
San Andreas Fault
San Jacinto Fault
A'

Figure 17

characterizes the rather limited upland regions.

The Transverse Ranges vary significantly in their bulk lithology, from almost entirely sedimentary terrane at the western end to mostly crystalline at the eastern end. The San Bernardino Mountain unit is composed chiefly of gneisses, schists, plutonics, and a sequence of marbles, quartzites, and carbonates on the northern flank. Exposed over large areas of the San Bernardinos are plutonic rocks whose average composition appears to be in the quartz monzonite range.

The Mojave Desert region is often considered to be the expression of the Basin and Range Province in this part of California; however, it lacks the thick Paleozoic sections and uniform block faulting of more typical Basin and Range regions to the north and east. Geologic mapping in the Mojave region has been done by Dibblee (1964), Hewett (1956), Gardner (1940), Bassett and Kupfer (1964), Bowen (1954), and McCulloh (1954). The regional geology has been outlined by Hewett (1954) and Bassett and Kupfer (1964). The Lucerne Valley area has been mapped by Gardner (1940) and more recently by Dibblee (1964). The name "Mojave Block" is applied to the part of the Mojave region that lies north of the San Andreas fault on the southwest and the San Bernardino Mountains on the southeast, and south of the Garlock fault (see index map, Figure 7). The eastern extent of the block is not as well defined, but might be considered to be along the southern projection of the Death Valley fault system. The block can be further broken into two units, an eastern part and a western part with a boundary at about the Mojave River (Figure 7). The western

part is characterized by an alluvial surface sloping gradually to the east with isolated buttes of Mesozoic plutonic and Tertiary volcanic rocks projecting from beneath the cover. The eastern portion is characterized by more irregular topography with locally great relief. The mountainous masses consist predominately of highly resistant Mesozoic plutonic rocks of average quartz monzonitic composition. Extensive pediment surfaces are common on mountain flanks and often underlie the broad sloping intermontane regions. This part of the Mojave Block contains many closed, playa-covered basins, some containing thick sections of continental Tertiary and Pleistocene sediments. The region is also cut by numerous northwest-southeast trending faults. The Lucerne Valley area lies within this eastern portion.

The San Andreas fault lies along the base of the steep southwestern-facing escarpment of the San Bernardino Mountains. South of the Transverse Ranges the San Andreas splits into several equally large and currently active segments. The regions through which these faults pass are characterized by significant non-seismic activity, i.e. creep (Whitten, 1955), numerous intermediate and small magnitude earthquakes (Allen, St. Amand, Richter, and Nordquist, 1965), and significant micro-earthquake activity (Brune and Allen, 1967); whereas the San Andreas fault proper, on the north side of the Transverse Ranges, is believed to be the source of large magnitude ($\sim$8) earthquakes with apparently no other form of strain energy release occurring along this segment (Allen, et al., 1965).

Temperature profiles for SB-2, 5, and 10 are shown in Figures 18, 20, and 21; summaries of the hole data are given in Tables 8, 9, and 10. The temperature profile and hole summary for LV-1 are given in Figure 22 and Table 11, respectively.

In the case of SB-2, core for thermal conductivity measurements was originally available only for the bottom 30 meters of the hole. (Recently, additional core, covering the bottom 60 meters, was acquired, and conductivity measurements made on this core are included in Appendix VII.) The bottom 30 meters were logged using a 2 meter depth spacing, and the heat flow was calculated from the product of the mean harmonic conductivity and mean gradient in this interval. Figure 19 shows the last 60 meters of temperatures plotted versus an expanded depth scale. SB-2 gives a heat flow of 1.6 HFU.

The lithology in hole SB-5 was similar to that in SB-2. However, it is seen that the heat flow is only 1.2 HFU. This value is probably an erroneous representation of the heat flow at this locality, due most likely to ground water movement. We might briefly examine the evidence for this. First, the drilling reports show that the formation drilled was highly fractured; loss of drilling fluid circulation frequently occurred, and the hole was not grouted. Second, the hole is located on an extremely steep slope, an environment which facilitates ground water movement; the bottom of the hole is still above the base level of the surrounding topography. Third, temperatures were extremely unstable during logging of the hole with drifts of several hundredths of a degree per minute common. Fourth, a large

SB-2 SAN BERNARDINO MTNS., CALIFORNIA

LOCATION and ELEVATION		DRILLING HISTORY	
Latitude	34° 15.0' N	Started	10/15/58
Longitude	117° 19.2' W	Stopped	1/28/59
Collar Elevation	4600 feet	Total Depth	1510 feet
Distance from Fault Trace	5 km	Hole Size	NX-Standard Cased $1\frac{1}{4}$" pipe (perf.)

DEPTH	GEOLOGIC LOG
0 - 1200 feet	Alternating Gneissic Diorite and Quartz Monzonite
1200 - 1305 feet	Hornblende Porphyry
1305 - 1510 feet	Same as 0-1200 ft (extensive fracturing from 1425-1480 ft)

CONDUCTIVITY, GRADIENT, HEAT FLOW, RADIOACTIVITY

Mean Resistivity . . . . . (26)		$164.3 \pm 8.0 \frac{\text{cm} \cdot \text{sec} \cdot °\text{C}}{\text{cal}}$
Mean Harmonic Conductivity		$6.08 \pm 0.3 \frac{\text{mcal}}{\text{cm} \cdot \text{sec} \cdot °\text{C}}$
Uncorrected Gradient . . . . . (430-462 m)		24.56 ± 0.30 °C/km
Corrected Gradient	Steady State	26.85 ± 0.33 °C/km
	Topographic Evolution	26.51 ± 0.33 °C/km
Uncorrected Heat Flow		1.50 ± 0.08 HFU
Corrected Heat Flow	Steady State	1.63 ± 0.08 HFU
	Topographic Evolution	1.61 ± 0.08 HFU
Limit of Topographic Influence		30 km
Radioactive Heat Production		Not determined (see SB-10)

Table 8

SB-5 SAN BERNARDINO MTNS., CALIFORNIA

LOCATION and ELEVATION		DRILLING HISTORY	
Latitude	34° 16.3' N	Started	5 5/4/65
Longitude	117° 19.7' W	Stopped	9/19/65
Collar Elevation	4160 feet	Total Depth	925 feet
Distance from Fault Trace	7 km	Hole Size	NX-Wireline Cased 1" pipe (perf.)

DEPTH	GEOLOGIC LOG
0 - 925 feet	Gneissic Granite (alternating biotite- and orthoclase-rich zones)

CONDUCTIVITY, GRADIENT, HEAT FLOW, RADIOACTIVITY

Mean Resistivity	(16)	$168.2 \pm 10.2 \frac{\text{cm} \cdot \text{sec} \cdot °\text{C}}{\text{cal}}$
Mean Harmonic Conductivity		$5.95 \pm 0.4 \frac{\text{mcal}}{\text{cm} \cdot \text{sec} \cdot °\text{C}}$
Uncorrected Gradient	(200-270 m)	17.66 ± 0.63 °C/km
Corrected Gradient	Steady State	18.20 ± 0.66 °C/km
	Topographic Evolution	----
Uncorrected Heat Flow		1.05 ± 0.10 HFU
Corrected Heat Flow	Steady State	1.08 ± 0.10 HFU
	Topographic Evolution	----
Limit of Topographic Influence		30 km
Radioactive Heat Production		Not determined (see SB-10)

Table 9

SB-10 SAN BERNARDINO MTNS., CALIFORNIA

LOCATION and ELEVATION		DRILLING HISTORY	
Latitude	34° 15.1' N	Started	5/12/65
Longitude	117° 19.7' W	Stopped	10/21/65
Collar Elevation	4760 feet	Total Depth	1700 feet
Distance from Fault Trace	5 km	Hole Size	NX-Wireline Cased 2" pipe (plastic; perf.)

DEPTH	GEOLOGIC LOG
0 - 1700 feet	Alternating Gneissic Quartz Diorite and Quartz Monzonite (fracture zone from 1620 - 1650 feet)

CONDUCTIVITY, GRADIENT, HEAT FLOW, RADIOACTIVITY

Mean Resistivity	(67)	$160.0 \pm 5.0 \frac{\text{cm} \cdot \text{sec} \cdot °\text{C}}{\text{cal}}$
Mean Harmonic Conductivity		$6.25 \pm 0.2 \frac{\text{mcal}}{\text{cm} \cdot \text{sec} \cdot °\text{C}}$
Uncorrected Gradient	(300-440 m)	22.19 ± 0.13 °C/km
Corrected Gradient — Steady State		25.23 ± 0.16 °C/km
Corrected Gradient — Topographic Evolution		24.87 ± 0.15 °C/km
Uncorrected Heat Flow		1.39 ± 0.04 HFU
Corrected Heat Flow — Steady State		1.58 ± 0.05 HFU
Corrected Heat Flow — Topographic Evolution		1.55 ± 0.05 HFU
Limit of Topographic Influence		30 km
Radioactive Heat Production		$3.7 \pm 1.5 \frac{\times 10^{-13} \text{cal}}{\text{cm}^3 \cdot \text{sec}}$

Table 10

LV-1 LUCERNE VALLEY, CALIFORNIA

LOCATION and ELEVATION		DRILLING HISTORY	
Latitude	34° 37.0' N	Started	8/22/60; 5/9/66
Longitude	116° 43.4' W	Stopped	10/28/60; 5/17/66
Collar Elevation	3685 feet	Total Depth	2300 feet
Distance from Fault Trace	50 km	Hole Size	0-500 ft NX-Wireline 500-2300 ft BX-Wireline Cased $1\frac{1}{4}$" pipe

DEPTH	GEOLOGIC LOG
0 - 2900 feet	Core lost (core log indicates diorite)
2000 - 2090 feet	Hornblende Diorite
2090 - 2150 feet	Aphanitic Andesite Dike (chilled margins)
2150 - 2300 feet	Hornblende Diorite

CONDUCTIVITY, GRADIENT, HEAT FLOW, RADIOACTIVITY

Mean Resistivity . . . . . (30)		$173.5 \pm 5.4 \frac{cm \cdot sec \cdot °C}{cal}$
Mean Harmonic Conductivity		$5.77 \pm 0.2 \frac{mcal}{cm \cdot sec \cdot °C}$
Uncorrected Gradient . . . . . (600-700 m)		29.27 ± 0.15 °C/km
Corrected Gradient	Steady State	28.60 ± 0.14 °C/km
	Topographic Evolution	27.38 ± 0.14 °C/km
Uncorrected Heat Flow		1.69 ± 0.05 HFU
Corrected Heat Flow	Steady State	1.65 ± 0.05 HFU
	Topographic Evolution	1.58 ± 0.05 HFU
Limit of Topographic Influence		30 km
Radioactive Heat Production		$2.3 \pm 0.7 \frac{\times 10^{-13} cal}{cm^3 \cdot sec}$

Table 11

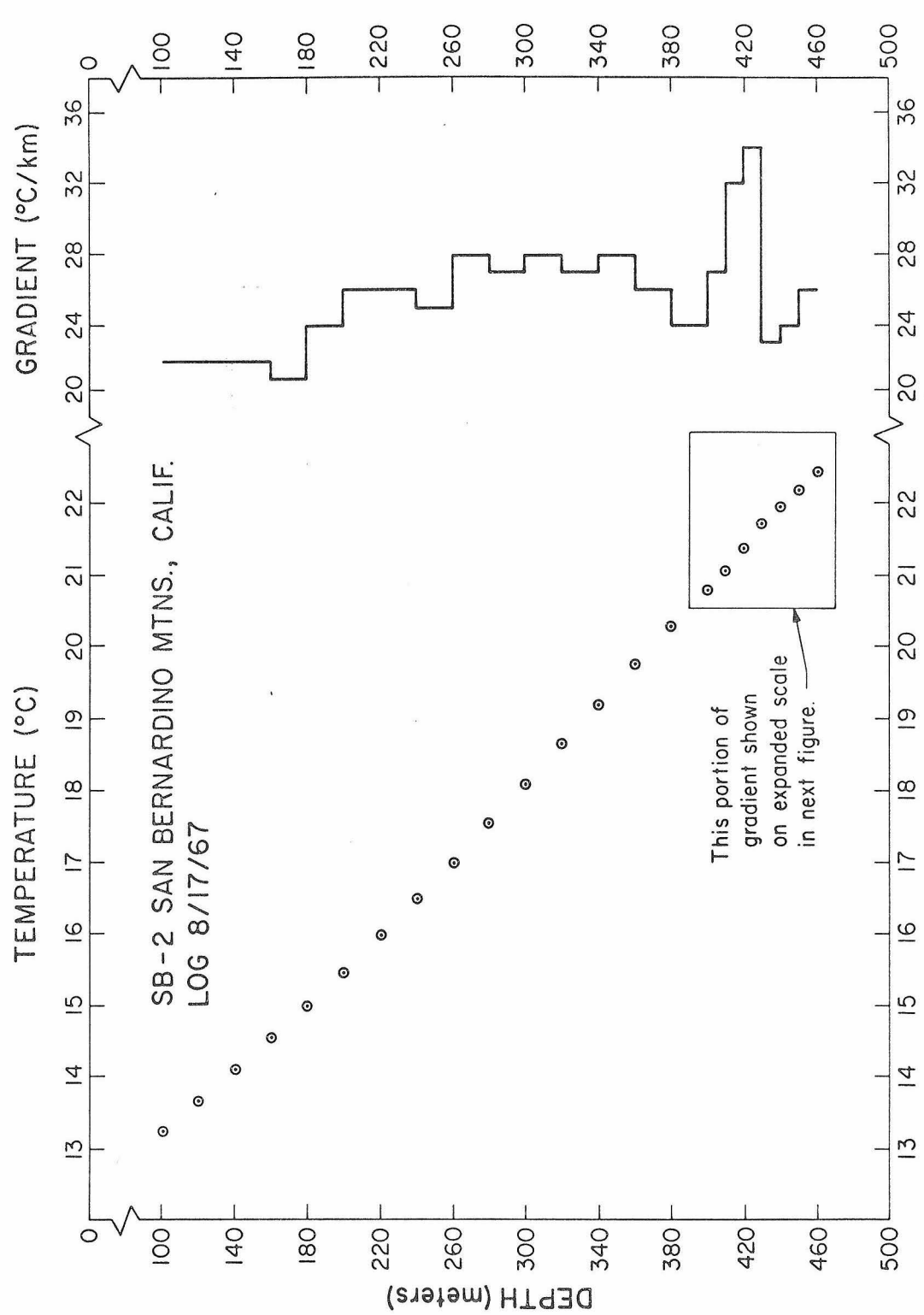
TEMPERATURE (°C)
GRADIENT (°C/km)
DEPTH (meters)
SB-2 SAN BERNARDINO MTNS., CALIF.
LOG 8/17/67
This portion of gradient shown on expanded scale in next figure.

Figure 18

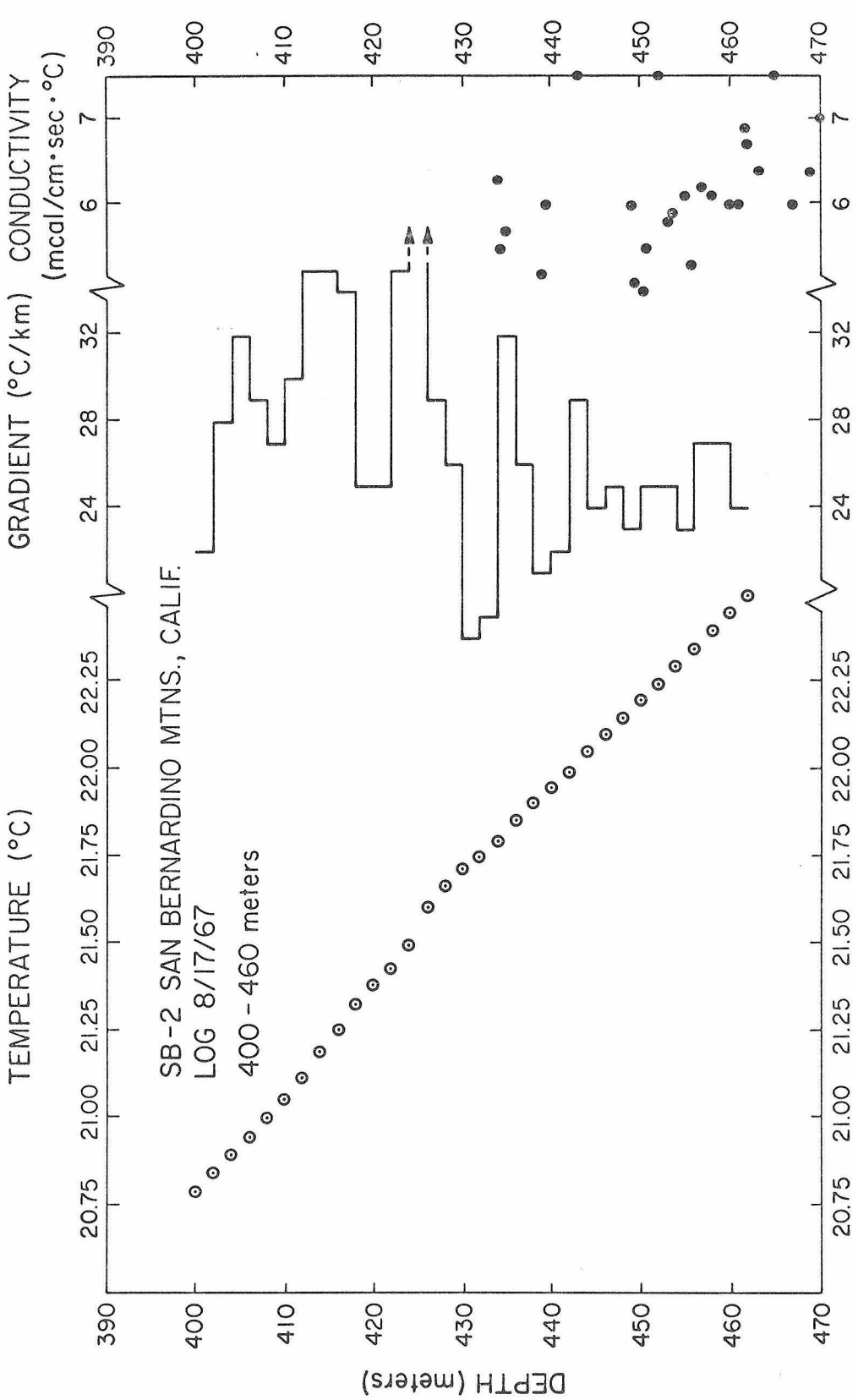
TEMPERATURE (°C)
GRADIENT (°C/km)
CONDUCTIVITY (mcal/cm·sec·°C)
SB-2 SAN BERNARDINO MTNS., CALIF.
LOG 8/17/67
400 - 460 meters
DEPTH (meters)
20.75
21.00
21.25
21.50
21.75
22.00
22.25
24
28
32
6
7
390
400
410
420
430
440
450
460
470

Figure 19

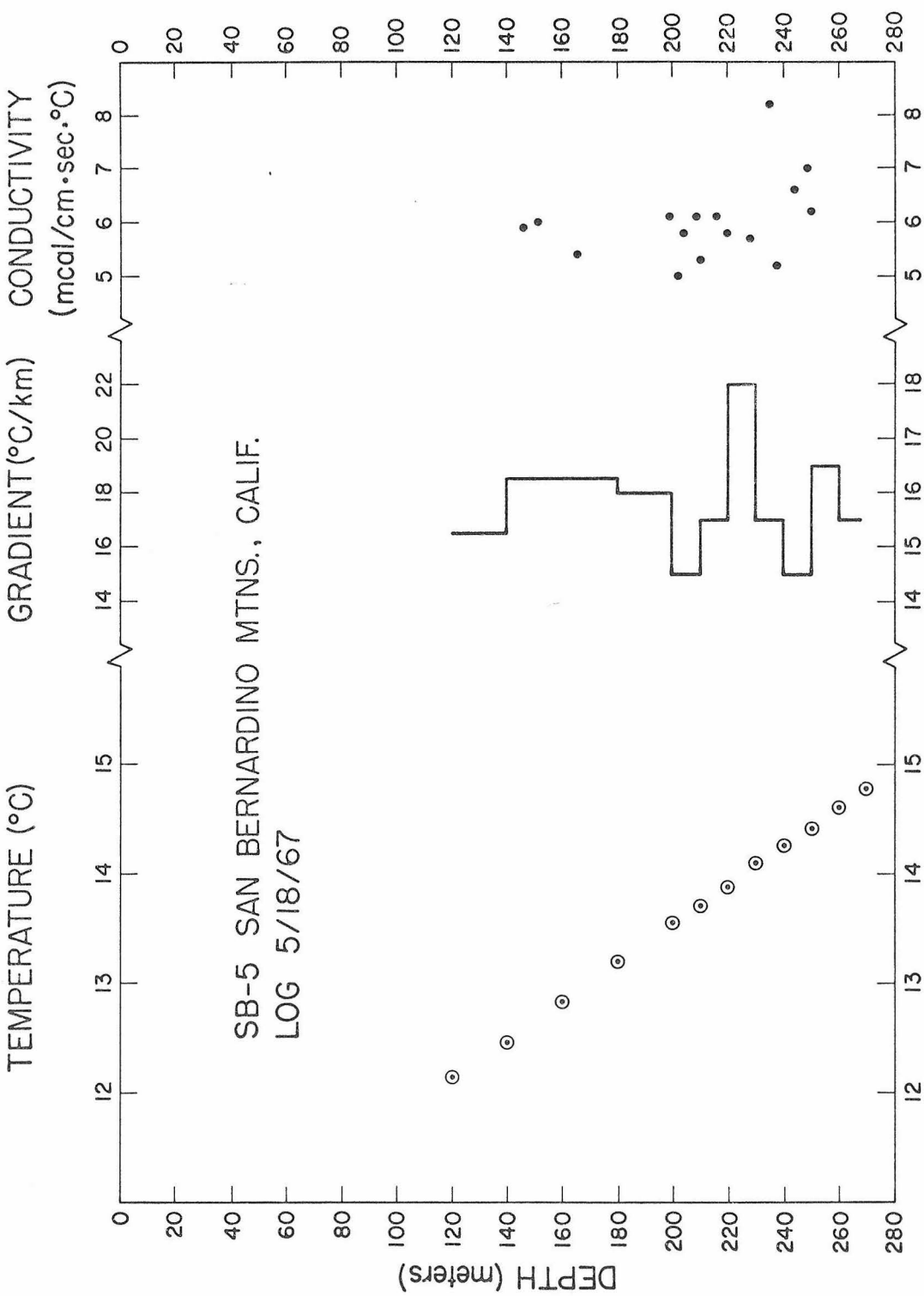
TEMPERATURE (°C)
GRADIENT (°C/km)
CONDUCTIVITY (mcal/cm·sec·°C)
SB-5 SAN BERNARDINO MTNS., CALIF.
LOG 5/18/67
DEPTH (meters)

Figure 20

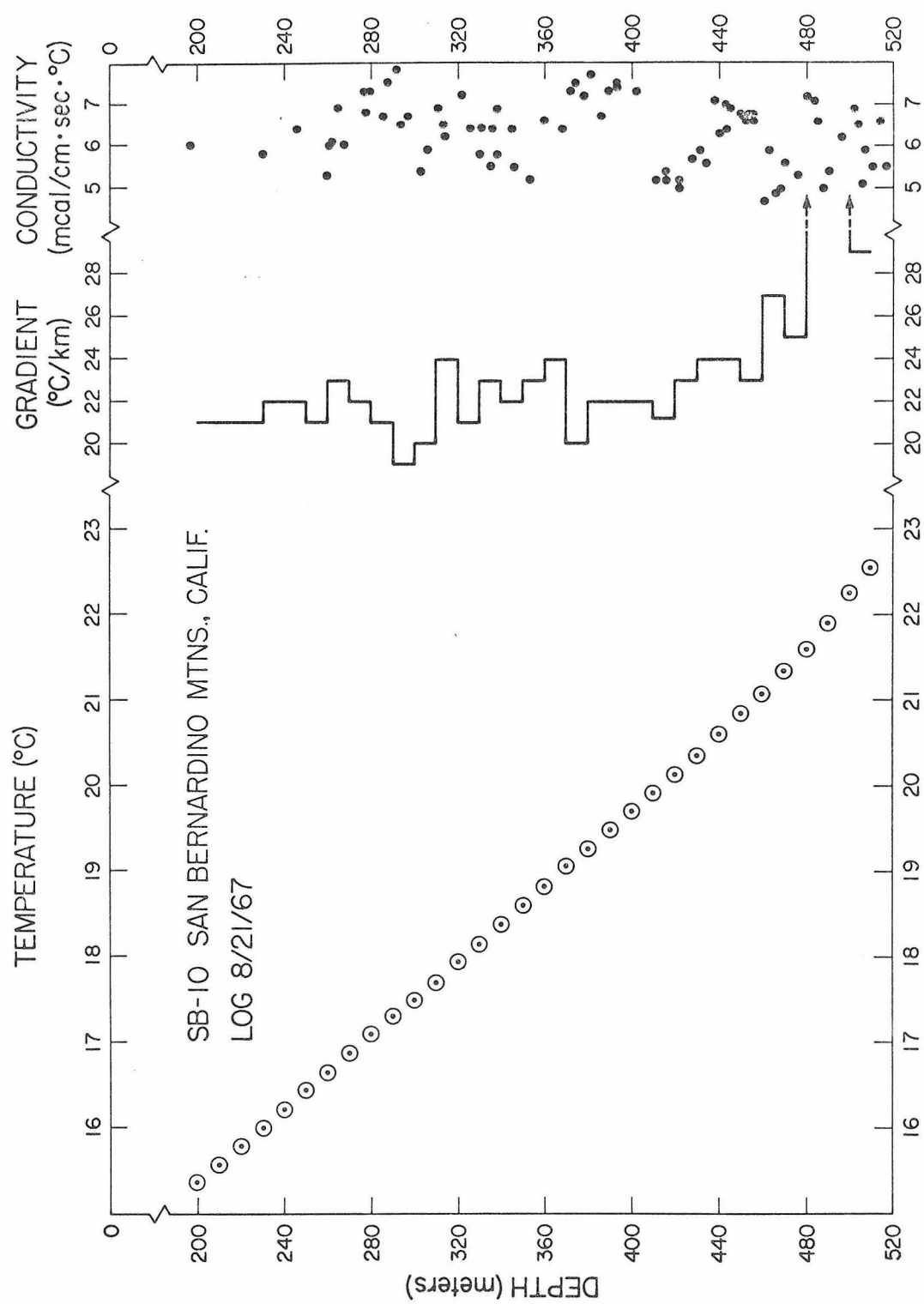
TEMPERATURE (°C)
GRADIENT (°C/km)
CONDUCTIVITY (mcal/cm·sec·°C)
SB-10 SAN BERNARDINO MTNS., CALIF.
LOG 8/21/67
DEPTH (meters)

Figure 21

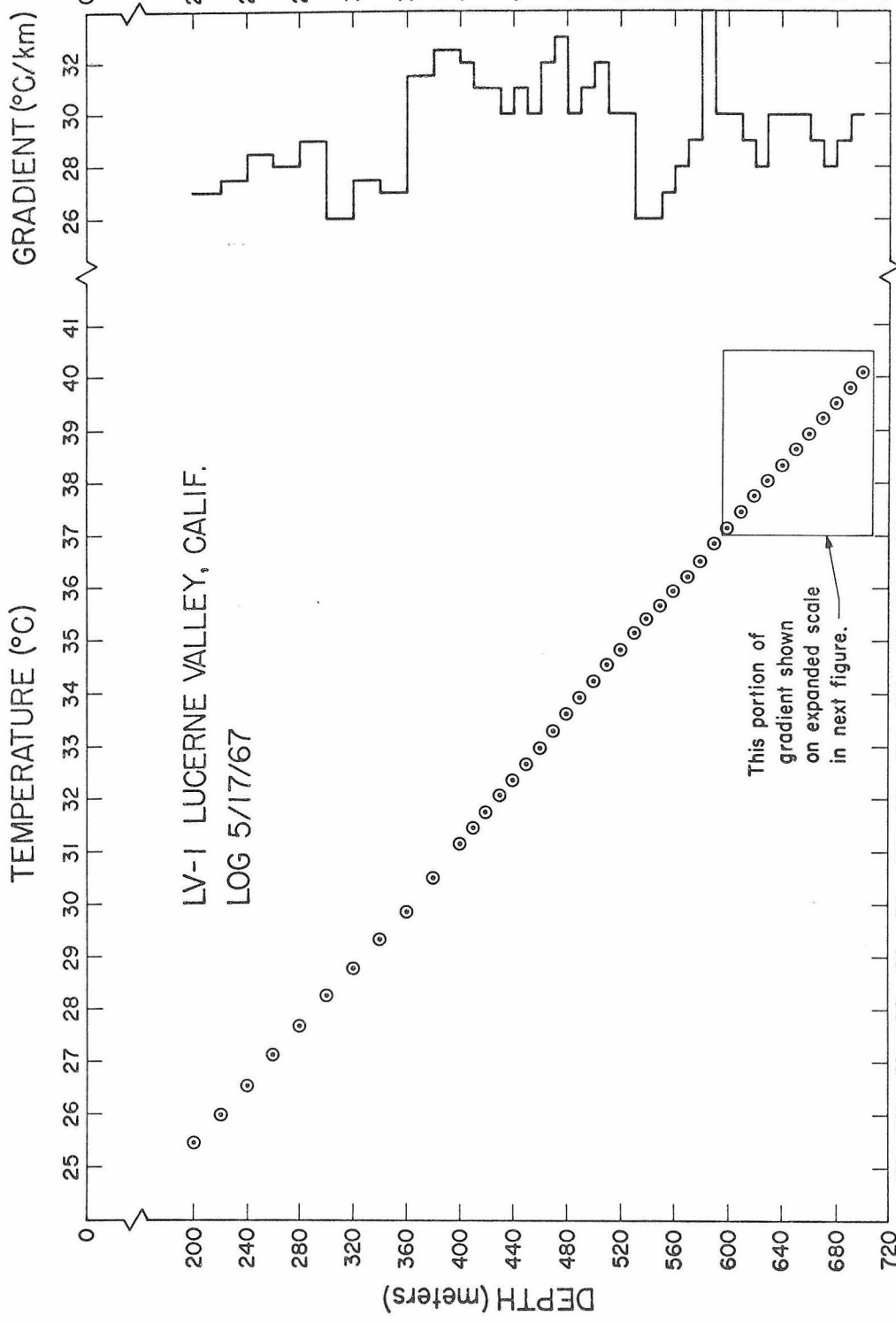
TEMPERATURE (°C)
GRADIENT (°C/km)
DEPTH (meters)
LV-1 LUCERNE VALLEY, CALIF.
LOG 5/17/67
This portion of gradient shown on expanded scale in next figure.

Figure 22

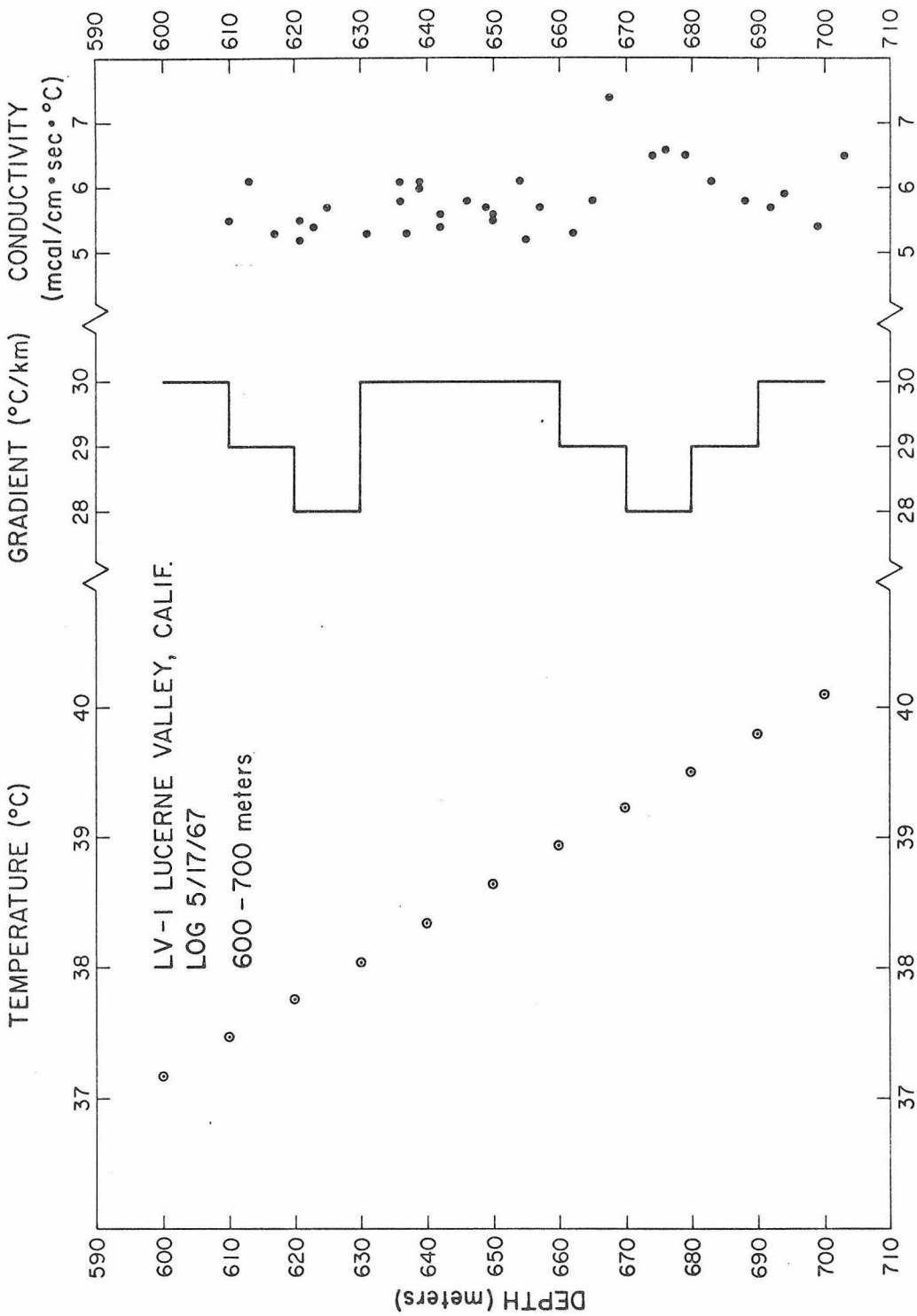
TEMPERATURE (°C)
GRADIENT (°C/km)
CONDUCTIVITY (mcal/cm • sec • °C)
LV-1 LUCERNE VALLEY, CALIF.
LOG 5/17/67
600 - 700 meters
DEPTH (meters)

Figure 23

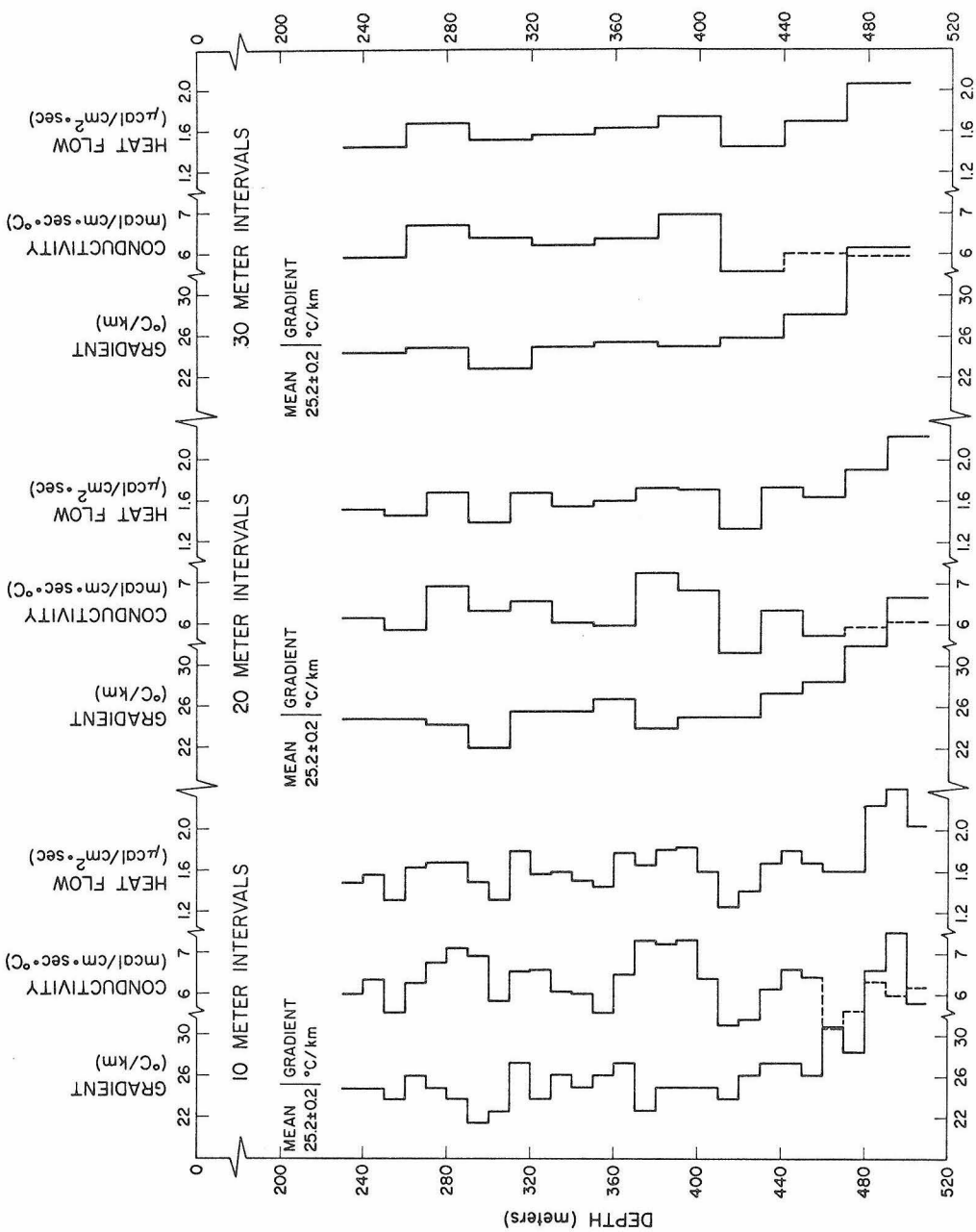
10 METER INTERVALS
20 METER INTERVALS
30 METER INTERVALS
GRADIENT (°C/km)
CONDUCTIVITY (mcal/cm·sec·°C)
HEAT FLOW (μcal/cm²·sec)
MEAN 25.2±0.2 °C/km
DEPTH (meters)
SB-10, SAN BERNARDINO MTNS., CALIF. INTERVAL HEAT FLOW

Figure 24

spring and horizontal well at the base of the slope directly below the drill hole site indicate that water is flowing out of fractures below the bottom of the drill hole.

SB-10 again has the same lithology as the other two holes. From Figure 21 we see that the gradient increases at about 450 meters. This increase in the gradient, from 450 m to the bottom of the hole, can be explained by two factors in conductivity: 1) a decrease of the average conductivity in this interval by 10% as can be seen from Appendix VII, SB-10, and 2) a faulted and fractured zone between 480 and 500 meters where most of the anomalous change in gradient occurs. The very bottom appears to be returning to the normal gradient. The conductivity of the fractured zone could not be determined; the core was too badly damaged to obtain disks for measuring. Thus on the basis of these considerations, the portion of the hole between 440 meters and the bottom was excluded from the heat flow determination. SB-10 then gives the same heat flow as SB-2, 1.6 HFU. Figure 24 shows the results of interval heat flows (corrected for steady-state topography) calculated for 10, 20, and 30 meter intervals for SB-10. The number of conductivity samples per 10, 20, and 30 meter interval averaged 3, 5, and 8, respectively. The average of the interval heat flows between 300 and 440 meters (the interval given in Table 10) are 1.59, 1.58, and 1.58 HFU for the 10, 20, and 30 meter interval cases, respectively. These values are in good agreement with the corrected heat flow from Table 10 obtained by the product method.

The radioactive heat production for the San Bernardino group of holes was determined using the core from SB-10. Measurements were made on one composite of ten randomly spaced $1\frac{1}{2}$ inch samples throughout the length of the hole. Appendix V gives the value for the equivalent uranium and Table 10, the heat productivity.

LV-1 was originally drilled (1960) to a depth of 600 meters by Southern Pacific Land Company. The core could not be located after extensive inquiry, and consequently the hole was deepened an additional 100 meters. The original lithologic log (Dorsey, Southern Pacific Land Co., 1960) indicates the entire hole was drilled in a fine to coarse grained hornblende diorite. The core obtained from the bottom 100 meters was found to be a coarse grained hornblende diorite with numerous andesitic dikes dipping at 45°. The dike material was found to have the same conductivity as the diorite, and thus refraction effects near the dikes were not encountered (see Roy, 1963, p. 18). The temperature gradient (see Figure 22) shows a distinct increase at about 300 meters from 26°C/km to 31°C/km, suggesting a decrease in conductivity below 300 meters. To determine if this change in gradient was correlated with a change in conductivity, a 15 meter hole was drilled 100 meters south of LV-1 in a surface outcrop mapped as quartz monzonite (Dibblee, 1954). It was found that the product of its conductivity and the gradient in the upper part of the hole gave about the same heat flow as that determined by using the conductivity and gradient from the bottom of the hole. The value of 1.6 HFU obtained from the bottom 100 meters of LV-1 is the same as a heat

flow value obtained by Roy, et al. (1968) about $6\frac{1}{2}$ km to the northeast in a complex geological environment.

The radioactivity measurements were made on two composites from the bottom 100 meters of the hole. $1\frac{1}{2}$ inch samples were taken every 25 feet and each composite contained samples from alternate 25 foot intervals, or every 50 feet. Their values are given in Appendix V. A single 6 inch sample from the quartz monzonite was also measured and gave a somewhat higher value (see Appendix V). The value of the radioactive heat production assumed representative of LV-1 is given in Table 11.

The general geologic history of the San Bernardino Mountains has probably paralleled that of the Peninsular Ranges. The San Bernardino Mountains are a large fault-bound block similar to those of the Peninsular Ranges, perhaps also having undergone major displacements with respect to their surroundings. SB-2 and SB-10 are located in the subdued upland portion (Bailey and Jahns, 1954) of the range. Again as in the Peninsular Ranges, the subdued upland relief probably represents the pre-mid-Miocene erosion surface which has undergone little significant erosion since mid-Miocene, the major erosion being confined to the deeply incised canyons along the fault scarps. Bateman and Wahrhaftig (1966) suggest the same for the Sierra Nevada; that is, perhaps several thousand feet of erosion in the deep canyons and essentially none from the intercanyon regions in the last 10 m.y. They further suggest that virtually no erosion has occurred in the last 3.5 m.y.

Following the same geologic time history as for the Anza region, we might suggest that the topography as we see it today has evolved in the last 16 m.y., and we have had 1.7 km of uplift with 0.1 km of erosion at SB-2 and SB-10. Results of calculations based on these figures are shown in Tables 8 and 10, and are not appreciably different from the results for the steady-state case.

The geologic history of the Mojave Desert seems quite difficult to interpret, especially in light of the close spatial relationship of this region with adjacent provinces which are physiographically so dissimilar. There are regions in the Mojave Block where the geology suggests extreme local erosion, and deposition has occurred in Cenozoic time (Hewett, 1954; R. P. Sharp, personal communication). The events from Middle Cretaceous to mid-Miocene time can be thought of as similar to the other areas we have discussed; Hewett (1954) estimates that the block was uplifted perhaps 7 km and eroded as it rose during this time. In contrast to neighboring regions, however, the Mojave Block was probably positive with respect to its surroundings from Late Mesozoic to present times and remained above sea level, as evidenced by the lack of Cenozoic marine sedimentation. Cenozoic deformation apparently took place most strongly during Pliocene time and involved broad warping and thrusting which appear to be most pronounced in the eastern part of the block, dying off to the west. Local basins and troughs were formed and the drainage gradually became internal. This period of orogenesis was then followed by significant erosion, "...sufficient to reduce the thrust

plates...to isolated blocks or klippen, " (Hewett, 1954). Furthermore, locally thick sections of upper Tertiary sediments (e.g. near Lucerne Valley, see Dibblee, 1964) and Pleistocene volcanics (which often cap positive features) lead one to suspect that at some time these deposits were more widespread and have subsequently been stripped away. Many of these features, however, may be fault controlled, or reflect locations of Tertiary basins and surfaces of deposition.

From the foregoing discussion, one might suspect that it is difficult to hypothesize an uplift and erosion rate for the Lucerne Valley area of the Mojave Desert; periods of rapid deposition intermingled with uplift and erosion further complicate the picture. The 7 km of erosion estimated by Hewett for Late Cretaceous and Early Tertiary time would have little effect on the present heat flow, essentially the same as that discussed for the Anza region. As for the Late Cenozoic history, we will consider two time dependent models, differing only by the amount of erosion, and suggest that along with the steady-state case each is equally probable, and for that matter, any case with an amount of erosion between that of the steady-state case (no erosion) and the case having the maximum erosion. The two cases are: 1) topographic evolution took place in the last 9 m.y. with no uplift and 1 km of erosion, and 2) topography evolved in the last 9 m.y. with no uplift and 2 km of erosion. The topographic evolution is assumed to commence with the region's Pliocene orogeny (Hewett, 1954) which also permitted the drainage to become external. The level of erosion can then be considered to be controlled by the base

level of the external drainage, and the amount, by the thickness of sediments, the thickness also depending on the nature of the depositional surface during Tertiary time. If the warps were pronounced and the basins well developed during the Tertiary, locally thick sections could develop, and it would not be necessary to assume any significant erosion of the pre-Tertiary crystalline terrane. If, however, these warps, in which the Tertiary sediments are preserved, were developed during the Pliocene orogeny, and the pre-orogenic surface was relatively uniform (with the exception of mountain masses, such as the Ord Mountains, Cady Mountains, etc., which probably represent residual, pre-Tertiary relief), it is possible that several km of debris could have been removed from all of the intermontane regions. No uplift is postulated because, as we indicated before, it is not necessary to invoke regional uplift to explain the onset or level of erosion, and furthermore, the Pliocene orogeny appears to be associated with thrusting and warping, but no generally recognizable uplift.

The value corrected for case 1) above is 1.58 HFU (Table 11). The value for case 2) is 1.52 HFU. Thus, if as much as 2 km of erosion actually occurred in the Mojave Block since early Pliocene, the measured heat flow at Lucerne Valley would be significantly higher (~0.2 HFU) than the normal heat flow for that area. Had a km of material been eroded in that last 1 m.y., the effects would be quite pronounced -- the corrected heat flow would be 1.46 HFU (Appendix VIII). Thus heat flow results would be seriously in doubt if it were discovered that erosion occurred at rates on the order of 1 km/m.y.

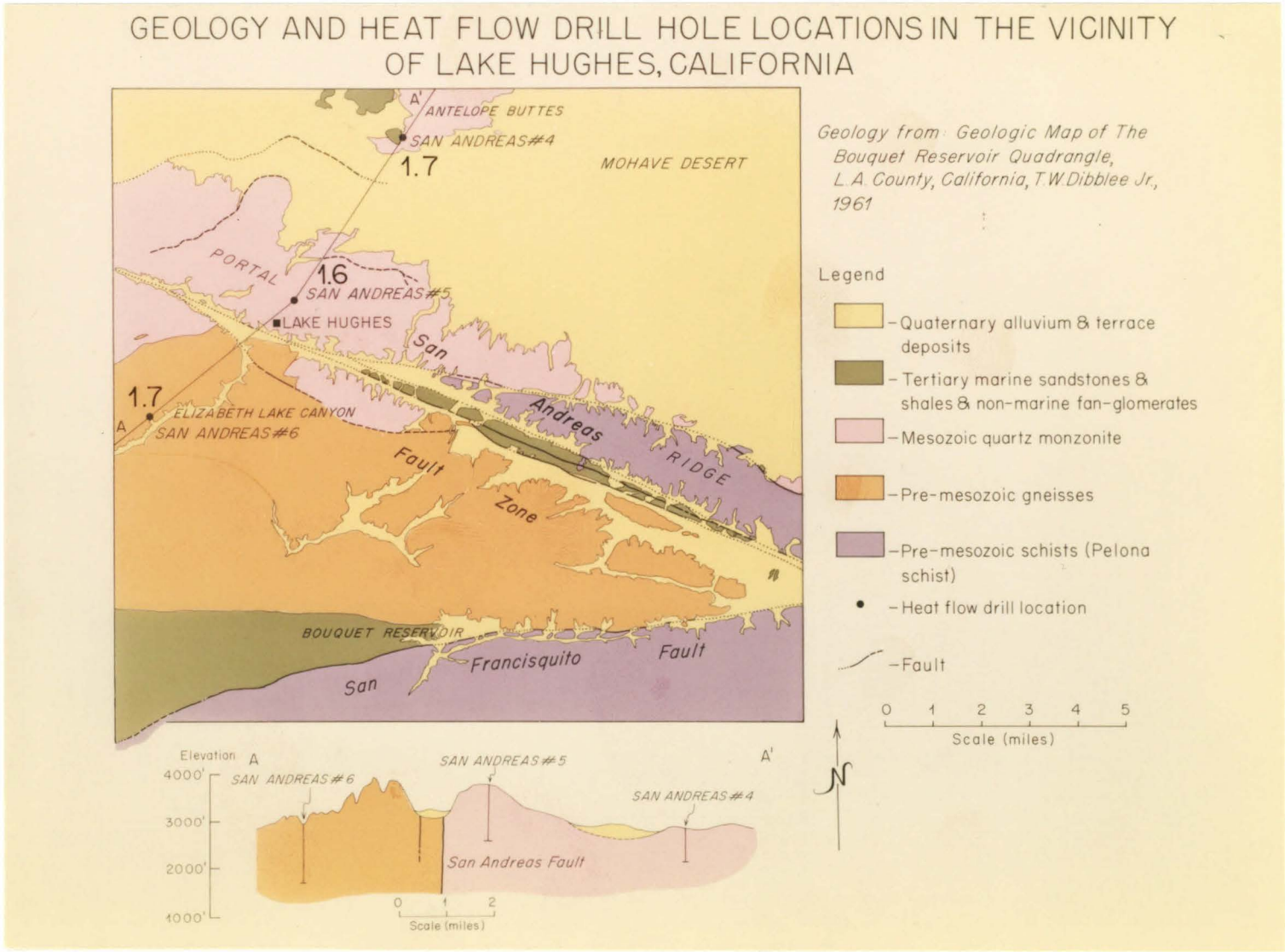
GEOLOGY AND HEAT FLOW DRILL HOLE LOCATIONS IN THE VICINITY OF LAKE HUGHES, CALIFORNIA
A'
ANTELOPE BUTTES
SAN ANDREAS #4
1.7
MOHAVE DESERT
PORTAL
1.6
SAN ANDREAS #5
LAKE HUGHES
San
1.7
A
ELIZABETH LAKE CANYON
SAN ANDREAS #6
Andreas
RIDGE
Fault
Zone
BOUQUET RESERVOIR
Francisquito
Fault
San
Geology from Geologic Map of The Bouquet Reservoir Quadrangle, L.A. County, California, T.W. Dibblee Jr., 1961
Legend
– Quaternary alluvium & terrace deposits
– Tertiary marine sandstones & shales & non-marine fan-glomerates
– Mesozoic quartz monzonite
– Pre-mesozoic gneisses
– Pre-mesozoic schists (Pelona schist)
– Heat flow drill location
– Fault
0 1 2 3 4 5
Scale (miles)
N
Elevation
A
A'
4000'
3000'
2000'
1000'
SAN ANDREAS #6
SAN ANDREAS #5
SAN ANDREAS #4
San Andreas Fault
0 1 2
Scale (miles)

Figure 25

It is hard to reconcile erosion rates of even 1-2 km/9 m.y. over such a large region, with those hypothesized for the neighboring provinces (e.g. Sierra Nevada), and we suggest that the steady-state value at LV-1 is the best value.

D. Heat Flow near Lake Hughes, California

Three holes (LH-1, LH-2, and LH-3) were drilled in pre-Tertiary crystalline rocks (Mesozoic?) in the vicinity of the San Andreas fault near Lake Hughes, California (see Figure 7). Two holes are located northeast of the fault and one southwest. Figure 25 shows the relation of the drill sites to the local geology. Note that LH-1, LH-2, and LH-3 are designated as San Andreas #4, #5, and #6, respectively, in Figure 25. The geology of the Lake Hughes area has been discussed by Simpson (1934), and more recently, has been mapped by Dibblee (1961).

The San Andreas fault in the Lake Hughes area forms the boundary between the western Mojave Block and the central Transverse Ranges. The western Mojave, as we indicated before, consists for the most part of an alluvial plain with isolated buttes of Tertiary volcanics and sediments and Mesozoic plutonics piercing the alluvium. It is terminated about 20 miles to the northwest in wedge-like fashion by the Garlock and San Andreas faults. Well and gravity data (Wiese and Fine, 1950; Mabey, 1960) suggest that the Cenozoic sedimentary fill beneath the alluvial surfaces in this portion of the Mojave may reach depths of five or six thousand feet.

LH-1 LAKE HUGHES, CALIFORNIA

LOCATION and ELEVATION		DRILLING HISTORY	
Latitude	34° 44.1' N	Started	9/21/65
Longitude	118° 23.7' W	Stopped	10/11/65
Collar Elevation	2800 feet	Total Depth	700 feet
Distance from Fault Trace	8 km	Hole Size	BX-Wireline Cased $1\frac{1}{4}$" pipe

DEPTH	GEOLOGIC LOG
0 - 700 feet	Quartz Monzonite (weathered and decomposed)

CONDUCTIVITY, GRADIENT, HEAT FLOW, RADIOACTIVITY

Mean Resistivity	(30)	$161.0 \pm 2.6 \frac{cm \cdot sec \cdot °C}{cal}$
Mean Harmonic Conductivity		$6.21 \pm 0.1 \frac{mcal}{cm \cdot sec \cdot °C}$
Uncorrected Gradient	(120-210 m)	27.70 ± 0.20 °C/km
Corrected Gradient	Steady State	27.68 ± 0.21 °C/km
	Topographic Evolution	27.52 ± 0.21 °C/km
Uncorrected Heat Flow		1.72 ± 0.03 HFU
Corrected Heat Flow	Steady State	1.72 ± 0.03 HFU
	Topographic Evolution	1.71 ± 0.03 HFU
Limit of Topographic Influence		20 km
Radioactive Heat Production		$8.7 \pm 4.0 \frac{x10^{-13} cal}{cm^3 \cdot sec}$

Table 12

LH-2 LAKE HUGHES, CALIFORNIA

LOCATION and ELEVATION		DRILLING HISTORY	
Latitude	34° 41.2' N	Started	1/24/63; 10/19/65
Longitude	118° 26.1' W	Stopped	3/13/63; 11/15/65
Collar Elevation	3773 feet	Total Depth	1225 feet
Distance from Fault Trace	1 km	Hole Size	0-680 ft NX-Wireline 680-1200 ft BX-Wireline Cased $1\frac{1}{4}$" pipe

DEPTH	GEOLOGIC LOG
0 - 1200 feet	Quartz Diorite (badly weathered and decomposed; ~50% clay and/or fault gouge)

CONDUCTIVITY, GRADIENT, HEAT FLOW, RADIOACTIVITY

Mean Resistivity	(25)	$160.0 \pm 5.2 \frac{\text{cm} \cdot \text{sec} \cdot °\text{C}}{\text{cal}}$
Mean Harmonic Conductivity		$6.15 \pm 0.2 \frac{\text{mcal}}{\text{cm} \cdot \text{sec} \cdot °\text{C}}$
Uncorrected Gradient	(180-280 m)	22.21 ± 0.10 °C/km
Corrected Gradient — Steady State		24.89 ± 0.06 °C/km
Corrected Gradient — Topographic Evolution		24.68 ± 0.06 °C/km
Uncorrected Heat Flow		1.39 ± 0.05 HFU
Corrected Heat Flow — Steady State		1.56 ± 0.05 HFU
Corrected Heat Flow — Topographic Evolution		1.54 ± 0.05 HFU
Limit of Topographic Influence		20 km
Radioactive Heat Production		$3.4 \pm 1.2 \frac{\times 10^{-13} \text{cal}}{\text{cm}^3 \cdot \text{sec}}$

Table 13

LH-3 LAKE HUGHES, CALIFORNIA

LOCATION and ELEVATION		DRILLING HISTORY	
Latitude	34° 39.1' N	Started	12/3/65
Longitude	118° 29.2' W	Stopped	1/6/66
Collar Elevation	2900 feet	Total Depth	1200 feet
Distance from Fault Trace	4 km	Hole Size	0-520 ft NX-Wireline 520-1200 ft BX-Wireline Cased $1\frac{1}{4}$" pipe

DEPTH	GEOLOGIC LOG
0 - 1200 feet	Quartz Diorite (slightly foliated; extensive fracture zone from 800 - 1000 feet)

CONDUCTIVITY, GRADIENT, HEAT FLOW, RADIOACTIVITY

Mean Resistivity . . . . . (52)		$171.0 \pm 5.4 \frac{cm \cdot sec \cdot °C}{cal}$
Mean Harmonic Conductivity		$5.85 \pm 0.2 \frac{mcal}{cm \cdot sec \cdot °C}$
Uncorrected Gradient . . . . . (150-250 m)		*32.80 ± 0.31 °C/km
Corrected Gradient	Steady State	28.74 ± 0.39 °C/km
	Topographic Evolution	28.43 ± 0.39 °C/km
Uncorrected Heat Flow		1.92 ± 0.06 HFU
Corrected Heat Flow	Steady State	1.68 ± 0.06 HFU
	Topographic Evolution	1.66 ± 0.06 HFU
Limit of Topographic Influence		20 km
Radioactive Heat Production		$2.6 \pm 0.6 \frac{\times 10^{-13} cal}{cm^3 \cdot sec}$

*Gradient fitted to interval shown, plus 360 m point (see text, p. 115)

Table 14

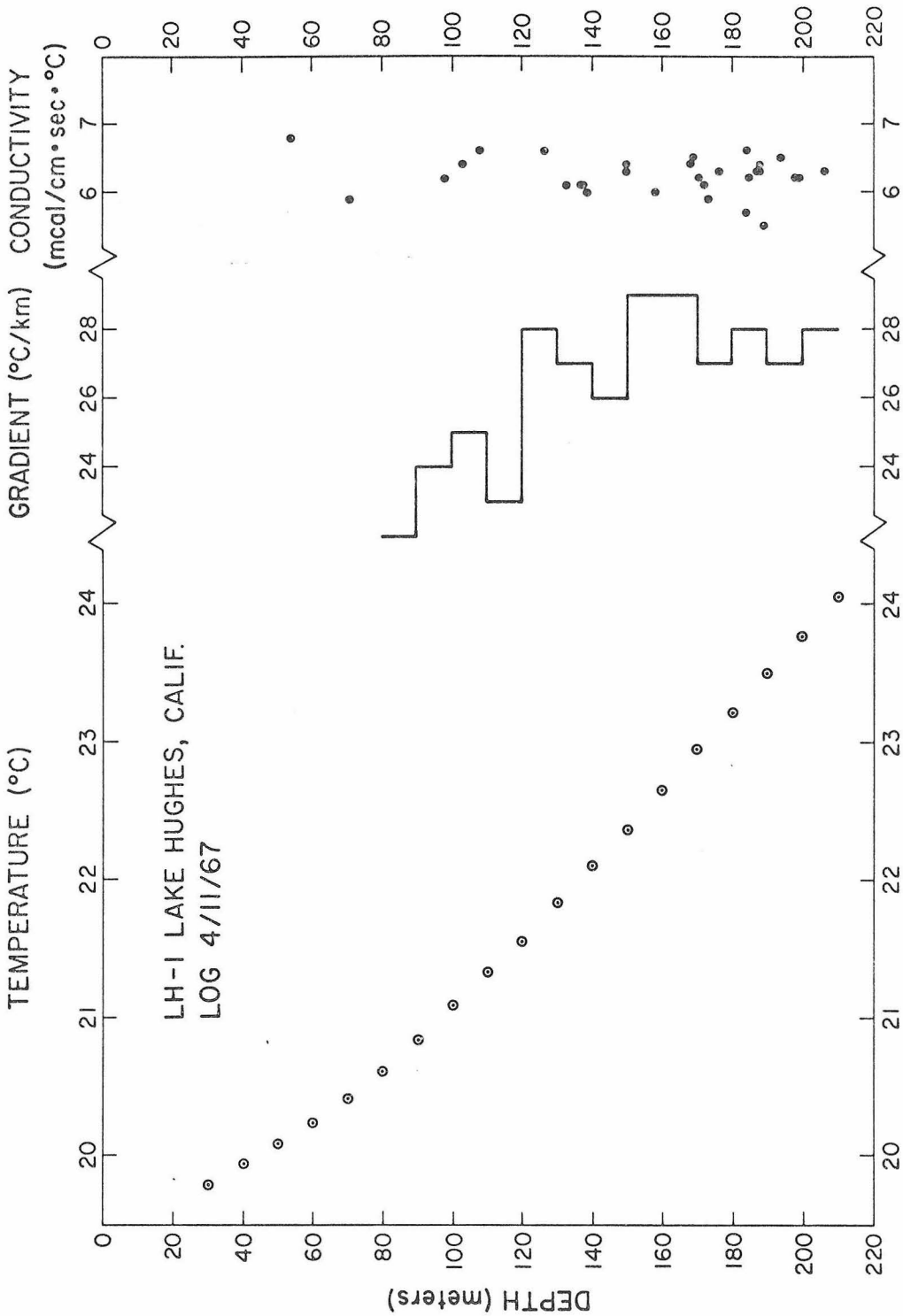
TEMPERATURE (°C)
GRADIENT (°C/km)
CONDUCTIVITY (mcal/cm•sec•°C)
LH-1 LAKE HUGHES, CALIF.
LOG 4/11/67
DEPTH (meters)

Figure 26

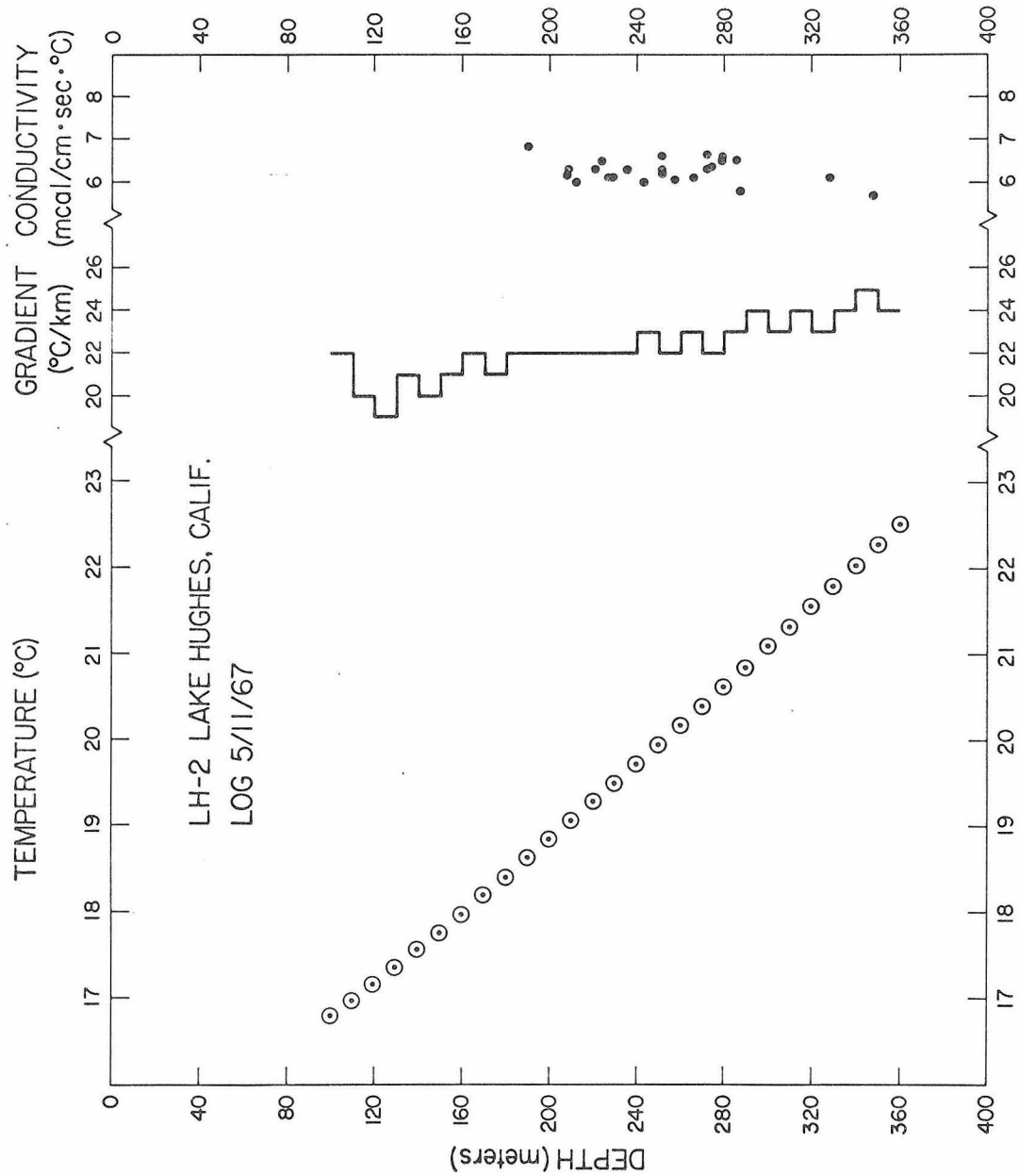
TEMPERATURE (°C)
GRADIENT (°C/km)
CONDUCTIVITY (mcal/cm·sec·°C)
LH-2 LAKE HUGHES, CALIF.
LOG 5/11/67
DEPTH (meters)

Figure 27

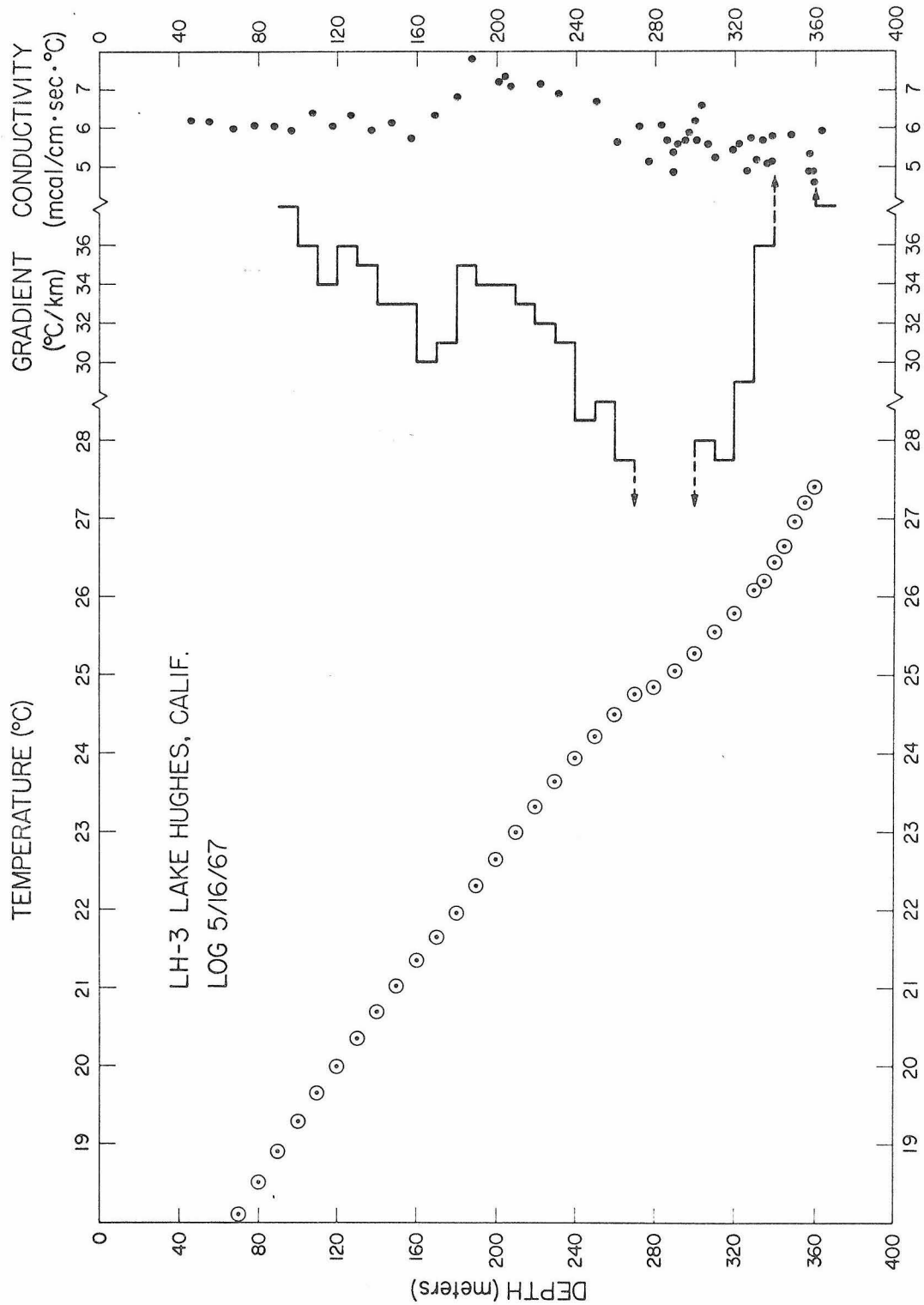
TEMPERATURE (°C)
GRADIENT (°C/km)
CONDUCTIVITY (mcal/cm·sec·°C)
LH-3 LAKE HUGHES, CALIF.
LOG 5/16/67
DEPTH (meters)

Figure 28

The central portion of the Transverse Ranges near Lake Hughes might be called the Liebre Mountains-Sierra Pelona Block, and consists of a narrow wedge of crystalline and metamorphic rocks between the San Andreas fault to the northeast and the Tertiary Ridge Basin and San Gabriel fault to the southwest. The crystalline rocks include quartz-monzonites of presumably Mesozoic age and gneissic diorites, also probably Mesozoic. The southern part of the region consists of a pre-Mesozoic quartz-biotite schist called throughout southern California, the Pelona schist, which is everywhere found in fault contact with the granitic rocks.

The San Andreas fault in the Lake Hughes area is characterized by one of the most spectacular and continuous rift valleys of any along its entire length. Many large sag ponds exist within the rift valley, which transects the regional drainage pattern. Major offsets along the fault occurred near Lake Hughes during the 1857 Fort Tejon earthquake. Since that time, however, the region has been very quiet seismically, and no creep offsets have been recognized in the area (Meade, 1963; Allen, et al., 1965).

LH-1 and LH-2 were drilled northeast of the San Andreas in rock types mapped as quartz monzonite (Dibblee, 1961). LH-2 was originally drilled to a depth of 180 meters by the California State Department of Water Resources in 1963 along a proposed tunnel alignment. It was deepened an additional 180 meters during our drilling operations in the Lake Hughes area. Of specific concern was a possible perturbation in temperature due to the existing Elizabeth

Lake Canyon tunnel which was installed in 1913 and passes at a depth of 200 meters at a distance of 300 meters to the south. We can consider the tunnel to bound internally the region $r > a$ where a is the radius of the tunnel, with the surface $r = a$ maintained at constant temperature V. The solution for the temperature, v, in the region $r > a$, initially at temperature zero, is given for a later time t by Carslaw and Jaeger (1959, p. 335), in integral form. Values are tabulated by Jaeger (1956, p. 316). For our case of $\frac{r}{a} \simeq 100$ and $\frac{\varkappa t}{a^2} \simeq 170$, $\frac{v}{V}$ is of the order of 10^{-4}. If we assume that $V \simeq 5°C$ (the difference between the mean annual surface temperature at Lake Hughes -- the water is probably at the surface temperature before entering the tunnel -- and the temperature at 200 meters), we get the temperature disturbance at the drill hole

$$v \simeq 0.0005°C$$

Thus the effect of water flowing through the tunnel is negligible.

In both LH-1 and LH-2, extreme weathering persisted to the bottom of the hole -- 210 meters in the case of LH-1 and 370 meters in the case of LH-2. The biotites for the most part were entirely chloritized and the feldspars extensively kaolinized. The core was just good enough to obtain suitable conductivity samples over a representative depth interval, but it should be pointed out that since only the best core could be used, a bias may have been introduced into the mean conductivity. However, the gradients were quite regular and thus the bias was assumed negligible, the conductivity essentially representing the bulk composition of the rock in these cases, with the

fractures having been filled in with silt or clay. The fact that the fractures probably have been filled in was undoubtedly responsible for the fact that no water circulation problems were encountered in these holes. Water pressure tests by the California State Department of Water Resources in LH-2 showed essentially no water could be injected into the formation. It might be noted that the slight progressive increase in gradient below 280 meters in the LH-2 (see Figure 27) could conceivably be due to the extreme weathered condition of the rock (greater fraction of clay) below this depth. Only two conductivity samples could be obtained from 290 meters depth to the bottom. For these reasons, this part of the gradient was not used for computing the heat flow. The increased gradient is not a terrain effect since the curvature in the gradient was not removed by the terrain correction.

LH-3 was drilled southwest of the fault in a slightly foliated gneissic diorite of uniform composition. The core was fresh and hard throughout the entire depth of the hole. A large fracture zone was encountered between about 240 and 270 meters. After the hole was completed, grouting with cement was attempted, but apparently failed as can be seen from Figure 28; the temperature-depth profile shows a post-drilling temperature disturbance at about 270 meters, indicative of the downward movement of water in the hole. During logging, the temperatures in the fractured interval were unstable and drifted as much as a few hundredths of a degree during measurement, while above this zone they were stable to better than ±0.01°C, suggesting that the temperatures are probably reliable above 250 meters.

In addition, the temperatures above 250 meters were reproducible from one logging to another. The bottom hole temperature was also found to be stable and reproducible. Thus, the gradient for calculating the heat flow was chosen by taking a portion of the temperature-depth curve above the disturbed region, together with the bottom hole temperature.

The heat flow values at LH-1, 2, and 3 are 1.7, 1.6, and 1.7 HFU, respectively, and are the same values within the statistical limits.

The radioactive content of the core from LH-1 was determined from two composites consisting of $1\frac{1}{2}$ inch samples taken at alternate 50-foot intervals from 50 feet deep to the bottom of the hole. One composite of $1\frac{1}{2}$ inch samples taken every 50 feet from 700 feet to the bottom was used to determine the radioactive content of the core from LH-2. The only reliable value for the radioactive heat productivity for the Lake Hughes area is from LH-3, since this determination was made on unweathered core. Two composites were evaluated from LH-3 consisting of $1\frac{1}{2}$ inch samples taken at alternate 50-foot depths from 50 feet to the bottom. The values of heat production are given in Tables 12, 13, and 14.

It is likely that the geologic and physiographic history at each of the drill sites near Lake Hughes may have been quite different. LH-1 is situated in the Mojave Block, LH-2 in a transition region between the Mojave Block and the Liebre Mountain-Sierra Pelona Block, and LH-3 in a deeply incised canyon within this latter region.

The present topographic evolution is assumed to have commenced in mid- to upper-Miocene as elsewhere in southern California.

LH-1 is located in the Antelope Buttes, a positive feature with respect to the surrounding western Mojave Block of low relief. The presence of these buttes may be related to a subsurface fault trending northeast-southwest a short distance to the east, or may reflect a northeast-southwest doming or warping of the basement and overlying sediments. A basal conglomerate and Tertiary section of volcanic debris unconformably overlie the crystalline basement to the west, and dip homoclinally westward toward a region known to have a great thickness of Cenozoic sediments. Because the hole was drilled near the contact with the basal conglomerate, the deep weathering can probably be explained by the fact that this was the pre-Tertiary erosion surface and without further erosion became the depositional surface for Tertiary sediments. For this reason, we will assume that no erosion of the crystalline basement has occurred since mid-Tertiary time. The main concern is how much Tertiary sedimentation was deposited on this surface and subsequently stripped away. The exposed section of volcanic pyroclastics and fanglomerates immediately to the northwest is about 2500 feet thick (Dibblee, 1961). However, because of the nature of these sediments, they are likely to be shingled and locally thin or thick, depending upon the relief of the original erosion surface. It is therefore quite tenuous to speculate on the depth of burial at the drill site on the basis of these reported thicknesses. The presence of fanglomerates suggest that

the region was positive with respect to its surroundings during Tertiary; and the absence of marine sediments, which are found farther west, indicates the area was above sea level, although perhaps not by much, since it is likely the western tip of the Mojave was the outlet to the sea for a large part of the block (Wiese, 1950). However, the dipping volcanics are suggestive of a certain amount of uplift (or subsidence to the west) although, because of the nature of this debris, part of this dip may be the result of the original environment of deposition. On the basis of the foregoing discussion and the present collar elevation, we will assume 0.3 km of uplift and a minimum of 0.3 km of erosion has occurred at LH-1 in the last 16 m.y.

LH-2 is located on Portal Ridge, a northwest-southeast trending high, paralleling the San Andreas fault. It is characterized by a crest having subdued relief and flanks that are deeply incised. Evidence regarding uplift and erosion at LH-2 is somewhat more obscure than at LH-1. The deep weathering of the crystalline terrane around LH-2 may be explained in the same way as that near LH-1, or may alternatively be due to this zone's proximity to the San Andreas fault, having repeatedly undergone fracturing and shearing due to movement along the fault, allowing the downward migration of surface fluids throughout. No evidence exists for an extensive or continuous Tertiary cover, although a locally thick section (perhaps as much as 5000 feet) of andesitic flows and tuff beds rest unconformably on the crystalline rocks of Portal Ridge about 10 miles to the northwest. It seems likely, however, that if we assume 0.3 km of uplift and 0.3 km

of erosion to occur 5 miles to the north (at Antelope Buttes), we must have about the same occurring at LH-2. This assumption is not valid, however, when considering the region on the opposite side of the San Andreas fault. LH-3 is situated southwest of the San Andreas in Elizabeth Lake Canyon, a deep incision into the gneissic complex just south of Liebre and Sawmill Mountains. The Liebre-Sawmill Mountain area has probably been positive with respect to its surroundings since upper Miocene, being a major contributor of sediments to the Ridge Basin area, the debris coming from the deeply eroded flanks and canyons of the southwestern-facing portion of these mountains. Assuming that the present tops of the ridges in this region represent approximately the pre-upper Miocene erosion surface, we might suggest that there has been 1.5 km of uplift and 0.5 km of erosion at LH-3 in the last 16 m.y.

Tables 12, 13, and 14 give the case of a 16 m.y. topographic evolution near Lake Hughes with 0.3 km of uplift and 0.3 km of erosion at LH-1 and LH-2, and 1.5 km of uplift and 0.5 km of erosion at LH-3; and, again, none of the values are significantly different from the results of the steady-state cases. It might be noted that in the case of LH-3, even if Elizabeth Lake Canyon had evolved in the last 1 m.y., the present heat flow would be high by only about 10% (see Appendix VIII, p.367).

E. Heat Flow in the Tehachapi Mountains, California

Six holes, drilled by the California State Department of Water Resources as part of an extensive drilling program along the alignment of the California aqueduct system through the Tehachapi Mountains near Gorman, California, were used for heat flow determinations (see Figure 7). One hole was deepened an additional 60 meters, and all were cleaned and cased with perforated $1\frac{1}{4}$ inch iron pipe. The six holes (DH-14, DH-15A, DH-43, DH-65, DH-67, and DH-70, as designated by the Department of Water Resources) are in a perpendicular profile across the Garlock fault, DH-43, 65, and 67 to the north and DH-14, 15A, and 70 to the south. Figure 29 shows the relation of the drill holes to the local geology.

DH-65 and 67 were drilled in a gneissic hornblende diorite, very hard and fresh, and highly foliated, which forms a large portion of the north flank of the Tehachapi Mountains in the vicinity of Pastoria and Grapevine Canyons. The age is tentatively placed as Jurassic (?) (Wiese, 1950), and the foliation is believed to be an original feature, having resulted from flowage during intrusion. DH-43 was drilled (deepened 60 meters during the course of this investigation) between the two branches of the Garlock fault in a quartz-mica schist assigned to the Pelona schist series of pre-Cambrian (?) age. DH-14, 15A, and 70 were drilled south of the Garlock fault in a salmon colored, coarse-grained, uniform, equigranular granite, also of Jurassic (?) age (Wiese, 1950), which crops out over a large area on the southern flank of the Tehachapi Mountains in the Cottonwood and Oso Canyons

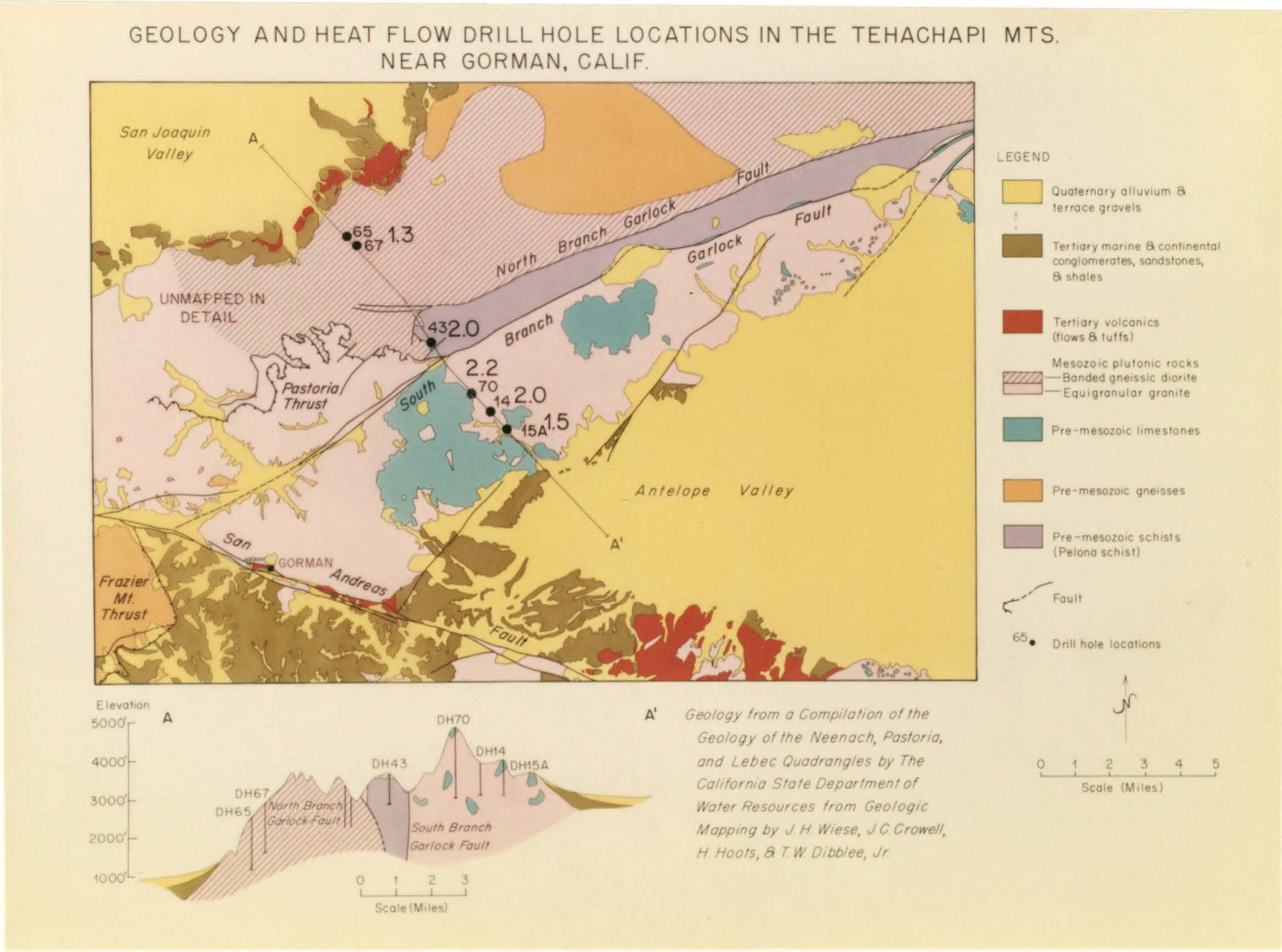
GEOLOGY AND HEAT FLOW DRILL HOLE LOCATIONS IN THE TEHACHAPI MTS.
NEAR GORMAN, CALIF.
San Joaquin Valley
A
65
67
1.3
North Branch Garlock Fault
Garlock Fault
UNMAPPED IN DETAIL
43
2.0
Branch
2.2
70
14
2.0
15A
1.5
Pastoria Thrust
South
Antelope Valley
A'
San Andreas Fault
GORMAN
Frazier Mt. Thrust
LEGEND
Quaternary alluvium & terrace gravels
Tertiary marine & continental conglomerates, sandstones, & shales
Tertiary volcanics (flows & tuffs)
Mesozoic plutonic rocks
Banded gneissic diorite
Equigranular granite
Pre-mesozoic limestones
Pre-mesozoic gneisses
Pre-mesozoic schists (Pelona schist)
Fault
Drill hole locations
0 1 2 3 4 5
Scale (Miles)
Elevation
5000'
4000'
3000'
2000'
1000'
A
A'
DH70
DH14
DH15A
DH43
DH67
DH65
North Branch Garlock Fault
South Branch Garlock Fault
0 1 2 3
Scale (Miles)
Geology from a Compilation of the Geology of the Neenach, Pastoria, and Lebec Quadrangles by The California State Department of Water Resources from Geologic Mapping by J.H. Wiese, J.C. Crowell, H. Hoots, & T.W. Dibblee, Jr.

Figure 29

DH-14 TEHACHAPI MTNS., CALIFORNIA

LOCATION and ELEVATION		DRILLING HISTORY	
Latitude	34° 51.7' N	Started	11/28/62
Longitude	118° 4415' W	Stopped	12/22/62
Collar Elevation	3905 feet	Total Depth	800 feet
Distance from Fault Trace	$3\frac{1}{2}$ km	Hole Size	NX-Wireline Cased $1\frac{1}{4}$" pipe (perf.)

DEPTH	GEOLOGIC LOG
0 - 800 feet	Granite

CONDUCTIVITY, GRADIENT, HEAT FLOW, RADIOACTIVITY

Mean Resistivity . . . . . (10)		$120.0 \pm 2.2 \frac{\text{cm} \cdot \text{sec} \cdot ^\circ\text{C}}{\text{cal}}$
Mean Harmonic Conductivity		$8.33 \pm 0.1 \frac{\text{mcal}}{\text{cm} \cdot \text{sec} \cdot ^\circ\text{C}}$
Uncorrected Gradient . . . . . (150-220 m)		26.23 ± 0.13 °C/km
Corrected Gradient	Steady State	24.36 ± 0.18 °C/km
	Topographic Evolution	23.89 ± 0.18 °C/km
Uncorrected Heat Flow		2.19 ± 0.04 HFU
Corrected Heat Flow	Steady State	2.03 ± 0.04 HFU
	Topographic Evolution	1.99 ± 0.04 HFU
Limit of Topographic Influence		30 km
Radioactive Heat Production		$7.7 \pm 2.3 \frac{\times 10^{-13} \text{cal}}{\text{cm}^3 \cdot \text{sec}}$

Table 15

DH-15A TEHACHAPI MTNS., CALIFORNIA

LOCATION and ELEVATION		DRILLING HISTORY	
Latitude	34° 51.3' N	Started	1/30/63
Longitude	118° 44.0' W	Stopped	3/28/63
Collar Elevation	3980 feet	Total Depth	931 feet
Distance from Fault Trace	$4\frac{1}{2}$ km	Hole Size	0-825 ft 3" tricone 825-931 ft BX-Wireline Cased $1\frac{1}{4}$" pipe (perf.)

DEPTH	GEOLOGIC LOG
0 - 825 feet	No core
825 - 931 feet	Granite (altered, weak and friable; ~50% clay

CONDUCTIVITY, GRADIENT, HEAT FLOW, RADIOACTIVITY

Mean Resistivity	(0)	No core (see text, p.140)
Mean Harmonic Conductivity		" "
Uncorrected Gradient	(150-220 m)	18.33 ± 0.14 °C/km
Corrected Gradient	Steady State	17.65 ± 0.11 °C/km
	Topographic Evolution	17.24 ± 0.11 °C/km
Uncorrected Heat Flow		1.54 ± 0.04 HFU
Corrected Heat Flow	Steady State	1.48 ± 0.04 HFU
	Topographic Evolution	1.44 ± 0.04 HFU
Limit of Topographic Influence		30 km
Radioactive Heat Production		Not determined (see DH-14)

Table 16

DH-43 TEHACHAPI MTNS., CALIFORNIA

LOCATION and ELEVATION		DRILLING HISTORY	
Latitude	34° 53.4' N	Started	12/3/63; 3/23/66
Longitude	118° 46.3' W	Stopped	3/5/64; 3/30/66
Collar Elevation	3671 feet	Total Depth	800 feet
Distance from Fault Trace	1 km	Hole Size	0-464 ft $5\frac{3}{4}$" tricone 464-618 ft NX-Wireline 618-800 ft BX-Wireline Cased $1\frac{1}{4}$" pipe (perf.)

DEPTH	GEOLOGIC LOG
0 - 124 feet	Gneissic Diorite
124 - 183 feet	Overthrust Fault Zone
183 - 800 feet	Quartz and Mica Schist (Pelona)

CONDUCTIVITY, GRADIENT, HEAT FLOW, RADIOACTIVITY

Mean Resistivity . . . . . (22)		$120.8 \pm 8.2 \frac{cm \cdot sec \cdot °C}{cal}$
Mean Harmonic Conductivity		$8.28 \pm 0.5 \frac{mcal}{cm \cdot sec \cdot °C}$
Uncorrected Gradient . . . . . (170-230 m)		23.80 ± 0.39 °C/km
Corrected Gradient	Steady State	24.45 ± 0.38 °C/km
	Topographic Evolution	24.04 ± 0.38 °C/km
Uncorrected Heat Flow		1.97 ± 0.14 HFU
Corrected Heat Flow	Steady State	2.02 ± 0.14 HFU
	Topographic Evolution	1.99 ± 0.14 HFU
Limit of Topographic Influence		30 km
Radioactive Heat Production		$2.1 \pm 0.6 \frac{x10^{-13} cal}{cm^3 \cdot sec}$

Table 17

DH-65 TEHACHAPI MTNS., CALIFORNIA

LOCATION and ELEVATION		DRILLING HISTORY	
Latitude	34° 56.1' N	Started	10/30/64
Longitude	118° 48.8' W	Stopped	12/19/64
Collar Elevation	2594 feet	Total Depth	1420 feet
Distance from Fault Trace	8 km	Hole Size	NX-Wireline Cased $1\frac{1}{4}$" pipe (perf.)

DEPTH	GEOLOGIC LOG
0 - 1420 feet	Gneissic Diorite

CONDUCTIVITY, GRADIENT, HEAT FLOW, RADIOACTIVITY

Mean Resistivity . . . . . (51)		$145.5 \pm 7.6 \frac{cm \cdot sec \cdot °C}{cal}$
Mean Harmonic Conductivity		$6.87 \pm 0.4 \frac{mcal}{cm \cdot sec \cdot °C}$
Uncorrected Gradient . . . . . (320-420 m)		17.99 ± 0.63 °C/km
Corrected Gradient	Steady State	18.28 ± 0.60 °C/km
	Topographic Evolution	17.95 ± 0.60 °C/km
Uncorrected Heat Flow		1.24 ± 0.08 HFU
Corrected Heat Flow	Steady State	1.26 ± 0.08 HFU
	Topographic Evolution	1.23 ± 0.08 HFU
Limit of Topographic Influence		30 km
Radioactive Heat Production		$1.1 \pm 1.1 \frac{x10^{-13} cal}{cm^3 \cdot sec}$

Table 18

DH-67 TEHACHAPI MTNS., CALIFORNIA

LOCATION and ELEVATION		DRILLING HISTORY	
Latitude	34° 55.9' N	Started	2/13/65
Longitude	118° 48.5' W	Stopped	4/5/65
Collar Elevation	2929 feet	Total Depth	1330 feet
Distance from Fault Trace	$7\frac{1}{2}$ km	Hole Size	NX-Wireline Cased $1\frac{1}{4}$" pipe (perf.)

DEPTH	GEOLOGIC LOG
0 - 1330 feet	Gneissic Diorite (brecciated and altered zone from 1007-1089 ft, including fault gouge)

CONDUCTIVITY, GRADIENT, HEAT FLOW, RADIOACTIVITY

Mean Resistivity . . . . . (40)		$144.7 \pm 7.7 \frac{cm \cdot sec \cdot °C}{cal}$
Mean Harmonic Conductivity		$6.92 \pm 0.4 \frac{mcal}{cm \cdot sec \cdot °C}$
Uncorrected Gradient . . . . . (320-390 m)		18.23 ± 1.14 °C/km
Corrected Gradient	Steady State	19.22 ± 1.20 °C/km
	Topographic Evolution	18.82 ± 1.19 °C/km
Uncorrected Heat Flow		1.26 ± 0.10 HFU
Corrected Heat Flow	Steady State	1.33 ± 0.11 HFU
	Topographic Evolution	1.30 ± 0.11 HFU
Limit of Topographic Influence		30 km
Radioactive Heat Production		Not determined (see DH-65)

Table 19

DH-70 TEHACHAPI MTNS., CALIFORNIA

LOCATION and ELEVATION		DRILLING HISTORY	
Latitude	34° 52.3' N	Started	7/23/64
Longitude	118° 45.1' W	Stopped	2/25/65
Collar Elevation	4832 feet	Total Depth	1070 ft (see text, p. 139)
Distance from Fault Trace	2 km	Hole Size	$4\frac{3}{4}$" tricone Cased $1\frac{1}{4}$" pipe

DEPTH	GEOLOGIC LOG
0 - 1070 feet	Granite (generally weathered or altered and highly fractured)

CONDUCTIVITY, GRADIENT, HEAT FLOW, RADIOACTIVITY

Mean Resistivity . . . . . (14)		$118.9 \pm 1.3 \frac{cm \cdot sec \cdot °C}{cal}$
Mean Harmonic Conductivity		$8.41 \pm 0.1 \frac{mcal}{cm \cdot sec \cdot °C}$
Uncorrected Gradient . . . . . (210-320 m)		21.22 ± 0.08 °C/km
Corrected Gradient	Steady State	26.27 ± 0.28 °C/km
	Topographic Evolution	25.73 ± 0.27 °C/km
Uncorrected Heat Flow		1.78 ± 0.02 HFU
Corrected Heat Flow	Steady State	2.21 ± 0.03 HFU
	Topographic Evolution	2.16 ± 0.03 HFU
Limit of Topographic Influence		30 km
Radioactive Heat Production		Not determined (see DH-14)

Table 20

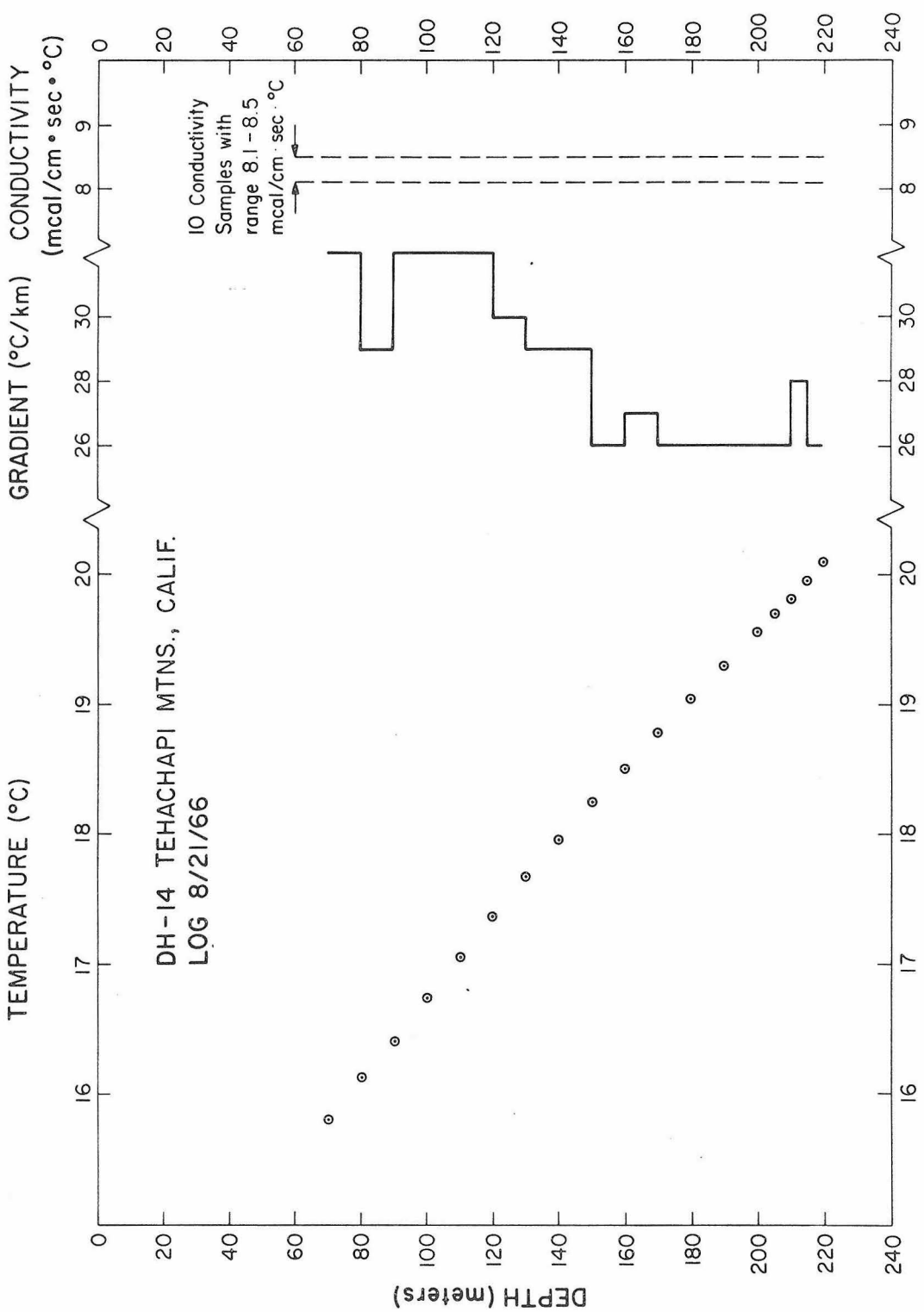
TEMPERATURE (°C)
GRADIENT (°C/km)
CONDUCTIVITY (mcal/cm • sec • °C)
DH-14 TEHACHAPI MTNS., CALIF.
LOG 8/21/66
10 Conductivity Samples with range 8.1 - 8.5 mcal/cm · sec · °C
DEPTH (meters)

Figure 30

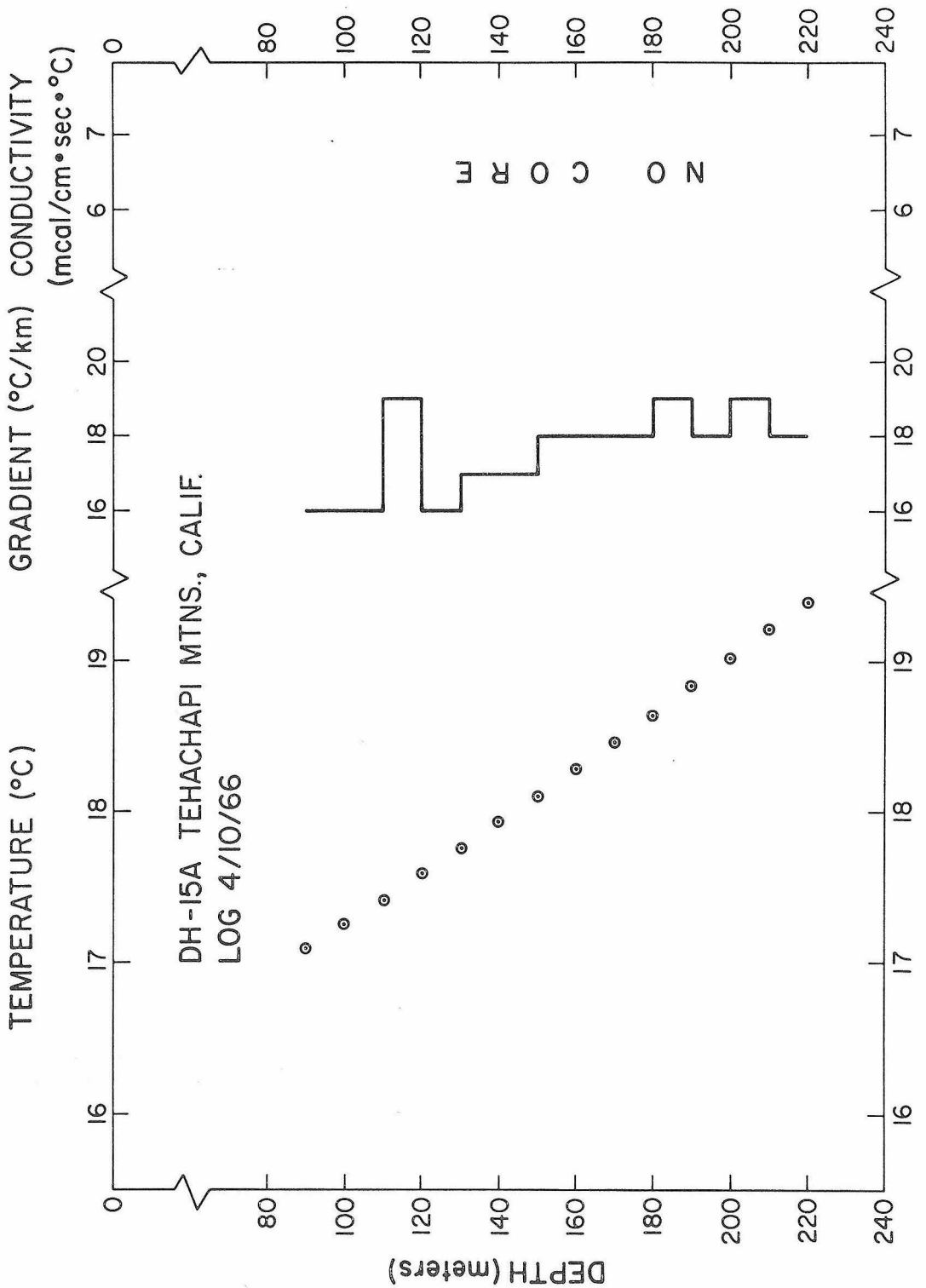
TEMPERATURE (°C)
GRADIENT (°C/km)
CONDUCTIVITY (mcal/cm•sec•°C)
DH-15A TEHACHAPI MTNS., CALIF.
LOG 4/10/66
NO CORE
DEPTH (meters)
0
80
100
120
140
160
180
200
220
240
16
17
18
19
20
6
7

Figure 31

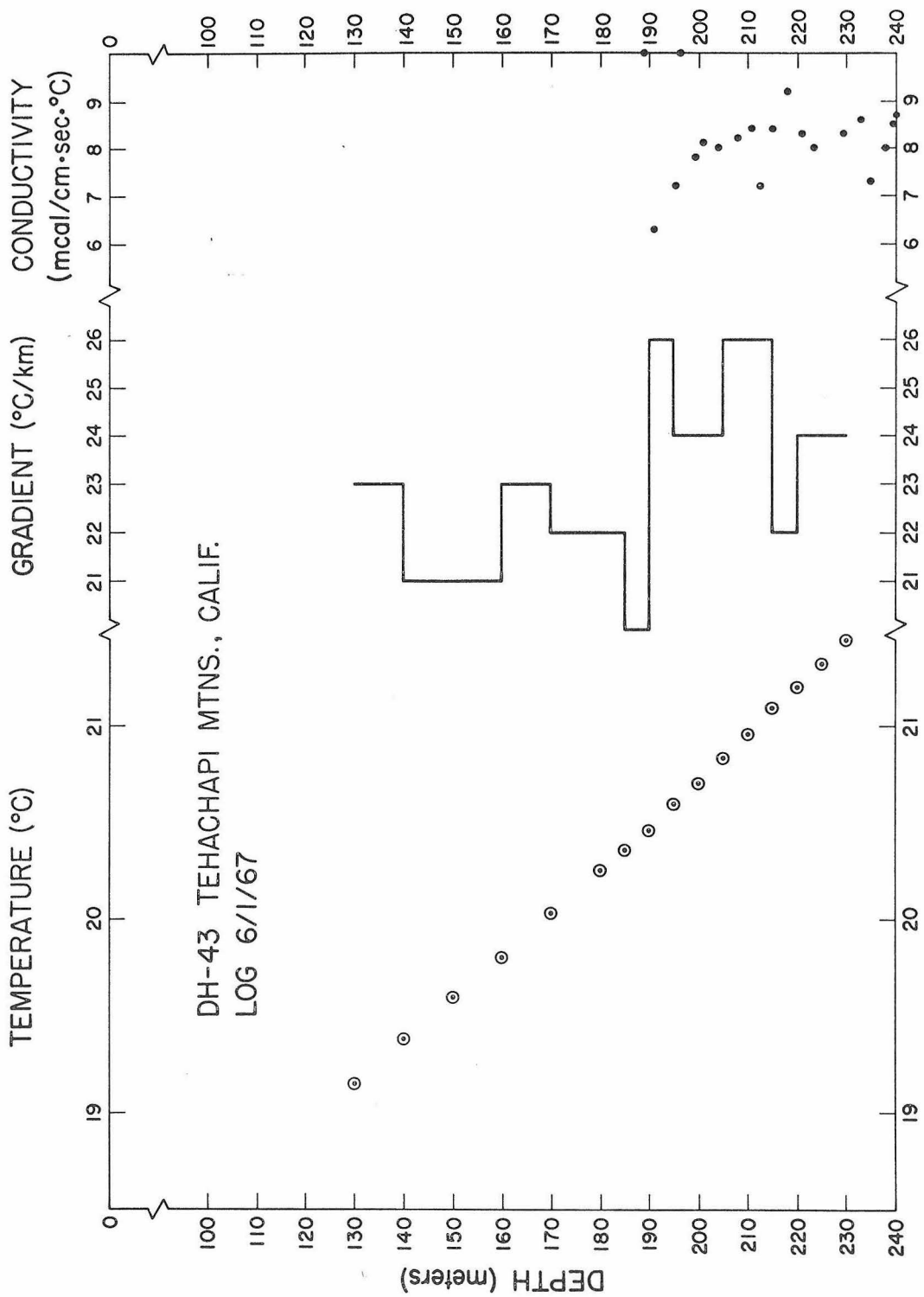
TEMPERATURE (°C)
GRADIENT (°C/km)
CONDUCTIVITY (mcal/cm•sec•°C)
DH-43 TEHACHAPI MTNS., CALIF.
LOG 6/1/67
DEPTH (meters)

Figure 32

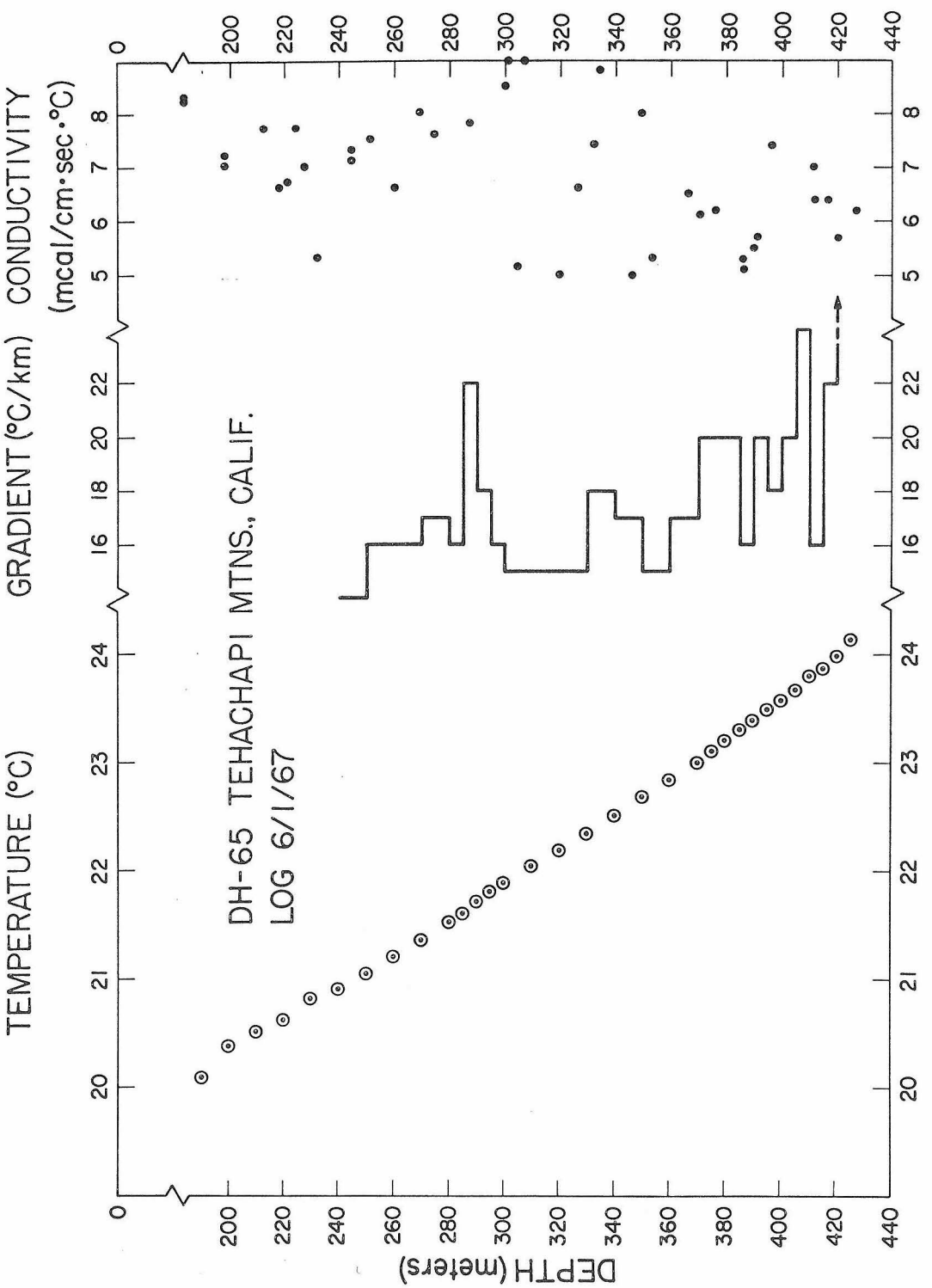
TEMPERATURE (°C)
GRADIENT (°C/km)
CONDUCTIVITY (mcal/cm·sec·°C)
DH-65 TEHACHAPI MTNS., CALIF.
LOG 6/1/67
DEPTH (meters)

Figure 33

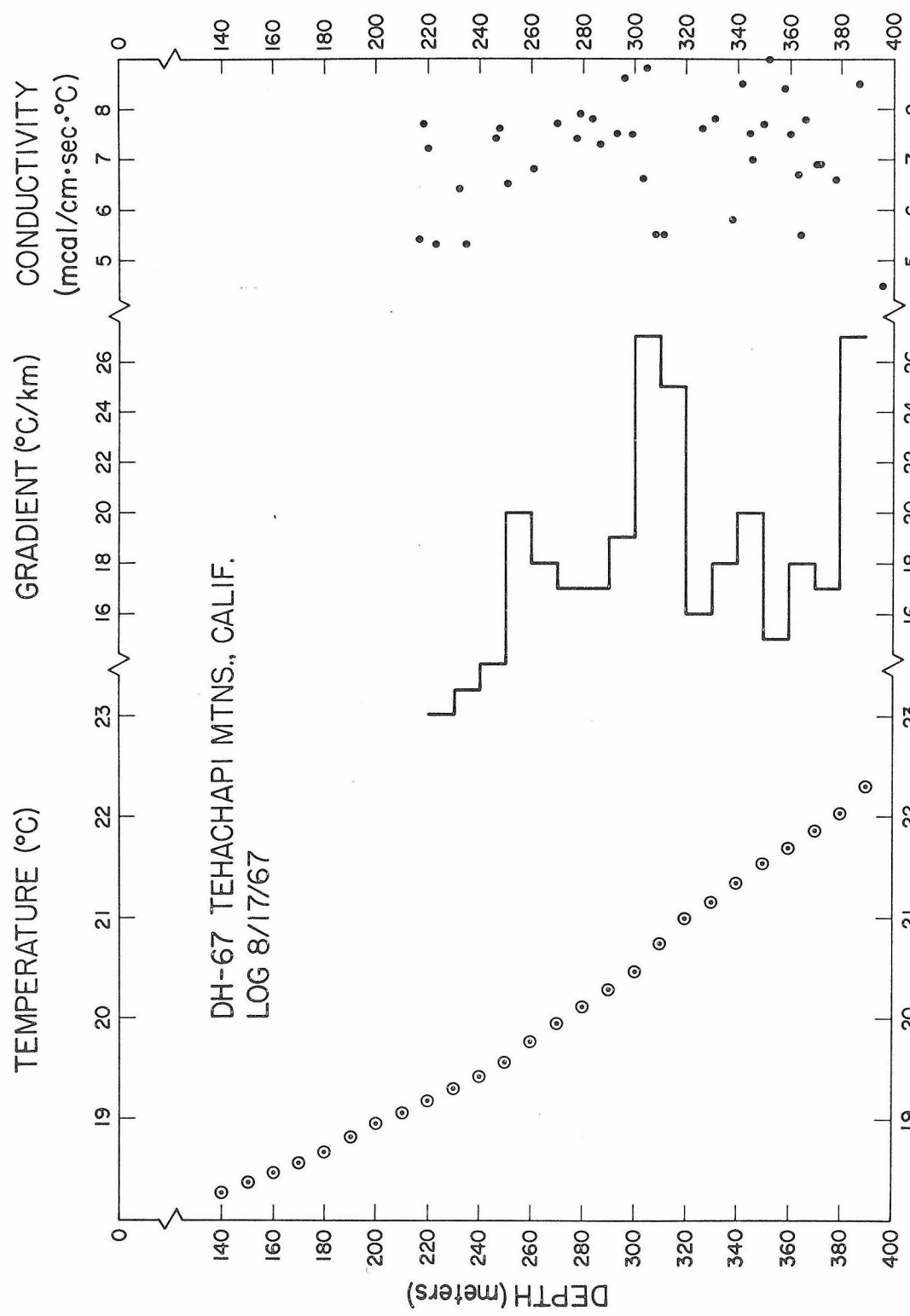
TEMPERATURE (°C)
GRADIENT (°C/km)
CONDUCTIVITY (mcal/cm·sec·°C)
DH-67 TEHACHAPI MTNS., CALIF.
LOG 8/17/67
DEPTH (meters)

Figure 34

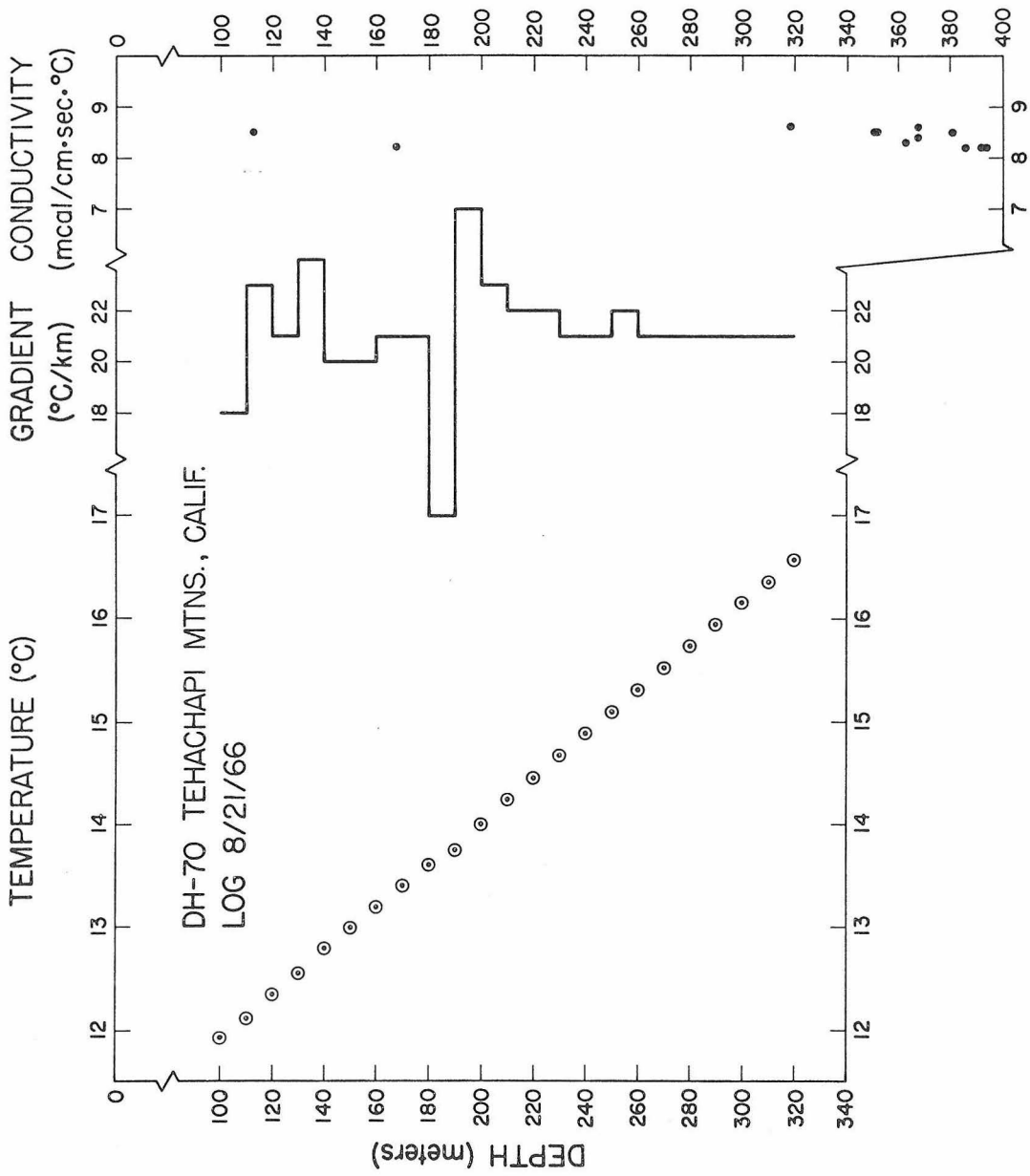
TEMPERATURE (°C)
GRADIENT (°C/km)
CONDUCTIVITY (mcal/cm·sec·°C)
DH-70 TEHACHAPI MTNS., CALIF.
LOG 8/21/66
DEPTH (meters)

Figure 35

region. The rock weathers so readily that outcrops of fresh rock are scarce even in the deeply eroded canyons. Deep weathering to at least 100 meters was common in all drill holes.

Geologic mapping in the vicinity of the drill holes in the Tehachapi Mountains has been carried out by Wiese (1950), Crowell (1952), and Dibblee (1955). A summary of the geology of the Tehachapi Mountains is presented by Buwalda (1954).

The Tehachapi Mountains are generally regarded as part of the Sierra Nevada physiographic province (see Figure 7) and are often geologically considered as the southern end of the rigid, westward-tilted Sierra Nevada block; however, there are some differences in their structure and geologic history. Instead of being an unbroken fault block tilted toward the San Joaquin Valley, the Tehachapi Mountains resemble a broad horst with strong warping and faulting along both margins.

The most extensively distributed rocks in the Tehachapi Mountains are plutonic types of pre-Cretaceous age, generally coarse grained and of diverse mineralogical composition, size, and shape. The average composition is in the quartz dioritic range, much like the Sierra Nevada to the north, but somewhat different from the average quartz monzonitic composition of plutons in the Mojave Block to the south. Residual pendants of pre-intrusive marbles and quartzites are widely scattered south of the Garlock fault and cap the ridge tops and high relief forms in the area. The

only other significant rock type in the area is the strip ($1\frac{1}{2}$ km wide by 30 km long) of Pelona schist which, as we indicated before, is found between the two branches of the Garlock fault.

Tertiary sediments, within the range, are absent in this region, although farther east non-marine strata of Oligocene to Late Miocene age underlie an area of perhaps 50 square miles, suggesting that at least the eastern part of the range stood above sea level during the bulk of Tertiary time.

The area under consideration is one of the most structurally complex regions in California. The intersection of the Garlock and San Andreas faults about 10 km to the west is the meeting point of five major physiographic provinces; the Coast Range, Central Valley, Sierra Nevada, Mojave Desert, and Transverse Range Provinces. The Garlock fault, which lies within the range in this portion of the Tehachapi's, is composed of a north and south branch to the east of the heat flow profile with only the south branch traceable to the west; the north branch is apparently covered by a large thrust sheet (Pastoria Thrust). It is generally recognized on the basis of geomorphological and structural relations that the south branch has been the most recently active segment of the fault, and we will consider it in our discussion to represent the actual trace of the Garlock. However, evidence for Recent activity is lacking along the length of the fault. Smith (1960) argues, on the basis of the relation of dated lake bed sediments to rather fresh-appearing fault scarps along the eastern extent of the Garlock fault, that movement along this portion

has not occurred in the last 50,000 years. Furthermore, seismic and non-seismic strain energy release as determined by seismicity (see Allen, et al., 1965) and strain accumulation (see Meade, 1963) surveys along the Garlock are negligible or lacking when compared with other fault zones in southern California. Thus, while the Garlock is perhaps second to the San Andreas in regional structural importance, it lacks the historical activity of the latter.

Temperature profiles for the six drill holes (DH-14, 15A, 43, 65, 67, and 70) are shown in Figures 30 to 35. Summaries of the pertinent data are given in Tables 15 to 20. Because these holes were drilled by the California State Department of Water Resources specifically for determining the geologic conditions at tunnel level and for the subsequent monitoring of water table depths (similar to the three holes in the San Bernardino Mountains), they were not as suited for heat flow measurements as we would have liked. In some instances, core was not taken in the upper part of the hole or was discarded after drilling. Furthermore, the holes could not be grouted, and perforated casing had to be inserted to allow freedom of water movement. Nevertheless, the results of the measurements appear to be consistent, with one exception as we will note later, and hence are regarded as equally good determinations with respect to the rest of the San Andreas data.

DH-65 and 67 were drilled about 2/3 km apart, 8 km north of the Garlock fault. The heat flow values from both holes are consistent within the statistical limits, each rounding to 1.3 HFU. It will

be noted that only the bottom 70 meters (320-390 m) were used to determine the gradient for DH-67. This was done because the anomalous gradient (high ~ 2.7°C/km) between 300 and 320 meters (see Figure 34) correlates very closely with an anomalous lithology (low conductivity ~ 5.5 mcal/cm· sec· °C) between 307 and 332 meters (see Table 19). Two conductivity measurements were made in the anomalous interval (see Appendix VII), and the product of the average gradient and conductivity for this interval agree with that determined from the final 70 meters. The fact that the anomalous gradient is apparently offset upwards from the anomalous lithologic zone is not surprising since this is to be expected in the practical case of a dipping contact between two mediums of differing conductivity (Jaeger, 1965); and it is likely that this zone has a significant dip. Finally, it can be seen that the gradient above 300 meters returns to the same gradient as that below the 300-320 meter zone.

Figure 36 shows the results of interval heat flows (corrected for steady-state topography) calculated for 10, 20, and 30 meter intervals for DH-67. The number of conductivity samples per 10, 20, and 30 meter interval averaged 2, 4, and 6.5, respectively. The averages of the interval heat flows between 250 and 390 meters are 1.47 HFU, 1.49 HFU, and 1.48 HFU for the respective 10, 20, and 30 meter intervals. These values are significantly higher than the 1.33 HFU value from Table 19. The reason for this inconsistency is that the interval heat flow averages have been unfavorably weighted, a) by the zone of high gradient between 300 and 320 meters (discussed

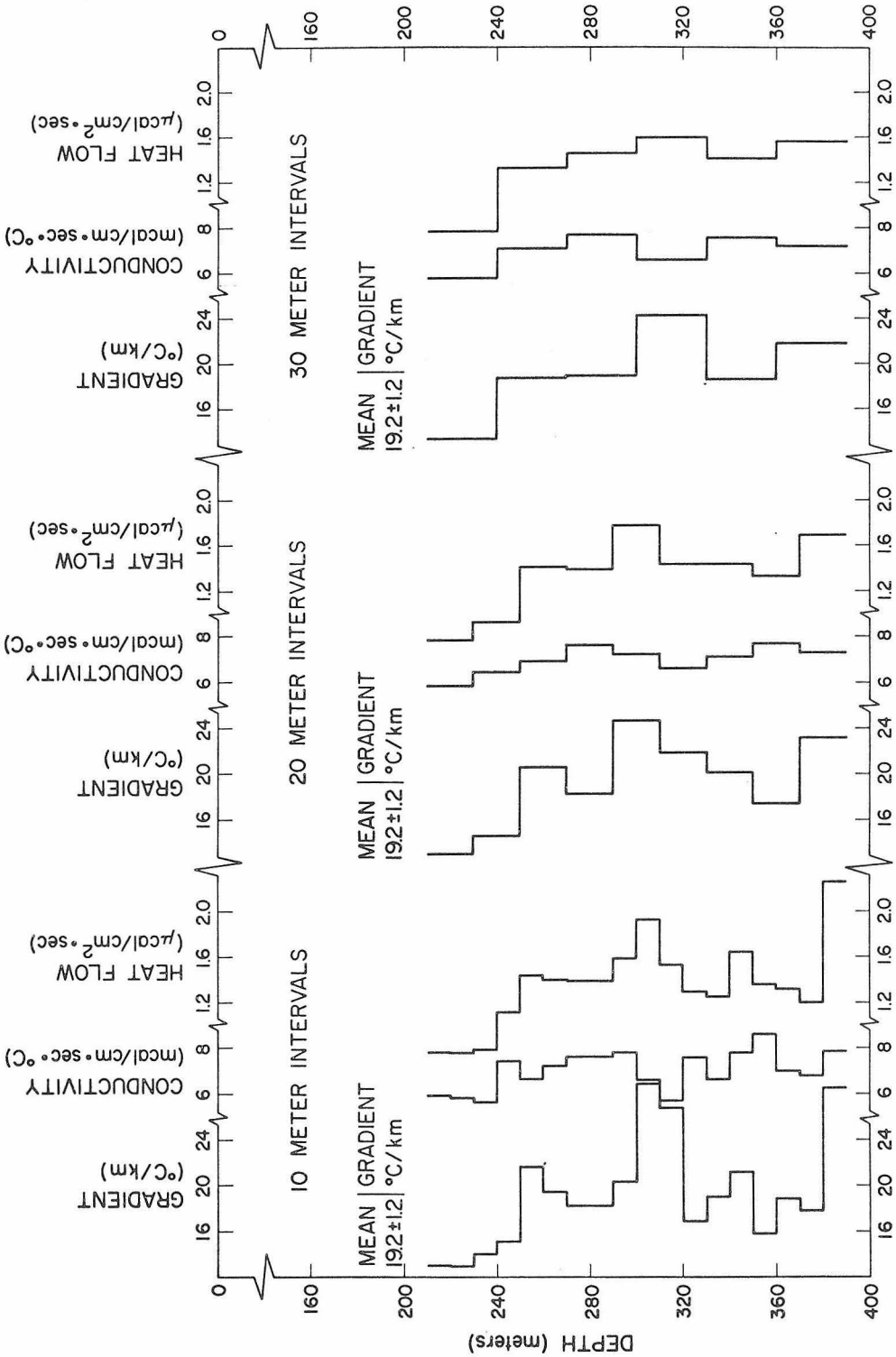

DH-67 TEHACHAPI MTNS., CALIF. INTERVAL HEAT FLOW

Figure 36

previously) for which only two values of the poor conductor were included in the conductivity, and b) by the last 10 meter interval in which the gradient was anomalously high. Removal of these two intervals from the interval averages brings them into line with the 1.33 HFU value.

DH-43 was drilled between the two branches of the Garlock (see Figure 32), where the north branch apparently becomes concealed by the Pastoria thrust fault. The hole was started in gneissic diorite, but at 40 meters apparently encountered the overthrust zone and at 55 meters entered fresh quartz-mica schist which continued to the bottom. The hole was deepened 55 meters, in addition to the 190 meters originally drilled by the Department of Water Resources. All of the temperature measurements relevant to the heat flow determination were made in this final 55 meters, well below the overthrust zone. The heat flow measured here gives a value of 2.0 HFU, significantly higher than the two determinations 7 km to the north.

DH-14 and 70 were drilled $3\frac{1}{2}$ and 2 km, respectively, from the Garlock. DH-14 is located in a canyon bottom and DH-70 on a ridge top in a region of rather severe topography. Both holes are located in the Tejon Lookout Granite (Crowell, 1952), a salmon colored, coarse-grained granite of uniform composition. The range of conductivity values measured on this core was extremely small (see Appendix VII), and only a few samples were really necessary to determine the mean values to high precision. Thus because the core from DH-14 was discarded, without markings, at the drill site, it

was adequate to simply pick up random samples of the discarded core for conductivity measurements. A similar problem was encountered for DH-70. The hole was originally drilled to a depth of 550 meters, but when cased a year later, only the 330 meter depth could be reached. Only spot core was obtained from the surface to this depth, and more continuous coring did not begin until about 370 meters. Again because of the uniformity of the rock, it was judged that measurements of core outside the interval logged would be representative of the entire hole. From Appendix VII (DH-70), we see that the conductivity values obtained for core below 330 meters agree with those values from the spot core above 330 meters. It should be mentioned, however, that the geologic log of the hole (Burckhalter, Calif. State Dept. of Water Resources, 1964-65) indicates that perhaps 50-75% of the rock drilled was altered and/or decomposed, as well as being highly fractured, and it is conceivable the conductivity as determined from the fresh, competent samples overestimated the average in-situ conductivity. Thus it is suggested that the 0.2 HFU higher heat flow obtained at DH-70 compared to the value of 2.0 HFU at DH-14, $1\frac{1}{2}$ km to the south, may be due to either as much as a 10% overestimate of the average conductivity at DH-70, or, more likely, to the inadequacy of the terrain correction for such severe topography. It is somewhat surprising that the heat flows differ by only slightly more than the sum of the statistical limits of error -- 2.0 HFU at DH-14 and 2.2 HFU at DH-70 -- when one considers the magnitude of the terrain corrections (see Tables 30 and 35).

The last of the Tehachapi holes, DH-15A, was drilled about $4\frac{1}{2}$ km south of the Garlock. No core was taken throughout the length of the hole with the exception of the bottom 30 meters (250-280 m) where a few broken and decomposed samples were obtained. The remainder of the geologic log was determined by inference from drill cuttings and drilling action (Jackson, Calif. State Dept. of Water Resources, 1963). As a result, no conductivity determinations could be made. However, the geologic map of the area and the broken core samples suggested that the granite is the same as that at DH-14 and 70. For this reason, the average of the values obtained at these other two holes was used for calculating the heat flow for DH-15A. As can be seen (Table 31), the heat flow of 1.5 HFU appears anomalously low -- even with the high conductivity used. Because the hole was drilled near a contact with limestone, the low heat flow suggested the possibility that the limestone had been dolomitized, and was either causing a refraction effect or perhaps even controlling the temperature gradient in the region, the granite being a dike within the dolomite. Dolomites have conductivities characteristically in the range 10-13 mcal/cm· sec· °C (Clark, 1966). A piece of limestone core from near the contact was measured and found to have a conductivity of about 7 mcal/cm· sec· °C, actually somewhat lower than the granite and in the limestone range. Temperature measurements in the hole were quite stable and the gradient uniform, suggesting no circulation of water in the hole, itself. In the absence of measured conductivities, it is necessary to regard the determination at DH-15A as second class,

and it is futile to speculate on large scale ground water circulation below the hole without any evidence.

Before proceding with the discussion of the geologic history, we want to consider a possible effect on the heat flow of the lithologic change across the Garlock fault. The conductivity of the gneissic diorite north of the north branch of the Garlock fault is about 6.9 mcal/cm· sec· °C (from DH-65 and 67), while to the south it is about 8.3 mcal/cm· sec· °C (from DH-43, 14, and 70) -- a 20% change across the fault. As a result of this situation, it is likely that heat flow determinations made near the boundary will require a correction for the refraction of heat from the poorer conductor into the better one. We can idealize the problem in the following way. Consider the composite infinite slab $0 < z < d$, of which $x > 0$ is of conductivity k_1 and $x < 0$ is of conductivity k_2 with the boundary conditions (Figure 37, p. 140)

$$v = 0, \quad z = 0, \quad -\infty < x < \infty$$

$$v = V_1, \quad z = d \quad x > 0$$

$$v = V_2, \quad z = d \quad x < 0$$

where v is the temperature; then if V_1 and V_2 are the temperatures for $x > 0$ and $x < 0$, respectively, we have (Carslaw and Jaeger, §16.4, 1959)

$$v_1 = \frac{zV_1}{d} - \frac{2k_2(V_2 - V_1)}{\pi(k_1 + k_2)} \sum_{n=1}^{\infty} \frac{(-1)^n}{n} \sin \frac{n\pi z}{d} e^{-\frac{n\pi x}{d}}, \qquad x > 0$$

$$v_2 = \frac{zV_2}{d} + \frac{2k_1(V_2-V_1)}{\pi(k_1+k_2)} \sum_{n=1}^{\infty} \frac{(-1)^n}{n} \sin\frac{n\pi z}{d}\, e^{\frac{n\pi x}{d}}, \qquad x < 0$$

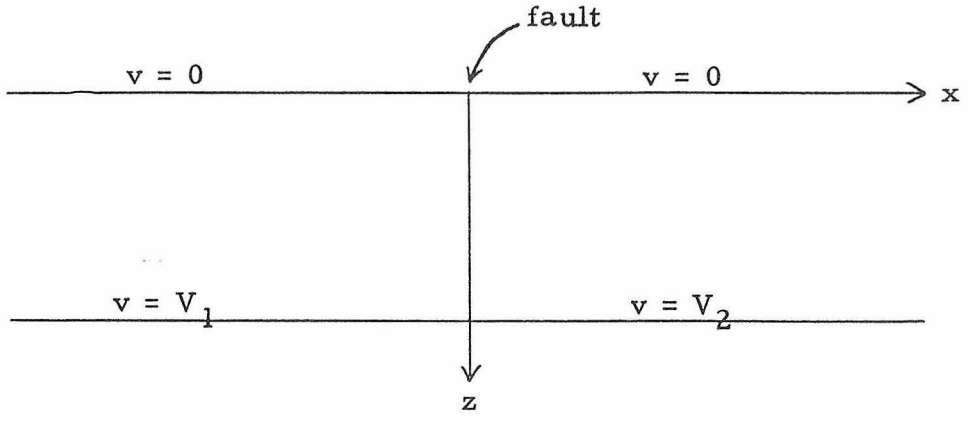

Figure 37

Now if we want to consider the flux at the surface, we have,

$$k_1 \frac{\partial v_1}{\partial z}\Big|_{z=o} = \frac{k_1 V_1}{d} - \frac{2k_1k_2(V_2-V_1)}{d(k_1+k_2)} \sum_{n=1}^{\infty} (-1)^n e^{-\frac{n\pi x}{d}}, \qquad x > 0$$

$$k_2 \frac{\partial v_2}{\partial z}\Big|_{z=o} = \frac{k_2 V_2}{d} + \frac{2k_1k_2(V_2-V_1)}{d(k_1+k_2)} \sum_{n=1}^{\infty} (-1)^n e^{\frac{n\pi x}{d}}, \qquad x < 0 \qquad (23)$$

Now let us consider a crude physical model. First of all, we will take k_1 = 6.9 mcal/cm· sec· °C and k_2 = 8.3 mcal/cm· sec· °C. If we assume that the plutons extend to a depth of 10 km, we set d = 10 km. Let us arbitrarily set V_1 = 200°C on the basis of a 20°C/km gradient, then if we make the assumption that the fluxes from below 10 km into both plutons are equivalent as $|x| \to \infty$ we have

$$k_1 V_1 = k_2 V_2$$

or

$$V_2 = \frac{k_1 V_1}{k_2} \simeq 166°C$$

Putting these numerical values into (23), we have

$$\begin{aligned} k_1 \frac{\partial v_1}{\partial z}\Big|_{z=o} = q_1 &= 1.38 + 0.256 \sum_{n=1}^{\infty} (-1)^n e^{-\frac{n\pi x}{10}} \text{ HFU}, \quad x > 0 \\ k_2 \frac{\partial v_2}{\partial z}\Big|_{z=o} = q_2 &= 1.38 - 0.256 \sum_{n=1}^{\infty} (-1)^n e^{\frac{n\pi x}{10}} \text{ HFU}, \quad x < 0 \end{aligned} \tag{24}$$

Now

$$\left[\sum_{n=1}^{\infty} (-1)^n e^{-\frac{n\pi x}{10}}, \quad x > 0\right] = \left[\sum_{n=1}^{\infty} (-1)^n e^{\frac{n\pi x}{10}}, \quad x < 0\right]$$

$$\simeq -0.43 \text{ for } x = 1 \text{ km}$$

$$\simeq -0.28 \text{ for } x = 3 \text{ km}$$

$$\simeq -0.04 \text{ for } x = 10 \text{ km}$$

Putting these into (24), we get

$q_1 = 1.49$ HFU; $q_2 = 1.27$ HFU for $|x| = 1$ km

$q_1 = 1.45$ $q_2 = 1.31$ for $|x| = 3$ km

$q_1 = 1.39$ $q_2 = 1.37$ for $|x| = 10$ km

Thus a 20% change in conductivity produces a 17% apparent difference in heat flow at locations 1 km on either side of the discontinuity, an 11% difference at 3 km, and at 10 km, i.e. $\sim d$, the effect is down to about $1\frac{1}{2}$%. If we apply these results to the actual case of the drill holes in the Tehachapi's, we have that

DH-43	2.0 HFU	High by $8\frac{1}{2}$ % → 1.8 HFU
DH-70	2.2	High by $5\frac{1}{2}$ % → 2.1
DH-14	2.0	No change
DH-15A	1.5	No change
DH-65	1.3	No change
DH-67	1.3	No change

In the case of the Tehachapi's, we might be able to somewhat improve the model since we probably do not have the condition that as $|x| \to \infty$ the fluxes approach the same value. Rather, we have that the flux in region (1) is perhaps 25% lower at "infinity" than in region (2). However, the estimates which we have given will probably be about the same, within the uncertainties of the model. Due to our imprecise knowledge of the actual geology, as well as the inexactness of the model, these corrections must remain as speculative.

Tables 15 to 20 give the heat flow values for a physiographic evolution of 12 m. y. The Tehachapi Mountains, as we suggested earlier, probably have had a somewhat different history from the Sierra Nevada to the northeast and, for that matter, the Coast Range to which they connect to the northwest. The Tertiary deformation has probably been somewhat intermediate, in time and magnitude, between that of the two adjacent provinces.

The pre-Tertiary history of the Tehachapi's as far as can be told is similar to the rest of southern and eastern California. At the time of the Nevadan orogeny in Late Jurassic or Early Cretaceous,

the region was covered with perhaps 15 km of strata (Dibblee, 1955), such that they were subjected to regional metamorphism. At this depth they were intruded by molten magma, chiefly quartz diorite, at which time uplift occurred, with a long interval of erosion through Cretaceous and Early Tertiary time to a crystalline surface of low relief. Whether or not the Tehachapi Mountains were ever largely covered by Tertiary sedimentary formations similar to those in the Coast Ranges is not known. It is clear that some of the interior parts in the eastern part of the range were not (Buwalda, 1954). There, sections of continental Oligocene to Miocene deposits are found. However, Dibblee suggests that the western part of the range may have remained barely submerged until Pliocene time. Evidence for this is the fact that the Tehachapi's merge into the San Emigdio Range to the west which contains thick Tertiary marine sections, and that the ancestral continental-marine shoreline is found in the westernmost tip of the Mojave Desert, which Dibblee says can be correlated with the similar line in the southern San Joaquin Valley, suggesting continuity of this depositional environment across the Tehachapi's in Miocene time.
It is likely then that the Tehachapi region was included in the general westward tilt, which became more intense to the north, creating a continental to marine environment upon which was later superimposed the general Tehachapi uplift at the beginning of Pliocene time (Dibblee, 1955). The Tertiary sections exposed along the flanks of the mountains now dip away at moderate to steep angles indicating vigorous deformation in Tertiary and post-Tertiary time. We suggest that

uplift from essentially sea level commenced some 12 m. y. ago.

Just how much erosion has occurred is again more difficult to evaluate. Crowell (1952) has suggested that some of the upland areas may be remnants of old erosion surfaces. In the western part of the range, south of the Garlock fault, the high relief is commonly capped with the old pre-intrusive metasediments. Because the range is so narrow and deeply incised, however, these surfaces are small and not well defined. Furthermore, we have no evidence for the amount of Tertiary cover that might have been stripped away. Generally, Tertiary sections are observed to thicken rapidly away from the mountains, suggesting the Tertiary cover within the range might have been relatively thin. To make the minimum, yet probably good approximation for the evolution of topography, we will assume that in the last 12 m. y. we have had an uplift of a surface of low relief from sea level to 1. 5 km south of the Garlock and 1. 3 km north of the fault (elevations of highest surfaces and tops of metasedimentary remnants), with an amount of erosion at each drill site equal to the difference between its collar elevation and the average maximum elevations, thereby assuming no initial Tertiary cover (Buwalda estimates a minimum of 1. 6 km of uplift). We would then have the following 12 m. y. summary for each drill hole

DH-14	1.5 km uplift	0.3 km erosion
DH-15A	1.5 " "	0.3 " "
DH-43	1.3 " "	0.2 " "
DH-65	1.3 " "	0.5 " "
DH-67	1.3 " "	0.4 " "
DH-70	1.5 " "	0.0 " "

It is likely that part of the elevation difference at DH-65 and 67 could be a result of the slope of the original flexure, especially when one considers the way in which the Tertiary sediment-crystalline contact is dipping to the north, into the valley away from the range. For this reason, we have corrected the previous figures of DH-65 and 67, based on a 30° dip of the contact surface (Hoots, 1930), to

DH-65	1.1 km uplift	0.3 km erosion
DH-67	1.2 " "	0.3 " "

From Tables 15 to 20, it is seen that at each hole the heat flow value corrected for a 12 m.y. topographic evolution is within 0.05 HFU of the steady-state value.

F. Heat Flow near Hollister, California

A single hole, HO-1, was drilled near Hollister, California, as part of the initial San Andreas fault project. However, because of the extreme interest in the rather unique fault activity found along the fault south of Hollister, an additional seven holes were drilled as part

of a continuing program, at various distances from the fault in the same region as HO-1 (see Figure 7) (R. F. Roy, J. N. Brune, and T. L. Henyey, Heat flow in a zone of high creep rate along the San Andreas fault, in preparation). The heat flow values for these sites are still in a preliminary state, but are precise enough to help complete the fault and regional picture; they will be discussed in terms of PHFU (preliminary heat flow units).

HO-1 is located 3 km west of the San Andreas fault zone in a quartz diorite, part of the Gabilan Mountains batholith. The Gabilan Mountains are part of the Coast Ranges physiographic province and represent the largest outcropping of crystalline rock in the province between the Klammath Mountains of northwestern California and the Tehachapi Mountains. The California Coast Ranges form a northwest-southeast trending structural belt bordering the Pacific Ocean from the Transverse Ranges northward.

Figure 38 shows HO-1 relative to the local geology. Also shown are the locations and preliminary heat flow values for the other seven holes. Detailed geologic mapping does not exist for the region immediately surrounding the location of HO-1; however, adjacent regions have been mapped in some detail, primarily in the sedimentary sequence to the east (see, for example, Allen, 1946; Wilson, 1943; Andrews, 1936; and Bowen and Gray, 1959). Although the San Andreas fault lies within the Coast Ranges Province in the Hollister region, the geologic environments on opposite sides of the fault, dominated to the east by the Franciscan core complex and to

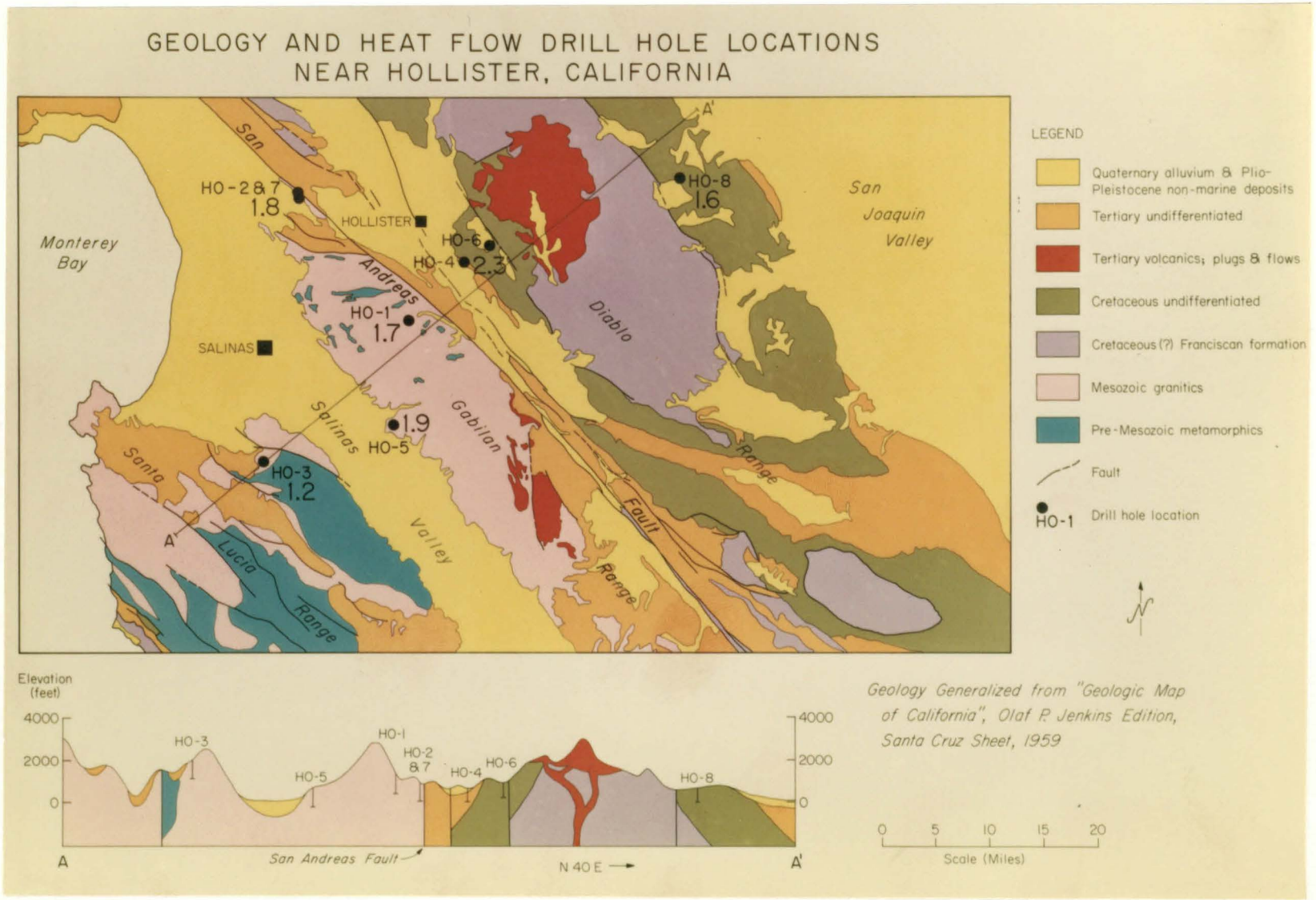
GEOLOGY AND HEAT FLOW DRILL HOLE LOCATIONS
NEAR HOLLISTER, CALIFORNIA
Monterey Bay
San Andreas
HO-2&7 1.8
HOLLISTER
HO-6
HO-4 2.3
HO-1 1.7
SALINAS
HO-8 1.6
San Joaquin Valley
Diablo Range
Gabilan Range
Salinas Valley
HO-5 1.9
HO-3 1.2
Santa Lucia Range
Fault
A
A'
LEGEND
Quaternary alluvium & Plio-Pleistocene non-marine deposits
Tertiary undifferentiated
Tertiary volcanics; plugs & flows
Cretaceous undifferentiated
Cretaceous (?) Franciscan formation
Mesozoic granitics
Pre-Mesozoic metamorphics
Fault
HO-1 Drill hole location
Elevation (feet)
4000
2000
0
HO-3
HO-5
HO-1
HO-2 &7
HO-4
HO-6
HO-8
San Andreas Fault
N 40 E
Geology Generalized from "Geologic Map of California", Olaf P. Jenkins Edition, Santa Cruz Sheet, 1959
0 5 10 15 20
Scale (Miles)

Figure 38

the west by the Salinian granitic-metamorphic core complex, are as dissimilar and mutually incompatible as any other two adjacent terranes along the entire length of the fault. Healy (1963) and Stewart (1967) have also found from seismic refraction profiles a significant difference in crustal structure between these two regions. They suggest a thin 23 km crust for the Gabilan block and a 32 km thick crust under the Diablo Range, with abnormally high crustal velocities.

The Franciscan consists of a diverse assemblage of eugeosynclinal rocks of presumably Cretaceous age, lacking systematic structure and regional metamorphism. No granitic rocks are found as part of the sequence although intrusions of ultramafic rock, primarily serpentines, are common associates of the Franciscan assemblage. Sandstones, chiefly graywackes, are the most prevalent rock types with shales, greenstones, and cherts making up the rest of the major lithic components. Overlying and in fault contact with the Franciscan core is a thick section of upper Cretaceous marine deposits, consisting largely of sandstones, shales, and conglomerates. Thick sections of marine Tertiary strata unconformably overlie the Cretaceous deposits, especially to the east of the Coast Ranges.

The granitic-metamorphic complex to the west of the San Andreas is termed the Salinian Block. It is bounded on the west by the Nacimiento fault, where the block is again juxtaposed with Franciscan rocks. Thus the Salinian granitic and metamorphic rocks, which are only locally exposed, form a long tract extending from the

Transverse Ranges to the northern extent of the San Andreas fault, the northern part largely under the sea and extending to the edge of the continental shelf. The northern Santa Lucia Range (see Figure 38) west of the Salinas Valley, consists of a composite of granitics and metamorphics, while the basement in the Gabilan Range, east of the valley, consists almost entirely of granitic rocks, with only minor metamorphic remnants or pendants. The San Andreas fault on the east flank of the Gabilan Range exhibits active creep in the vicinity of HO-1. The famed Almadén winery, several structures of which sit astride an active segment of the fault, is only about 3 km to the east of the drill site.

Figure 39 and Table 21 give the pertinent data from HO-1. The hole was drilled in a quartz dioritic body of unknown extent, which for the most part is quite fresh and unfractured. However, a large fracture zone was encountered from about 210 to 260 meters and is the cause of the temperature disturbance seen in Figure 39, most pronounced at about 260 meters. Cement grouting of the entire hole was attempted, but, if successful at all, was only so in the last 20 meters, which was the part of the hole used to derive the gradient. Temperatures in this zone were quite stable and the gradient could be consistently reproduced.

Descriptions of the seven preliminary heat flow determinations near Hollister will not be given in detail here. The following table summarizes the heat flow for these holes. Only a limited number of conductivity determinations have been made for these holes, and a

HO-1 HOLLISTER, CALIFORNIA

LOCATION and ELEVATION		DRILLING HISTORY	
Latitude	36° 43.3' N	Started	5/27/66
Longitude	121° 24.4' W	Stopped	6/28/66
Collar Elevation	1080 feet	Total Depth	1000 feet
Distance from Fault Trace	3 km	Hole Size	BX-Wireline Cased $1\frac{1}{4}$" pipe

DEPTH	GEOLOGIC LOG
0 - 300 feet	Quartz Monzonite
300 - 1000 feet	Quartz Diorite (badly fractured zone from 700-850 feet)

CONDUCTIVITY, GRADIENT, HEAT FLOW, RADIOACTIVITY

Mean Resistivity . . . . . (27)		$152.0 \pm 1.8 \frac{cm \cdot sec \cdot °C}{cal}$
Mean Harmonic Conductivity		$6.58 \pm 0.1 \frac{mcal}{cm \cdot sec \cdot °C}$
Uncorrected Gradient . . . . . (278-300 m)		30.22 ± 0.13 °C/km
Corrected Gradient	Steady State	26.00 ± 0.09 °C/km
	Topographic Evolution	----
Uncorrected Heat Flow		1.99 ± 0.02 HFU
Corrected Heat Flow	Steady State	1.71 ± 0.02 HFU
	Topographic Evolution	----
Limit of Topographic Influence		10 km
Radioactive Heat Production		$3.4 \pm 1.0 \frac{x10^{-13} cal}{cm^3 \cdot sec}$

Table 21

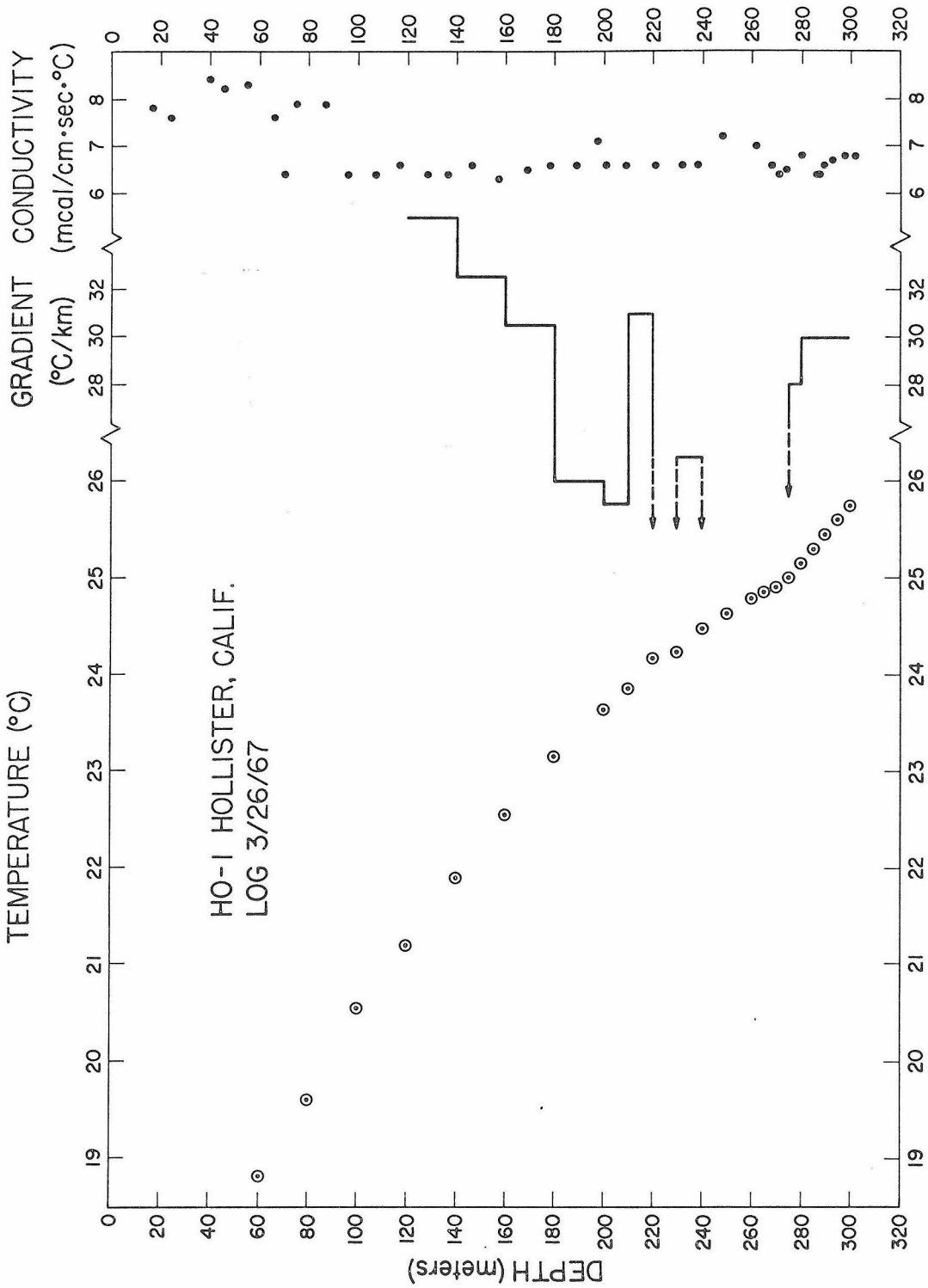
TEMPERATURE (°C)
GRADIENT (°C/km)
CONDUCTIVITY (mcal/cm·sec·°C)
HO-1 HOLLISTER, CALIF.
LOG 3/26/67
DEPTH (meters)

Figure 39

rough terrain correction to only 10 km. The values are probably good to ±10%.

Hole	Corrected H. F. (steady-state)
HO-2	1.7 PHFU
HO-3	1.2
HO-4	2.3
HO-5	1.9
HO-6	2.3
HO-7	1.7
HO-8	1.4*

* Incorrect on map

Table 22

G. Heat Flow between San Diego and El Centro, California

Figure 40 shows the locations of six preliminary heat flow determinations between San Diego and El Centro, California, from work by Roy and Brune (personal communication). The following table summarizes the heat flow. Again, only a limited number of conductivity determinations have been made, and no terrain corrections have been made. The values are probably good to ±15%.

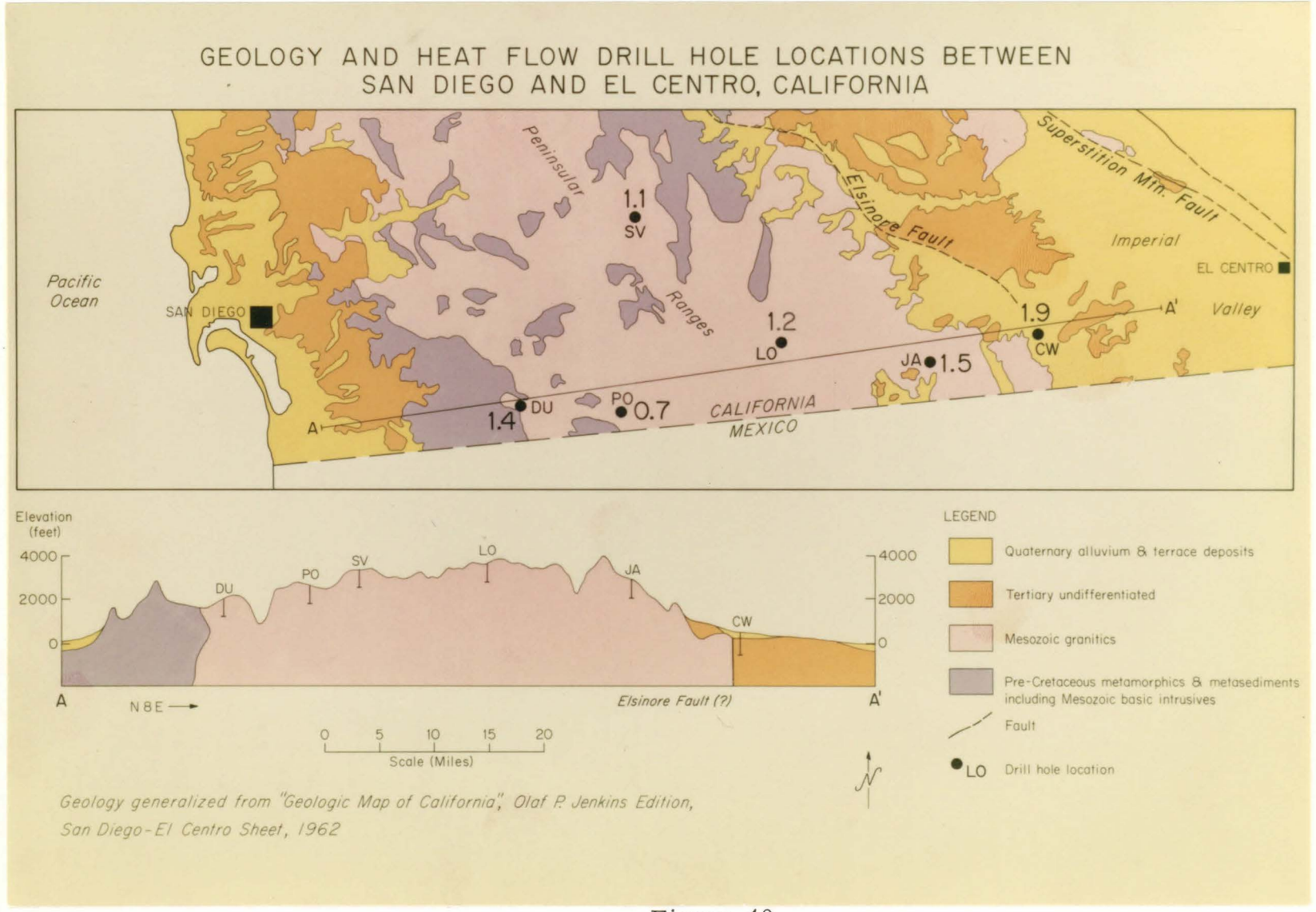
GEOLOGY AND HEAT FLOW DRILL HOLE LOCATIONS BETWEEN SAN DIEGO AND EL CENTRO, CALIFORNIA
Pacific Ocean
SAN DIEGO
Peninsular Ranges
Elsinore Fault
Superstition Mtn. Fault
Imperial Valley
EL CENTRO
1.1 SV
1.2 LO
1.9 CW
1.5 JA
1.4 DU
0.7 PO
A
A'
CALIFORNIA
MEXICO
Elevation (feet)
4000
2000
0
DU
PO
SV
LO
JA
CW
N 8 E
Elsinore Fault (?)
0 5 10 15 20
Scale (Miles)
LEGEND
Quaternary alluvium & terrace deposits
Tertiary undifferentiated
Mesozoic granitics
Pre-Cretaceous metamorphics & metasediments including Mesozoic basic intrusives
Fault
LO Drill hole location
Geology generalized from "Geologic Map of California", Olaf P. Jenkins Edition, San Diego-El Centro Sheet, 1962

Figure 40

Hole	Uncorrected H. F.
LO	1. 1 PHFU
PO	0. 8*
SV (2 holes)	1. 2
JA	1. 5
CW	1. 9
DU	1. 3

*Incorrect on map

Table 23

These data complete the presentation of the recently obtained data directly pertinent to the study of heat flow near the major strike-slip faults in central and southern California. Additional values from California and parts of the western United States bearing on the regional heat flow pattern will be presented simply in map form in the last section.

VIII. DISCUSSION

A. General Statement

The purpose of this investigation was to determine the extent to which heat generated by the San Andreas fault system affected heat flow in the vicinity of the fault as compared to the regional heat flow in central and southern California. Primary consideration is given to the hypothesis that fault zones are direct sources of heat due to strain energy conversion via non-elastic processes. A semi-quantitative basis for estimating the magnitude of the strain energy effect is presented in terms of fault mechanisms in the first part of this section. Included in this part are some theoretical models of heat flow from faults of different geometries. In the second part, the heat flow data are discussed in light of these considerations. The heat flow determinations of other investigators are then used to help complete the regional picture in central and southern California. The association of the San Andreas fault system with the regional heat flow pattern is examined. These major structural features will be interpreted, not as sources of heat, but primarily as boundaries between provinces characterized by different heat flows.

B. Energy Regime of a Fault

Whether or not a heat flow anomaly is associated with a fault depends upon the answers to several questions; first, is the fault or motion along the fault capable of producing an observable amount of

heat? Second, if these sources (providing they existed) were spatially distributed in a reasonable way, would the anomaly still be measurable; and third, can this anomaly be isolated from equally significant anomalies attributable to other energy sources and/or geologic and topographic conditions in the neighborhood of the heat flow measurements? It is hoped the following discussion will provide at least a partial answer to these queries.

Stored strain energy can be converted via elastic and numerous non-elastic processes to other forms of energy in the neighborhood of a fault zone. In principle, it is not necessary for a large earthquake to occur for release of strain energy. Recently, widespread investigations throughout California suggest that creep movements may be responsible for major fault offsets and perhaps considerable energy release (see Whitten, 1955; Steinbrugge, et al., 1960; Meade, 1963 and 1966; Cluff and Steinbrugge, 1966; Radbruch, 1967). We will consider the following scheme as representative of the partition of strain energy release in the vicinity of a fault:

1) Seismic Wave Energy. A significant part of the strain energy released during earthquakes is converted to seismic waves via an elastic process, and this energy is removed for the most part from the fault zone and dissipated throughout the entire earth through non-elastic processes. The amount of energy involved in wave propagation has been investigated empirically as a function of earthquake magnitude by various investigators (Gutenberg and Richter, 1956; Salovyov, 1959; Båth, 1958; DeNoyer, 1958 and 1959). This

is the only part of the energy regime whose absolute value is known with any degree of certainty. The relationship derived by Gutenberg and Richter (1956) expresses the total energy E (in ergs), radiated as seismic waves, in terms of the Richter source magnitude M in the following way

$$\log_{10} E = 11.8 + 1.5\,M \qquad (25)$$

If it is assumed that on the average two magnitude 8.3 earthquakes per century occur along the length of the San Andreas fault (based on the two known such events in the last 100 years), it follows from (25) that ~0.3 calories per second per cm of fault length of seismic energy are produced along the 800 km length of the fault.

A more recent investigation of earthquake energies by Wu (1966) suggests that the Gutenberg-Richter relation (henceforth abbreviated to G-R relation) predicts seismic energies which are low by an order of magnitude. Thus 0.3 cal/sec/cm of fault should be considered a lower bound on seismic energy release.

2) Heat Production due to Anelastic Behavior. Creep and to a lesser extent plastic deformation are non-elastic processes which may involve significant amounts of energy release in the vicinity of active fault zones. Creep can occur across a single fault plane or across an entire zone many km on either side of the fault trace, as, for example, near Hollister. These processes, which involve strain energy conversion to heat via internal friction, are most intense in a zone near the fault plane, and therefore represent a primary fault heat source. Large earthquakes undoubtedly trigger creep and plastic

deformation, although, as indicated earlier, creep may be responsible for fault displacements over a given length of time equivalent to primary offsets due to faulting at the time of a seismic event. A recent earthquake near Parkfield, California (July, 1966), involving several inches of primary ground displacement has been accompanied by an equivalent amount of creep offset since the earthquake occurred.

For the purposes of energy calculations, this zone will be represented by a plane, and the motions projected on the plane such that the sum of all relative displacements occurs across this plane. Thus, creep will be thought of as the gradual movement of the two fault surfaces past one another under the influence of sliding friction.

3) Heat Production due to Sliding Friction during a Rapid Fault Dislocation. This process should probably be considered as a corollary to 2) since it may be considered a singular case of creep. However, we want to distinguish it from the general creep mechanism because it may be an important factor of energy release during the primary offset accompanying a major earthquake. We will discuss the energy release during the process of slip in terms of an average stress and a stress-drop.

4) Formation of Higher Energy Minerals or Phases. Zones of mylonitization, cataclasis, and crushed rock are common along major faults (Sharp, 1965); high energy mineral assemblages and hot springs (see Stearns, Stearns, and Waring, 1937) are also common along zones of faulting. Formation of these various lithologies, minerals, and phases involve endothermic or endoenergetic

processes. These processes will be assumed insignificant relative to the total energy regime of a fault in this discussion.

5) The Movement of Masses with and Against Gravity. The effect of this process on the energy regime may be important in dip-slip faulting and may be either positive or negative, depending upon the relative movement of the center of mass of both fault blocks with respect to the center of the earth, but is probably insignificant over a long period of time in the case of strike-slip faulting since we can assume the total contribution has averaged zero. It is interesting to note that dip-slip movements can be sources or sinks of significant amounts of energy when they involve large blocks of crustal material. For example, if we consider a block of crust undergoing say an uplift at a rate r, the work done per unit time would be given by

$$E = \rho V g r$$

where ρ is the density of the material, V the volume of the block, and g the average value of the acceleration of gravity. If we consider a 10 km wide strip of 30 km thick crustal material to be uplifted at a rate of 7.5 meters per 1000 years (Shumm, 1963), the work done will be about 5 cal/sec/cm of strip length, or perhaps 10 times the amount of energy associated with seismic wave generation along a major fault.

How then, from consideration of this sort of an energy scheme, might one attempt to estimate the amount of strain energy converted to heat in the vicinity of the fault? We have suggested that the bulk

of the strain energy released along a fault will be converted either to seismic waves through elastic processes or to heat by dissipative processes. Let us consider first what we know most reliably about the energy scheme, namely, the amount of energy converted to elastic waves as given by the G-R relation. Based on limited earthquake statistics and the validity of the G-R relation, the statement has been made that it is reasonable to expect 0.3 calories per second of seismic energy to be liberated per cm of fault. We can then add that, depending upon the efficiency of seismic wave generation, it is conceivable that an equivalent amount of energy will be converted to heat in the neighborhood of the fault. Heat production on the order of 1 cal/sec/cm of fault length might be expected to produce a significant increase in heat flow (depending on fault geometry) in the vicinity of a major fault zone. Thus the point of this line of reasoning has been that energies, reasonably associated with major strike-slip faults (albeit seismic energy), are consistent with a measurable surface heat flow.

A second approach is to determine, if possible, the energy difference in the shear fields before and after faulting and subtract the energies not available for local heat production -- in particular, the seismic energy. Energy differences have been investigated theoretically by several people who consider uniform dislocations in ideal linear elastic media (Knopoff, 1958; Byerly and DeNoyer, 1958; Keylis-Borok, 1959; and Teisseyre, 1960). Energies calculated from these theoretical models, which depend on the not too well-known physical fault parameters, generally give values, although of the same order of magnitude,

lower than that associated with seismic wave energies and predict fault depths inconsistent with hypocenter determinations. For example, Knopoff gets

$$E = \frac{1}{16}\mu\pi s^2 L = 4 \times 10^{23} \text{ ergs}$$

for the 1906 8.3 magnitude earthquake, where μ is the rigidity, s the fault dislocation at the surface, and L the length of the break. Byerly and DeNoyer, using an empirical determination of the displacement field and basically the same theoretical approach, get

$$E \approx 1 \times 10^{23} \text{ ergs}$$

The G-R relation on the other hand, predicts for an 8.3 magnitude event

$$E = 1.8 \times 10^{24} \text{ ergs}$$

These models, however, would be expected to predict a lower bound on the total energy since the tacit assumption is made that an initial stress distribution drops to zero in the final state. Generally, this assumption is probably not valid; the pre-stress existing in the medium may be quite different from the stress-drop (Burridge and Knopoff, 1966). This effect can best be seen if we consider the change in energy at the fault plane. By definition (Orowan, 1960; Brune, 1968), the total work done by the elastic forces, E_t, is equal to the product of the area of the slip surface A, times the average stress operating $\bar{\sigma}$, times the mean dislocation or displacement $\bar{u}$

$$E_t = \bar{\sigma} A \bar{u} \qquad (26)$$

Thus if the stress dropped from 1 bar to zero bars across the fault plane, we would have

$$\bar{\sigma} = 0.5 \text{ bars}$$

and

$$E_t = 0.5 \; A \bar{u}$$

whereas if the stress dropped from 10 bars to 9 bars, then

$$\bar{\sigma} = 9.5 \text{ bars}$$

and

$$E_{t2} = 9.5 \, A \, \bar{u} = 19 \, E_{t1}$$

In both cases the stress-drop amounted to 1 bar. Due to the linearity of static elasticity, we may superpose an additional shear stress field on that considered say by Knopoff, and thereby obtain larger total energies at the fault plane. Burridge and Knopoff (1966) have done this and amend Knopoff (1958) obtaining

$$E = \frac{1}{16} \pi \mu \left(\frac{1 + \gamma}{1 - \gamma} \right) s^2 L \qquad (27)$$

where γ is the ratio of the initial shear stress to the final shear stress on the fault plane, $0 \leq \gamma \leq 1$. It can be seen that depending on the value of γ, E can conceivably take on any value from

$$E_{min} = \frac{1}{16} \pi \mu s^2 L$$

to $E = \infty$. Thus this approach of static elasticity would be helpful only if we had a clue as to what the magnitude of pre-stresses were. Seismological techniques aimed at determining the absolute stress

have so far proved unfruitful. At best we can say that the stress-drop, which can be calculated from knowledge of the physical fault parameters according to relations of the form (Knopoff, 1958)

$$\sigma_{sd} = \frac{1}{2} \frac{U_m \mu}{a} \tag{28}$$

where U_m is the maximum displacement (at ground surface), μ the rigidity, and a the fault depth, gives a lower bound on absolute stress. Maximum stress-drops on the order of 100 bars have been reported for strike-slip faulting (Brune and Allen, 1967a). A simple, yet highly convincing argument presented by Orowan (1960) suggests that consideration of that portion of the energy in elastic waves can only lead to information on stress-drops while also, interestingly, suggesting that inversion of heat flow data coupled with stress-drop information could lead to a determination of absolute stress. We have from (26)

$$E_t = A \bar{u} \bar{\sigma}$$

If we put

$$\bar{\sigma} = \frac{\sigma_1 + \sigma_2}{2}$$

where σ_1 is the initial stress and σ_2 the final stress, then

$$E_t = A \bar{u} \frac{\sigma_1 + \sigma_2}{2} \tag{29}$$

Now

$$E_t = E_s + E_f \tag{30}$$

where E_s is the seismic energy and E_f the frictional or heat energy.

We can write

$$E_f = f\bar{u} = \sigma_f A \bar{u} \tag{31}$$

where f is the frictional force and σ_f the frictional stress across the fault plane. Now let us assume $\sigma_f = \sigma_2$; that is, the frictional stress determines the final state of stress on the fault plane -- when $\bar{\sigma} \leq \sigma_f$, the fault ceases to be able to slip -- a reasonable assumption; then from (31)

$$E_f = A\bar{u}\sigma_2 \tag{32}$$

or from (29), (30), and (32)

$$E_s = E_t - E_f$$

$$= A\bar{u}\left(\frac{\sigma_1 - \sigma_2}{2}\right)$$

or the seismic wave energy, E_s, is a function of the average stress-drop $\frac{\sigma_1 - \sigma_2}{2}$ only, while the frictional or heat energy is a function of the final stress σ_2. Thus, assuming the validity of (32), we can, by determining E_f from heat flow measurements and knowing the fault parameters A and $\bar{u}$, solve for σ_2 in (32). If we then calculate the stress-drop $\sigma_1 - \sigma_2$, say from (28), we then know σ_1. If no measurable heat flow anomaly is found associated with the fault, we should be able to put an upper bound on the initial stress.

A third way of considering heat production along a fault is to consider the dissipative processes in terms of a coefficient of friction μ. We recall from (31)

$$E_f = A\,\bar{\sigma}_f\,\bar{u}$$

$$= A\,\bar{u}\,\bar{\tau}\,\mu \qquad (33)$$

where $\bar{\tau}_f$ is the average normal (to the fault plane) frictional stress and μ the coefficient of sliding friction. We can write

$$\bar{\tau}_f = \bar{\tau}_h + \bar{\tau}_t - \bar{\tau}_p \qquad (34)$$

where $\bar{\tau}_h$ is the mean hydrostatic pressure, $\bar{\tau}_t$ is the average of any tectonic stress acting perpendicular to the fault plane, and $\bar{\tau}_p$ the average fluid pore pressure. $\bar{\tau}_h$ is commonly taken (for shallow depths, below yield point of rock) as $\frac{2}{3}\bar{\tau}_\ell$ where $\bar{\tau}_\ell$ is the average lithostatic load. Now

$$\bar{\tau}_\ell = \rho g \frac{D}{2} \qquad (35)$$

or

$$\bar{\tau}_h = \frac{2}{3}\rho g \frac{D}{2} = \rho g \frac{D}{3} \qquad (36)$$

where D is the depth of faulting. If we neglect $\bar{\tau}_t$ and $\bar{\tau}_p$ for the moment, we get from (33), (34), (35), and (36)

$$E_f = A\,\bar{u}\mu\rho g \frac{D}{3} = \rho g \frac{D}{3} L\bar{u}\mu$$

Putting in numerical values appropriate for the 1906 San Francisco earthquake, namely: $\rho = 3.0$ gm/cm^3, $g = 10^3$ cm/sec^2, $D = 20$ km, $L = 300$ km, $U_m = 550$ cm (U_m = maximum surface displacement; $\bar{u} = \frac{\pi}{4} U_m$ from Knopoff's static model, 1958), we get

$$E_f \simeq 4.8 \times 10^{25}\mu \text{ ergs} \qquad (37)$$

Inclusion of $\overline{\tau}_t$ and $\overline{\tau}_p$ may alter (37) by a factor of two, but would probably not change the order of magnitude; as a matter of fact, the two effects tend to cancel. Neither $\overline{\tau}_t$ nor $\overline{\tau}_p$ would be expected to substantially exceed the lithostatic load.

Thus the problem with this approach is can we assign a reasonable value to the coefficient of friction μ? It has been assumed that strike-slip faulting is representative of uniaxial compression at 30° from the slip direction, which is compatible with a coefficient of internal friction of about 0.6 (Anderson, 1951). In addition, experiments involving rocks under triaxial confinement, with a uniaxially applied differential stress (Handin, 1966), indicate most crystalline rocks shear along planes inclined ~30° to the differentially stressed axis. However, it seems somewhat unreasonable to suggest a possible value for μ on the basis of internal friction of fresh, unfractured rock since existing faults by definition represent inherent zones of weakness and are perhaps more like the boundary between two polished surfaces. Coefficients of smooth kinetic friction are about 0.1. If we put this value in (37) for μ, we have

$$E_f \simeq 4.8 \times 10^{24} \text{ ergs}$$

It is interesting to note that this approach predicts about the same value of energy as does the G-R relation and is about an order of magnitude higher than the minimum value of Knopoff (1958).

Finally, we wish to assess heat production in terms of creep, a process which is intrinsically dissipative if assumed to occur

under a non-zero shear stress. The work done by the elastic forces causing creep will be converted to heat in the vicinity of the fault where the creep is occurring. As we have indicated earlier, creep has been shown to be responsible for significant amounts of fault offset along various segments of the San Andreas fault system, and may even be the primary form of strain energy release in some regions. For example, the west side of the Salton Trough has been observed to be moving northward relative to the east side at a rate of 8 cm/yr. Relative creep offset amounting to about 5 cm/yr is observed across the San Andreas fault and a zone 25 km or either side, just south of Hollister. One-third of this offset is occurring across a single break at the fault (Allen, et al., 1965, after Whitten, 1955, and Meade, 1963). If the offsets from creep of between 2 and 5 cm/yr are summed over a 100 year period (probable recurrence rate for an ~8 magnitude event at a given location along the San Andreas), we would have total displacements amounting to between 2 and 5 meters, or equivalent to displacements to be expected from ~8 magnitude earthquakes. Thus if the creep mechanism is equally significant at depth in the fault zone and can be assumed to be a continuing process, we might conclude that the process involves equally as much energy release per cm of fault per second as recurring earthquakes with similar offsets. This conclusion assumes that the shear stresses under which creep occurs are comparable to those under which faulting takes place.

Creep energy can be treated quantitatively, as we indicated earlier, in the same way we discussed frictional energy due to faulting.

Instead of using equation (26) for the energy per event, namely

$$E = A\bar{\sigma}\bar{u}$$

and introducing a time dependence from an earthquake recurrence rate, we have for the energy liberated per unit time

$$E = A\bar{\sigma}\dot{\epsilon} \tag{38}$$

where $\dot{\epsilon}$ is the creep rate. For the energy liberated per unit time per unit fault length, we would have

$$E = D\bar{\sigma}\dot{\epsilon}$$

where D is the depth of faulting.

The purpose of the foregoing discussion has been to present a "plausibility argument" for heat production along a fault. We have suggested on the basis of what is known about the energy regime of a fault that it is not unreasonable to expect on the order of 1 cal/sec of energy to be liberated per cm of fault. In the next section, we wish to consider what the surface heat flow, corresponding to this energy release, would look like for various models of fault geometry.

C. Fault Geometry and Heat Production

Until now we have been discussing the question of what quantity of energy might be released in the form of heat by various physical processes in the vicinity of the fault, but have not yet considered the problem of whether or not this heat could contribute to an observable heat flow anomaly at the surface near a major fault.

In other words, we want to ask how would these heat sources have to be distributed in time and space to produce surface heat flow anomalies, or given a physically realizable spatial and time distribution of these sources, might we be able to detect their presence and perhaps magnitude with surface measurements?

For the time distribution of heat producing mechanisms, we must rely on a relatively short history of recorded statistics and field observations. We know that in the last 100 years there have been two ~8 magnitude earthquakes along the San Andreas fault, and with the additional evidence of possible rates of strain accumulation and fault displacements, is it reasonable to assume that perhaps we have had on the average two such events along the length of the San Andreas during a good part of the geologic past? Benioff has suggested that maybe this is a reasonable guess. With regard to creep phenomena, we must ask whether or not it is a continuously occurring process; does it occur at various points along the fault at various times, or, as Allen has suggested (1967), are only selected segments of the fault characterized by creep while others are susceptible to large earthquakes? Or, finally, one might ask if creep is merely a process which occurs prior to or following earthquakes and is not a significant form of displacement in itself? Indeed, without time-limited statistics and field observations, these questions are at best difficult to answer. As geologists we are perhaps unduly influenced by the law of uniformitariansim, yet this is the approach we choose to take, undoubtedly from want of a better one.

With regard to the spatial situation, the problem comes in setting up a physically realizable model; that is, how are the heat sources distributed with depth (and breadth) in the fault zone and what criteria might we apply to define a realizable model? Here we have touched on perhaps the most crucial question -- to what extent can we project to depth our surface observations regarding such phenomena as fault displacement, creep, and strain accumulation? The answer to this question can only come from comparison of our observations with various models.

The theory of line sources (Carslaw and Jaeger, Chapter X, 1959) allows us to conveniently describe models of heat production for various fault geometries. This has been done in Appendix IV. Continuous heat producing line, strip, and zone sources have been considered for the cases of heat production being a) constant with depth, and b) a linear function of depth. Relations (8), (11), (12), (13), and (14) from Appendix IV were programmed for the IBM 7094 for various combinations of fault dimensions to determine the relation between the heat flow Q and the horizontal distance from the fault trace y. A number of representative models are presented in Figures 41 to 49.

All of the cases shown have been normalized to the same total heat production, namely 1 cal/cm of fault length/sec. Thus, for example, a fault zone which has twice the volume of another will have only one-half the density of heat sources. If one desires to know the shape of the curves and the values of Q versus y for say a 2 cal/cm of

fault length/sec heat production or twice the heat source density, it is only necessary to multiply the value of Q at a given y by the factor 2. In general, then, for a total heat production of n cal/cm of fault/length/sec, the shape of the curve can be found by multiplying the value of the heat flow Q for the value of y desired by n; i.e., whereas the heat flow at $y = y_o$ is given by Q for 1 cal/cm of fault/sec, the value at $y = y_o$ for n cal/cm of fault/sec is given by nQ. Thus by inversion of the above process, we can compare the shape of any actual heat flow anomaly of this type with one of the models presented in Figures 41 to 49. For example, by taking the ratio of Q for the maximum of the actual anomaly and Q_{max} for a given model and applying this ratio in the same sense to the rest of the curve (usually discrete points) for the actual anomaly, we would normalize to the given model.

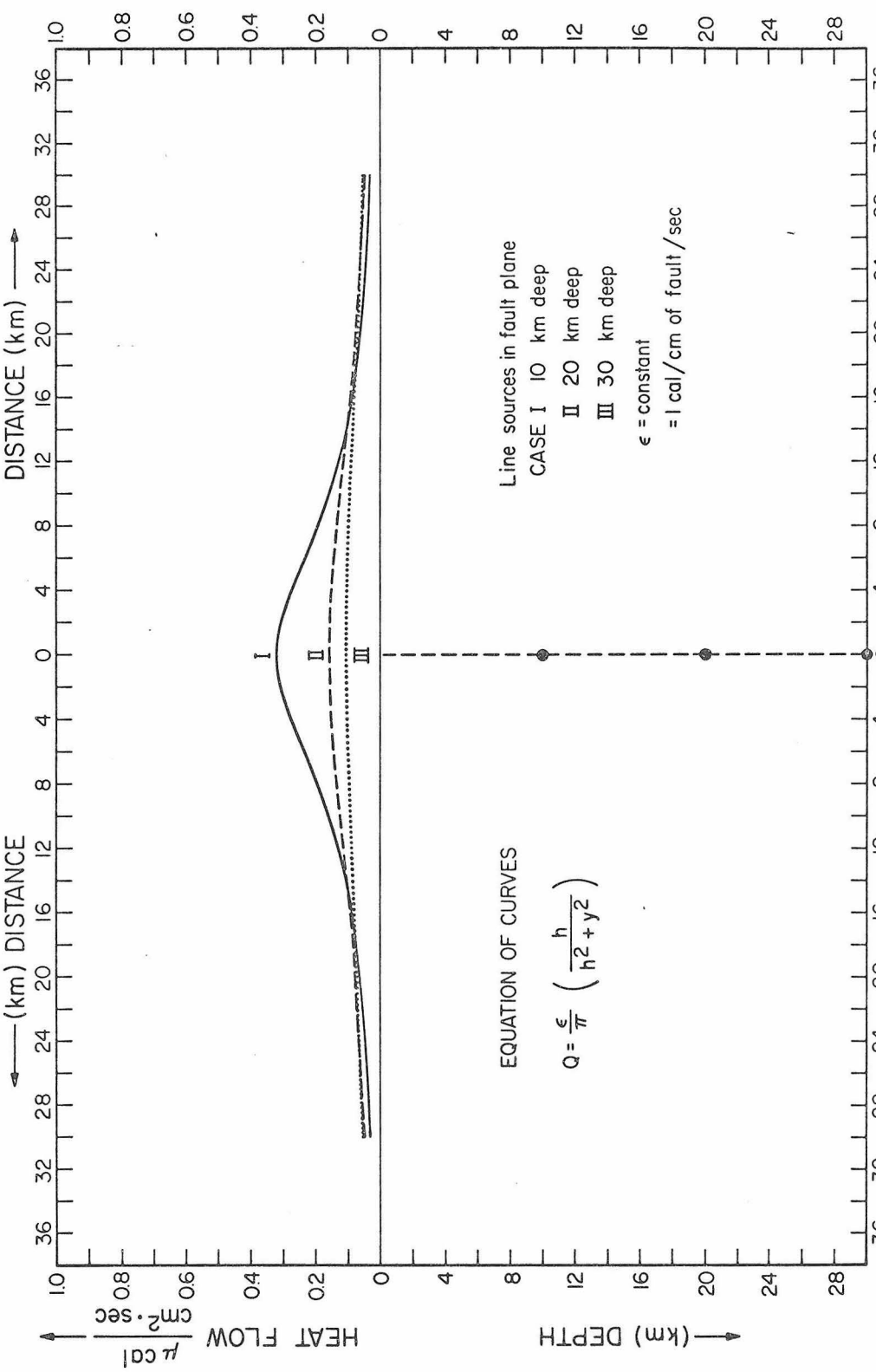
DISTANCE (km)
(km) DISTANCE
HEAT FLOW
μ cal / cm² · sec
(km) DEPTH
I
II
III
Line sources in fault plane
CASE I 10 km deep
II 20 km deep
III 30 km deep
ϵ = constant
= 1 cal/cm of fault/sec
EQUATION OF CURVES
$Q = \frac{\epsilon}{\pi}\left(\frac{h}{h^2 + y^2}\right)$

Figure 41

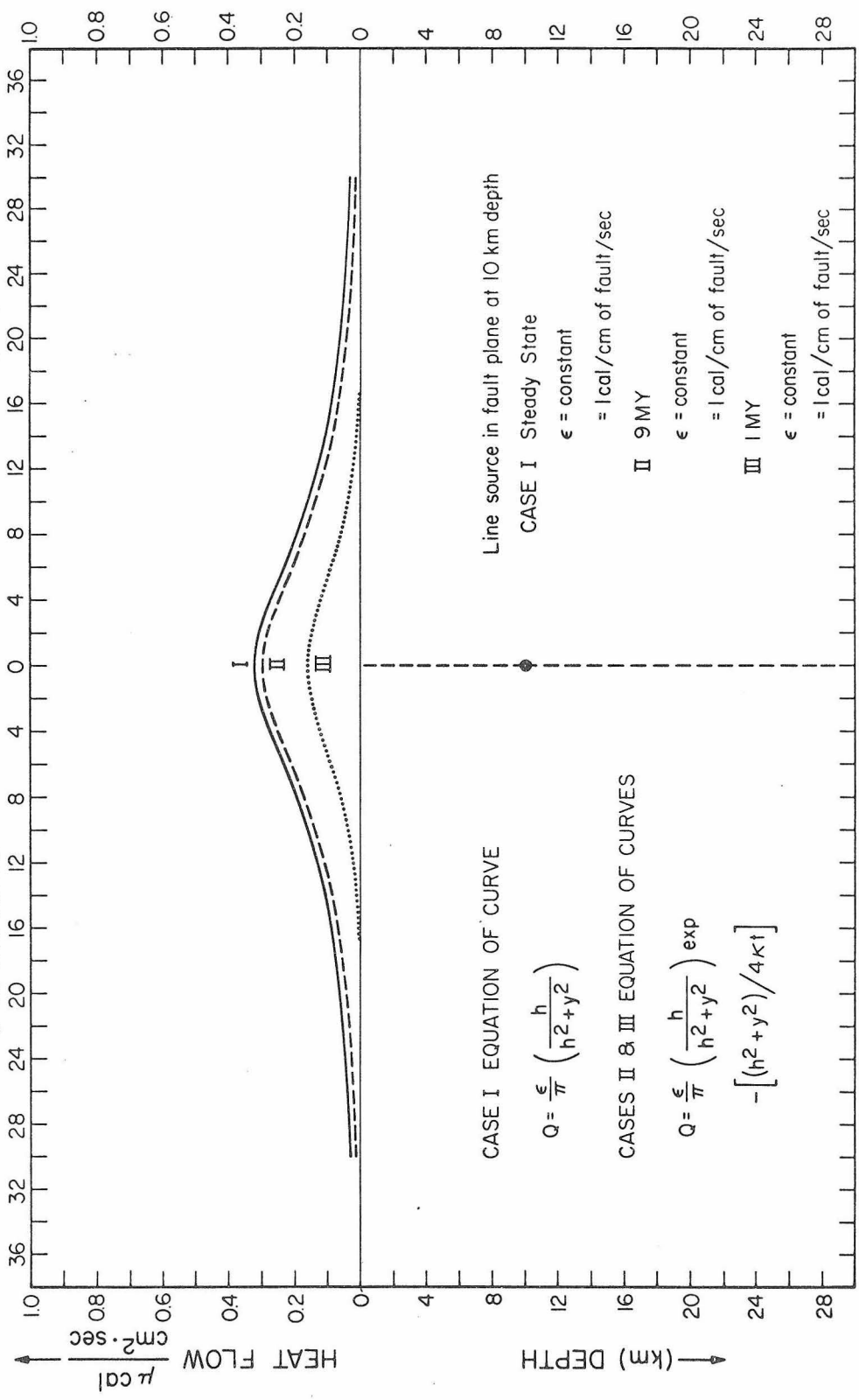
DISTANCE (km)
(km) DISTANCE
HEAT FLOW
μ cal / cm² · sec
(km) DEPTH
I
II
III
Line source in fault plane at 10 km depth
CASE I Steady State
ε = constant
= 1 cal/cm of fault/sec
II 9 MY
ε = constant
= 1 cal/cm of fault/sec
III 1 MY
ε = constant
= 1 cal/cm of fault/sec
CASE I EQUATION OF CURVE
$Q = \frac{\epsilon}{\pi}\left(\frac{h}{h^2+y^2}\right)$
CASES II & III EQUATION OF CURVES
$Q = \frac{\epsilon}{\pi}\left(\frac{h}{h^2+y^2}\right)\exp -\left[(h^2+y^2)/4\kappa t\right]$

Figure 42

Figure 43

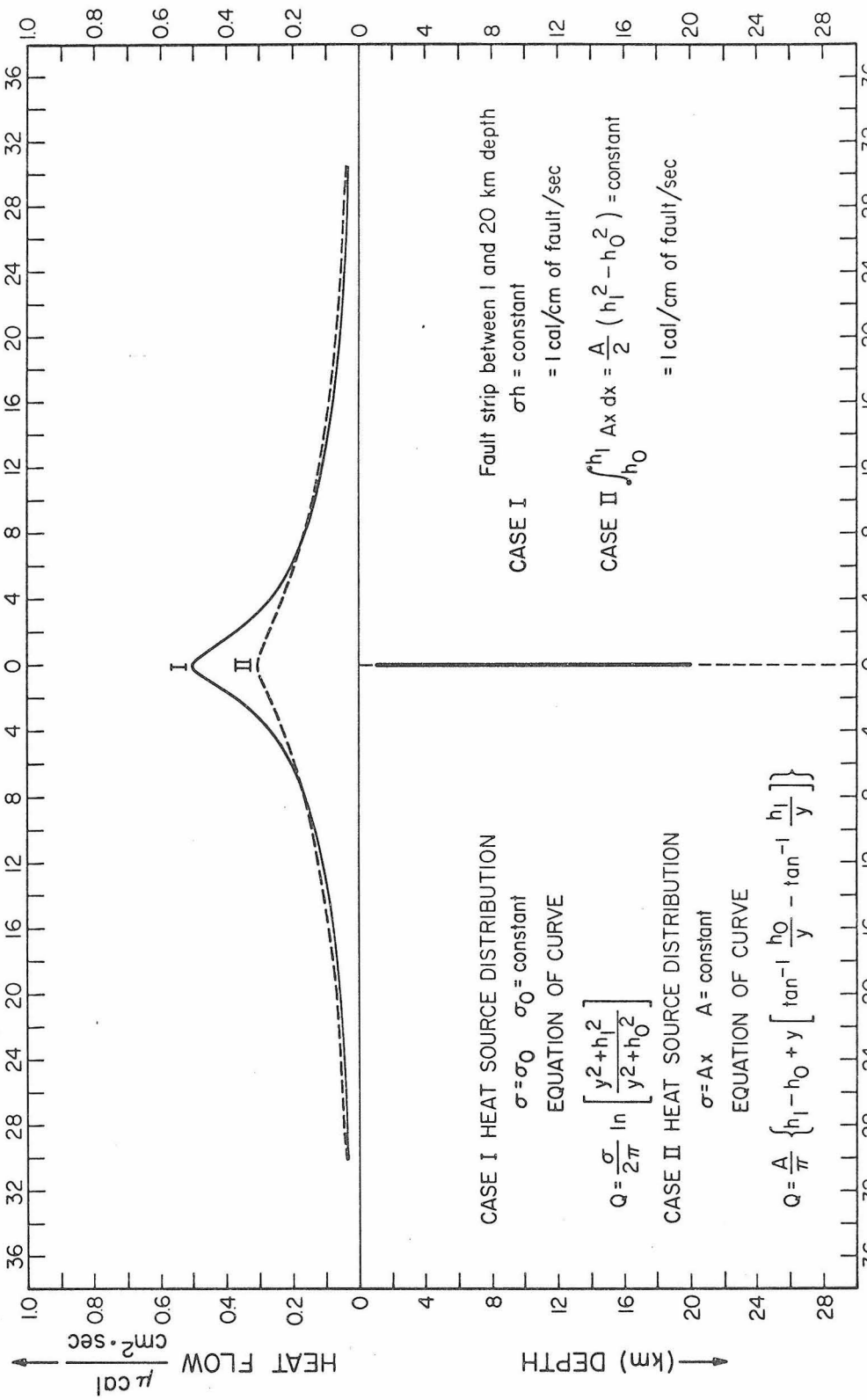
DISTANCE (km)
(km) DISTANCE
HEAT FLOW μcal / cm² · sec
(km) DEPTH
I
II
Fault strip between 1 and 20 km depth
CASE I σh = constant
= 1 cal/cm of fault/sec
CASE II $\int_{h_0}^{h_1} Ax\,dx = \frac{A}{2}(h_1^2 - h_0^2)$ = constant
= 1 cal/cm of fault/sec
CASE I HEAT SOURCE DISTRIBUTION
$\sigma = \sigma_0$ σ_0 = constant
EQUATION OF CURVE
$Q = \frac{\sigma}{2\pi} \ln\left[\frac{y^2+h_1^2}{y^2+h_0^2}\right]$
CASE II HEAT SOURCE DISTRIBUTION
$\sigma = Ax$ A = constant
EQUATION OF CURVE
$Q = \frac{A}{\pi}\left\{h_1 - h_0 + y\left[\tan^{-1}\frac{h_0}{y} - \tan^{-1}\frac{h_1}{y}\right]\right\}$

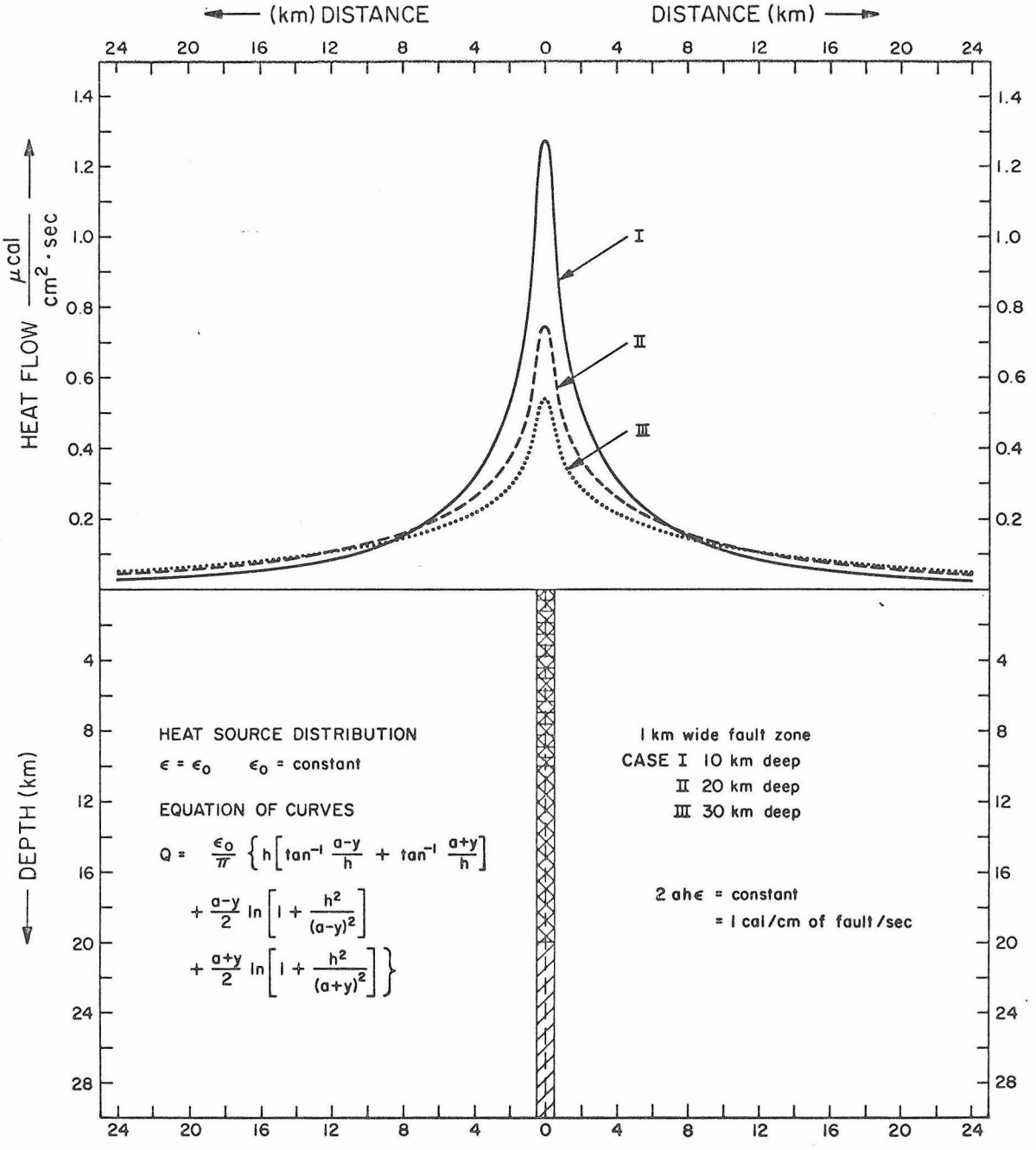
(km) DISTANCE
DISTANCE (km)
HEAT FLOW μcal / cm² · sec
DEPTH (km)
I
II
III
HEAT SOURCE DISTRIBUTION
ε = ε₀ ε₀ = constant
EQUATION OF CURVES
Q = ε₀/π { h[tan⁻¹ (a-y)/h + tan⁻¹ (a+y)/h]
+ (a-y)/2 ln[1 + h²/(a-y)²]
+ (a+y)/2 ln[1 + h²/(a+y)²] }
1 km wide fault zone
CASE I 10 km deep
II 20 km deep
III 30 km deep
2 ahε = constant
= 1 cal/cm of fault/sec

Figure 44

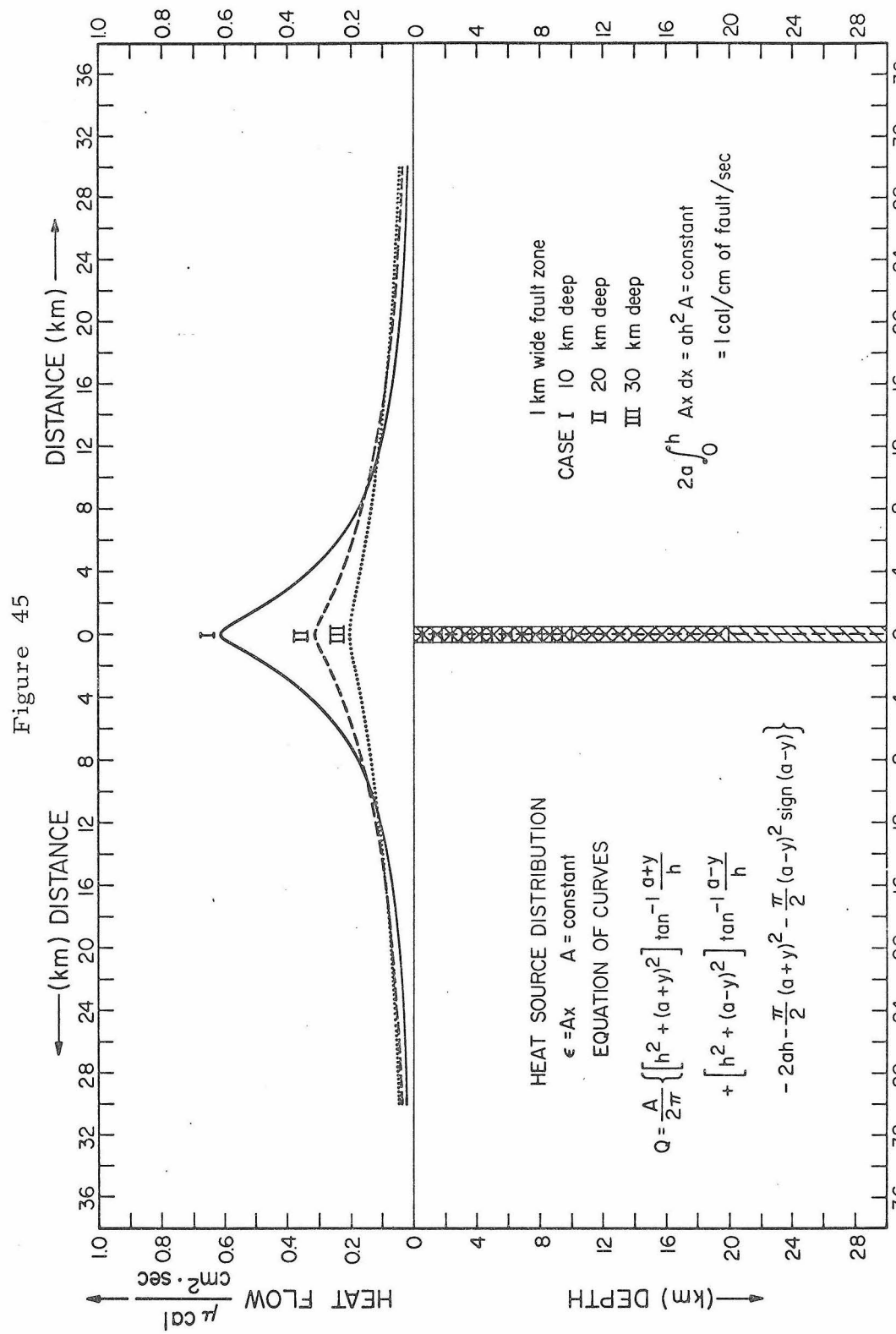
DISTANCE (km)
(km) DISTANCE
HEAT FLOW
μ cal / cm² · sec
(km) DEPTH
I
II
III
1 km wide fault zone
CASE I 10 km deep
II 20 km deep
III 30 km deep
$2a\int_0^h Ax\,dx = ah^2A$ = constant
= 1 cal/cm of fault/sec
HEAT SOURCE DISTRIBUTION
$\epsilon = Ax$ A = constant
EQUATION OF CURVES
$Q = \frac{A}{2\pi}\left\{\left[h^2+(a+y)^2\right]\tan^{-1}\frac{a+y}{h} + \left[h^2+(a-y)^2\right]\tan^{-1}\frac{a-y}{h} - 2ah - \frac{\pi}{2}(a+y)^2 - \frac{\pi}{2}(a-y)^2\,\text{sign}\,(a-y)\right\}$

Figure 45

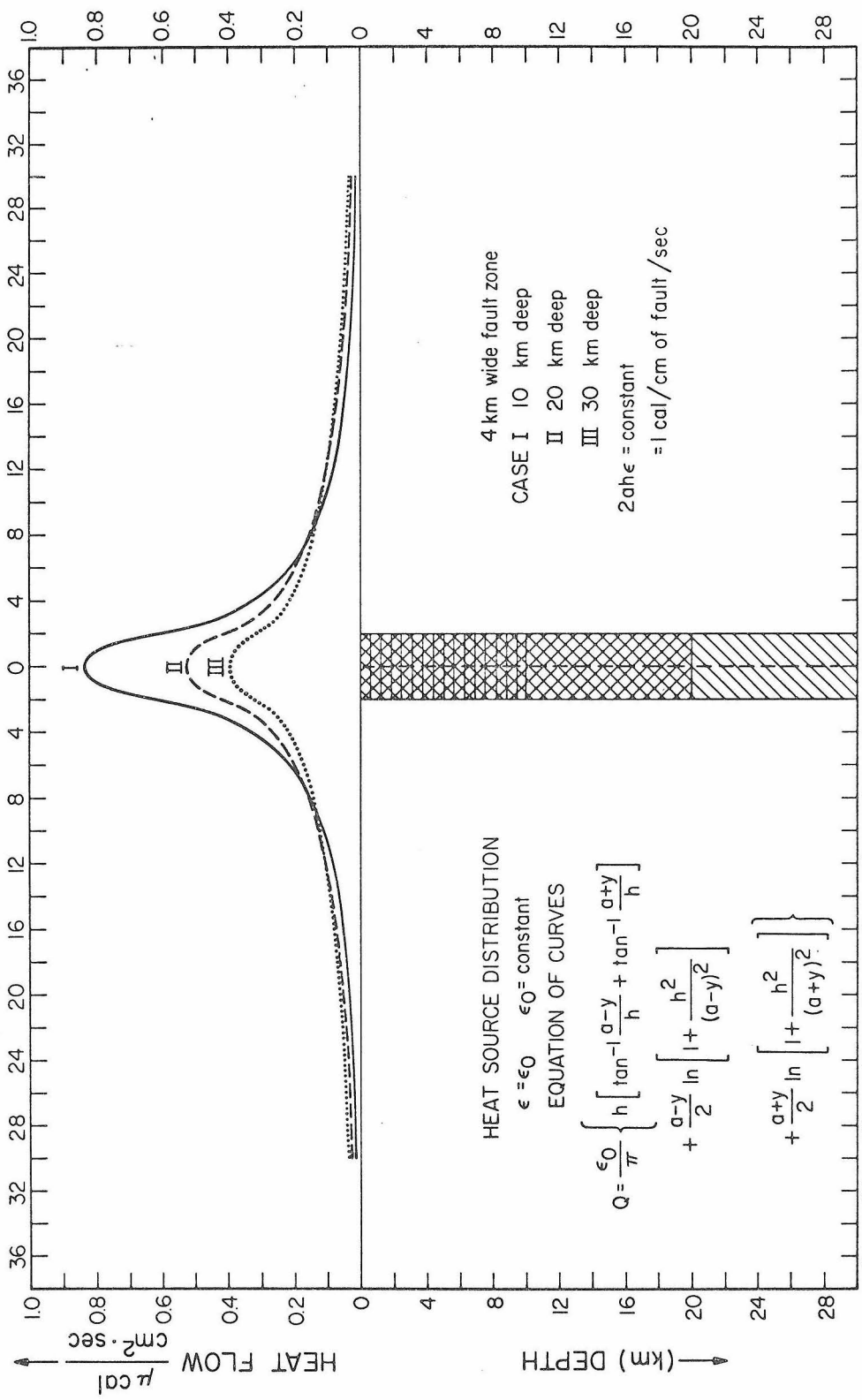
DISTANCE (km)
(km) DISTANCE
HEAT FLOW μcal / cm² · sec
(km) DEPTH
I
II
III
4 km wide fault zone
CASE I 10 km deep
II 20 km deep
III 30 km deep
2ahε = constant
= 1 cal/cm of fault/sec
HEAT SOURCE DISTRIBUTION
ε = ε0 ε0 = constant
EQUATION OF CURVES
$Q = \frac{\epsilon_0}{\pi}\left\{h\left[\tan^{-1}\frac{a-y}{h} + \tan^{-1}\frac{a+y}{h}\right] + \frac{a-y}{2}\ln\left[1+\frac{h^2}{(a-y)^2}\right] + \frac{a+y}{2}\ln\left[1+\frac{h^2}{(a+y)^2}\right]\right\}$

Figure 46

Figure 47

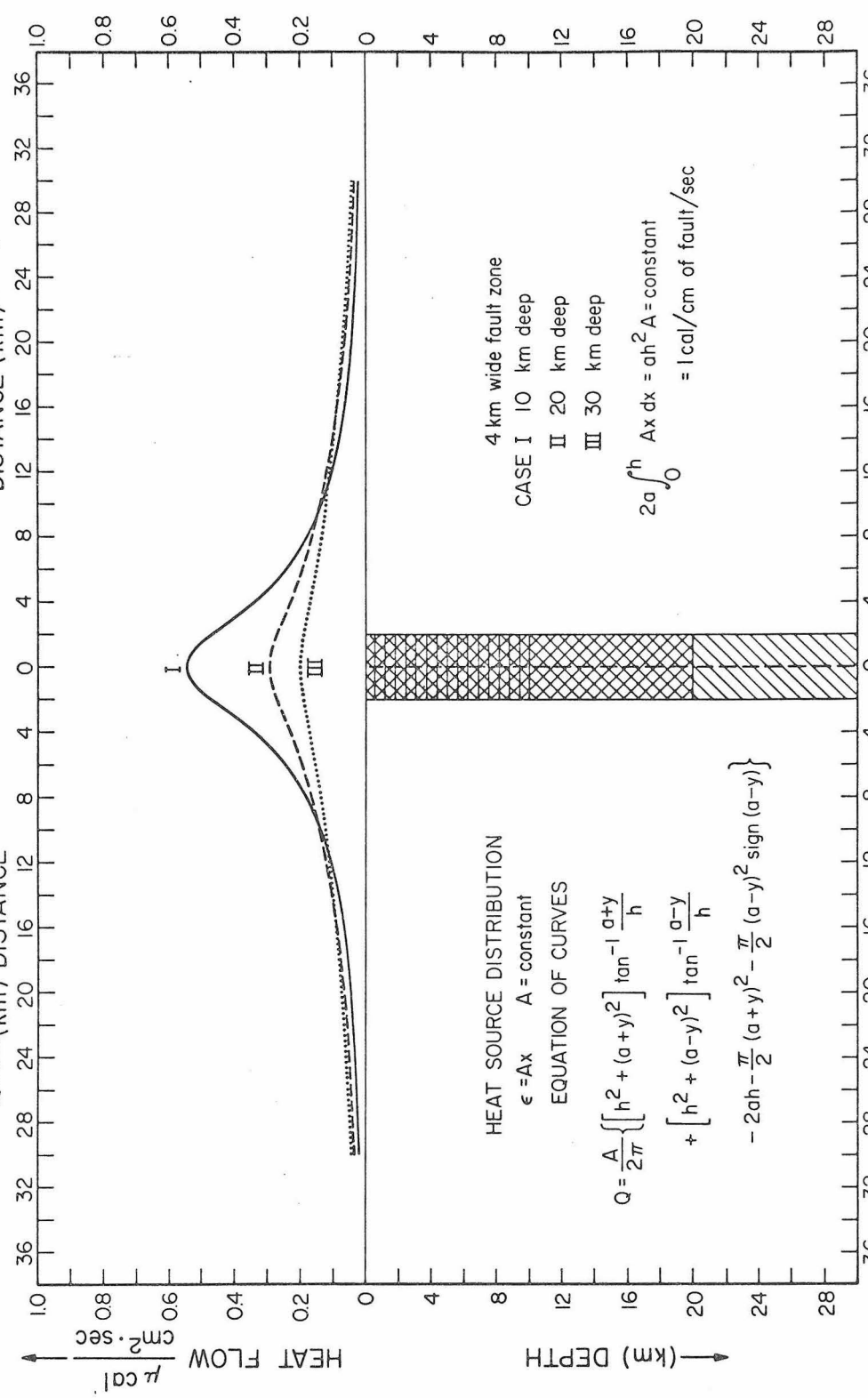
DISTANCE (km)
(km) DISTANCE
HEAT FLOW
μ cal / cm² · sec
(km) DEPTH
I
II
III
4 km wide fault zone
CASE I 10 km deep
II 20 km deep
III 30 km deep
2a ∫₀ʰ Ax dx = ah² A = constant
= 1 cal/cm of fault/sec
HEAT SOURCE DISTRIBUTION
ϵ = Ax A = constant
EQUATION OF CURVES
Q = A/2π { [h² + (a+y)²] tan⁻¹ (a+y)/h
+ [h² + (a-y)²] tan⁻¹ (a-y)/h
- 2ah - π/2 (a+y)² - π/2 (a-y)² sign (a-y) }

Figure 48

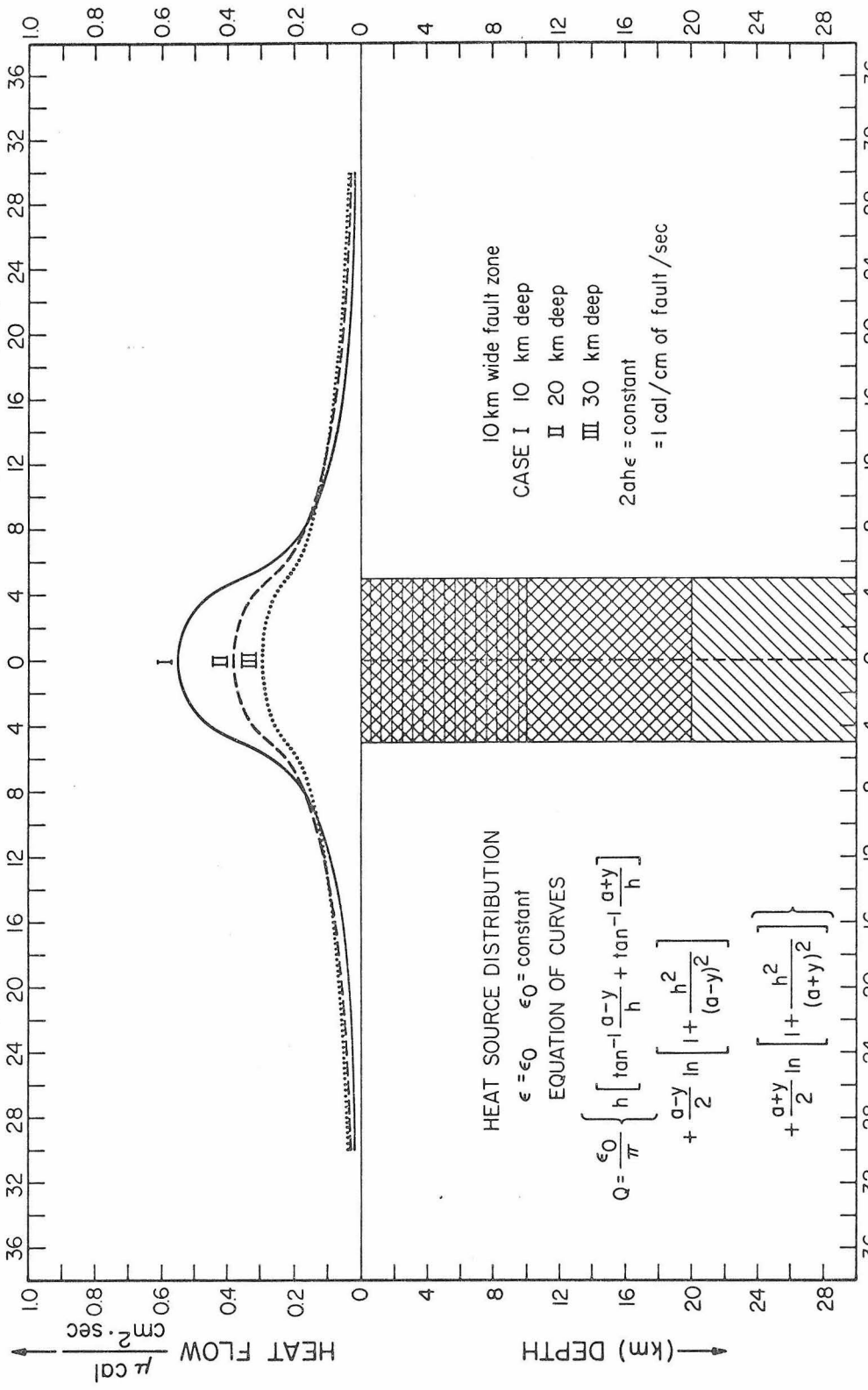
(km) DISTANCE
DISTANCE (km)
HEAT FLOW $\frac{\mu \text{ cal}}{\text{cm}^2 \cdot \text{sec}}$
(km) DEPTH
I
II
III
10 km wide fault zone
CASE I 10 km deep
II 20 km deep
III 30 km deep
$2ah\epsilon$ = constant
= 1 cal/cm of fault/sec
HEAT SOURCE DISTRIBUTION
$\epsilon = \epsilon_0$ ϵ_0 = constant
EQUATION OF CURVES
$Q = \frac{\epsilon_0}{\pi} \left\{ h \left[\tan^{-1} \frac{a-y}{h} + \tan^{-1} \frac{a+y}{h} \right] + \frac{a-y}{2} \ln \left[1 + \frac{h^2}{(a-y)^2} \right] + \frac{a+y}{2} \ln \left[1 + \frac{h^2}{(a+y)^2} \right] \right\}$

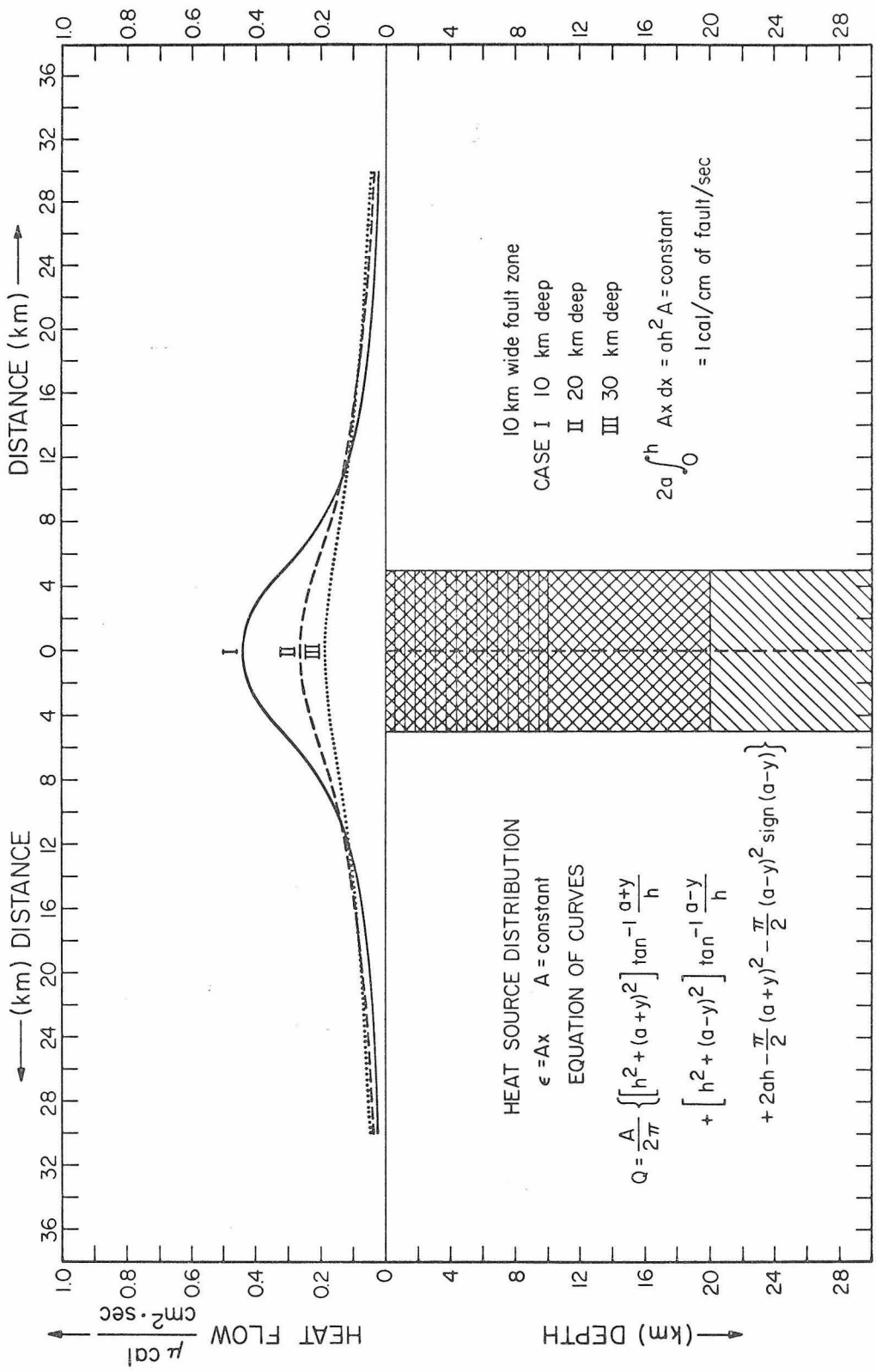
DISTANCE (km)
(km) DISTANCE
HEAT FLOW μ cal / cm² · sec
(km) DEPTH
I
II
III
10 km wide fault zone
CASE I 10 km deep
II 20 km deep
III 30 km deep
$2a\int_0^h Ax\,dx = ah^2A$ = constant
= 1 cal/cm of fault/sec
HEAT SOURCE DISTRIBUTION
$\epsilon = Ax$ A = constant
EQUATION OF CURVES
$Q = \frac{A}{2\pi}\left\{\left[h^2+(a+y)^2\right]\tan^{-1}\frac{a+y}{h}\right.$
$+\left[h^2+(a-y)^2\right]\tan^{-1}\frac{a-y}{h}$
$\left.+2ah-\frac{\pi}{2}(a+y)^2-\frac{\pi}{2}(a-y)^2\,\mathrm{sign}\,(a-y)\right\}$

Figure 49

IX. INTERPRETATION OF DATA

A. General Statement

The purpose of this section is to examine the relation of the heat flow data to the major strike-slip faults of California in light of our previous discussion regarding strain energy release. We have suggested that it is not unreasonable to associate a minimum of 10^{24} ergs of energy with the largest known seismic events along the San Andreas fault and have further hypothesized, on the basis of an assumed frequency of occurrence of these events, that at least a few tenths of a cal per sec of seismic energy is being liberated per cm along the fault. In addition, we have alluded to the fact that it is not unreasonable to expect an amount of heat of equivalent magnitude to be produced per cm of fault length, especially in instances where creep is responsible for significant fault offset. Finally, we have shown in the last section what heat flow anomalies might look like for various fault geometries where heat is being released at the rate of 1 cal/cm of fault/sec. What now can we say that the data tell us regarding heat production along the faults which we have studied? Are there or are there not heat flow anomalies? Can we tell anything about fault geometry or fault history? What does the level of heat production tell us about the absolute stress, about the efficiency of seismic wave generation, and about the total energy? These are questions we want to consider in the following discussion.

B. Discussion

The different regions along the various faults which were investigated are representative of a spectrum of contemporary fault and seismic activity. The region near Hollister is characterized by significant creep across the San Andreas fault; geodetic surveys (Whitten, 1955) indicate that points 25 km or so on either side of the fault are creeping relative to one another at a rate of 5 cm/yr. No large magnitude earthquakes (>7) are known to have occurred along this segment of the fault. The break from the 1906 San Francisco earthquake was traced southward as far as San Juan Bautista, about 10 miles to the north of HO-1. Conversely, the Lake Hughes region is located along a portion of the San Andreas which broke during the 1857 Fort Tejon earthquake. Triangulation surveys across this part of the fault show no measurable strain is occurring, and it has been suggested (Allen, St. Amand, Richter, and Nordquist, 1965) that this segment is likely to experience another large magnitude shock.

The holes in the San Bernardino Mountains lie near the southern extent of the 1857 break along the San Andreas and at a major bifurcation point of the San Andreas fault system. From the Transverse Ranges southward, no single one of the numerous large strike-slip faults stands out so uniquely as does the San Andreas to the north. The heat flow sites in the Anza region are located near the San Jacinto fault, one of the major branches of the San Andreas fault and, presently, the most active. The region near Anza is

characterized by numerous small magnitude (up to 7) shocks and significant micro-earthquake activity. The profile in the Tehachapi Mountains crosses the Garlock fault, which is presently seismically inactive and shows no evidence of creep offset or strain accumulation. Finally, the profile of Roy and Brune between San Diego and El Centro is in a region free, for the most part, of large strike-slip faults. To the east, the profile ends at the Elsinore fault which here strikes along the boundary of the Peninsular Ranges and Salton Trough.

Figure 50 shows a summary of the heat flow data in relation to the nearest major strike-slip fault. The measured heat flow at each drill hole has been plotted versus the distance in km along a normal to the fault. Dashed lines have been drawn between the data points to illustrate the assumed trends. In several instances, heat flow values for locations farther than 40 km from the fault (limit of the horizontal scale in Figure 50), yet near enough to be assumed representative of 40 km away, have been plotted at 40 km to help complete the picture; these points are indicated by a heavy underlining of the hole number. The two heavy bars on the eastern parts of the Anza and San Diego - El Centro profiles indicate the average value of the heat flow (1.8 HFU) representative of a large portion of the Salton Trough (Rex, 1966, and personal communication). C.I.T. is a preliminary value of Roy located at the Caltech Seismological Laboratory in Pasadena. It's value, uncorrected for terrain and determined from only a limited number of conductivity measurements

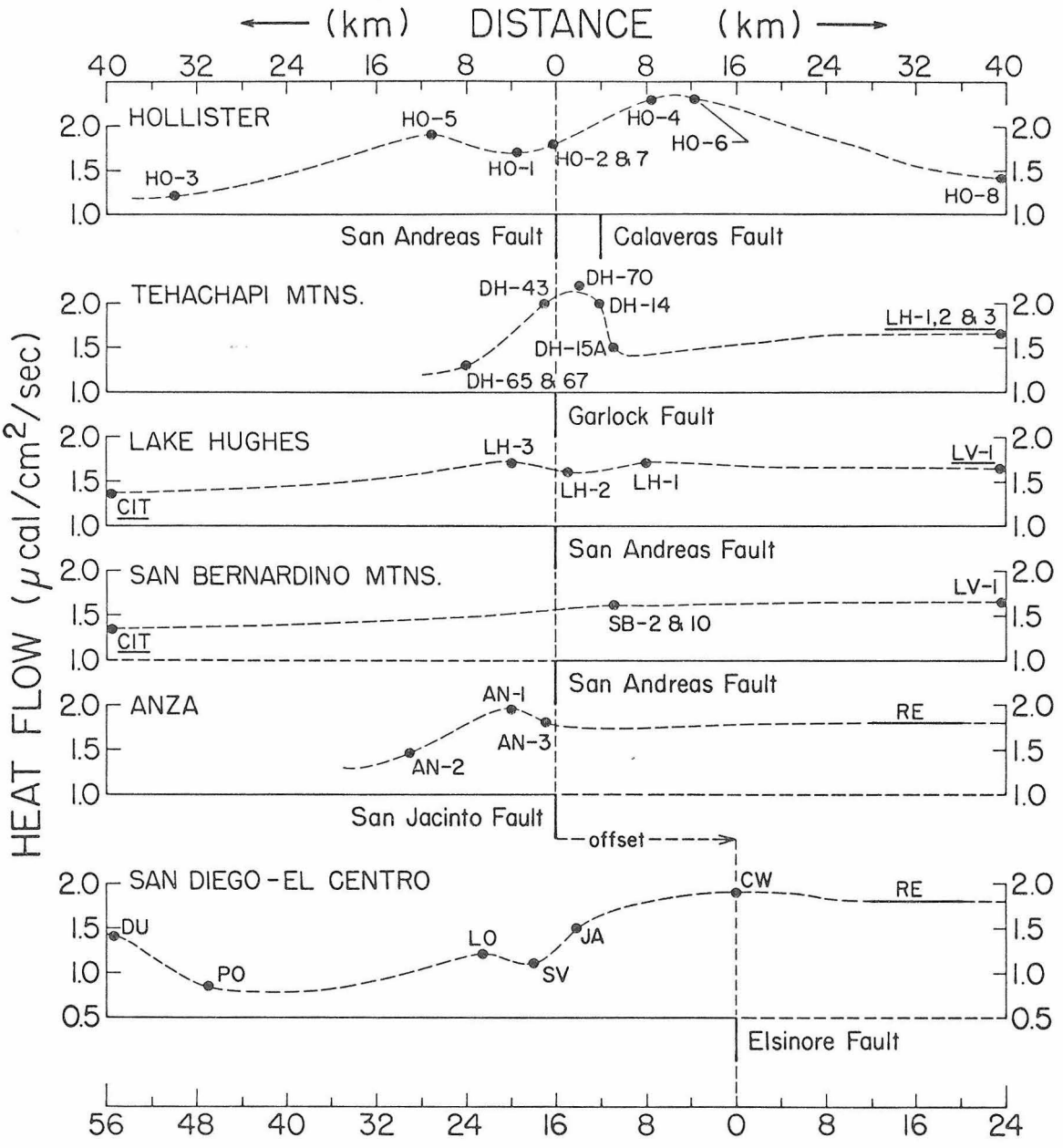

Data used from other investigators:

HO-6, HO-8, CIT, DU, PO, LO, SV, JA, CW — Roy and Brune (personal communication)

RE — Rex (1966, and personal communication)

Heat Flow Data in California Plotted Versus Distance From Nearest Major Strike Slip Fault

Figure 50

is 1.4 HFU. This value is good to ±5% (Roy, personal communication).

The San Diego - El Centro and Anza profiles are both located in the Peninsular Range Province. The trend of the heat flow values at Anza appears very similar to the trend of the heat flow in the eastern part of the San Diego - El Centro profile. In both cases the heat flow rises from about 1.5 HFU 14 km west of the fault to about 1.8-1.9 HFU at the fault. Rex's data indicate that the Salton Trough is a region of high heat flow, averaging 1.8 HFU, and thus the transition from low heat flow to high heat flow along the San Diego - El Centro profile can be directly related to a transition between provinces of inherently different lower crust-upper mantle heat flows without having to appeal to fault-produced heat. In the case of the Anza region, however, the San Jacinto fault lies a full 25 km west of the physiographic boundary between the Peninsular Ranges and Salton Trough, and lacking any heat flow determinations between this boundary and the fault, we cannot clearly relate the rise in heat flow west of the fault to the transition between provinces. We might note that the difference in radioactive heat production between AN-1 - AN-3 and AN-2 cannot explain the difference in heat flow. It would take an unrealistic thickness of 30 km of granitic rock (infinite slabs) having the near surface radioactivity at each site to account for the difference.

Thus, we suggest that the change in heat flow west of the San Jacinto is most probably related to either a transition between provinces of inherently different heat flow or to heat production in a zone

along the San Jacinto fault. Accepting the first alternative would imply that the San Jacinto fault approximately delimits a region of high heat flow to the east and low heat flow to the west irrespective of what the physiography and geology might otherwise suggest. The similarity between the eastern portion of the San Diego - El Centro profile and the Anza profile lends some credence to this hypothesis.

If we accept the second alternative, what can we say about heat production and fault geometry? First of all, we note that the anomaly does not appear symmetrical about the fault -- the heat flow determination at AN-3 (closest to the fault) being about 0.1 HFU lower than at AN-1. This fact could be interpreted to mean one of two things; either the heat flow anomaly is displaced west from the present trace of the fault, or, assuming AN-1 and AN-3 are the same value within statistics, an extremely broad anomaly exists over the fault. Because in reality the values of AN-1 and AN-3 are the same within statistics, we must reasonably accept the second case. Second, we would like to know what the value of heat flow would be if the disturbance of the fault were not there, in order to determine the magnitude of the anomaly. On the basis of the values at LO and SV in the San Diego - El Centro profile, we might suppose that this "base" level would be of the order of 1.2 HFU. This gives a value of 0.65 HFU for the anomaly maximum with a value of 0.3 HFU at 13 km (AN-3), and no appreciable decline in heat flow for 4 km on either side of the fault trace. From the curves in Figures 41 to 49, we see that this anomaly can be fit by either of two extreme cases, a line source at

about 15 km (Figure 41, between curves I and II) or a zone source 10 km wide and 25 km deep, with a linear-with-depth heat source distribution (Figure 49, between curves II and III). Both distributions would imply an energy release of about 3 cal/cm of fault/sec. The line source is unreasonable in that this model from equation (31) would require stresses of several thousand bars acting across a short interval of fault plane. Accepting the zone source model would imply that energy release is not confined to the region below the fault trace which is less than a km wide in this region. This does not seem reasonable in the case of earthquakes since we would expect the heat to be released where the ground broke. We might appeal to creep within the zone. Creep displacements across the San Jacinto and related faults south of Anza have been determined to be of the order of 3 cm/yr (Sharp, 1965). Under the assumption that this is also the creep rate across the 10 km wide strip along the San Jacinto near Anza, relation (38) would imply an average stress of about 500 bars acting across the fault plane, assuming a uniform creep rate with depth; or 1000 bars at 25 km. These values are consistent with Jeffreys' estimate of the strength of the crust (1959), but are higher than stresses which seem likely should exist in the vicinity of a major fracture or zone of weakness. Finally, it might be argued that the high heat flow in the Salton Trough is a result of the entire region undergoing right-lateral creep at the total rate of 8 cm/yr between points on the two sides of the trough (Whitten, 1955). If we consider the region to be approximated by a long, uniform heat producing zone 80 km wide and 20 km

deep, by equation (11), Appendix IV, and relation (38), we would need an average stress on the order of 500 bars to produce an observed anomaly of 0.6 μcal/cm^2/sec, as before. It seems more reasonable to invoke the similar explanation for high heat flow in the Salton Trough as for the Basin and Range Province adjacent to the east where the heat flow values remain equally high, that is, high temperatures in the lower crust and upper mantle (Roy, Blackwell, Decker, and Birch, 1968a).

The two regions studied immediately to the north of the Transverse Ranges, San Bernardino and Lake Hughes, have similar heat flows with one another of about 1.65 HFU with no apparent increase in heat flow near the San Andreas fault. This negative result, i.e. no heat flow anomaly along the San Andreas fault between San Bernardino and the Tehachapi Mountains where a large magnitude earthquake is known to have occurred, suggests an upper limit on the absolute stress. The absence of an anomaly (i.e. heat flow due to the fault is of the order of 0.1 μcal/cm^2/sec or less at the fault) implies (from Figures 1, 3, 4, or 5) that for a 20 km deep fault less than 1 km wide, heat is being produced at a rate of 0.3 cal/cm of fault length/sec or less. If we assume the average long term motion due to large earthquakes is about 3 cm/yr along this segment of the fault, we have that 0.3 cal/cm of fault length/sec is consistent with an average absolute stress of 60 bars. 0.3 cal/cm of fault length/sec is also of the same order as the amount of energy converted to seismic waves per cm of fault length per second assuming two 8 magnitude events per century (see section VIII) and hence implies an efficiency

of seismic wave generation of 50% or better for events occurring along this segment of the fault. If events along this segment of the fault have all been of the large magnitude type, this result is consistent with suggestions that the efficiency increases and the fractional stress-drop approaches unity with increasing magnitude (King and Knopoff, 1968). If we assume the validity of equation (32), section VIII, we would have that 60 bars would be an upper limit on the final state of stress and from calculations of stress-drops on strike-slip faults (Brune and Allen, 1967a), we could then put an upper bound of between 100 and 200 bars on the average pre-stress to be expected.

The profile across the Garlock fault in the Tehachapi Mountains exhibits a large heat flow maximum, ~2.0 HFU, in the vicinity of the fault. It is suggested that a portion of the high heat flow can be explained on the basis of radioactivity content of the local rock and on refraction near the fault.

As will be recalled, we showed in section VI (Tehachapi data) that the corrected heat flows due to refraction at the Garlock fault might reasonably be given by the following

DH-65 and 67	1.3 HFU unchanged
DH-43	1.8
DH-70	2.1
DH-14	2.0 unchanged
DH-15A	1.5 unchanged

Recent work by Blackwell (personal communication), which we will

not discuss here, suggests that the heat flow value at DH-70 should be further reduced by about 0.1 HFU due to the pattern of the subsurface isotherms, a result of the unusual distribution of mean annual soil temperatures prevailing in this region. We then have the corrected heat flow values reading

DH-65 and 67	1.3 HFU
DH-43	1.8
DH-70	2.0
DH-14	2.0
DH-15A	1.5 (?)

Next we want to consider the effect of the local radioactivity. We see from Figure 29 that a widespread region south of the Garlock fault is underlain by granite with a heat productivity of about 8×10^{-13} cal/cm^3/sec (from DH-14, Table 15), while a large region north of the fault is comprised of diorite with a heat productivity of about 1×10^{-13} cal/cm^3/sec (from DH-65, Table 18). Assuming that these plutons are semi-infinite sheets 10 km thick, we can, by adding and subtracting the effects of semi-infinite sheets and infinite strips (of the form, equation 11, Appendix IV), determine the effects at each of the drill sites of the local radioactivity. Thus we have that an infinite sheet 10 km thick with the assumed geometrical distribution of radioactivity would contribute the following to the heat flow at each of the drill holes

DH-65 and 67	0.21 HFU
DH-43	0.45
DH-70	0.56
DH-14	0.62
DH-15A	0.64

If we subtract these values from the last set of corrected heat flows, we get residual values at the drill holes given by

DH-65 and 67	1.09 HFU
DH-43	1.35
DH-70	1.44
DH-14	1.38
DH-15A	0.86 (?)

Finally, a correction might be necessary due to the fact that the profile across the Garlock also traverses the entire Tehachapi Range, from the Central Valley to the Mojave Desert, two provinces that are probably characterized by inherently different regional heat flows. This situation would be responsible for a gradient in heat flow across the range. If we consider the heat flow values at Lake Hughes, ~1.65 HFU, to be representative of the western Mojave Block (dismissing the value at DH-15A as anomalously low), and the value at DH-65 and 67, ~1.30 HFU, to be representative of the southern end of the Central Valley, we can assume a 0.1 HFU/10 km gradient, increasing from north to south across the Tehachapi Mountains. Applying this to our last corrected values (normalizing to DH-65 and 67), we get for the final residual heat flows

DH-65 and 67	1.09 HFU
DH-43	1.28
DH-70	1.34
DH-14	1.24
DH-15A	0.74 (?)

These would be the minimum expected residuals. Decreasing the effect of the local radioactivity and neglecting the heat flow transition only enhance the anomaly. As can be seen, we are unable to explain the difference of ~0.2 HFU between the three determinations near the Garlock fault and the value 8 km to the north. We might suggest that the residual above background be arbitrarily represented by the curve in Figure 51, although we have only two points on either side of the maximum to define its shape.

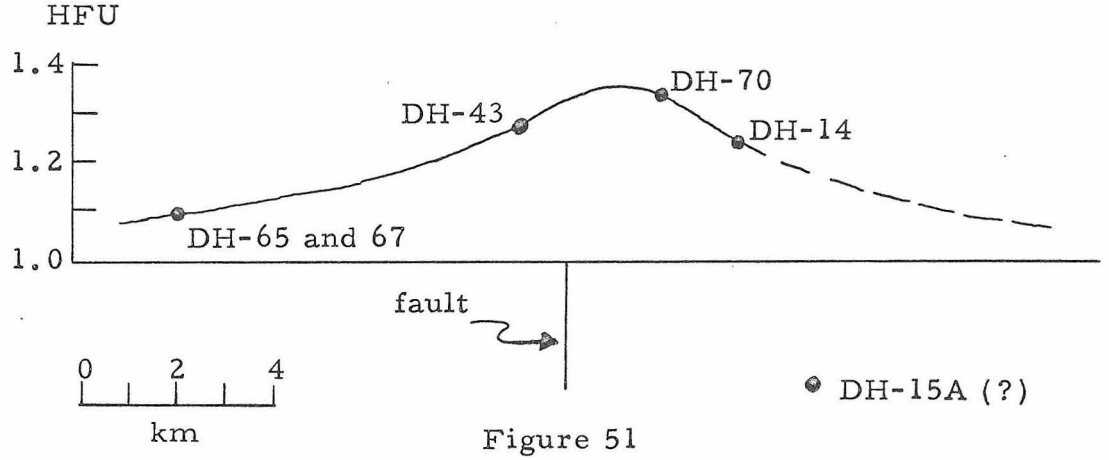

Figure 51

We have arbitrarily introduced a 0.1 HFU residual at DH-65 and 67 since, if the anomaly is due to the fault, we see from Figures 41 to 49 that unless the source is essentially at the surface, the value of Q at 8 km is <u>not</u> negligible. We have approximated the data by a curve

whose shape is similar to that of curve II in Figure 45, that is, a 20 km deep fault with energy production a linear function of depth, and at a rate of 1 cal/sec/cm of fault. This model is, of course, by no means unique. Because the Garlock fault is presently inactive, we do not know what sort of fault mechanism to assign the heat production to or what sort of rates of displacement have occurred. For displacement rates compatible to the San Andreas fault, the heat flow anomaly over the Garlock is consistent with a frictional stress of about 100 bars.

The last profile across the San Andreas fault is that near Hollister (see Figure 50). We will discuss here only the relation of the heat flow to the fault. A more complete discussion of the profile will be discussed by Roy, Brune, and Henyey (Heat flow in a zone of high creep rate along the San Andreas fault, California; in preparation). The fact that is most readily apparent from the profile is the high heat flow (~2.3 HFU) located a full 10 km east of the San Andreas fault and 6 km east of the Calaveras fault, a major branch of the San Andreas. This heat flow anomaly appears to be related to high temperatures at depth beneath the Diablo Range (see Figure 38), which consists in large part of the Franciscan complex of rocks. Any symmetric component about the San Andreas fault, if it existed, would be almost completely masked. On the basis of the value of 1.5 HFU at HO-8, 30 km east of the apparent maximum between HO-4 and HO-6 and the values of 1.7-1.8 HFU at HO-1 and HO-2 and 7, this symmetric component would not be expected to have a maximum

larger than 0.3 HFU. An 0.3 HFU anomaly associated with a 20 km deep fault creeping at the rate of 5 cm/yr is consistent with an average stress of about 100 bars.

C. Conclusions

From the previous discussion of the data, it is clear that in central and southern California we have not succeeded in finding a heat flow anomaly directly attributable to the San Andreas or its related faults. In the cases where the heat flow pattern is somewhat in doubt, it seems clear that we can place an upper limit of the order of a couple of tenths of an HFU fault-produced heat under a wide range of fault activity. These figures imply that if strain energy is released primarily through faulting, we should not expect the absolute stresses to exceed ~200 bars; while if creep is the primary mechanism of energy release, absolute stress should be no larger than ~100 bars.

The heat flow data from the San Andreas fault study are consistent from region to region along the fault. The mean value of 23 determinations in the vicinity of the major strike-slip faults (excluding SB-5 and the data of Roy and Brune between San Diego and El Centro) is 1.7 HFU ± 0.1 s.d., with a range of 1.2 to 2.3 HFU. This regional average can be compared to general data from middle North America and, in particular, the rest of the southwestern United States (see Figure 52).

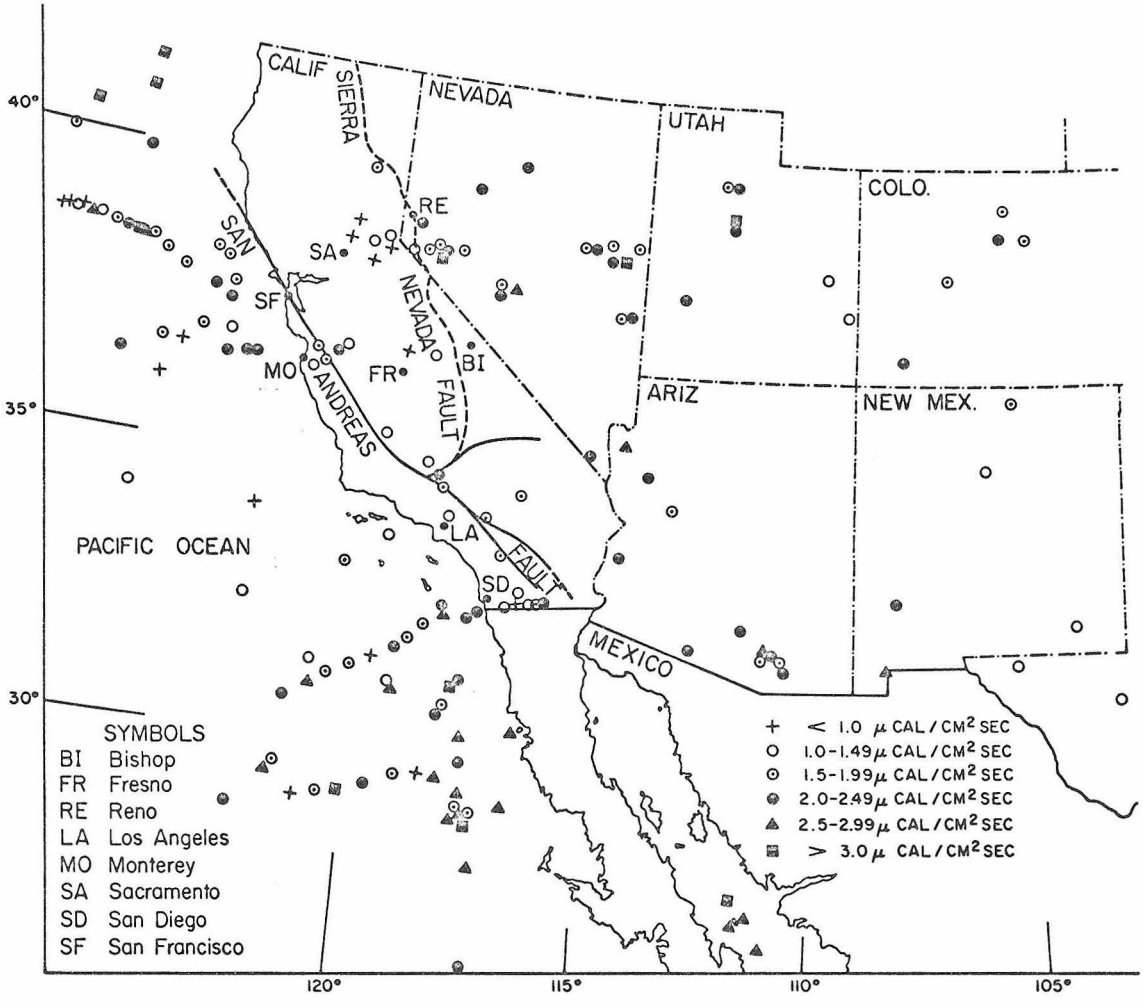

Map Contains Data from the Following Investigators:

Benfield (pub.)
Birch (pub.)
Burns and Grim (pub.)
Clark (pub.)
Foster (pub.)
Henyey and Wasserburg (this work)
Herrin and Clark (pub.)
Lachenbruch, Wollenberg, Greene and Smith (pub.)
Roy and Brune (personal comm.)
Roy, Decker, Blackwell and Birch (in press)
Spicer (pub.)
Von Herzen (pub.)
Wright and Costain (pub.)

Heat Flow Data from Southwestern U.S. Published or Reported Prior to January, 1968. Compiled by Roy and Blackwell and Reproduced here with their Permission (1968).

Figure 52

Lee and Uyeda (1965) discuss the heat flow data from North America in terms of four regions, the Canadian Shield, Interior Lowlands, Appalachian System, and Western Cordillera. They suggest that the average regional heat flows for these regions are as follows: 0.9 HFU for the Canadian Shield, 1.2 HFU for the Interior Lowlands, 1.0 HFU for the Appalachian System, and 1.7 HFU for the Western Cordillera. Recent heat flow data of Roy, Decker, Blackwell, and Birch (1968), however, raise the simple averages of the Appalachian System and Western Cordillera to 1.3 HFU and ≥2.0 HFU, respectively. Thus it appears that the Appalachian Region and Interior Lowlands have essentially the same heat flow, while the Western Cordillera remains significantly higher. In terms of regional averages, the mean value of 1.7 HFU for the San Andreas data would appear to be intermediate between the Interior Lowlands and Western Cordillera. However, recent work by Roy, Blackwell, Decker, and Birch (1968a) suggested that regional averages are meaningless unless the effect of the local radioactivity is taken into consideration. They prefer to define regional or provincial averages in terms of a "reduced" heat flow determined by the method presented in Figure 53. In each province, the surface heat flow (Q_S, $\mu cal/cm^2/sec$) and heat generation (A, 10^{-13} $cal/cm^3/sec$) of the local rock are related by an equation of the form $Q_S = Q_D + AD$. The heat flow Q_D, as given by the intercept in Figure 53, would be defined as the regional average with superposed infinite slabs of thickness D and heat generation A contributing to the remainder of the heat flow at each locality. Roy,

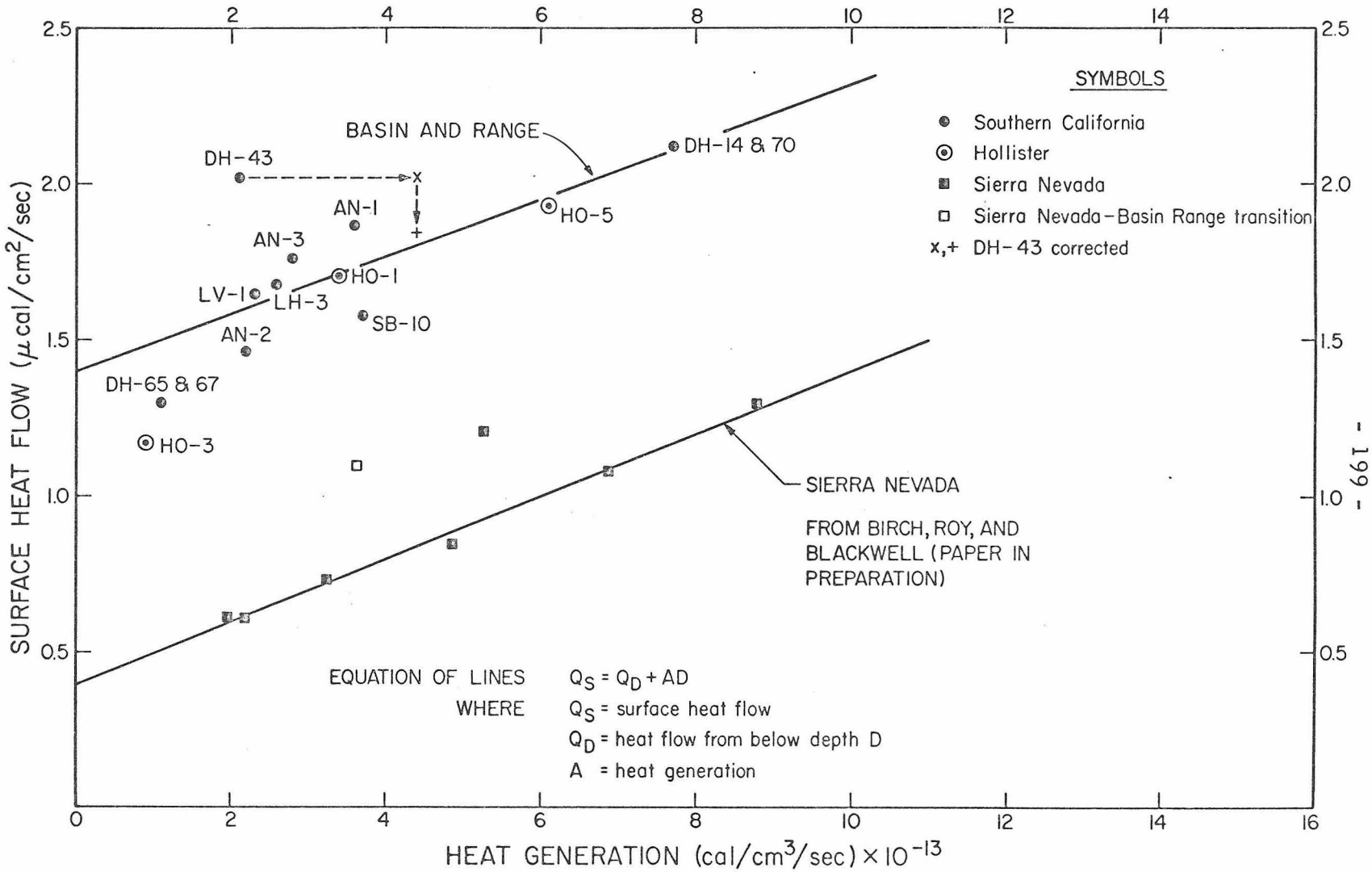
SURFACE HEAT FLOW (μcal/cm^2/sec)
HEAT GENERATION (cal/cm^3/sec) $\times 10^{-13}$
BASIN AND RANGE
SIERRA NEVADA
FROM BIRCH, ROY, AND BLACKWELL (PAPER IN PREPARATION)
DH-43
DH-14 & 70
HO-5
AN-1
AN-3
HO-1
LV-1
LH-3
SB-10
AN-2
DH-65 & 67
HO-3
SYMBOLS
Southern California
Hollister
Sierra Nevada
Sierra Nevada-Basin Range transition
x,+ DH-43 corrected
EQUATION OF LINES $Q_S = Q_D + AD$
WHERE Q_S = surface heat flow
Q_D = heat flow from below depth D
A = heat generation

Figure 53

et al. (1968a) and Roy (personal communication), using this approach, arrive at values for Q_D of 0.8 μcal/cm^2/sec for the Northern Appalachians and Interior Lowlands, 0.4 μcal/cm^2/sec for the Sierra Nevada (see Figure 53), and 1.4 μcal/cm^2/sec for the Basin and Ranges (Figure 53). Figure 53 also shows the reliable data from the San Andreas fault study plotted in a similar fashion. The points cluster around the Basin and Range line, suggesting a regional heat flow in the vicinity of the San Andreas not significantly different from the Basin and Range Province. DH-43 is the only point which falls appreciably above the line, but when corrected for refraction and the geometrical effect on the distribution of radioactivity due to the presence of the Garlock fault, the point falls close to the line. It is also seen that four points fall somewhat below the Basin and Range line. Locations whose points fall below the line would be expected to have a lower regional average. Two of the four points, AN-2 and HO-3, lie farthest west of the San Jacinto-San Andreas fault in their respective profiles, and DH-65 lies farthest north of the Garlock fault in its profile. In addition, all locations west of JA in the San Diego-El Centro profile must have heat flow - heat generation points which fall below the Basin and Range line. This suggests that as one proceeds from the fault toward one of these locations, one is going from a region of intrinsically higher heat flow to one of lower heat flow.

Figure 52 shows a summary of heat flow data from the southwestern United States. The regions to the west of the Sierra Nevada fault and north of the Garlock fault are regions of low to normal heat

flow. The data from the strip between the San Andreas-San Jacinto fault and the continental margin also suggest this to be a region of low to normal heat flow. Thus the major faults of California appear to lie on transitions between or delimit regions characterized by different heat flows from the lower crust and upper mantle. It should be emphasized that these regions are not of the subcontinental scale, but in many instances only of geologic province size, suggesting a complex tectonic pattern in the southwestern United States.

REFERENCES CITED

Aldrich, L. T. and Wetherill, G. W. (1958) Geochronology by radioactive decay: Ann. Rev. Nucl. Sci., 8, 257-298.

Allen, C. R. (1967) Different modes of strain energy release along the San Andreas fault (abst): Conference on Geologic Problems of the San Andreas Fault System, Stanford University.

Allen, C. R., St. Amand, P., Richter, C. F., and Nordquist, J. M. (1965) Relationship between seismicity and geologic structure in the southern California region: Bull. Seismo. Soc. Amer., 55, 753-797.

Allen, J. E. (1946) Geology of the San Juan Bautista quadrangle: Calif. Div. Mines Bull. 133, 9-75.

Anderson, E. M. (1951) The dynamics of faulting: Edinburgh, Oliver and Boyd, 206 p.

Andrews, P. (1936) Geology of the Pinnacles National Monument: Calif. Univ., Dept. Geol. Sci., Bull. 24, 1-38.

Bailey, T. L. and Jahns, R. H. (1954) Geology of the Transverse Range Province, southern California: Calif. Div. Mines Bull. 170, Chapt. II, 83-106.

Banks, P. O. and Silver, L. T. (1964) Material balance in the whole rock U-Pb system of a young granite (abst): Trans. Amer. Geophys. Union, 45, 108.

Bartlett (1965) Geologic log of drill hole SB-10, San Bernardino Mountains, California: Calif. State Dept. of Water Resources.

Bassett, A. M. and Kupfer, D. H. (1964) A geologic reconnaissance in the southeastern Mojave Desert: Calif. Div. Mines Spec. Rpt. 83, 43 p.

Bateman, P. C. and Wahrhaftig, C. (1966) Geology of the Sierra Nevada: Calif. Div. Mines Bull. 190, 107-172.

Båth, M. (1958) The energies of seismic body waves and surface waves: Contr. in Geophys. (Gutenberg Vol.) 1, 1-16.

Beck, A. E. (1957) A steady-state method for the rapid measurement of the thermal conductivity of rocks: Jour. Sci. Instr., 40, 452-454.

Beers, Y. (1957) Theory of error: Reading, Mass., Addison-Wesley Pub. Co., 66 p.

Benfield, A. E. (1947) A heat flow value for a well in California: Am. Jour. Sci., 245, 1-18.

Birch, F. (1950) Flow of heat in the Front Range, Colorado: Bull. Geol. Soc. Amer., 61, 567-630.

Birch, R. (1954) Heat from radioactivity in Neclear Geology, ed. H. Faul: New York, John Wiley and Sons, p. 148-174.

Birch, F., Roy, R. F., and Blackwell, D. D. (in prep.) Heat flow in the Sierra Nevada, California.

Blackwell, D. D. (1967) Terrestrial heat flow in the northwestern United States: Ph.D. Thesis, Harvard University.

Bowen, O. E., Jr. (1954) Geology and mineral resources of the Barstow Quadrangle: Calif. Div. Mines Bull. 165, 208 p.

Bowen, O. E., Jr. and Gray, C. H., Jr. (1959) Geology and economic possibilities of the limestone and dolomite deposits of the northern Gabilan Range, California: Calif. Div. Mines Spec. Rpt. 56, 40 p.

Bowen, R. (1966) Paleotemperature analysis: Amsterdam, Elsevier Pub. Co., 265 p.

Brooks, C. E. P. (1949) Climate through the ages: New York, McGraw-Hill, 395 p.

Brune, J. N. (1968) Seismic moment, seismicity, and rate of slip along major fault zones: Jour. Geophys. Res., 73, 777-784.

Brune, J. N. and Allen, C. R. (1967) A microearthquake survey of the San Andreas fault system in southern California: Bull. Seismo. Soc. Amer., 57, 277-296.

Brune, J. N. and Allen, C. R. (1967a) A low stress-drop, low-magnitude earthquake with surface faulting: The Imperial, California earthquake of March 4, 1966: Bull. Seismo. Soc. Amer., 57, 501-514.

Bullard, E. C. (1939) Heat flow in South Africa: Proc. Roy. Soc. London, Series A, 173, 474-502.

Bullard, E. C. (1947) The time necessary for a borehole to attain temperature equilibrium: Monthly Notices Roy. Astron. Soc., Geophys. Suppl., 5, 127-130.

Burckhalter (1964-65) Geologic log of drill hole DH-70, Tehachapi Mountains, California: Calif. State Dept. of Water Resources.

Burns, R. E. and Grim, P. J. (1967) Heat flow in the Pacific Ocean off central California: Jour. Geophys. Res., 72, 6239-6247.

Burridge, R. and Knopoff, L. (1966) The effect of initial stress or residual stress on elastic energy calculations: Bull. Seismo. Soc. Amer., 56, 421-424.

Buwalda, J. P. (1954) Geology of the Tehachapi Mountains, California: Calif. Div. Mines Bull. 170, Chapt. II, 131-142.

Byerly, P. and DeNoyer, J. (1958) Energy in earthquakes as computed from geodetic observations: Contr. in Geophys. (Gutenberg Vol.) 1, 17-35.

Carslaw, H. S. and Jaeger, J. C. (1959) Conduction of heat in solids: London, Oxford University Press, 497 p.

Clark, S. P. (1957) Heat flow at Grass Valley, California: Trans. Amer. Geophys. Union, 38, 239-244.

Clark, S. P. (1966) Thermal conductivity in Handbook of Physical Constants: Geol. Soc. Amer. Mem. 97, 459-482.

Clark, S. P., Peterman, Z. E., and Heier, K. S. (1966) Abundances of uranium, thorium, and potassium in Handbook of Physical Constants: Geol. Soc. Amer. Mem. 97, 521-541.

Cluff, L. S. and Steinbrugge, K. V. (1966) Hayward fault slippage in the Irvington-Niles districts of Fremont, California: Bull. Seismo. Soc. Amer., 56, 257-279.

Crowell, J. C. (1952) Geology of the Lebec Quadrangle, California: Calif. Div. Mines Spec. Rpt. 24, 23 p.

DeNoyer, J. (1958) Determination of the energy in body and surface waves (Part I): Bull. Seismo. Soc. Amer., 48, 355-368.

DeNoyer, J. (1959) Determination of the energy in body and surface waves (Part II): Bull. Seismo. Soc. Amer., 49, 1-10.

Dibblee, T. W., Jr. (1954) Geology of the Imperial Valley region, California: Calif. Div. Mines Bull. 170, Chapt. II, 21-28.

Dibblee, T. W., Jr. (1955) Geology of the southeastern margin of the San Joaquin Valley, California: Calif. Div. Mines Bull. 171, 23-34.

Dibblee, T. W., Jr. (1961) Geologic map of the Bouquet Reservoir Quadrangle, Los Angeles County, California: U. S. Geol. Survey Min. Inv. Field Studies Map MF-79.

Dibblee T. W., Jr. (1964) Geologic map of the Lucerne Valley Quadrangle, San Bernardino County, California: U. S. Geol. Survey Misc. Geol. Inv. Map I-426.

Dibblee, T. W., Jr. (1964) Geologic map of the Rodman Mountains Quadrangle, San Bernardino County, California: U. S. Geol. Survey Misc. Geol. Inv. Map I-430.

Dorsey (1960) Geologic log of drill hole SP-1 (LV-1 in this work), Lucerne Valley, California: Southern Pacific Land Company.

Dudley, P. H. (1935) Physiographic history of a portion of the Perris block, southern California: Calif. Jour. Mines and Geol., 31, 487-506.

Fenneman, N. M. (1931) Physiography of western United States: New York, McGraw-Hill, 534 p.

Foster, T. D. (1962) Heat flow measurements in the northeast Pacific and in the Bering Sea: Jour. Geophys. Res., 67, 2991-2993.

Gardner, D. L. (1940) Geology of the Newberry and Ord Mountains, San Bernardino County, California: Calif. Jour. Mines and Geol., 36, 257-292.

Geiger, R. (1950) The climate near the ground: Cambridge, Harvard University Press, 482 p.

Gough, D. I. (1963) Heat flow in the southern Karoo: Proc. Roy. Soc. London, Series A, 272, 207-230.

Gutenberg, B. and Richter, C. F. (1956) Earthquake magnitude, intensity, energy, and acceleration: Bull. Seismo. Soc. Amer., 46, 105-145.

Handin, J. (1966) Strength and ductility in Handbook of Physical Constants: Geol. Soc. Amer. Mem. 97, 223-289.

Healy, J. H. (1963) Crustal structure along the coast of California from seismic refraction measurements: Jour. Geophys. Res., 68, 5777-5787.

Herrin, E. and Clark, S. P. (1956) Heat flow in west Texas and eastern New Mexico: Geophysics, 21, 1087-1098.

Hewett, D. F. (1954) General geology of the Mojave Desert region, California: Calif. Div. Mines Bull. 170, Chapt. II, 5-20.

Hewett, D. F. (1956) Geology and mineral resources of the Ivanpah Quadrangle, Nevada-California: U. S. Geol. Survey Prof. Paper 275, 172 p.

Hoots, H. W. (1930) Geology and oil resources along the southern border of San Joaquin Valley, California: U. S. Geol. Survey Bull. 812-D, 243-332.

Jackson (1963) Geologic log of drill hole DH-15A, Tehachapi Mountains, California: Calif. State Dept. of Water Resources.

Jaeger, J. C. (1956) Numerical values for the temperature in radial heat flow: Jour. Math. and Phys., 34, 316-321.

Jaeger, J. C. (1961) The effect of the drilling fluid on temperatures measured in boreholes: Jour. Geophys. Res., 66, 563-569.

Jaeger, J. C. (1964) Thermal effects of intrusions: Revs. Geophys., 2, 443-466.

Jaeger, J. C. (1965) Application of the theory of heat conduction to geothermal measurements in Terrestrial Heat Flow: Amer. Geophys. Union Monograph 8, 7-23.

Jaeger, J. C. and Beck, A. (1955) The calculation of heat flow through disks and its application to conductivity measurements. Brit. Jour. Appl. Phys., 6, 15-16.

Jahns, R. H. (1954) Geology of the Peninsular Range Province, southern California and Baja California: Calif. Div. Mines Bull. 170, Chapt. II, 29-52.

Jeffreys, H. (1940) The disturbance of the temperature gradient in the earth's crust by inequalities of height: Monthly Notices Roy. Astron. Soc., Geophys. Suppl., 4, 309-312.

Jeffreys, H. (1959) The Earth: Cambridge University Press, 420 p.

Kelis-Borok, V. I. (1959) On estimation of the displacement in an earthquake source and of source dimensions: Annali Geofisica, 12, 205-214.

Kendrew, W. G. (1953) The climates of the continents: Oxford, Clarendon Press, 607 p.

King, C. and Knopoff, L. (1968) Stress drop in earthquakes: Bull. Seismo. Soc. Amer., 58, 249-257.

Knopoff, L. (1958) Energy release in earthquakes: Geophys. Jour., 1, 44-52.

Lachenbruch, A. H. and Brewer, M. C. (1959) Dissipation of the temperature effect of drilling a well in arctic Alaska: U. S. Geol. Survey Bull. 1083-C, 73-109.

Lachenbruch, A. H., Wollenberg, H. A., Greene, G. W., and Smith, A. R. (1966) Heat flow and heat production in the central Sierra Nevada, Preliminary results (abst): Trans. Amer. Geophys. Union, 47, 179.

Larsen, E. S., Jr. (1941) The batholith of southern California: Science, 93, 442-443.

Larsen, E. S., Jr. (1945) Time required for the crystallization of the great batholith of southern and lower California: Am. Jour. Sci., 243-A, 399-416.

Larsen, E. S., Jr. (1948) Batholith and associated rocks of Corona, Elsinore, and San Luis Rey Quadrangles, southern California: Geol. Soc. Amer. Mem. 29, 182 p.

Lee, W. H. K. and Uyeda, S. (1965) Review of heat flow data in Terrestrial Heat Flow: Amer. Geophys. Union Monograph 8, 87-190.

Mabey, D. R. (1960) Gravity survey of the western Mojave Desert, California: U. S. Geol. Survey Prof. Paper 316-D, 51-73.

McCulloh, T. H. (1954) Problems of the metamorphic and igneous rocks of the Mojave Desert: Calif. Div. Mines Bull. 170, Chapt. VII, 13-24.

Meade, B. K. (1963) Horizontal crustal movements in the United States: Rpt. to Comm. on Recent Crustal Movements, Int. Union of Geodesy and Geophys., General Assembly, Berkeley.

Meade, B. K. and Small, J. B. (1966) Current and recent movement on the San Andreas fault: Calif. Div. Mines Bull. 190, 385-391.

Miller, W. J. (1935) Geomorphology of the southern Peninsular Range of California: Geol. Soc. Amer. Bull., 46, 1535-1562.

Nairn, A. E. M., ed. (1963) Problems in Paleoclimatology: London, Interscience Pub., 705 p.

Orowan, E. (1960) Mechanism of seismic faulting: Geol. Soc. Amer. Mem. 79, 323-345.

Radbruch, D. H. (1967) New evidence of recent fault activity in Alameda, Contra Costa, and Santa Clara Counties, California (abst): Conference on Geologic Problems of the San Andreas Fault System, Stanford University.

Ratcliffe, E. H. (1959) Conductivity of fused and crystalline quartz: Brit. Jour. Appl. Phys., 10, 22-25.

Rex, R. W. (1966) Heat flow in the Imperial Valley of California (abst): Trans. Amer. Geophys. Union, 47, 181.

Roy, R. F. (1963) Heat flow measurements in the United States: Ph.D. Thesis, Harvard University.

Roy, R. F. and Blackwell, D. D. (1966) Heat flow in the Sierra Nevada and western Great Basin (abst): Trans. Amer. Geophys. Union, 47, 179-180.

Roy, R. F., Blackwell, D. D., Decker, E. R., and Birch, F. (1968a) Heat generation of surface rocks and heat flow provinces (abst): Trans. Amer. Geophys. Union, 49, 319.

Roy, R. F., Brune, J. N., and Henyey, T. L. (in prep.) Heat flow in a zone of high creep rate along the San Andreas fault, California.

Roy, R. F., Decker, E. R., Blackwell, D. D., and Birch, F. (1968) Heat flow in the United States: Jour. Geophys. Res., in press.

Salovyov, S. L. (1959) Magnitude and energy of earthquakes: Publ. Bur. Centr. Seism. Int. A 20, 39-53.

Sauer, C. (1929) Land forms in the Peninsular Range of California as developed about Warner's Hot Springs and Mesa Grande: Univ. Calif. Publ. in Geography, 3, 199-290.

Sharp, R. V. (1965) Geology of the San Jacinto fault zone in the Peninsular Ranges of southern California: Ph.D. Thesis, California Institute of Technology.

Shumm, S. A. (1963) Disparity between present rates of denudation and orogeny: U. S. Geol. Survey Prof. Paper 454-H, 13 p.

Simpson, E. C. (1934) Geology and mineral deposits of the Elizabeth Lake Quadrangle, California: Calif. Jour. Mines and Geol., 30, 371-415.

Smith, G. I. (1960) Time of last displacement on the middle part of the Garlock fault, California: U. S. Geol. Survey Prof. Paper 400-B, 280.

Spicer, H. C. (1964) Geothermal gradients and heat flow in the Salt Valley Anticline, Utah: Boll. Geofis. Teorica Appl., 6, 263-282.

Stearns, N. D., Stearns, H. T., and Waring, G. A. (1937) Thermal springs in the United States: U. S. Geol. Survey Water Supply Paper 679-B, 59-191.

Steinbrugge, K. V., Zacher, E. G., Tocher, D., Whitten, C. A., and Claire, C. N. (1960) Creep on the San Andreas fault: Bull. Seismo. Soc. Amer., 50, 389-415.

Stewart, S. W. (1967) Preliminary comparison of seismic travel times and inferred crustal structure adjacent to the San Andreas fault in the Diablo and Gabilan Ranges (abst): Conference on Geologic Problems of the San Andreas Fault System, Stanford University.

Teisseyre, R. (1960) A dislocation model of the earthquake mechanism and the influence of discontinuity surfaces on seismic energy release: Acta Geophys. Polonica, 8, 107-113.

U. S. Weather Bureau (1964) Climatography of the United States, No. 86-4, Climatic summary of the United States, Supplement for 1951-1960, California, 215 p.

Von Herzen, R. P. (1963) Geothermal heat flow in the Gulfs of California and Aden: Science, 140, 1207-1208.

Von Herzen, R. P. (1964) Ocean-floor heat-flow measurements west of the United States and Baja California: Marine Geol., 1, 225-239.

Walsh, J. B. and Decker, E. R. (1966) Effect of pressure and saturating fluid on the thermal conductivity of compact rock: Jour. Geophys. Res., 71, 3053-3061.

Wasserburg, G. J., MacDonald, G. J. F., Hoyle, F., and Fowler, W. (1964) Relative contributions of uranium, thorium, and potassium to heat production in the earth: Science, 143, 465-467.

White, D. E. (1957) Thermal waters of volcanic origin: Bull. Geol. Soc. Amer., 68, 1637-1658.

Whitten, C. A. (1955) Measurements of earth movements in California: Calif. Div. Mines Bull. 171, 75-80.

Wiese, J. H. (1950) Geology and mineral resources of the Neenach Quadrangle, California: Calif. Div. Mines Bull. 153, 51 p.

Wiese, J. H. and Fine, S. F. (1950) Structural features of western Antelope Valley, California: Amer. Assoc. Pet. Geol. Bull., 34, 1647-1658.

Wilson, I. F. (1943) Geology of the San Benito Quadrangle, California: Calif. Jour. Mines and Geol., 39, 183-270.

Wright, M. P. and Costain, J. K. (1968) Heat flow and geothermal gradient measurements in Utah (abst): Trans. Amer. Geophys. Union, 49, 325.

Wu, F. (1966) The lower limit of total energy and partitioning of energy for three earthquakes (abst): Trans. Amer. Geophys. Union, 47, 163.

APPENDIX I

A. Determination of Heat Production due to U-Th from α-Particle Counting

Symbols and values of physical constants and specific α-activities (see Aldrich and Wetherill, 1958) used in the following discussion are given below

$$1 \text{ year} = 3.156 \times 10^{7} \text{ seconds}$$
$$= 5.26 \times 10^{5} \text{ minutes}$$

$$t_m = 5.26 \times 10^{5} \text{ minutes/year}$$

$$1 \text{ ev} = 3.829 \times 10^{-20} \text{ cal}$$

$$U^{235}/U^{238} \simeq 1/139.5 \qquad \text{(ratio by weight)}$$

$$n_{238} \text{ (specific activity of } U^{238}) = 742.7 \times 10^{3} \ \frac{U^{238}\text{dis}}{\text{min}\cdot\text{gm } U^{238}}$$

$$n_{235} \text{ (specific activity of } U^{235}) = 4740 \times 10^{3} \ \frac{U^{235}\text{dis}}{\text{min}\cdot\text{gm } U^{235}}$$

$$n_{232} \text{ (specific activity of } Th^{232}) = 246.3 \times 10^{3} \ \frac{Th^{232}\text{dis}}{\text{min}\cdot\text{gm } Th^{232}}$$

First we determine how many ppm of U^{235} and how many ppm of U^{238} are in 1 ppm of U (ordinary uranium). We have

$$\frac{U^{235}}{U^{238}} = \frac{1}{139.5}$$

Let

$$x = \#\text{ ppm of } U^{235} \text{ in 1 ppm U}$$

$$y = \#\text{ ppm of } U^{238} \text{ in 1 ppm U}$$

$$\therefore \quad x + y = 1$$

$$\frac{x}{y} = \frac{1}{139.5}$$

We have neglected the contribution from the other uranium nuclides.

Solving we get

$$x = \frac{1}{140.5} \frac{\text{ppm } U^{235}}{\text{ppm U}}$$

$$y = \frac{139.5}{140.5} \frac{\text{ppm } U^{238}}{\text{ppm U}} \qquad (1)$$

Now let us determine the α-activity of 1 ppm U^{235} in equilibrium with its daughters. This is given by

$$n_{235} \cdot t_m \cdot (\#\ \alpha\text{-decays in } U^{235} \text{ series} = 7)$$

Note that we are assuming radioactive equilibrium, and for each decay of a U^{235} atom, we have a decay at each decay point through the entire U^{235} series.

Therefore we can write

$$4740 \times 10^3 \frac{U^{235}\text{ dis}}{\text{min} \cdot \text{gm } U^{235}} \cdot 3.26 \times 10^5 \frac{\text{min}}{\text{yr}} \cdot 7 \frac{\alpha\text{-dis}}{U^{235}\text{ dis}}$$

$$= 1.74 \times 10^{13} \frac{\alpha\text{-dis}}{\text{yr} \cdot \text{gm } U^{235}} \qquad (2)$$

Now if we note that by definition

$$1 \text{ ppm } U^{235} \equiv 10^{-6} \frac{\text{gm } U^{235}}{\text{gm of rock}}$$

we can multiply (2) by

$$10^{-6} \frac{\text{gm } U^{235}}{\text{gm of rock} \cdot \text{ppm } U^{235}}$$

and we have

$$1.74 \times 10^{13} \frac{\alpha\text{-dis}}{\text{yr} \cdot \text{gm } U^{235}} \cdot \frac{\text{gm } U^{235}}{\text{gm of rock} \cdot \text{ppm } U^{235}}$$

$$= 1.74 \times 10^{7} \frac{\alpha\text{- dis}}{\text{yr} \cdot \text{ppm } U^{235} \cdot \text{gm of rock}} \quad (3)$$

Now we do the similar thing for U^{238}, that is the α-activity of 1 ppm U^{238}, is given by

$$n_{238} \cdot t_m \cdot (\#\ \alpha\text{-decays} = 8) \cdot 10^{-6} \frac{\text{gm } U^{238}}{\text{gm of rock} \cdot \text{ppm } U^{238}}$$

$$= 3.12 \times 10^{6} \frac{\alpha\text{-dis}}{\text{ppm } U^{238} \cdot \text{gm of rock}} \quad (4)$$

Now we want to determine the activity of 1 ppm U. From eqns. (1), (3), and (4), we have for the activity of 1 ppm U

$$\frac{1}{140.5} \cdot 1.74 \times 10^{7} + \frac{139.5}{140.5} \cdot 3.12 \times 10^{6}$$

$$= 3.22 \times 10^{6} \frac{\alpha\text{ - dis}}{\text{yr} \cdot \text{ppm U} \cdot \text{gm of rock}} \quad (5)$$

Now we ask as before what the α-activity of 1 ppm of Th^{232} is. It is given as before by

$$n_{232} \cdot t_m \cdot (\#\ \alpha\text{-decays} = 6) \cdot 10^{-6}\ \frac{\text{gm Th}^{232}}{\text{gm of rock} \cdot \text{ppm Th}^{232}}$$

$$= 7.77 \times 10^5\ \frac{\alpha\text{ - dis}}{\text{yr} \cdot \text{ppm Th}^{232} \cdot \text{gm of rock}} \qquad (6)$$

We now want to develop the concept of equivalent uranium, or 1 ppm of equivalent uranium, which we will abbreviate 1 ppm eU. If we say that a substance has χ ppm eU, we mean that it has the α-activity equivalent to that of χ ppm U. Thus we see, for example, from taking the ratio of (5) to (6) that 1 ppm U has the same activity as 4.14 ppm Th^{232}. That is

$$\frac{3.22 \times 10^6}{7.77 \times 10^5} = 4.14 \qquad (7)$$

So, for example, if we are given a rock that contains 5 ppm U and 20 ppm Th^{232}, we will say that it contains

$$5 + \frac{20}{4.14} = 5 + 4.83 = 9.83 \text{ ppm eU}$$

that is, 9.83 ppm equivalent uranium. When counting α-particles, we do not know whether they are coming from uranium or thorium or a combination, and so we express everything in terms of eU. Before proceeding to energy calculations, we will need several more numbers. First, we want to know, in 1 ppm U, what fraction of the decays come from U^{235} and what fraction from U^{238}. We get these values from the determination of (5), namely, the fraction of decays from U^{235} is

$$\frac{\frac{1}{140.5} \cdot 1.74 \times 10^7}{3.22 \times 10^6} = 0.038 \qquad (8)$$

and similarly the fraction of decays from U^{238} is

$$\frac{\frac{139.5}{140.5} \cdot 3.12 \times 10^{6}}{3.22 \times 10^{6}} = 0.962 \qquad (9)$$

Second, what can we say about the fraction of decays from thorium and the fraction from uranium in 1 ppm eU? As we said before we do not know where the decays are coming from, but if we make at this point the reasonable assumption that in normal rock

$$\frac{U}{Th} \approx \frac{1}{4.14} \quad \text{(by weight)} \qquad (10)$$

we will note from our discussion of equation (7) that now we would have in 1 ppm eU exactly half the decays coming from the uranium and half from thorium, so

$$\begin{aligned} &\text{fraction of decays from U} = 0.500 \\ &\text{fraction of decays from Th} = 0.500 \end{aligned} \qquad (11)$$

We will see later that the assumption of the U-Th ratio of 1:4.14 can only lead to errors in the heat production determination of at most several per cent for cases of pure thorium or pure uranium. We have from column 3 of Table 3 (in Mev per atom)

U^{238}	47.4
U^{235}	45.2
Th^{232}	39.8

Now in the U^{238} decay series, we have 8 α-particles given off per decay of one U^{238} atom. Thus one α-decay in the U^{238} series is representative of

$$\frac{47.4 \text{ Mev}}{8 \text{ dis}} = 5.924 \frac{\text{Mev}}{\text{dis}} \qquad (12)$$

Similarly for U^{235} we get

$$\frac{45.2 \text{ Mev}}{7 \text{ dis}} = 6.457 \frac{\text{Mev}}{\text{dis}} \qquad (11')$$

and for Th^{232}

$$\frac{39.8 \text{ Mev}}{6 \text{ dis}} = 6.633 \frac{\text{Mev}}{\text{dis}} \qquad (11'')$$

Now if we know the amount of eU in a sample, we know the number of decays per unit time,and we know each decay represents one of the energies in (11). But in (8), (9), and (10), we considered the relative contributions of each species to the activity. Therefore, let us weight the energies in (11) by these relative contributions. We have for the uranium

$$0.962(5.925) + 0.038(6.457) = 5.952 \frac{\text{Mev}}{\text{dis}}$$

Thus if our decays were due to only U, we would have each decay representing 5.952 Mev. But from (11) we see that we have 50% Th and 50% U. Thus each decay represents

$$0.500(5.952) + 0.500(6.633) = 6.292 \frac{\text{Mev}}{\text{dis}} \qquad (13)$$

It can now be seen if we have only U in our sample, we should have taken 5.952 Mev/decay and we would be off

$$\frac{6.292 - 5.952}{6.292} \sim 5\%$$

by using (13). If we had only thorium, we should have used 6.633 Mev/decay and we would be off

$$\frac{6.633 - 6.292}{6.292} \sim 5\%$$

So at most, our values for energy production will be in error by ±5%, and in normal rock we will generally be within ±1%. Now we can make the final determination of the amount of energy available for heat per ppm eU. We multiply (13) by (5)

$$6.292 \frac{\text{Mev}}{\text{dis}} \cdot 3.22 \times 10^{6} \frac{\text{dis}}{\text{yr} \cdot \text{ppm eU} \cdot \text{gm of rock}}$$

since by definition 1 ppm eU means the activity equivalent to 1 ppm U. This is equal to

$$2.03 \times 10^{7} \frac{\text{Mev}}{\text{yr} \cdot \text{ppm eU} \cdot \text{gm of rock}} \qquad (14)$$

Now we have the conversion factors

$$3.829 \times 10^{-14} \frac{\text{cal}}{\text{Mev}}$$

$$3.156 \times 10^{7} \frac{\text{sec}}{\text{yr}}$$

So (14) is equivalent to

$$2.46 \times 10^{-14} \frac{\text{cal}}{\text{sec} \cdot \text{ppm eU} \cdot \text{gm of rock}} \qquad (15)$$

If we assume an average rock density of 2.7 gm/cm^3, (15) becomes

$$\boxed{0.66 \times 10^{-13} \frac{\text{cal}}{\text{sec} \cdot \text{cm}^3 \cdot \text{ppm eU}}} \qquad (16)$$

where (10) is <u>implicitly assumed.</u>

B. Heat Production from Ordinary Uranium, Thorium, and Potassium

We can write down expressions similar to (16) for ordinary uranium and thorium alone. From Table 3 and using a rock density of 2.7 gm/cm^3, we get

$$0.62 \times 10^{-13} \frac{\text{cal}}{\text{sec} \cdot \text{cm}^3 \cdot \text{ppm U}_{\text{ordinary}}}$$

$$0.17 \times 10^{-13} \frac{\text{cal}}{\text{sec} \cdot \text{cm}^3 \cdot \text{ppm Th}}$$

Similarly for ordinary potassium, we have (in terms of per cent $K_{ordinary}$)

$$0.23 \times 10^{-13} \frac{\text{cal}}{\text{sec} \cdot \text{cm}^3 \cdot \%\ K_{\text{ordinary}}} \qquad (17)$$

If only the equivalent uranium is determined for a sample, we can make the assumption (Wasserburg, MacDonald, Hoyle, and Fowler, 1964)

$$\frac{K}{U} = 10^4 \qquad (18)$$

Then since

$$\frac{K}{U} = 10^4 \rightarrow \frac{1\%K}{\text{ppm U}} \rightarrow \frac{\frac{1}{2}\%K}{\frac{1}{2}\text{ ppm U}}$$

and a ratio (be weight) Th/U = 4.14/1 implies that 1 ppm eU is made up of $\frac{1}{2}$ ppm Th and $\frac{1}{2}$ ppm U, we can combine (16) and (17) into a single relation, namely

$$0.775 \times 10^{-13} \frac{\text{cal}}{\text{sec} \cdot \text{cm}^3 \cdot \text{ppm eU*}}$$

where now (18) and (10) are implicitly assumed along with a rock density of 2.7 gm/cm^3.

* Includes the potassium content

APPENDIX II

The Effect on α-Activity due to Possible Radon Loss from a Crushed Rock Sample

The rebuilding of a radioactive species which has been removed from an equilibrium decay series is given by the following equation

$$\frac{dN}{dt} = \lambda_o N_o - \lambda N$$

where $\frac{dN}{dt}$ is the rate of buildup, N is the number of that species, λ its decay constant, and N_o and λ_o are the number and decay constant, respectively, for the parent. This equation has the solution (if all of the species were lost)

$$N = \frac{\lambda_o N_o}{\lambda}\left[1-e^{-\lambda t}\right]$$

If we want to determine how long the lost species takes to build up to say 90% of its equilibrium value, we note

$$N_\infty = \frac{\lambda_o N_o}{\lambda}$$

or

$$\frac{N}{N_\infty} = 1-e^{-\lambda t} = 0.90$$

and solving for t we get

$$t = \frac{\ell n\ 10}{\lambda} = \frac{\ell n\ 10}{\ell n\ 2} t_{1/2} \approx 3t_{1/2}$$

where $t_{1/2}$ is the half-life of the species in question. It should also be noted that decays of short lived daughters, of the species which is

removed, are also affected. We have for the decay of a species which is not being replenished

$$\frac{dN}{dt} = -\lambda N$$

with the notation as before. This has the solution

$$N = N_o e^{-\lambda t}$$

where N_o is the number at the time replenishment ceased. Thus if we ask when the number of decays reaches say 10% of normal, or equivalently when the number of particles, N, is 10% of N_o, we have

$$\frac{N}{N_o} = e^{-\lambda t} = 0.1$$

or solving for t

$$t = \frac{\ell n\ 10}{\ell n\ 2}\, t_{1/2} \approx 3t_{1/2}$$

Thus we see it takes characteristically three half-lives for a species which is removed to replenish itself and also about three half-lives for a daughter of a species not being replenished to essentially disappear. We can now examine the half-lives of radon and their daughters to see whether or not loss of radon might introduce significant effects. The Th^{232} series involves Rn^{219} with a half-life of 3.92 seconds; obviously equilibrium will be re-established in this series in a matter of seconds. The U^{235} series decays to Rn^{220} with a half-life of 54 seconds. Again equilibrium will be rapidly re-established, this time in a few minutes. The U^{238} series decays to Rn^{222} with a half-life of 3.82 days. Thus if all radon were lost,

we might find it necessary to wait a week or two before equilibrium is re-established. Furthermore, if we look at the decay products of Rn^{222} to Bi^{210}

Rn^{222}	Po^{218}	α-decay	$t_{1/2} = 3.82$ d
Po^{218}	Pb^{214}	α-decay	$t_{1/2} = 3$ m
Pb^{214}	Bi^{214}	β-decay	$t_{1/2} = 27$ m
Bi^{214}	Po^{214}	β-decay	$t_{1/2} = 20$ m
Po^{214}	Pb^{210}	α-decay	$t_{1/2} = 10^{-4}$ sec
Pb^{210}	Bi^{210}	β-decay	$t_{1/2} = 22$ yrs

we see that all the daughters up to Pb^{210} (during the decays of which two additional α-particles are involved) are appreciably depleted within a matter of one hour if not replenished; hence their depletion and buildup follow that of Rn^{222}. So if the radon escapes with crushing, three α-decays are affected; this is 3/14 or 21% of the total α-decays which are affected. Conceivably then, one could introduce up to a 21% error in heat productivity by not waiting a week or two for equilibrium to be re-established.

APPENDIX III

Derivation of the Topographic Correction for Measurement of Heat Flow in Drill Holes

The temperature, v, at an interior point (x, y, z, t) of a semi-infinite half space of uniform thermal diffusivity $\varkappa$ produced by surface temperature f(x', y', t) $t > 0$, can be represented by (Birch, 1950, eqn. 3)

$$v(x, y, z, t) = \frac{4\varkappa z}{\pi^{3/2}} \int_{-\infty}^{\infty}\int_{-\infty}^{\infty}\int_{o}^{t} \frac{f(x', y', t')}{[4\varkappa(t-t')]^{5/2}} \exp -\left[\frac{R^2}{4\varkappa(t-t')}\right] dx'dy'dt' \qquad (1)$$

where

$$R^2 = (x-x')^2 + (y-y')^2 + (z-z')^2$$

If we assume the time variation to be linear, and also transform to cylindrical polar coordinates, we can integrate (1) with respect to the time variable and find that the temperature v at a time t is given by (Birch, 1950, eqn. 8)

$$v(x, y, z, t) = \frac{z}{2\pi} \int_{o}^{\infty}\int_{o}^{2\pi} f(r, \varphi, t)\, E(\beta)\, \frac{r\, dr\, d\varphi}{R^3} \qquad (2)$$

where

$$E(\beta) = 2 \operatorname{erfc} \beta - 4i^2 \operatorname{erfc} \beta$$

$$\beta = \frac{R}{\sqrt{4\varkappa t}}$$

and

$$r^2 = (x-x')^2 + (y-y')^2$$

φ being measured in the x-y plane.

Birch then demonstrates (pp. 588-590, 1950) that temperature variations on the present irregular surface which began as a plane boundary (original surface) on which the temperature had been uniform and constant for a long time, and which might have undergone a certain amount of uniform vertical uplift and concomitant erosion, can be distributed, to a good approximation, over a reference plane passing through a point on the surface directly above the interior point at which the effect of the surface temperature distribution is to be applied. (This would be the collar in the case of a drill hole). Furthermore, it is shown that the temperature change at a general point on the reference plane due to uplift and erosion is (the near surface gradient having been approximated by the undisturbed geothermal gradient)

$$-\alpha' L - (\alpha - \alpha')\,[d + h(r, \varphi)] \qquad (3)$$

where L is the amount of uplift of the original surface, d the amount of erosion, α the true undisturbed geothermal gradient, α' the change of surface or soil temperature with elevation, and $h(r, \varphi)$ the measured relief from the reference plane at time t. It must be emphasized that d does not represent an average erosion over the region surrounding the drill site, but rather the actual position of the collar of the hole in question with respect to the original surface. Thus the change at an internal point (x, y, z), which can be represented by

$$T(z) - T_s - \alpha[d + z] \qquad (4)$$

T_s being the original surface temperature and T(z) the present temperature at depth z, is found using equation (2) where (3) has been

substituted for $f(r, \varphi, t)$. Thus we have

$$T(z) - T_s - \alpha[d+z] = \frac{z}{2\pi} \int_0^{\infty} \int_0^{2\pi} \left\{ -\alpha' L - (\alpha - \alpha')[d + h(r, \varphi)] \right\} E(\beta) \frac{r\, dr\, d\varphi}{R^3} \tag{5}$$

$$= \frac{z}{2\pi} [-\alpha' L - (\alpha - \alpha') d] \int_0^{\infty} \int_0^{2\pi} E(\beta) \frac{r\, dr\, d\varphi}{R^3}$$

$$- \frac{z}{2\pi} (\alpha - \alpha') \int_0^{\infty} \int_0^{2\pi} h(r, \varphi) E(\beta) \frac{r\, dr\, d\varphi}{R^3} \tag{6}$$

$$= \frac{z}{2\pi} [-\alpha' L - (\alpha - \alpha') d] I_1 - \frac{z}{2\pi} (\alpha - \alpha') I_2 \tag{7}$$

where I_1 and I_2 are the two integrals in (6), respectively. Now I_1 can be integrated directly and gives

$$I_1 = \frac{2\pi}{z} \left[4i^2 \operatorname{erfc} \left(\frac{z}{\sqrt{4\varkappa t}} \right) \right] \tag{8}$$

$$\simeq \frac{2\pi}{z} \left(1 - \frac{2z}{\sqrt{\pi \varkappa t}} \right) \tag{9}$$

I_2 can be evaluated in a form applicable to numerical evaluation of three-dimensional problems. Consider the reference plane divided into radii r_1, r_2, r_3, $r_4 \ldots$; then we can write

$$\frac{z}{2\pi} I_2 = \frac{z}{2\pi} \int_0^{\infty} \int_0^{2\pi} h(r, \varphi) E(\beta) \frac{r\, dr\, d\varphi}{R^3} \tag{10}$$

$$= \frac{z}{2\pi} \left[\int_0^{r_1} \int_0^{2\pi} h(r, \varphi) E(\beta) \frac{r\, dr\, d\varphi}{R^3} + \int_{r_1}^{r_2} \int_0^{2\pi} h(r, \varphi) E(\beta) \frac{r\, dr\, d\varphi}{R^3} \right.$$

$$\left. + \int_{r_2}^{r_3} \int_0^{2\pi} h(r, \varphi) E(\beta) \frac{r\, dr\, d\varphi}{R^3} + \ldots \right] \tag{11}$$

Let us look at one of these terms, say

$$\frac{z}{2\pi}\int_{r_1}^{r_2}\int_{o}^{2\pi} h(r,\varphi)E(\beta)\,\frac{r\,dr\,d\varphi}{R^3} \tag{12}$$

if $\overline{h}_r$ and $\overline{E}_r$ are the mean values of $h(r,\varphi)$ and $E(\beta)$, respectively, for the ring $r_1 < r < r_2$, then we can write (12) as

$$\frac{z}{2\pi}\,\overline{E}_r\overline{h}_r\int_{r_1}^{r_2}\int_{o}^{2\pi}\frac{r\,dr\,d\varphi}{R^3} \tag{13}$$

From geometric considerations, we know an element of solid angle $d\Omega$ subtended by an element of surface area $d\sigma$ at a distance R from the vertex of $d\Omega$ can be written

$$d\Omega = \frac{\overline{n}\cdot\overline{R}}{R^3}\,d\sigma \tag{14}$$

where $\overline{n}$ is the unit normal to the surface σ. Thus it can be seen that in (13)

$$\frac{z\,r\,dr\,d\varphi}{R^3}$$

is the element of solid angle $d\Omega$, subtended at the point (x, y, z) by the element of surface $r\,dr\,d\varphi$ of the plane $z = 0$, and

$$\Delta\Omega_r = \int_{r_1}^{r_2}\int_{o}^{2\pi}\frac{z\,r\,dr\,d\varphi}{R^3} \tag{15}$$

is just the element of solid angle subtended by the ring $r_1 < r < r_2$. Integrating, we have

$$\Delta\Omega_r = 2\pi\left[\left(\frac{r_1^2}{z^2}+1\right)^{-1/2} - \left(\frac{r_2^2}{z^2}+1\right)^{-1/2}\right] \tag{16}$$

So (13) becomes

$$\frac{1}{2\pi}\bar{E}_r\bar{h}_r\Delta\Omega_r \tag{17}$$

and hence (11) can be written

$$\frac{z}{2\pi}I_2 = \sum_{\text{rings}}\bar{h}_r\bar{E}_r\frac{\Delta\Omega_r}{2\pi} \tag{18}$$

Substituting (18) and (9) into (7), we have

$$T(z) - T_s - \alpha(d+z) = \left[-\alpha' L - (\alpha-\alpha')d\right]\left[1 - \frac{2z}{\sqrt{\pi\varkappa t}}\right]$$

$$-(\alpha-\alpha')\sum_{\text{rings}}\bar{h}_r\bar{E}_r\frac{\Delta\Omega_r}{2\pi} \tag{19}$$

or multiplying out, cancelling terms, and rearranging, we have the final equation

$$T(z) - \alpha'[azL - azd + \bar{h}] = T_s - \alpha'[L-d] + \alpha[z + azd - \bar{h}] \tag{20}$$

where

$$a = \frac{2}{\sqrt{\pi\varkappa t}}$$

$$\bar{h} = \sum_{\text{rings}}\bar{h}_r\bar{E}_r\frac{\Delta\Omega_r}{2\pi}$$

We can generalize (20) in the following way, writing it as

$$T_{cor} = T_o + \alpha z_{cor}$$

where $T_{cor} = T(z) - \alpha'[azL - adz + \bar{h}]$ is the topographically corrected temperature at the corrected depth $z_{cor} = z + azd - \bar{h}$ and $T_o = T_s - \alpha'[L-d]$ is just the surface temperature at the present surface (collar of hole). Thus it can be seen that a plot of z_{cor} versus T_{cor}

will give a straight line with slope α, the undisturbed geothermal gradient, and intercept T_o. It should be noted that T_{cor} and z_{cor} have little physical significance.

In the steady-state case where the topography has persisted indefinitely in its present state, since a = 0, $E(\beta) \to 1$ ($t = \infty$) and $L = \delta = 0$, equation (20) reduces to

$$T(z) - \alpha' \bar{h}(\infty) = T_s + \alpha[z - \bar{h}(\infty)] \qquad (21)$$

where $\bar{h}(\infty) = \sum_{\text{rings}} \bar{h}_r \frac{\Delta\Omega_r}{2\pi}$ and T_s is the present surface temperature. T_{cor} and z_{cor} are now somewhat simplified. The $\bar{h}_r$'s are determined from topographic maps and are simply the difference between the collar elevation (C.E.) of the drill hole and the average elevations (AVE.) of the different rings, negative for C.E. < AVE., positive for C.E. > AVE. Appendix VIII gives the radii of the actual rings (in meters) used for the topographic corrections for each hole in this work. For a 200 to 300 meter hole, the topography within the first 0.5 km is the most crucial, as can be seen if one plots the weighting function (16).

APPENDIX IV

Development of Line Source Theory

The basic theory of line sources is presented by Carslaw and Jaeger (1959, Chapter X), and we will draw heavily on their work.

The two-dimensional differential equation of heat conduction,

$$\frac{\partial^2 T(x, y, t)}{\partial x^2} + \frac{\partial^2 T(x, y, t)}{\partial y^2} = \frac{1}{\varkappa} \frac{\partial T(x, y, t)}{\partial t}$$

has the solution

$$T(x, y, t) = \frac{Q}{4\pi\varkappa t} \exp -\left[(x-x')^2 + (y-y')^2 / 4\varkappa t \right] \qquad (1)$$

subject to the initial condition

$$T(x, y, 0) = Q\,\delta(x-x')\,\delta(y-y')$$

where $\varkappa$ is the thermal diffusivity and Q a source strength. $\delta(\xi-\xi')$ is the Dirac delta function; $\int \delta(\xi-\xi')d\xi' = 1$, and $\delta(\xi-\xi') = 0$ for $\xi \neq \xi'$. (1) is the solution for the temperature in an infinite homogeneous medium due to an instantaneous line source of strength Q at $t = 0$, parallel to the z-axis and passing through the point (x', y'). The strength Q is defined as the temperature to which the amount of heat liberated per unit length of the line would raise unit volume of the substance. Thus the heat liberated per unit length of the line is $Q\rho c$, where ρ is the density and c is the heat capacity.

For a semi-infinite solid, we require that the plane $x = 0$ remain at temperature $T = 0$. We can find the analogous solution to (1) if we put an instantaneous line source of strength $-Q$ through the point

$(-x', y')$, thus we have

$$T(x, y, t) = \frac{Q}{4\pi\kappa t} \left\{ \exp-\left[(x-x')^2+(y-y')^2/4\kappa t \right] \right.$$

$$\left. - \exp-\left[(x+x')^2+(y-y')^2/4\kappa t \right] \right\} \quad x > 0 \qquad (2)$$

The flux at the surface is given by

$$k\frac{\partial T}{\partial x}\Big|_{x=o} = \frac{Qkx'}{4\pi\kappa^2 t^2} \exp-\left[x'^2+(y-y')^2/4\kappa t \right] \qquad (3)$$

where k is the thermal conductivity.

The temperature field for a continuous (from time = 0 to time t) line source passing through the point (x', y') with T = 0 at x = 0 can be derived by setting $t = t-t'$ in equation (2) and integrating with respect to t' from 0 to t; we obtain the result

$$T(x, y, t) = \frac{-q}{4\pi\kappa} \left[Ei\left(-\frac{r^2}{4\kappa t}\right) - Ei\left(-\frac{r_1^2}{4\kappa t}\right)\right] \qquad (4)$$

where $q\rho c$ is now the heat liberated per unit length per unit time, and

$$r^2 = (x-x')^2+(y-y')^2$$
$$r_1^2 = (x+x')^2+(y-y')^2$$

and where

$$-Ei(-\xi) = \int_{\xi}^{\infty} \frac{e^{-u}}{u} \, u$$

To find the surface flux after time t, we differentiate (4) with respect to x and set x = 0 obtaining

$$k\frac{\partial T}{\partial x}\Big|_{x=o} = \frac{kq}{\pi\kappa} \frac{x'}{x'^2+(y-y')^2} \exp - \left[x'^2+(y-y')^2/4\kappa t \right]$$

or since $\varkappa = \frac{k}{\rho c}$ and $\epsilon = q\rho c$ where ϵ is the energy liberated per unit length per unit time, we have

$$k \frac{\partial T}{\partial x}\Big|_{x=o} = \frac{\epsilon}{\pi} \frac{x'}{x'^2+(y-y')^2} \exp -\left[x'^2+(y-y')^2/4\varkappa t \right] \qquad (5)$$

For small values of ξ, we have

$$Ei(-\xi) = \gamma + \ell n\xi - \xi + \frac{1}{4}\xi^2 + O(\xi^3)$$

where $\gamma = 0.5772$ (Euler's constant). Thus for large values of t, (4) becomes

$$T(x, y, \infty) = \frac{q}{4\pi\varkappa} \ell n \frac{r_1^2}{r^2} \qquad (6)$$

and the surface flux is given by

$$k \frac{\partial T(x, y, \infty)}{\partial x}\Big|_{x=o} = \frac{kq}{\pi\varkappa} \frac{x'}{x'^2+(y-y')^2} \qquad (7)$$

Or again since $\varkappa = \frac{k}{\rho c}$ and $\epsilon = q\rho c$ where ϵ is the energy liberated per unit length per unit time, we have

$$k \frac{\partial T(x, y, \infty)}{\partial x}\Big|_{x=o} = \frac{\epsilon}{\pi} \frac{x'}{x'^2+(y-y')^2}$$

The result is also obtained by setting $t = \infty$ in (5). If we put the source at a depth h through y = 0; that is, through the point (h , 0) we would have

$$k \frac{\partial T}{\partial x}\Big|_{x=o} = q = \frac{\epsilon}{\pi} \frac{h}{h^2+y^2} \qquad (8)$$

Thus (8) gives the surface flux due to a line source buried at depth h below a surface kept at temperature T = 0, and which has been continuously producing heat at the rate E energy units per unit time per

unit length for a long time.

Plane sources of spatially variable (or constant) strength can be composed from a superposition in space of a discrete number of line sources of different (or the same) strengths. The greater the number of line sources, the better the approximation. Rather than writing an expression, we will simply say that the temperature or flux can be found by summing the individual effects of each of the line sources. We will find this procedure useful when discussing fault problems.

The "zone source" or the problem of steady-state heat production in the region $h_o \leq x \leq h_1$, $|y| \leq a$ has been investigated by Wasserburg and Ramo (personal communication). We have from (6) the temperature due to a line source of constant strength passing through the point (x', y') given by ($T = 0$ for $x = 0$)

$$T(x,y,\infty) = -\frac{q}{4\pi\kappa} \ell n \frac{r^2}{r_1^2} = -\frac{\epsilon}{4\pi k} \ell n \left[\frac{(x-x')^2 + (y-y')^2}{(x+x')^2 + (y-y')^2} \right] \qquad (9)$$

Thus the problem that must be solved is a superposition of these line sources in two dimensions, namely

$$T(x,y) = -\frac{\epsilon}{4\pi k} \int_{-a}^{+a} \int_{h_o}^{h_1} dx' dy' \ell n \left[\frac{(x-x')^2 + (y-y')^2}{(x+x')^2 + (y-y')^2} \right] \qquad (10)$$

where ϵ is now the heat liberated per unit time per unit volume (constant throughout volume), since we have distributed line sources of strength $q dx' dy'$ throughout the volume $h_o \leq x \leq h_1$, $|y| \leq a$. It might be noted that a vertical strip source can be treated the same way with integration with respect to only the x' variable. Since in heat flow we are only interested in the surface flux, we will solve

instead

$$k \frac{\partial T(x,y)}{\partial x}\Big|_{x=o} = \frac{\epsilon}{\pi} \int_{-a}^{+a}\int_{h_o}^{h_1} dx'dy' \frac{x'}{(x')^2+(y-y')^2}$$

gotten by differentiating (10) with respect to x and setting x = 0. If we integrate first with respect to the y' variable and second with respect to x', we obtain the desired result, namely

$$k\frac{\partial T}{\partial x}\Big|_{x=o} = \frac{\epsilon}{\pi}\Bigg\{h_1\left[\tan^{-1}\frac{a-y}{h_1} + \tan^{-1}\frac{a+y}{h_1}\right] + \frac{a-y}{2}\ln\left[1+\frac{h_1^2}{(a-y)^2}\right]$$

$$+\frac{a+y}{2}\ln\left[1+\frac{h_1^2}{(a+y)^2}\right] - h_o\left[\tan^{-1}\frac{a-y}{h_o} + \tan^{-1}\frac{a+y}{h_o}\right]$$

$$-\frac{a-y}{2}\ln\left[1+\frac{h_o^2}{(a-y)^2}\right] - \frac{a+y}{2}\ln\left[1+\frac{h_o^2}{(a+y)^2}\right]\Bigg\} \qquad (11)$$

The solution for the strip source, that is, after integration of (9) with respect to x' as indicated above and located on the plane y'=0, is given by (T = 0 for x = 0)

$$k\frac{\partial T}{\partial x}\Big|_{x=o} = \frac{\sigma}{2\pi}\ln\left[\frac{y^2+h_1^2}{y^2+h_o^2}\right] \qquad (12)$$

where σ is the heat liberated per unit time per unit surface area, and h_o and h_1 are the top depth and bottom depth of the strip, respectively. It should be noted that in relation (8)

$$\lim_{h \to 0} k\frac{\partial T}{\partial x}\Big|_{x=o} \to \infty$$

and in relation (12)

$$\lim_{\substack{h_o \to 0 \\ y \to 0}} k\frac{\partial T}{\partial x}\Big|_{x=o} \to \infty$$

or we have singularities at the surface in case any of the heat producing elements reach the surface. This mathematical ambiguity does not exist, however, in the case of a zone source, as can be seen by examining relation (11).

It is not necessary, of course, to have ϵ = constant in (10). We will note later that for fault zones a more realistic distribution of heat sources will be given by

$$\epsilon = \epsilon(x) = Ax$$

where A is some constant given by say

$$\int_{h_o}^{h_1} Ax\, dx = \langle \epsilon \rangle (h_1 - h_o)$$

where $\langle \epsilon \rangle$ is some average value of the energy liberated per unit time per unit volume. We will then want to perform the integration

$$k \frac{\partial T}{\partial x}\Big|_{x=o} = \frac{1}{\pi} \int_{-a}^{+a} \int_{h_o}^{h_1} dx' dy' \epsilon(x') \frac{x'}{x'^2 + (y-y')^2}$$

$$= \frac{A}{\pi} \int_{-a}^{+a} \int_{h_o}^{h_1} dx' dy' \frac{x'^2}{x'^2 + (y-y')^2}$$

since $\epsilon(x') = Ax'$. The solution to this is given by

$$k \frac{\partial T}{\partial x}\Big|_{x=o} = \frac{A}{2\pi} \left\{ \left[h_1^2 + (a+y)^2 \right] \tan^{-1} \frac{a+y}{h_1} + \left[h_1^2 + (a-y)^2 \right] \tan^{-1} \frac{a-y}{h_1} + 2ah_1 \right.$$

$$\left. - \left[h_o^2 + (a+y)^2 \right] \tan^{-1} \frac{a+y}{h_o} - \left[h_o^2 + (a-y)^2 \right] \tan^{-1} \frac{a-y}{h_o} - 2ah_o \right\} \quad (13)$$

A similar analysis may be performed for the strip source. For the strip located on the plane $y' = 0$, the solution is given by

$$k\frac{\partial T}{\partial x}\Big|_{x=o} = \frac{A}{\pi}\left\{h_1-h_o + y\left[\tan^{-1}\frac{h_o}{y} - \tan^{-1}\frac{h_1}{y}\right]\right\} \qquad (14)$$

where

$$\sigma(x) = Ax \qquad A = \text{constant}$$

and

$$\int_{h_o}^{h_1} Ax\,dx = \langle\sigma\rangle\,(h_1-h_o)$$

$\langle\sigma\rangle$ is some average value of the energy liberated per unit time per unit area.

APPENDIX V

Equivalent Uranium and Potassium Analyses of Core Samples from Drill Holes

Location	Sample	eU (ppm)		% K_2O	% K
Anza	AN-1-W	9.4	*	2.75	2.28
	AN-1-H	4.8		3.00	2.49
	AN-1-F	4.6		2.75	2.28
	AN-2-W	5.7	*	2.10	1.74
	AN-2-H	2.5		2.00	1.66
	AN-2-F	2.9		2.00	1.66
	AN-3-W	2.6	*	2.75	2.28
	AN-3-H	4.4		2.35	1.95
	AN-3-F	3.0		2.55	2.12
Lake Hughes	LH-1-H	10.8	* §	2.65	2.20
	LH-1-F	14.0	* §	2.77	2.30
	LH-2-CO	4.4	* §	2.65	2.20
	LH-3-H	3.3		2.05	1.70
	LH-3-F	3.3		2.50	2.08
San Bernardino	SB-10-CO	4.9		---	---
Lucerne Valley	LV-H-F	2.0	†	1.60	1.33
	LV-TF-SF	3.1		1.55	1.29
	LV-50	4.4	‡	1.25	1.04
Tehachapi Mountains	DH-14-CO	10.4		4.90	4.07
	DH-43-CO	2.8	⊙	1.85	1.54
	DH-65-H	2.0		1.80	1.49
	DH-65-F	0.2		1.00	0.83
Hollister	HO-1-W	5.0		4.55	3.78
	HO-1-H	4.3		3.15	2.61
	HO-1-F	4.4		2.25	1.87

Location	Sample	eU (ppm)	% K_2O	% K
Hollister (continued)	HO-3-CO	1.0	---	---
	HO-5-CO	8.2	---	---
Mt. Rubidoux Standard	----	9.2 ⊕	4.43	3.68

* Weathered Samples - not included in average value for determination of heat production unless the only value(s) from hole (§).

† Sample contains ~40% andesite dike with eU < 1.0 ppm. Only LV-TF-SF used for heat production in LV-1.

‡ Surface sample from near LV-1. Not used in average value for LV-1.

⊙ Pelona schist.

⊕ This value determined from isotope dilution analysis.

APPENDIX VI

TEMPERATURE - DEPTH DATA

(Depths are given in meters, Temperatures in degrees C;
All measurements were made below the water table)

1. AN-1 Anza, California; 1200 foot hole completed 4/16/65; three loggings

LOG 7/9/65 Probe - Harvard FEI 5-K250-1

*Depth(m)	Temp(°C)	*Depth(m)	Temp(°C)	*Depth(m)	Temp(°C)
Zero set for thermistor at collar elev.		160	21.16 ± .01	260	23.71 ± .01
		170	21.43	270	23.98
.	.	180	21.63	280	24.23
.	.	190	21.92	290	24.49
.	.	200	22.20	300	24.70
100	19.62 ± .01	210	22.44	310	24.97
110	19.88	220	22.70	320	25.19
120	20.14	230	22.93	330	25.44
130	20.39	240	23.19	340	25.73
140	20.66	250	23.46		
150	20.91				

LOG 3/27/66 Probe - C.I.T. #1

Depth(m)	Temp(°C)	Depth(m)	Temp(°C)	Depth(m)	Temp(°C)
Zero set for thermistor 0.63 m below collar elevation		65	18.71 ± .01	105	19.70 ± .01
		70	18.82	110	19.84
		75	18.94	115	19.97
.	.	80	19.07	120	20.10
.	.	85	19.18	125	20.24
.	.	90	19.31	130	20.37
50	18.36 ± .01	95	19.45	135	20.50
55	18.46	100	19.59	140	20.62
60	18.58				

*Depth in meters below zero setting

AN-1 LOG 3/27/66 (continued)

Depth(m)	Temp(°C)	Depth(m)	Temp(°C)	Depth(m)	Temp(°C)
145	20.75 ± .01	220	22.67 ± .01	295	24.56 ± .01
150	20.87	225	22.80	300	24.69
155	20.99	230	22.93	305	24.83
160	21.12	235	23.06	310	24.96
165	21.25	240	23.16	315	25.07
170	21.38	245	23.28	320	25.20
175	21.51	250	23.44	325	25.30
180	21.63	255	23.57	330	25.40
185	21.77	260	23.70	335	25.53
190	21.89	265	23.84	340	25.63
195	22.02	270	23.95	345	25.76
200	22.15	275	24.10	350	25.92
205	22.28	280	24.22	355	26.01
210	22.39	285	24.34		
215	22.55	290	24.48		

LOG 5/12/67 Probe - C.I.T. #2

Depth(m)	Temp(°C)	Depth(m)	Temp(°C)	Depth(m)	Temp(°C)
Zero level not recorded		130	20.39 ± .01	250	23.43 ± .01
		140	20.64	260	23.71
.	.				
.	.	150	20.88	270	23.97
.	.	160	21.14	280	24.20
50	18.39 ± .01	170	21.40	290	24.45
60	18.61	180	21.65	300	24.70
70	18.84	190	21.90	310	24.95
80	19.08	200	22.16	320	25.18
90	19.33	210	22.41	330	25.40
100	19.60	220	22.66	340	25.66
110	19.86	230	22.93	350	25.88
120	20.12	240	23.17	360	26.12

2. AN-2 Anza, California; 1000 foot hole completed 6/14/65; four loggings

LOG 7/9/65 Probe - Harvard FEI 5-K250-1

Depth(m)	Temp(°C)	Depth(m)	Temp(°C)	Depth(m)	Temp(°C)
Zero set for thermistor at collar elev.		150	20.05 ± .01	240	22.12 ± .01
		160	20.25	250	22.22
.	.	170	20.52	260	22.48
.	.	180	20.68	270	22.64
100	18.82 ± .01	190	20.92	280	23.02
110	19.08	200	21.11	290	23.09
120	19.32	210	21.34	300	23.27
130	19.51	220	21.58		
140	19.76	230	21.82		

LOG 8/19/65 Probe - Harvard FEI 5-K250-1

Depth(m)	Temp(°C)	Depth(m)	Temp(°C)	Depth(m)	Temp(°C)
Zero set for thermistor at collar elev.		110	19.04 ± .01	210	21.35 ± .01
		120	19.27	220	21.61
.	.	130	19.50	230	21.85
.	.	140	19.73	240	22.09
50	17.98 ± .01	150	19.99	250	22.25
60	18.12	160	20.22	260	22.48
70	18.27	170	20.48	270	22.70
80	18.44	180	20.68	280	22.96
90	18.63	190	20.92	290	23.09
100	18.82	200	21.13	300	23.29

LOG 3/27/66 Probe - C.I.T. #1

Depth(m)	Temp(°C)	Depth(m)	Temp(°C)	Depth(m)	Temp(°C)
Zero set for thermistor 0.76 m below collar elevation		20	17.52 ± .02	40	17.79 ± .02
		30	17.70	45	17.84
		35	17.75	50	17.90 ± .01
.	.				

AN-2 LOG 3/27/66 (continued)

Depth(m)	Temp(°C)	Depth(m)	Temp(°C)	Depth(m)	Temp(°C)
55	17.96 ± .01	140	19.64 ± .01	225	21.64 ± .01
60	18.03	145	19.75	230	21.75
65	18.11	150	19.87	235	21.87
70	18.19	155	19.99	240	21.98
75	18.28	160	20.11	245	22.08
80	18.37	165	20.25	250	22.18
85	18.46	170	20.38	255	22.28
90	18.57	175	20.49	260	22.39
95	18.65	180	20.60	265	22.51
100	18.75	185	20.72	270	22.62
105	18.85	190	20.83	275	22.75
110	18.96	195	20.95	280	22.86
115	19.06	200	21.06	285	22.94
120	19.18	205	21.17	290	23.03
125	19.31	210	21.29	295	23.12
130	19.42	215	21.40	300	23.22
135	19.55	220	21.52		

LOG 5/12/67 Probe - C.I.T. #2

Depth(m)	Temp(°C)	Depth(m)	Temp(°C)	Depth(m)	Temp(°C)
Zero level not recorded		110	18.97 ± .01	220	21.52 ± .01
		120	19.19	230	21.74
.	.	130	19.41	240	21.96
.	.	140	19.63	250	22.18
.	.	150	19.88	260	22.39
40	17.79 ± .01	160	20.13	270	22.60
50	17.91	170	20.37	280	22.85
60	18.04	180	20.59	290	23.01
70	18.20	190	20.82	300	23.20
80	18.37	200	21.05		
90	18.56	210	21.28		
100	18.75				

3. AN-3 Anza, California; 700 foot hole completed 7/15/65; four loggings

LOG 7/21/65 Probe - Harvard FEI 5-K250-1

Depth(m)	Temp(°C)	Depth(m)	Temp(°C)	Depth(m)	Temp(°C)
Zero set for thermistor at collar elev.		80	16.49 ± .01	150	18.10 ± .01
		90	16.70	160	18.32
.	.				
.	.	100	16.94	170	18.67
.	.	110	17.17	180	18.84
50	16.03 ± .01	120	17.42	190	19.03
60	16.09	130	17.64	200	19.28
70	16.26	140	17.89	210	19.53

LOG 8/19/65 Probe - Harvard FEI 5-K250-1

Depth(m)	Temp(°C)	Depth(m)	Temp(°C)	Depth(m)	Temp(°C)
Zero set for thermistor at collar elev.		80	16.31 ± .01	150	18.01 ± .01
		90	16.55	160	18.25
.	.				
.	.	100	16.80	170	18.51
.	.	110	17.02	180	18.73
50	15.80 ± .01	120	17.29	190	18.95
60	15.87	130	17.54	200	19.20
70	16.08	140	17.78	210	19.44

LOG 3/27/66 Probe - C.I.T. #1

Depth(m)	Temp(°C)	Depth(m)	Temp(°C)	Depth(m)	Temp(°C)
Zero set for thermistor 0.84 m below collar elevation		35	15.46 ± .02	75	16.07 ± .01
		40	15.48	80	16.19
		45	15.52	85	16.31
10	15.62 ± .02	50	15.58 ± .01	90	16.45
15	15.52	55	15.66	95	16.58
20	15.50	60	15.74	100	16.69
25	15.48	65	15.85	105	16.81
30	15.46	70	15.96	110	16.96

AN-3 LOG 3/27/66 (continued)

Depth(m)	Temp(°C)	Depth(m)	Temp(°C)	Depth(m)	Temp(°C)
115	17.08 ± .01	150	17.93 ± .01	185	18.76 ± .01
120	17.20	155	18.05	190	18.88
125	17.34	160	18.17	195	19.00
130	17.46	165	18.29	200	19.11
135	17.58	170	18.41	205	19.24
140	17.70	175	18.53	210	19.35
145	17.81	180	18.64		

LOG 5/12/67 Probe - C.I.T. #2

Depth(m)	Temp(°C)	Depth(m)	Temp(°C)	Depth(m)	Temp(°C)
Zero level not recorded		80	16.18 ± .01	160	18.16 ± .01
		90	16.43	170	18.40
.	.	100	16.68	180	18.64
30	15.48 ± .01	110	16.94	190	18.87
40	15.50	120	17.19	200	19.10
50	15.59	130	17.44	210	19.34
60	15.74	140	17.68		
70	15.95	150	17.92		

4. LH-1 Lake Hughes, California; 700 foot hole completed 10/11/65; four loggings

LOG 11/5/65 Probe - Harvard FEI 5-K250-1

Depth(m)	Temp(°C)	Depth(m)	Temp(°C)	Depth(m)	Temp(°C)
Zero set for thermistor at collar elev.		80	20.76 ± .01	150	22.47 ± .01
.	.	90	20.96	160	22.76
30	19.98 ± .01	100	21.18	170	23.03
40	20.05	110	21.42	180	23.32
50	20.17	120	21.67	190	23.58
60	20.33	130	21.94	200	23.86
70	20.55	140	22.20	210	24.12

LH-1 LOG 1/29/66 Probe - Harvard FEI K-250-1

Depth(m)	Temp(°C)	Depth(m)	Temp(°C)	Depth(m)	Temp(°C)
Zero set for thermistor 1.10 m below collar elevation		130	21.88 ± .01	190	23.53 ± .01
		140	22.13	200	23.81
		150	22.41	210	24.15
.	.	160	22.70		
.	.	170	22.97		
.	.	180	23.26		
120	21.59 ± .01				

NOTE: This logging was started with another probe which went bad at 120 m, thus disturbing the hole above 120 m for the relog.

LOG 8/15/66 Probe - Harvard FEI 4-K396-1

Depth(m)	Temp(°C)	Depth(m)	Temp(°C)	Depth(m)	Temp(°C)
Zero set for thermister 0.88 m below collar elevation		80	20.66 ± .01	160	22.73 ± .01
		90	20.88	170	23.01
		100	21.12	180	23.29
.	.	110	21.39	190	23.56
.	.	120	21.62	200	23.84
.	.	130	21.89	210	24.11
50	20.10 ± .01	140	22.16		
60	20.26	150	22.43		
70	20.46				

LOG 4/11/67 Probe - C.I.T. #2

Depth(m)	Temp(°C)	Depth(m)	Temp(°C)	Depth(m)	Temp(°C)
Zero level not recorded		80	20.62 ± .01	160	22.66 ± .01
		90	20.84	170	22.95
.	.	100	21.08	180	23.22
.	.	110	21.33	190	23.50
30	19.79 ± .01	120	21.56	200	23.77
40	19.94	130	21.84	210	24.05
50	20.08	140	22.11		
60	20.23	150	22.37		
70	20.42				

5. LH-2 Lake Hughes, California; 1225 foot hole, first 600 feet completed 3/13/63, 600-1225 feet completed 11/15/65; four loggings

LOG 12/21/65 Probe - Harvard FEI 5-K250-1

Depth(m)	Temp(°C)	Depth(m)	Temp(°C)	Depth(m)	Temp(°C)
Zero level not recorded		130	17.37 ± .01	260	20.21 ± .01
.	.	140	17.58	270	20.44
20	15.89 ± .02	150	17.79	280	20.66
30	15.97	160	17.99	290	20.90
40	16.01	170	18.22	300	21.14
50	16.07 ± .01	180	18.42	310	21.36
60	16.17	190	18.65	320	21.62
70	16.30	200	18.87	330	21.84
80	16.46	210	19.09	340	22.08
90	16.63	220	19.32	350	22.30
100	16.81	230	19.54	360	22.58
110	16.99	240	19.76	370	22.84
120	17.18	250	19.98		

LOG 3/22/66 Probe - C.I.T. #1

Depth(m)	Temp(°C)	Depth(m)	Temp(°C)	Depth(m)	Temp(°C)
Zero set for thermistor 0.67 m below collar elevation		90	16.57 ± .01	150	17.73 ± .01
		95	16.66	155	17.83
.	.	100	16.75	160	17.93
.	.	105	16.83	165	18.03
.	.	110	16.93	170	18.15
50	16.02 ± .01	115	17.02	175	18.26
55	16.07	120	17.12	180	18.37
60	16.12	125	17.22	185	18.47
65	16.18	130	17.31	190	18.59
70	16.24	135	17.41	195	18.69
75	16.32	140	17.52	200	18.80
80	16.40	145	17.62	205	18.91
85	16.48				

LH-2 LOG 3/22/66 (continued)

Depth(m)	Temp(°C)	Depth(m)	Temp(°C)	Depth(m)	Temp(°C)
210	19.03 ± .01	265	20.26 ± .01	320	21.58 ± .01
215	19.14	270	20.37	325	21.69
220	19.25	275	20.48	330	21.81
225	19.36	280	20.60	335	21.92
230	19.47	285	20.72	340	22.04
235	19.58	290	20.84	345	22.16
240	19.69	295	20.97	350	22.29
245	19.80	300	21.08	355	22.40
250	19.91	305	21.20	360	22.54
255	20.02	310	21.32	365	22.66
260	20.13	315	21.46	370	22.78

LOG 2/4/66 Probe - C.I.T. #1

Depth(m)	Temp(°C)	Depth(m)	Temp(°C)	Depth(m)	Temp(°C)
Zero set for thermistor 0.82 m below collar elevation		140	17.52 ± .01	270	20.37 ± .01
		150	17.72	280	20.60
.	.	160	17.93	290	20.84
.	.	170	18.15	300	21.08
50	16.02 ± .01	180	18.37	310	21.31
60	16.12	190	18.58	320	21.57
70	16.25	200	18.80	330	21.80
80	16.40	210	19.02	340	22.04
90	16.57	220	19.24	350	22.28
100	16.75	230	19.47	360	22.54
110	16.94	240	19.69	370	22.78
120	17.12	250	19.91		
130	17.31	260	20.13		

LH-2 LOG 8/15/66 Probe - Harvard FEI 4-K396-1

Depth(m)	Temp(°C)	Depth(m)	Temp(°C)	Depth(m)	Temp(°C)
Zero set for thermistor 0.91 m below collar elevation		140	17.53 ± .01	260	20.15 ± .01
		150	17.74	270	20.39
.	.	160	17.94	280	20.62
.	.	170	18.16	290	20.86
.	.	180	18.38	300	21.10
60	16.12 ± .01	190	18.60	310	21.34
70	16.25	200	18.82	320	21.59
80	16.41	210	19.04	330	21.83
90	16.57	220	19.26	340	22.07
100	16.75	230	19.48	350	22.33
110	16.94	240	19.70	360	22.58
120	17.13	250	19.93		
130	17.32				

LOG 5/11/67 Probe - C.I.T. #2

Depth(m)	Temp(°C)	Depth(m)	Temp(°C)	Depth(m)	Temp(°C)
Zero level not recorded		170	18.19 ± .01	280	20.62 ± .01
		180	18.40	290	20.85
.	.	190	18.62	300	21.09
.	.	200	18.84	310	21.32
.	.	210	19.06	320	21.56
100	16.78 ± .01	220	19.28	330	21.79
110	16.96	230	19.50	340	22.03
120	17.16	240	19.72	350	22.28
130	17.35	250	19.95	360	22.52
140	17.56	260	20.17		
150	17.76	270	20.40		
160	17.97				

6. LH-3 Lake Hughes, California; 1200 foot hole completed 1/6/66; four loggings

LOG 1/22/66 Probe - Harvard FEI 5-K250-1

Depth(m)	Temp(°C)	Depth(m)	Temp(°C)	Depth(m)	Temp(°C)
Zero set for thermistor 0.92 m below collar elevation		110	19.42 ± .01	240	23.97 ± .01
		120	19.79	250	24.25
.	.	130	20.22	260	24.53 ± .02
10	14.52 ± .02	140	20.65	270	24.82
20	15.85	150	21.00	280	24.95
30	16.38	160	21.32	290	25.11
40	16.80	170	21.64	300	25.37
50	17.22 ± .01	180	21.96	310	25.59
60	17.66	190	22.31	320	25.84
70	18.08	200	22.68	330	26.21
80	18.42	210	23.03	340	26.64
90	18.82	220	23.35	350	27.61
100	19.16	230	23.65	360	28.00

LOG 2/12/66 Probe - C.I.T. #1

Depth(m)	Temp(°C)	Depth(m)	Temp(°C)	Depth(m)	Temp(°C)
Zero set for thermistor 0.92 m below collar elevation		120	19.82 ± .01	250	24.22 ± .01
		130	20.22	260	24.50 ± .02
.	.	140	20.64	270	24.76
20	15.77 ± .02	150	20.98	280	24.88
30	16.31	160	21.28	290	25.06
40	16.76	170	21.62	300	25.30
50	17.20 ± .01	180	21.94	310	25.52
60	17.65	190	22.29	320	25.78
70	18.07	200	22.64	330	26.13
80	18.44	210	22.98	340	26.65
90	18.84	220	23.31	350	27.56
100	19.19	230	23.63	360	27.94
110	19.47	240	23.96		

LH-3 LOG 8/12/66 Probe - Harvard FEI 4-K396-1

Depth(m)	Temp(°C)	Depth(m)	Temp(°C)	Depth(m)	Temp(°C)
Zero set for thermistor 0.84 m below collar elevation		130	20.36 ± .01	250	24.28 ± .01
		140	20.72	260	24.55 ± .02
.	.	150	21.06	270	24.77
.	.	160	21.40	280	24.89
50	17.28 ± .01	170	21.69	290	25.07
60	17.73	180	22.01	300	25.32
70	18.15	190	22.35	310	25.53
80	18.54	200	22.69	320	25.80
90	18.93	210	23.03	330	26.12
100	19.30	220	23.37	340	26.78
110	19.65	230	23.69	350	27.60
120	20.00	240	24.01	360	27.99

LOG 5/16/67 Probe - C.I.T. #2

Depth(m)	Temp(°C)	Depth(m)	Temp(°C)	Depth(m)	Temp(°C)
Zero set for thermistor 0.91 m above collar elevation		130	20.34 ± .01	270	24.75 ± .02
		140	20.69	280	24.85
.	.	150	21.02	290	25.06
.	.	160	21.35	300	25.28
30	16.24 ± .01	170	21.65	310	25.54
40	16.77	180	21.96	320	25.79
50	17.23	190	22.31	330	26.08
60	17.68	200	22.65	335	26.20
70	18.10	210	22.99	340	26.44
80	18.51	220	23.32	345	27.15
90	18.90	230	23.64	350	27.47
100	19.28	240	23.95	355	27.71
110	19.64	250	24.22	360	27.91
120	19.98	260	24.50 ± .02		

7. SB-2 San Bernardino Mountains, California; 1500 foot hole completed 1/28/59; three loggings

LOG 7/27/66 Probe - C.I.T. #1

Depth(m)	Temp(°C)	Depth(m)	Temp(°C)	Depth(m)	Temp(°C)
Zero set for thermistor 0.58 m below collar elevation		230	15.67 ± .02	400	20.87 ± .02
		240	15.97	410	21.14
.	.	250	16.26	420	21.43
.	.	260	16.51	423.05	21.56
100	12.95 ± .02	270	16.83	426.10	21.65
110	13.11	280	17.27	430	21.74
120	13.29	290	17.71	433.05	21.80
130	13.43	300	18.07	436.10	---
140	13.70	310	18.39	440	21.98
150	13.90	320	18.70	443.05	22.03
160	14.13	330	18.96	446.10	22.11
170	14.34	340	19.25	450	22.21
180	14.49	350	19.54	453.05	22.30
190	14.72	360	19.83	456.10	22.38
200	15.05	370	20.12	460	22.47
210	15.19	380	20.39		
220	15.51	390	20.65		

LOG 5/17/67 Probe - C.I.T. #2

Depth(m)	Temp(°C)	Depth(m)	Temp(°C)	Depth(m)	Temp(°C)
Zero set for thermistor 1.50 m above collar elevation		200	15.52 ± .02	380	20.34 ± .02
		220	15.88	390	20.60
.	.	240	16.52	400	20.82
.	.	260	17.02	410	21.09
100	13.21 ± .02	280	17.57	420	21.38
120	13.66	300	18.14	430	21.73
140	14.11	320	18.68	440	21.95
160	14.57	340	19.22	450	22.20
180	14.96	360	19.80	460	22.44

SB-2 LOG 8/17/66 Probe - C.I.T. #1

Depth(m)	Temp(°C)	Depth(m)	Temp(°C)	Depth(m)	Temp(°C)
Zero set for thermistor 1.22 m above collar elevation		360	19.77 ± .02	430	21.717 ± .01
		380	20.30	432.03	21.754
.	.	400	20.793 ± .01	434.06	21.792
.	.	402.03	20.839	436.09	21.857
100	13.23 ± .02	404.06	20.896	438.12	21.910
120	13.67	406.09	20.952	440	21.950
140	14.11	408.12	21.010	442.03	21.994
160	14.56	410	21.060	444.06	22.052
180	---	412.03	21.120	446.09	22.100
200	15.47	414.06	21.191	448.12	22.150
220	15.98	416.09	21.262	450	22.193
240	16.49	418.12	21.331	452.03	22.244
260	16.99	420	21.378	454.06	22.294
280	17.55	422.03	21.428	456.09	22.341
300	18.09	424.06	21.499	458.12	22.396
320	18.66	426.09	21.611	460	22.447
340	19.20	428.12	21.669	462.03	22.496

8. SB-5 San Bernardino Mountains, California; 900 foot hole completed 9/19/65; one logging

LOG 5/18/67 Probe - C.I.T. #2

Depth(m)	Temp(°C)	Depth(m)	Temp(°C)	Depth(m)	Temp(°C)
Zero level not recorded		160	12.83 ± .02	240	14.27 ± .01
		180	13.20	250	14.42
.	.	200	13.56	260	14.61
.	.	210	13.71	270	14.78
120	12.13 ± .02	220	13.88		
140	12.46	230	14.10		

9. SB-10 San Bernardino Mountains, California; 1700 foot hole completed 10/21/65; two loggings

LOG 1/13/66 Probe - Harvard FEI 5-K250-1

Depth(m)	Temp(°C)	Depth(m)	Temp(°C)	Depth(m)	Temp(°C)
Zero level not recorded		260	16.72 ± .01	400	19.80 ± .01
		270	16.92	410	20.04
.	.	280	17.14	420	20.27
.	.	290	17.34	430	20.50
160	14.60 ± .01	300	17.55	440	20.74
170	14.81	310	17.78	450	20.98
180	15.03	320	18.00	460	21.21
190	15.25	330	18.23	470	21.47
200	15.46	340	18.44	480	21.75
210	15.67	350	18.69	490	22.00
220	15.88	360	18.95	500	22.34
230	16.08	370	19.16	510	22.63
240	16.33	380	19.36	Bottom	22.735
250	16.54	390	19.58		

LOG 8/21/67 Probe - C.I.T. #3

Depth(m)	Temp(°C)	Depth(m)	Temp(°C)	Depth(m)	Temp(°C)
Zero set for thermistor 0.76 m above collar elevation		260	16.64 ± .01	360	18.82 ± .01
		270	16.87	370	19.06
.	.	280	17.09	380	19.26
.	.	290	17.30	390	19.48
200	15.36 ± .01	300	17.49	400	19.70
210	15.57	310	17.69	410	19.92
220	---	320	17.93	420	20.13
230	15.99	330	18.14	430	20.36
240	16.21	340	18.37	440	20.60
250	16.43	350	18.59	450	20.84

SB-10 LOG 8/21/67 (continued)

Depth(m)	Temp(°C)	Depth(m)	Temp(°C)	Depth(m)	Temp(°C)
460	21.07 ± .01	490	21.90 ± .01	Bottom	22.750 ± .01
470	21.34	500	22.25		
480	21.59	510	22.54		

10. LV-1 Lucerne Valley, California; 2300 foot hole, first 2000 feet completed 10/28/60; 2000-2300 feet completed 5/17/66; three loggings

LOG 1/23/66 Probe - Harvard FEI 5-K250-1

Depth(m)	Temp(°C)	Depth(m)	Temp(°C)	Depth(m)	Temp(°C)
Zero set for thermistor 0.91 m below collar elevation		240	26.68 ± .01	390	31.08 ± .01
		250	26.96	400	31.41
.	.	260	27.25	410	31.74
.	.	270	27.53	420	32.01
130	23.66 ± .01	280	27.83	430	32.29
140	23.95	290	28.11	440	32.58
150	24.22	300	28.40	450	32.90
160	24.48	310	28.65	560	33.21
170	24.75	320	28.91	470	33.53
180	25.02	330	29.19	480	33.86
190	25.30	340	29.48	490	34.16
200	25.58	350	29.79	500	34.48
210	25.84	360	30.12	510	34.78
220	26.13	370	30.44	520	35.09
230	26.39	380	30.76	530	35.33

LV-1 LOG 8/26/66 Probe - Harvard FEI 4-K396-1

Depth(m)	Temp(°C)	Depth(m)	Temp(°C)	Depth(m)	Temp(°C)
Zero set for thermistor 1.00 m below collar elevation		240	26.61 ± .01	390	30.89 ± .01
		250	26.89	400	31.23
.	.	260	27.17	410	31.55
.	.	270	27.46	420	31.84
130	23.63 ± .01	280	27.75	430	32.15
140	23.90	290	28.04	440	32.44
150	24.15	300	28.33	450	32.74
160	24.40	310	28.59	460	33.06
170	24.67	320	28.84	470	33.38
180	24.94	330	29.10	480	33.71
190	25.23	340	29.40	490	34.02
200	25.50	350	29.66	500	34.33
210	25.77	360	29.95	510	34.63
220	26.05	370	30.27	520	34.94
230	26.34	380	30.58	530	35.18

LOG 5/17/67 Probe - C.I.T. #2

Depth(m)	Temp(°C)	Depth(m)	Temp(°C)	Depth(m)	Temp(°C)
Zero set for thermistor 1.00 m above collar elevation		360	29.87 ± .01	500	34.24 ± .01
		380	30.50	510	34.56
.	.	400	31.15	520	34.86
.	.	410	31.47	530	35.16
200	25.46 ± .01	420	31.76	540	35.42
220	26.00	430	32.07	550	35.68
240	26.55	440	32.37	560	35.95
260	27.12	450	32.68	570	36.23
280	27.68	460	32.98	580	26.52
300	28.26	470	33.30	590	36.87
320	28.78	480	33.63	600	37.17
340	29.33	490	33.93	610	37.47

LV-1 LOG 5/17/67 (continued)

Depth(m)	Temp(°C)	Depth(m)	Temp(°C)	Depth(m)	Temp(°C)
620	37.76 ± .01	650	38.64 ± .01	680	39.51 ± .01
630	38.04	660	38.94	690	39.80
640	38.34	670	39.23	700	40.10

11. DH-14 Tehachapi Mountains, California; 800 foot hole completed 12/22/62; two loggings

LOG 4/10/66 Probe - C.I.T. #1

Depth(m)	Temp(°C)	Depth(m)	Temp(°C)	Depth(m)	Temp(°C)
Zero set for thermistor 0.88 m below collar elevation		100	16.56 ± .01	170	18.73 ± .01
		110	16.93	180	19.00
.	.	120	17.32	190	19.25
.	.	130	17.61	200	19.52
70	15.57 ± .01	140	17.89	210	19.77
80	15.90	150	18.23	220	20.05
90	16.21	160	18.46		

LOG 8/21/66 Probe - Harvard FEI 4-K396-1

Depth(m)	Temp(°C)	Depth(m)	Temp(°C)	Depth(m)	Temp(°C)
Zero set for thermistor 0.85 m below collar elevation		110	17.05 ± .01	190	19.30 ± .01
		120	17.37	200	19.56
.	.	130	17.67	205	19.69
.	.	140	17.96	210	19.82
70	15.80 ± .01	150	18.25	215	19.96
80	16.12	160	18.51	220	20.09
90	16.41	170	18.78	Bottom	20.204
100	16.73	180	19.04		

12. DH-15A Tehachapi Mountains, California; 900 foot hole completed 3/28/63; one logging

LOG 4/10/66 Probe - C.I.T. #1

Depth(m)	Temp(°C)	Depth(m)	Temp(°C)	Depth(m)	Temp(°C)
Zero set for thermistor 0.3 m below collar elevation		110	16.92 ± .01	170	17.97 ± .01
		120	17.11	180	18.15
.	.	130	17.27	190	18.34
.	.	140	17.44	200	18.52
90	16.60 ± .01	150	17.61	210	18.71
100	16.76	160	17.79	220	18.89

13. DH-43 Tehachapi Mountains, California; 800 foot hole, first 600 feet completed 3/5/64, 600-800 feet completed 3/30/66; two loggings

LOG 5/21/65 Probe - Harvard FEI 5-K250-1

Depth(m)	Temp(°C)	Depth(m)	Temp(°C)	Depth(m)	Temp(°C)
Zero set for thermistor 0.30 m above collar elevation		110	18.75 ± .02		
		120	18.95		
.	.	130	19.13 ± .01		
.	.	140	19.35		
90	18.30 ± .02	Hole blocked at this depth			
100	18.49				

LOG 6/1/67 Probe - C.I.T. #2

Depth(m)	Temp(°C)	Depth(m)	Temp(°C)	Depth(m)	Temp(°C)
Zero set for thermistor 0.91 m above collar elevation		160	19.80 ± .01	205	20.83 ± .01
		170	20.03	210	20.96
.	.	180	20.25	215	21.09
.	.	185	20.36	220	21.20
130	19.15 ± .01	190	20.46	225	21.32
140	19.38	195	20.59	230	21.44
150	19.59	200	20.71		

14. DH-65 Tehachapi Mountains, California; 1400 foot hole completed 12/19/64; four loggings

LOG 5/21/65 Probe - Harvard FEI 5-K250-1

Depth(m)	Temp(°C)	Depth(m)	Temp(°C)	Depth(m)	Temp(°C)
Zero set for thermistor at collar elev.		240	---	350	22.90 ± .01
		250	21.13 ± .01	360	23.07
.	.	260	21.27	370	23.26
.	.	270	21.44	380	23.45
.	.	280	21.63	390	23.64
170	19.63 ± .01	290	21.80	400	23.83
180	19.80	300	21.98	410	24.00
190	20.08	310	22.16	420	24.19
200	20.54	320	22.34	430	24.32
210	20.62	330	22.54	Bottom	24.377
220	20.69	340	22.72		
230	20.80				

LOG 7/15/65 Probe - Harvard FEI 5-K250-1

Depth(m)	Temp(°C)	Depth(m)	Temp(°C)	Depth(m)	Temp(°C)
Zero set for thermistor at collar elev.		230	20.84 ± .01	330	22.59 ± .01
		240	20.99	340	22.77
.	.	250	21.14	350	22.94
.	.	260	21.30	360	23.12
.	.	270	21.44	370	23.30
170	19.66 ± .01	280	21.65	380	23.48
180	19.82	290	21.85	390	23.67
190	20.15	300	21.99	400	23.87
200	20.54	310	22.20	410	24.05
210	20.60	320	22.39	420	24.22
220	20.72				

DH-65 LOG 8/18/66 Probe - Harvard FEI 4-K396-1

Depth(m)	Temp(°C)	Depth(m)	Temp(°C)	Depth(m)	Temp(°C)
Zero set for thermistor at collar elev.		240	20.92 ± .01	350	22.74 ± .01
		250	21.05	360	22.94
.	.	260	21.22	370	23.10
.	.	270	21.38	380	23.27
.	.	280	21.55	390	23.47
170	19.66 ± .01	290	21.71	400	23.67
180	19.84	300	21.91	410	23.90
190	20.13	310	22.08	420	24.09
200	20.44	320	22.24	430	24.39
210	20.54	330	22.42		
220	20.64	340	22.57		
230	20.83				

LOG 6/1/67 Probe - C.I.T. #2

Depth(m)	Temp(°C)	Depth(m)	Temp(°C)	Depth(m)	Temp(°C)
Zero level not recorded		280	21.52 ± .01	380	23.20
		285	21.60	385	23.30
.	.	290	21.71	390	23.38
.	.	295	21.80	395	23.48
.	.	300	21.88	400	23.57
190	20.07 ± .02	310	22.03	405	23.67
200	20.37	320	22.18	410	23.79
210	20.50	330	22.33	415	23.87
220	20.61	340	22.51	420	23.98
230	---	350	22.68	425	24.13
240	---	360	22.83	Bottom	24.413
250	21.03 ± .01	370	22.00		
260	21.19	375	23.10		
270	21.35				

15. DH-67 Tehachapi Mountains, California; 1300 foot hole completed 4/5/65; two loggings

LOG 7/15/65 Probe - Harvard FEI 5-K250-1

Depth(m)	Temp(°C)	Depth(m)	Temp(°C)	Depth(m)	Temp(°C)
Zero set for thermistor at collar elev.		160	---	240	19.56 ± .01
		170	18.56 ± .01	250	19.71
.	.	180	18.68	260	19.89
.	.	190	18.82	270	20.06
120	18.04 ± .01	200	18.93	280	20.23
130	18.12	210	19.09	290	20.40
140	18.20	220	19.21	300	20.63
150	18.33	230	19.34		

LOG 8/17/66 Probe - Harvard FEI 4-K396-1

Depth(m)	Temp(°C)	Depth(m)	Temp(°C)	Depth(m)	Temp(°C)
Zero set for thermistor 0.86 m below collar elevation		210	19.05 ± .01	320	20.99 ± .01
		220	19.17	330	21.15
.	.	230	19.29	340	21.33
.	.	240	19.42	350	21.53
140	18.26 ± .01	250	19.56	360	21.68
150	18.37	260	19.76	370	21.86
160	18.47	270	19.94	380	22.03
170	18.56	280	20.11	390	22.30
180	18.67	290	20.28	Bottom	22.470
190	18.82	300	20.47		
200	18.95	310	20.74		

16. DH-70 Tehachapi Mountains, California; 1800 foot hole completed 2/25/66; one logging

LOG 8/21/66 Probe - Harvard FEI 4-K396-1

Depth(m)	Temp(°C)	Depth(m)	Temp(°C)	Depth(m)	Temp(°C)
Zero set for thermistor 0.74 m below collar elevation		160	13.18 ± .01	260	15.31 ± .01
		170	13.39	270	15.52
.	.	180	13.60	280	15.73
.	.				
.	.	190	13.74	290	15.94
100	11.92 ± .01	200	14.00	300	16.15
110	12.10	210	14.23	310	16.36
120	12.33	220	14.45	320	16.57
130	12.54	230	14.67	325	16.67
140	12.78	240	14.88		
150	12.98	240	15.09		

17. HO-1 Hollister, California; 1000 foot hole completed 5/28/66; three loggings

LOG 11/10/66 Probe - C.I.T. #1

Depth(m)	Temp(°C)	Depth(m)	Temp(°C)	Depth(m)	Temp(°C)
Zero set for thermistor 0.50 m above collar elevation		120	21.31 ± .01	250	24.69 ± .02
		130	21.66	260	24.83
.	.	140	22.02	270	24.962 ± .01
.	.				
.	.	150	22.38	272	24.984
30	15.43 ± .02	160	22.61	274	25.005
40	16.79	170	22.96	276	25.076
50	18.60	180	23.21	278	25.127
60	19.01	190	23.48	280	25.185
70	19.40 ± .01	200	23.68 ± .02	282	25.247
80	19.74	210	23.91	284	25.307
90	20.34	220	24.25	286	25.368
100	20.66	230	24.29	288	25.431
110	20.96	240	24.54	290	25.487

HO-1 LOG 11/10/66 (continued)

Depth(m)	Temp(°C)	Depth(m)	Temp(°C)	Depth(m)	Temp(°C)
292	25.542 ± .01	296	25.666 ± .01	300	25.798 ± .01
294	25.601	298	25.738	Bottom	25.906

LOG 1/12/67 Probe - C.I.T. #1

Depth(m)	Temp(°C)	Depth(m)	Temp(°C)	Depth(m)	Temp(°C)
Zero set for thermistor 0.61 m above collar elevation		170	22.94 ± .01	282	25.265 ± .01
		190	23.48	284	25.326
.	.	210	23.92 ± .02	286	25.388
.	.	230	24.31	288	25.446
30	15.51 ± .01	250	24.88	290	25.508
50	18.59	270	24.966 ± .01	292	25.567
70	19.28	272	24.984	294	25.630
90	20.28	274	25.002	296	25.690
110	20.91	276	25.099	298	25.748
130	21.63	278	25.143	300	25.807
150	22.35	280	25.205	302	25.857

LOG 3/26/67 Probe - C.I.T. #2

Depth(m)	Temp(°C)	Depth(m)	Temp(°C)	Depth(m)	Temp(°C)
Zero level not recorded		140	21.89 ± .01	260	24.778 ± .01
		160	22.54	265	24.856
.	.	180	23.15 ± .02	270	24.908
.	.	200	23.63	275	25.013
20	14.65 ± .01	210	23.86	280	25.149
40	16.71	220	24.17	285	25.300
60	18.82	230	24.23	290	24.453
80	19.60	240	24.48	295	25.605
100	20.54	250	24.63	300	25.753
120	21.19				

APPENDIX VII

CONDUCTIVITY DATA

(Depths are given in feet below collar elevation, Conductivity values in mcal/cm·sec·°C, Resistivity values in cm·sec·°C/cal. The temperature given is the mean sample temperature during measurement and the pressure, the axial pressure on the sample. All samples were water saturated unless otherwise noted.)

1. AN-1 Anza, California

Depth(ft)	k	R	Temp(°C)	Press(bars)
239	7.4	135	11	200
371	7.5	133	11	200
446	7.5	133	11	200
475	7.1	141	23	100
485	7.7	130	11	200
501	7.6	131	23	100
551	7.5	133	11	200
	7.2	139	31	200
552	7.3	137	23	100
576	7.4	136	23	100
597	7.5	133	11	200
624	7.6	132	23	100
659	7.6	132	23	100
689	7.9	127	11	200
728	7.5	133	11	200
750	7.3	136	23	100
775	7.2	139	23	100
822	6.8	148	23	100
836	7.1	141	11	200
850	6.7	150	23	100
872	7.8	128	11	200
	7.5	133	31	200
900	7.3	137	23	100
938	7.8	128	11	200

AN-1 Anza, California (continued)

Depth(ft)	k	R	Temp(°C)	Press(bars)
971	8.1	123	11	200
1002	7.4	135	23	100
1036	7.6	132	11	200
1050	7.4	135	23	100
1069	7.7	130	11	200
1075	7.4	135	23	100
1100	7.4	136	23	100
1102	7.5	134	23	100
1122	7.8	128	11	200
1125	7.4	135	23	100
1150	6.6	152	23	100
1173	7.4	136	23	100
1174	7.3	137	11	200
	6.9	145	31	200
1183A	7.4	136	23	100
1183B	7.5	134	23	100

2. AN-2 Anza, California

Depth(ft)	k	R	Temp(°C)	Press(bars)
154	6.4	156	11	200
226	7.0	143	23	200
286	6.9	145	11	200
334	6.8	147	11	200
	6.7	149	31	200
403	6.5	154	11	200
440A	6.9	145	11	200
440B	6.5	153	23	100
448	6.5	155	23	100
474	6.7	149	23	100
485	6.8	147	11	200

AN-2 Anza, California (continued)

Depth(ft)	k	R	Temp(°C)	Press(bars)
525	5.9	168	23	100
535	6.7	149	11	200
540	5.8	173	23	100
607	7.1	141	11	200
	6.8	147	31	200
625	6.5	153	23	100
650	6.6	152	23	100
666	7.0	143	11	200
675	6.8	147	23	100
700	6.6	151	23	100
722	7.0	143	11	200
725	6.5	154	23	100
750A	6.6	152	23	100
750B	6.5	153	23	100
755	7.1	141	11	200
775	7.2	139	11	200
825	6.5	154	23	100
850	6.4	157	23	100
898A	6.1	164	23	100
898B	6.2	161	23	100
902	5.8	172	11	200
925A	6.2	161	23	100
925B	6.5	155	23	100
947	7.3	137	11	200
	7.0	143	31	200
975	6.8	147	23	100
987	6.9	145	11	200
1000	6.9	145	11	200

3. AN-3 Anza, California

Depth(ft)	k	R	Temp(°C)	Press(bars)
285	6.3	159	11	200
426	7.3	137	11	200
	7.0	143	31	200
444	6.1	165	23	100
466	7.3	137	11	200
471	6.7	149	23	100
494	8.4	119	23	100
505	7.0	143	11	200
507	6.7	149	23	100
510	6.6	151	23	100
522	6.7	148	23	100
531	7.1	141	11	200
532	7.0	142	23	100
554	6.9	145	23	100
564	6.9	145	11	200
569	7.0	144	23	100
580	8.6	116	23	100
586	6.9	144	23	100
592	6.9	145	23	100
597	7.0	142	11	200
600	6.7	150	23	100
604	6.7	150	23	100
614	6.9	145	23	100
625	6.9	146	23	100
634	6.9	145	23	100
649	6.7	150	11	200
	6.5	155	31	200
650	5.0	199	23	100
654	6.7	149	23	100
656	6.8	148	23	100
675	7.0	143	23	100

AN-3 Anza, California (continued)

Depth(ft)	k	R	Temp(°C)	Press(bars)
676	6.9	146	23	100
728	7.2	139	11	200
754	7.0	142	11	200

4. LH-1 Lake Hughes, California

Depth(ft)	k	R	Temp(°C)	Press(bars)
177	6.4*	157	22	200
	6.8	148	22	200
233	5.7*	176	11	200
	6.0	167	11	200
321	5.0*	200	11	200
	6.3	159	11	200
332	6.4	156	21	50
354	6.2*	161	11	200
	6.7	149	11	200
414	6.6	152	21	50
436	5.7*	176	11	200
	6.2	161	11	200
449	5.8*	173	11	200
	6.2	161	11	200
450	6.1	164	22	50
453	6.0	167	22	50
489	6.1*	164	11	200
	6.4	157	11	200
490	6.4	157	22	50
519	6.0	167	22	50
550	6.4	157	22	50
554	6.0*	167	11	200
	6.6	152	11	200
	6.5	154	31	200

*Unsaturated

LH-1 Lake Hughes, California (continued)

Depth(ft)	k	R	Temp(°C)	Press(bars)
558	6.2	161	22	50
563	6.1	164	22	50
567	5.6*	178	11	200
	6.0	167	11	200
578	6.3	159	22	50
603	6.4*	157	11	200
	6.7	149	11	200
604	5.7	176	22	50
606	6.2	161	22	50
612	6.3	158	22	50
615	6.4	157	20	50
616	6.3	158	21	50
620	5.5	182	22	50
635	6.5	154	22	50
649	5.9*	170	11	200
	6.3	159	11	200
	6.1	164	31	200
651	6.2	161	21	50
676	6.3	159	22	50

5. LH-2 Lake Hughes, California

Depth(ft)	k	R	Temp(°C)	Press(bars)
623	6.9	145	11	200
	6.8	147	31	200
682	6.2	161	11	200
684	6.3	160	21	100
696	6.0	166	21	100
724	6.3	160	21	100
734	6.5	154	21	100
744	6.1	164	21	100

LH-2 Lake Hughes, California (continued)

Depth(ft)	k	R	Temp(°C)	Press(bars)
752	6.1	164	21	100
772	6.3	159	21	100
796	6.0	166	22	100
823	6.6	151	21	100
824	6.3	159	11	200
825	6.3	159	21	100
843	6.1	164	11	200
	6.0	166	31	100
872	6.1	165	21	100
892	6.7	149	11	200
893	6.3	159	21	100
899	6.4	156	11	200
914	6.5	153	21	100
915	6.6	152	11	200
936	6.5	154	21	100
940	5.8	173	21	100
1075	6.1	165	21	100
1140	5.7	174	22	100
1141	5.7	175	21	100

6. LH-3 Lake Hughes, California

Depth(ft)	k	R	Temp(°C)	Press(bars)
151	6.3	159	14	200
	6.1	164	34	200
182	6.2	161	14	200
	6.1	164	34	200
219	6.0	169	14	200
	6.0	169	34	200
257	6.1	164	14	200
	6.0	169	34	200

LH-3 Lake Hughes, California (continued)

Depth(ft)	k	R	Temp(°C)	Press(bars)
289	6.1	164	14	200
	6.0	169	34	200
317	6.0	169	14	200
	5.9	170	34	200
353	6.5	154	14	200
	6.3	159	34	200
385	6.1	164	14	200
	6.0	169	34	200
415	6.4	156	14	200
	6.3	159	34	200
449	6.0	167	14	200
	5.9	170	34	200
482	6.2	161	14	200
	6.1	164	34	200
514	5.8	172	14	200
	5.7	176	34	200
556	6.4	156	14	200
	6.3	159	34	200
590	6.9	145	14	200
	6.8	147	34	200
612	7.9	127	14	200
	7.6	132	34	200
659	7.3	137	14	200
	7.1	141	34	200
669	7.5	133	14	200
	7.2	139	34	200
679	7.2	139	14	200
	7.0	143	34	200
719	7.3	137	14	200
	7.0	143	34	200

LH-3 Lake Hughes, California (continued)

Depth(ft)	k	R	Temp(°C)	Press(bars)
759	7.0	143	14	200
	6.8	147	34	200
792	17.8	56	14	200
	17.1	58	34	200
819	6.8	147	14	200
	6.6	151	34	200
857	5.7	176	14	200
	5.6	179	34	200
891	6.1	164	14	200
	6.0	167	34	200
908	5.2	192	14	200
	5.1	197	34	200
927	6.1	164	21	100
939	5.7	176	14	200
	5.7	176	34	200
940	5.7	176	20	100
948	4.9	204	21	100
949	5.4	185	14	200
	5.4	185	34	200
955	5.6	179	21	100
968	5.7	176	21	100
973	5.9	170	21	100
983	6.2	161	14	200
	6.2	161	34	200
985	5.7	176	22	100
993	6.6	151	20	100
1004	5.6	179	22	100
1014	5.3	189	14	200
	5.2	192	34	200
1046	5.5	182	14	200
	5.4	185	34	200

LH-3 Lake Hughes, California (continued)

Depth(ft)	k	R	Temp(°C)	Press(bars)
1057	5.6	180	22	100
1071	4.9	203	22	100
1078	5.8	173	14	200
	5.7	176	34	200
1086	5.2	192	20	100
1095	5.7	176	22	100
1103	5.1	196	21	100
1111	5.8	173	22	100
1112	5.2	192	14	200
	5.1	196	34	200
1142	5.9	170	14	200
	5.8	173	34	200
1169	4.9	203	22	100
1172	5.4	185	14	200
	5.3	189	34	200
1178	4.9	203	22	100
1179	4.6	218	20	100
1191	6.0	167	14	200
	5.9	170	34	200

7. SB-2 San Bernardino Mountains, California

Depth(ft)	k	R	Temp(°C)	Press(bars)
1300	6.7	150	22	100
1310	5.5	180	22	100
1321	4.9	206	22	100
1328	4.7	213	22	100
1336	5.3	189	22	100
1356	5.1	197	22	100
1364	4.4	226	22	100
1372	4.6	217	22	100

SB-2 San Bernardino Mountains, California (continued)

Depth(ft)	k	R	Temp(°C)	Press(bars)
1384	4.7	214	22	100
1392	4.8	207	22	100
1401	4.9	204	22	100
1403	4.4	226	22	100
1421	5.3	189	22	100
1428	6.3	158	22	100
1429	5.5	181	22	100
1431	5.7	176	22	100
1442	5.6	177	22	100
1443	5.2	191	22	100
1444	6.0	167	22	100
1458	8.2	122	22	100
1477	6.1	165	22	100
1478	5.1	197	22	100
1482	5.0	202	22	100
1483	5.5	180	22	100
1484	7.6	131	22	100
1490	5.8	174	22	100
1492	5.9	168	22	100
1496	6.1	164	22	100
1498	5.3	190	22	100
1501	6.2	161	22	100
1507	6.1	163	22	100
1512	6.0	166	22	100
1516	6.0	167	22	100
1518	6.9	144	22	100
1519	6.7	148	22	100
1523	6.4	155	22	100
1529	7.5	134	22	100
1537	6.0	168	22	100
1542	6.4	156	22	100
1550	7.0	143	22	100

8. SB-5 San Bernardino Mountains, California

Depth(ft)	k	R	Temp(°C)	Press(bars)
478	5.9	170	23	100
494	6.0	167	23	100
542	5.4	186	23	100
652	6.1	165	23	100
661	5.0	199	23	100
668	5.8	173	23	100
684	6.1	165	23	100
689	5.3	188	23	100
709	6.1	163	23	100
719	5.8	171	23	100
748	5.7	177	23	100
770	8.2	121	23	100
778	5.2	191	23	100
801	6.6	151	23	100
815	7.0	144	23	100
818	6.2	161	23	100

9. SB-10 San Bernardino Mountains, California

Depth(ft)	k	R	Temp(°C)	Press(bars)
101	5.9	170	22	100
422	5.6	218	22	100
441	4.5	222	22	100
446	5.3	191	22	100
501	6.6	151	20	100
502	6.7	149	22	100
606	5.4	184	22	100
644	6.0	167	22	100
754	5.8	171	20	100
806	6.4	155	22	100
854	5.3	189	22	100
856	6.0	168	22	100

SB-10 San Bernardino Mountains, California (continued)

Depth(ft)	k	R	Temp(°C)	Press(bars)
860	6.1	164	22	100
868	6.9	145	22	100
880	6.0	154	22	100
910	7.3	136	22	100
912	6.8	147	22	100
920	7.3	137	21	100
937	6.7	150	22	100
946	7.5	134	20	100
956	7.8	129	23	100
963	6.5	153	23	100
975	6.7	148	23	100
995	5.4	187	22	100
1005	5.9	169	23	100
1021	6.9	144	23	100
1029	6.5	153	22	100
1032	6.2	160	22	100
1057	7.2	140	22	100
1070	6.4	157	22	100
1084	5.8	172	21	100
1086	6.4	156	22	100
1098	5.5	182	23	100
1102	6.4	157	23	100
1110A	5.8	172	22	100
1110B	6.9	145	24	100
1131	6.4	157	22	100
1136	5.5	180	22	100
1158	5.2	191	22	100
1182	6.6	151	22	100
1206	6.4	157	23	100
1220	7.3	137	22	100
1225	7.5	134	21	100

SB-10 San Bernardino Mountains, California (continued)

Depth(ft)	k	R	Temp(°C)	Press(bars)
1238	7.2	139	22	100
1251	7.7	130	22	100
1266	6.7	150	22	100
1276	7.3	137	21	100
1289A	7.5	134	22	100
1289B	7.4	136	20	100
1318	7.3	136	23	100
1349	5.2	192	22	100
1366A	5.4	185	22	100
1366B	5.2	192	20	100
1382A	5.0	198	22	100
1382B	5.2	193	19	100
1406	5.7	176	21	100
1412	5.9	170	23	100
1423	5.6	180	21	100
1439	7.1	140	23	100
1446	6.3	159	22	100
1456	6.4	156	23	100
1458	7.0	143	23	100
1460	6.9	145	23	100
1474	6.8	147	22	100
1477	6.7	149	22	100
1484	6.6	152	23	100
1489	6.8	148	22	100
1495	6.8	148	23	100
1496	6.6	151	23	100
1511	4.7	212	22	100
1521	5.9	169	23	100
1530	4.9	205	23	100
1538	5.0	201	23	100
1542	5.6	177	23	100
1560	5.3	189	23	100

SB-10 San Bernardino Mountains, California (continued)

Depth(ft)	k	R	Temp(°C)	Press(bars)
1576	7.2	140	23	100
1583	7.1	141	23	100
1592	6.6	152	23	100
1602	5.0	201	23	100
1607	5.4	186	23	100
1627	6.2	162	23	100
1646	6.9	144	23	100
1655	6.5	153	23	100
1659	5.1	196	23	100
1663	5.9	168	23	100
1674	5.5	182	23	100
1685	6.6	151	23	100
1697	5.5	182	23	100
1715	4.6	218	23	100

10. LV-1 Lucerne Valley, California

Depth(ft)	k	R	Temp(°C)	Press(bars)
† 33A	6.9	145	25	200
† 33B	6.7	149	25	200
† 44A	6.5	154	25	200
† 44B	6.2	161	25	200
2005	5.5	182	23	100
2015	6.1	165	23	100
2031	5.3	190	23	100
2041A	5.5	182	25	200
2041B	5.2	192	25	200
2048A	5.4	185	25	200
2048B	5.4	185	25	200
2053	5.7	176	23	100

† These samples taken from a 15 meter hole 100 meters south of LV-1.

LV-1 Lucerne Valley, California (continued)

Depth(ft)	k	R	Temp(°C)	Press(bars)
2075	5.3	190	23	100
2091A	5.8	172	25	200
2091B	6.1	164	25	200
2094	5.3	189	23	100
2099A	6.1	164	25	200
2099B	6.0	167	25	200
2108A	5.4	185	25	200
2108B	5.6	179	25	200
2123	5.8	173	23	100
2133	5.7	175	23	100
2137A	5.5	182	25	200
2137B	5.6	179	25	200
2147	6.1	165	23	100
2151	5.2	193	23	100
2160	5.7	176	23	100
2176	5.3	187	20	100
	5.3	187	42	100
2185	5.8	173	23	100
2194	7.4	135	23	100
2213	6.5	153	23	100
2222	6.6	152	23	100
2232	6.5	155	23	100
2243	6.1	164	23	100
2260	5.8	172	23	100
2272	5.7	174	23	100
2281	5.9	170	23	100
2295	5.4	185	23	100
2311	6.5	155	23	100

11. DH-14 Tehachapi Mountains, California

‡ Depth(ft)	k	R	Temp(°C)	Press(bars)
-1-	8.3	120	21	100
-2-	8.5	117	21	100
-3-	8.4	120	21	100
-4-	8.3	120	21	100
-5-	8.2	122	21	100
-6-	8.4	120	23	100
-7-	8.3	121	23	100
-8-	8.5	118	23	100
-9-	8.3	121	23	100
-10-	8.1	124	23	100

12. DH-15A Tehachapi Mountains, California

No core was available from this hole.

13. DH-43 Tehachapi Mountains, California

Depth(ft)	k	R	Temp(°C)	Press(bars)
620	12.2	82	23	100
627	6.3	158	23	100
641	7.2	139	23	100
644	14.3	70	23	100
654	7.8	128	23	100
660	8.1	123	23	100
670	8.0	125	23	100
682	8.2	122	23	100
692	8.4	119	23	100
696	7.2	138	23	100
704	8.4	119	23	100
715	9.2	109	23	100

‡ No depths available for this hole since core discarded on surface after drilling.

DH-43 Tehachapi Mountains, California (continued)

Depth(ft)	k	R	Temp(°C)	Press(bars)
723	8.3	121	23	100
733	8.0	125	23	100
752	8.3	121	23	100
764	8.6	116	23	100
770	7.3	137	23	100
781	8.0	125	23	100
786	8.5	118	23	100
791	8.7	114	23	100

14. DH-65 Tehachapi Mountains, California

Depth(ft)	k	R	Temp(°C)	Press(bars)
295A	8.4	119	22	200
295B	8.4	119	22	200
	7.8*	128	22	200
397A	9.0	111	22	200
397B	8.8	114	22	200
	8.3*	120	22	200
495A	7.6	132	22	200
495B	8.6	116	22	200
	8.0*	125	22	200
551A	7.8	128	22	200
551B	8.4	119	22	200
	7.8*	128	22	200
600A	8.2	122	22	200
600B	8.3	120	22	200
	7.6*	132	22	200
649A	7.0	143	22	200
649B	7.2	139	22	200
	6.7*	149	22	200

* Unsaturated

DH-65 Tehachapi Mountains, California (continued)

Depth(ft)	k	R	Temp(°C)	Press(bars)
696	7.7	130	22	100
715	6.6	151	22	100
724	6.7	148	21	100
735	7.7	129	22	100
745	7.0	143	22	100
760	5.3	188	21	100
800A	7.1	141	22	200
800B	7.3	137	22	200
	6.8*	147	22	200
823	7.5	133	22	100
851	6.6	152	23	100
882	8.0	124	23	100
898	7.6	132	23	100
942	7.8	128	23	100
984	8.5	118	23	100
987A	9.7	103	22	200
987B	9.2	109	22	200
	8.6*	116	22	200
997A	5.1	196	22	200
997B	5.2	192	22	200
	5.1*	196	22	200
1007	9.5	106	23	100
1051	5.0	199	23	100
1071	6.6	152	23	100
1090	7.4	135	21	100
1097	8.8	114	23	100
1136	5.0	200	21	100
1144	8.0	125	22	100
1158	5.3	188	20	100
1199	6.5	154	22	100

* Unsaturated

DH-65 Tehachapi Mountains, California (continued)

Depth(ft)	k	R	Temp(°C)	Press(bars)
1215	6.1	165	21	100
1232	6.2	160	21	100
1266A	5.3	189	22	200
1266B	5.1	196	22	200
	5.1*	196	22	200
1278	5.5	182	21	100
1282	5.7	176	22	100
1298	7.4	136	23	100
1347	7.0	143	23	100
1348	6.4	158	22	100
1365	6.4	156	22	100
1377	5.7	175	22	100
1398	6.2	160	23	100

15. DH-67 Tehachapi Mountains, California

Depth(ft)	k	R	Temp(°C)	Press(bars)
710	5.4	184	21	100
715	7.7	130	21	100
722	7.2	139	22	100
730	5.3	189	22	100
760	6.4	157	22	100
768	5.3	190	22	100
806	7.4	136	21	100
812	7.6	132	22	100
824	6.5	153	22	100
855	6.8	147	21	100
885	7.7	130	21	100
910	7.4	135	21	100
915	7.9	127	21	100

* Unsaturated

DH-67 Tehachapi Mountains, California (continued)

Depth(ft)	k	R	Temp(°C)	Press(bars)
930	7.8	128	22	100
940	7.3	138	20	100
961	7.5	133	23	100
970	8.6	117	21	100
980	7.5	133	22	100
993	6.6	151	22	100
998	8.8	113	21	100
1010	5.5	183	22	100
1020	5.5	181	21	100
1070	7.6	132	22	100
1085	7.8	129	22	100
1108	5.8	173	22	100
1120	8.5	118	22	100
1131	7.5	134	21	100
1135	7.0	143	21	100
1147	7.7	129	22	100
1153	9.1	109	22	100
1175	8.4	120	21	100
1180	7.5	133	21	100
1190	6.7	149	21	100
1195	5.5	183	21	100
1200	7.8	129	22	100
1215	6.9	145	21	100
1220	6.9	146	21	100
1239	6.6	151	22	100
1270	8.5	118	22	100
1300	4.5	221	21	100

16. DH-70 Tehachapi Mountains, California

Depth(ft)	k	R	Temp(°C)	Press(bars)
369	8.5	118	23	100
549	8.2	122	23	100
1047	8.6	116	23	100
1150	8.5	117	23	100
1154	8.5	118	23	100
1190	8.3	120	23	100
1206A	8.6	117	23	100
1206B	8.4	119	23	100
1250	8.5	118	23	100
1267	8.2	123	23	100
1287	8.2	121	23	100
1292	8.2	122	23	100
1526	8.6	117	23	100
1778	8.5	117	23	100

17. HO-1 Hollister, California

Depth(ft)	k	R	Temp(°C)	Press(bars)
57	8.0	125	14	200
	7.7	130	34	200
78	7.7	130	14	200
	7.5	133	34	200
130	8.5	118	14	200
	8.2	122	34	200
151	8.3	120	14	200
	8.0	125	34	200
181	8.4	119	14	200
	8.2	122	34	200
217	7.7	130	14	200
	7.4	135	34	200
229	6.5	154	14	200
	6.3	159	34	200

HO-1 Hollister, California (continued)

Depth(ft)	k	R	Temp(°C)	Press(bars)
246	8.0	125	14	200
	7.8	128	34	200
285	8.0	125	14	200
	7.8	128	34	200
315	6.4	156	14	200
	6.3	159	34	200
352	6.6	152	14	200
	6.2	161	34	200
385	6.6	152	14	200
	6.5	154	34	200
420	6.5	154	14	200
	6.4	156	34	200
447	6.5	154	14	200
	6.3	159	34	200
479	6.7	149	14	200
	6.5	154	34	200
514	6.4	156	14	200
	6.2	161	34	200
553	6.6	152	14	200
	6.4	156	34	200
583	6.7	149	14	200
	6.5	154	34	200
619	6.7	149	14	200
	6.5	154	34	200
648	7.2	139	14	200
	7.0	143	34	200
660	6.6	152	14	200
	6.5	154	34	200
686	6.7	149	14	200
	6.6	152	34	200
723	6.6	152	14	200
	6.5	154	34	200

HO-1 Hollister, California (continued)

Depth(ft)	k	R	Temp(°C)	Press(bars)
762	6.8	147	14	200
	6.4	156	34	200
782	6.7	149	14	200
	6.6	152	34	200
812	7.2	139	14	200
858	7.1	141	14	200
	7.0	143	34	200
878	6.6	152	14	200
	6.5	154	34	200
888	6.4	156	23	100
900	6.5	154	23	100
920	6.8	147	14	200
	6.7	149	34	200
938	6.4	156	23	100
942	6.4	156	23	100
947	6.6	152	14	200
	6.5	154	34	200
960	6.7	149	23	100
980	6.8	147	23	100
991	6.8	147	23	100

APPENDIX VIII

REDUCED GRADIENT AND HEAT FLOW DATA

Explanation of Terminology

RADII Outer radius of ring on terrain correction template.

ELDIFF Difference in elevation (in meters) between the drill hole collar elevation (C.E.) and the average elevation in a given ring (AVE.), i.e. C.E. - AVE.

T(O) Mean annual surface temperature deduced from extrapolation of temperature data in interval used for heat flow measurement to zero depth.

UNCORRECTED DATA Data uncorrected for topography or topographic evolution.

TOPOGRAPHIC CORRECTION Data corrected for topography according to the following notation:

SS CASE Topography has persisted in present state indefinitely.

1MY CASE Topography has evolved to present configuration in last 1 m.y.

4MY CASE Evolution in last 4 m.y.

etc.

GRAD Geothermal gradient determined by a least-squares linear fit to temperature-depth data.

REST Mean resistivity of core = mean harmonic conductivity.

FLUX Heat flow determined by taking the product of the gradient and the reciprocal of the resistivity.

DEPTH Depth in meters of a given measurement.

TEMP Temperature in °C at a given depth.

CORDEP Corrected depth; corrected according to the specified topographic situation (CORDEP = z_{cor}; see text, p. 227).

CORTEM Corrected temperature (CORTEM = T_{cor}; see text, p. 227).

SMOOTH Temperature in °C at a given depth as determined from parameters of least-squares fit.

RES Residual between the temperature calculated from parameters of the least-squares fit and the actual temperature at a given depth.

STER Standard error

of GRAD $$S_G = \left(\frac{\Sigma\,[y_i-(a+bx_i)]^2}{n-2}\right)^{\frac{1}{2}}\left(\frac{n}{n(\Sigma\,x_i^2)-(\Sigma\,x_i)^2}\right)^{\frac{1}{2}}$$

where a and b are the constants* from the least-squares linear fit to the temperature and depth data, y_i and x_i, and n is the number of temperature-depth points.

of REST $$S_R = \left(\frac{\Sigma\,(x_i-\bar{x})^2}{n(n-1)}\right)^{\frac{1}{2}} \quad \text{where } \bar{x} = \frac{\Sigma\,x_i}{n}$$

n being the number of determinations of resistivity x_i.

of FLUX $$S_F = \frac{G}{R}\left[\left(\frac{S_R}{R}\right)^2 + \left(\frac{S_G}{G}\right)^2\right]^{\frac{1}{2}}$$

where R and G are the mean resistivity and gradient, respectively.

95 CL 95% confidence limit

of GRAD = $t_2 S_G$

of REST = $t_1 S_R$

of FLUX = $$\frac{G}{R}\left[\left(\frac{t_1 S_R}{R}\right)^2 + \left(\frac{t_2 S_G}{G}\right)^2\right]^{\frac{1}{2}}$$

where t_1 and t_2 are the Student's multipliers for n-1 and

n-2 degrees of freedom, respectively.

The Units are Self Explanatory. e.g. MICROCAL/SQCMSEC = $\frac{\mu cal}{cm^2 \cdot sec}$

* The constants a and b are given by

$$a = \frac{(\Sigma y_i)(\Sigma x_i^2) - (\Sigma x_i)(\Sigma x_i y_i)}{n(\Sigma x_i^2) - (\Sigma x_i)^2}$$

$$b = \frac{n(\Sigma x_i y_i) - (\Sigma x_i)(\Sigma y_i)}{n(\Sigma x_i^2) - (\Sigma x_i)^2}$$

(see Beers, 1957, p. 37)

TOPOGRAPHIC DATA, ANZA AN-1

RADII	ELDIFF
100.0	-3.6
200.0	-8.5
300.0	-11.0
400.0	-2.7
500.0	8.5
700.0	22.0
900.0	38.0
1200.0	31.0
1500.0	22.0
2000.0	8.0
2500.0	-8.0
3000.0	-19.0
4000.0	-21.0
5000.0	3.0
7000.0	-54.0
10000.0	-118.0
15000.0	-204.0
20000.0	-102.0
30000.0	160.0
40000.0	-0.
50000.0	-0.
70000.0	-0.
100000.0	-0.

UNCORRECTED DATA, ANZA AN-1

DEPTH	TEMP	SMOOTH	RES
160.00	21.140	21.166	-0.026
170.00	21.400	21.416	-0.016
180.00	21.650	21.666	-0.016
190.00	21.900	21.917	-0.017
200.00	22.160	22.167	-0.007
210.00	22.410	22.418	-0.008
220.00	22.660	22.668	-0.008
230.00	22.930	22.919	0.011
240.00	23.170	23.169	0.001
250.00	23.430	23.420	0.010
260.00	23.710	23.670	0.040
270.00	23.970	23.920	0.050
280.00	24.200	24.171	0.029
290.00	24.450	24.421	0.029
300.00	24.700	24.672	0.028
310.00	24.950	24.922	0.028
320.00	25.180	25.173	0.007
330.00	25.400	25.423	-0.023
340.00	25.660	25.674	-0.014
350.00	25.880	25.924	-0.044
360.00	26.120	26.174	-0.054

T(0) = 17.158 DEG C

GRAD = 25.044 DEG/KM

STER = 0.1007 DEG/KM
95CL = 0.2109 DEG/KM

REST = 135.8 CMSECDEG/CAL

STER = 1.1 CMSECDEG/CAL
95CL = 2.3 CMSECDEG/CAL

FLUX = 1.844 MICROCAL/SQCMSEC

STER = 0.017 MICROCAL/SQCMSEC
95CL = 0.035 MICROCAL/SQCMSEC

TOPOGRAPHIC CORRECTION, SS CASE, ANZA AN-1

CORDEP	CORTEM	SMOOTH	RES
160.93	21.144	21.178	-0.033
170.66	21.403	21.425	-0.022
180.39	21.652	21.672	-0.020
190.14	21.901	21.919	-0.019
199.89	22.160	22.167	-0.008
209.66	22.408	22.415	-0.007
219.43	22.657	22.663	-0.006
229.22	22.926	22.912	0.015
239.02	23.166	23.161	0.005
248.83	23.425	23.410	0.015
258.66	23.704	23.659	0.045
268.49	23.963	23.909	0.054
278.34	24.193	24.159	0.033
288.21	24.442	24.410	0.032
298.09	24.691	24.660	0.031
307.97	24.941	24.911	0.029
317.88	25.170	25.163	0.008
327.79	25.390	25.415	-0.025
337.72	25.650	25.667	-0.017
347.66	25.869	25.919	-0.050
357.61	26.109	26.172	-0.062

T(0) = 17.091 DEG C

GRAD = 25.392 DEG/KM

STER = 0.1166 DEG/KM
95CL = 0.2440 DEG/KM

REST = 135.8 CMSECDEG/CAL

STER = 1.1 CMSECDEG/CAL
95CL = 2.3 CMSECDEG/CAL

FLUX = 1.870 MICROCAL/SQCMSEC

STER = 0.017 MICROCAL/SQCMSEC
95CL = 0.036 MICROCAL/SQCMSEC

TOPOGRAPHIC CORRECTION, 1MY CASE ANZA AN-1

UPLIFT = 1.3 KM EROSION = 0.1 KM

CORDEP	CORTEM	SMOOTH	RES
162.48	21.000	21.033	-0.033
172.31	21.250	21.272	-0.021
182.14	21.490	21.510	-0.020
191.98	21.730	21.748	-0.019
201.83	21.980	21.987	-0.008
211.69	22.220	22.226	-0.007
221.57	22.460	22.465	-0.006
231.45	22.720	22.705	0.015
241.35	22.950	22.945	0.005
251.26	23.200	23.185	0.015
261.18	23.470	23.426	0.045
271.11	23.720	23.666	0.054
281.06	23.941	23.908	0.033
291.02	24.181	24.149	0.032
300.99	24.422	24.391	0.031
310.98	24.662	24.633	0.029
320.98	24.883	24.875	0.008
330.99	25.093	25.118	-0.024
341.01	25.344	25.361	-0.017
351.05	25.555	25.604	-0.049
361.10	25.785	25.847	-0.062

T(0) = 17.095 DEG C

GRAD = 24.238 DEG/KM

STER = 0.1146 DEG/KM
95CL = 0.2399 DEG/KM

REST = 135.8 CMSECDEG/CAL

STER = 1.1 CMSECDEG/CAL
95CL = 2.3 CMSECDEG/CAL

FLUX = 1.785 MICROCAL/SQCMSEC

STER = 0.017 MICROCAL/SQCMSEC
95CL = 0.035 MICROCAL/SQCMSEC

TOPOGRAPHIC CORRECTION, 4MY CASE ANZA AN-1

UPLIFT = 1.3 KM EROSION = 0.1 KM

CORDEP	CORTEM	SMOOTH	RES
161.92	21.073	21.106	-0.033
171.71	21.328	21.349	-0.022
181.51	21.572	21.592	-0.020
191.31	21.816	21.835	-0.019
201.13	22.071	22.078	-0.008
210.96	22.315	22.322	-0.007
220.79	22.560	22.566	-0.006
230.64	22.824	22.810	0.015
240.50	23.059	23.054	0.005
250.38	23.314	23.299	0.015
260.27	23.589	23.544	0.045
270.16	23.843	23.789	0.054
280.08	24.068	24.035	0.033
290.00	24.313	24.281	0.032
299.94	24.558	24.527	0.031
309.89	24.803	24.774	0.029
319.86	25.028	25.021	0.008
329.83	25.244	25.268	-0.025
339.82	25.499	25.516	-0.017
349.82	25.714	25.764	-0.049
359.84	25.950	26.012	-0.062

T(0) = 17.093 DEG C

GRAD = 24.785 DEG/KM

STER = 0.1154 DEG/KM
95CL = 0.2416 DEG/KM

REST = 135.8 CMSECDEG/CAL

STER = 1.1 CMSECDEG/CAL
95CL = 2.3 CMSECDEG/CAL

FLUX = 1.825 MICROCAL/SQCMSEC

STER = 0.017 MICROCAL/SQCMSEC
95CL = 0.036 MICROCAL/SQCMSEC

TOPOGRAPHIC CORRECTION, 9MY CASE ANZA AN-1

UPLIFT = 1.3 KM EROSION = 0.1 KM

CORDEP	CORTEM	SMOOTH	RES
161.67	21.097	21.131	-0.033
171.44	21.353	21.375	-0.022
181.22	21.599	21.619	-0.020
191.02	21.845	21.864	-0.019
200.81	22.101	22.108	-0.008
210.63	22.347	22.353	-0.007
220.45	22.593	22.599	-0.006
230.28	22.859	22.844	0.015
240.13	23.095	23.090	0.005
249.98	23.351	23.336	0.015
259.85	23.628	23.583	0.045
269.74	23.884	23.830	0.054
279.64	24.110	24.077	0.033
289.55	24.357	24.324	0.032
299.47	24.603	24.572	0.031
309.40	24.850	24.820	0.029
319.35	25.076	25.069	0.008
329.31	25.293	25.318	-0.025
339.29	25.550	25.567	-0.017
349.27	25.767	25.816	-0.049
359.27	26.004	26.066	-0.062

T(0) = 17.093 DEG C

GRAD = 24.976 DEG/KM

STER = 0.1157 DEG/KM
95CL = 0.2422 DEG/KM

REST = 135.8 CMSECDEG/CAL

STER = 1.1 CMSECDEG/CAL
95CL = 2.3 CMSECDEG/CAL

FLUX = 1.839 MICROCAL/SQCMSEC

STER = 0.017 MICROCAL/SQCMSEC
95CL = 0.036 MICROCAL/SQCMSEC

TOPOGRAPHIC CORRECTION, 16MY CASE ANZA AN-1

UPLIFT = 1.3 KM EROSION = 0.1 KM

CORDEP	CORTEM	SMOOTH	RES
161.19	21.127	21.160	-0.033
170.94	21.384	21.406	-0.022
180.69	21.632	21.652	-0.020
190.46	21.880	21.898	-0.019
200.23	22.137	22.145	-0.008
210.01	22.385	22.392	-0.007
219.80	22.633	22.639	-0.006
229.60	22.901	22.886	0.015
239.42	23.139	23.134	0.005
249.25	23.397	23.382	0.015
259.09	23.675	23.630	0.045
268.94	23.933	23.879	0.054
278.81	24.162	24.128	0.033
288.69	24.410	24.378	0.032
298.58	24.658	24.627	0.031
308.49	24.907	24.877	0.029
318.41	25.135	25.128	0.008
328.34	25.354	25.378	-0.025
338.28	25.612	25.629	-0.017
348.24	25.831	25.880	-0.050
358.21	26.069	26.132	-0.062

T(0) = 17.092 DEG C

GRAD = 25.237 DEG/KM

STER = 0.1163 DEG/KM
95CL = 0.2433 DEG/KM

REST = 135.8 CMSECDEG/CAL

STER = 1.1 CMSECDEG/CAL
95CL = 2.3 CMSECDEG/CAL

FLUX = 1.858 MICROCAL/SQCMSEC

STER = 0.017 MICROCAL/SQCMSEC
95CL = 0.036 MICROCAL/SQCMSEC

TOPOGRAPHIC CORRECTION, 1MY CASE ANZA AN-1

UPLIFT = 1.5 KM EROSION = 0.3 KM

CORDEP	CORTEM	SMOOTH	RES
167.64	21.000	21.033	-0.033
177.79	21.250	21.271	-0.021
187.94	21.490	21.510	-0.020
198.11	21.730	21.748	-0.019
208.28	21.980	21.987	-0.008
218.46	22.220	22.226	-0.007
228.66	22.460	22.466	-0.006
238.87	22.720	22.705	0.014
249.08	22.950	22.945	0.005
259.32	23.200	23.185	0.015
269.56	23.470	23.426	0.044
279.82	23.720	23.667	0.054
290.09	23.941	23.908	0.033
300.37	24.181	24.149	0.032
310.67	24.422	24.391	0.031
320.97	24.662	24.633	0.029
331.30	24.883	24.875	0.008
341.63	25.093	25.118	-0.024
351.98	25.344	25.361	-0.017
362.33	25.555	25.604	-0.049
372.70	25.785	25.847	-0.062

T(0) = 17.097 DEG C

GRAD = 23.476 DEG/KM

STER = 0.1105 DEG/KM
95CL = 0.2313 DEG/KM

REST = 135.8 CMSECDEG/CAL

STER = 1.1 CMSECDEG/CAL
95CL = 2.3 CMSECDEG/CAL

FLUX = 1.729 MICROCAL/SQCMSEC

STER = 0.016 MICROCAL/SQCMSEC
95CL = 0.034 MICROCAL/SQCMSEC

TOPOGRAPHIC CORRECTION, 4MY CASE ANZA AN-1

UPLIFT = 1.5 KM EROSION = 0.3 KM

CORDEP	CORTEM	SMOOTH	RES
164.50	21.073	21.106	-0.033
174.45	21.328	21.349	-0.022
184.41	21.572	21.592	-0.020
194.38	21.816	21.835	-0.019
204.35	22.071	22.078	-0.008
214.34	22.315	22.322	-0.007
224.34	22.560	22.566	-0.006
234.35	22.824	22.810	0.015
244.37	23.059	23.054	0.005
254.41	23.314	23.299	0.015
264.46	23.589	23.544	0.045
274.52	23.843	23.789	0.054
284.59	24.068	24.035	0.033
294.68	24.313	24.281	0.032
304.78	24.558	24.527	0.031
314.89	24.803	24.774	0.029
325.02	25.028	25.021	0.008
335.15	25.244	25.268	-0.025
345.30	25.499	25.516	-0.017
355.47	25.714	25.764	-0.049
365.64	25.950	26.012	-0.062

T(0) = 17.095 DEG C

GRAD = 24.387 DEG/KM

STER = 0.1133 DEG/KM
95CL = 0.2372 DEG/KM

REST = 135.8 CMSECDEG/CAL

STER = 1.1 CMSECDEG/CAL
95CL = 2.3 CMSECDEG/CAL

FLUX = 1.796 MICROCAL/SQCMSEC

STER = 0.017 MICROCAL/SQCMSEC
95CL = 0.035 MICROCAL/SQCMSEC

TOPOGRAPHIC CORRECTION, 9MY CASE ANZA AN-1

UPLIFT = 1.5 KM EROSION = 0.3 KM

CORDEP	CORTEM	SMOOTH	RES
163.38	21.097	21.130	-0.033
173.27	21.353	21.375	-0.022
183.16	21.599	21.619	-0.020
193.06	21.845	21.864	-0.019
202.96	22.101	22.108	-0.008
212.88	22.347	22.353	-0.007
222.81	22.593	22.599	-0.006
232.75	22.859	22.844	0.015
242.70	23.095	23.090	0.005
252.67	23.351	23.336	0.015
262.65	23.628	23.583	0.045
272.64	23.884	23.830	0.054
282.64	24.110	24.077	0.033
292.66	24.357	24.325	0.032
302.69	24.603	24.572	0.031
312.74	24.850	24.821	0.029
322.79	25.076	25.069	0.008
332.86	25.293	25.318	-0.025
342.94	25.550	25.567	-0.017
353.03	25.767	25.816	-0.049
363.14	26.004	26.066	-0.062

T(0) = 17.094 DEG C

GRAD = 24.707 DEG/KM

STER = 0.1143 DEG/KM
95CL = 0.2392 DEG/KM

REST = 135.8 CMSECDEG/CAL

STER = 1.1 CMSECDEG/CAL
95CL = 2.3 CMSECDEG/CAL

FLUX = 1.819 MICROCAL/SQCMSEC

STER = 0.017 MICROCAL/SQCMSEC
95CL = 0.035 MICROCAL/SQCMSEC

TOPOGRAPHIC CORRECTION, 16MY CASE ANZA AN-1

UPLIFT = 1.5 KM EROSION = 0.3 KM

CORDEP	CORTEM	SMOOTH	RES
161.84	21.127	21.160	-0.033
171.63	21.384	21.406	-0.022
181.42	21.632	21.652	-0.020
191.22	21.880	21.898	-0.019
201.03	22.137	22.145	-0.008
210.85	22.385	22.392	-0.007
220.69	22.633	22.639	-0.006
230.53	22.901	22.886	0.015
240.39	23.139	23.134	0.005
250.25	23.397	23.382	0.015
260.14	23.675	23.631	0.045
270.03	23.933	23.879	0.054
279.94	24.162	24.128	0.033
289.86	24.410	24.378	0.032
299.79	24.658	24.627	0.031
309.74	24.907	24.877	0.029
319.70	25.135	25.128	0.008
329.67	25.354	25.378	-0.025
339.65	25.612	25.629	-0.017
349.65	25.831	25.880	-0.050
359.66	26.069	26.132	-0.062

T(0) = 17.092 DEG C

GRAD = 25.134 DEG/KM

STER = 0.1157 DEG/KM
95CL = 0.2422 DEG/KM

REST = 135.8 CMSECDEG/CAL

STER = 1.1 CMSECDEG/CAL
95CL = 2.3 CMSECDEG/CAL

FLUX = 1.851 MICROCAL/SQCMSEC

STER = 0.017 MICROCAL/SQCMSEC
95CL = 0.036 MICROCAL/SQCMSEC

TOPOGRAPHIC CORRECTION, 1MY CASE ANZA AN-1

UPLIFT = 1.7 KM EROSION = 0.5 KM

CORDEP	CORTEM	SMOOTH	RES
172.80	21.000	21.033	-0.032
183.27	21.250	21.271	-0.021
193.75	21.490	21.510	-0.020
204.23	21.730	21.748	-0.019
214.73	21.980	21.987	-0.008
225.24	22.220	22.226	-0.007
235.75	22.460	22.466	-0.006
246.28	22.720	22.705	0.014
256.82	22.950	22.945	0.005
267.38	23.200	23.185	0.014
277.94	23.470	23.426	0.044
288.52	23.720	23.667	0.054
299.11	23.941	23.908	0.033
309.72	24.181	24.149	0.032
320.34	24.422	24.391	0.031
330.97	24.662	24.633	0.029
341.61	24.883	24.875	0.008
352.27	25.093	25.118	-0.024
362.94	25.344	25.360	-0.017
373.62	25.555	25.604	-0.049
384.31	25.785	25.847	-0.061

T(0) = 17.100 DEG C

GRAD = 22.761 DEG/KM

STER = 0.1067 DEG/KM
95CL = 0.2233 DEG/KM

REST = 135.8 CMSECDEG/CAL

STER = 1.1 CMSECDEG/CAL
95CL = 2.3 CMSECDEG/CAL

FLUX = 1.676 MICROCAL/SQCMSEC

STER = 0.016 MICROCAL/SQCMSEC
95CL = 0.033 MICROCAL/SQCMSEC

TOPOGRAPHIC CORRECTION, 4MY CASE ANZA AN-1

UPLIFT = 1.7 KM EROSION = 0.5 KM

CORDEP	CORTEM	SMOOTH	RES
167.08	21.073	21.106	-0.033
177.19	21.328	21.349	-0.021
187.31	21.572	21.592	-0.020
197.44	21.816	21.835	-0.019
207.58	22.071	22.078	-0.008
217.73	22.315	22.322	-0.007
227.89	22.560	22.566	-0.006
238.06	22.824	22.810	0.015
248.24	23.059	23.054	0.005
258.44	23.314	23.299	0.015
268.65	23.589	23.544	0.044
278.87	23.843	23.789	0.054
289.10	24.068	24.035	0.033
299.35	24.313	24.281	0.032
309.61	24.558	24.527	0.031
319.89	24.803	24.774	0.029
330.17	25.028	25.021	0.008
340.47	25.244	25.268	-0.024
350.78	25.499	25.516	-0.017
361.11	25.714	25.763	-0.049
371.44	25.950	26.011	-0.062

T(0) = 17.096 DEG C

GRAD = 24.003 DEG/KM

STER = 0.1113 DEG/KM
95CL = 0.2329 DEG/KM

REST = 135.8 CMSECDEG/CAL

STER = 1.1 CMSECDEG/CAL
95CL = 2.3 CMSECDEG/CAL

FLUX = 1.767 MICROCAL/SQCMSEC

STER = 0.016 MICROCAL/SQCMSEC
95CL = 0.034 MICROCAL/SQCMSEC

TOPOGRAPHIC CORRECTION, 9MY CASE ANZA AN-1

UPLIFT = 1.7 KM EROSION = 0.5 KM

CORDEP	CORTEM	SMOOTH	RES
165.10	21.097	21.130	-0.033
175.10	21.353	21.375	-0.022
185.09	21.599	21.619	-0.020
195.10	21.845	21.864	-0.019
205.11	22.101	22.108	-0.008
215.14	22.347	22.353	-0.007
225.18	22.593	22.599	-0.006
235.22	22.859	22.844	0.015
245.28	23.095	23.090	0.005
255.36	23.351	23.337	0.015
265.44	23.628	23.583	0.045
275.54	23.884	23.830	0.054
285.65	24.110	24.077	0.033
295.78	24.357	24.325	0.032
305.92	24.603	24.572	0.031
316.07	24.850	24.821	0.029
326.23	25.076	25.069	0.008
336.41	25.293	25.318	-0.025
346.59	25.550	25.567	-0.017
356.79	25.767	25.816	-0.049
367.00	26.004	26.066	-0.062

T(0) = 17.094 DEG C

GRAD = 24.444 DEG/KM

STER = 0.1129 DEG/KM
95CL = 0.2363 DEG/KM

REST = 135.8 CMSECDEG/CAL

STER = 1.1 CMSECDEG/CAL
95CL = 2.3 CMSECDEG/CAL

FLUX = 1.800 MICROCAL/SQCMSEC

STER = 0.017 MICROCAL/SQCMSEC
95CL = 0.035 MICROCAL/SQCMSEC

TOPOGRAPHIC CORRECTION, 16MY CASE ANZA AN-1

UPLIFT = 1.7 KM EROSION = 0.5 KM

CORDEP	CORTEM	SMOOTH	RES
162.48	21.127	21.160	-0.033
172.31	21.384	21.406	-0.022
182.15	21.632	21.652	-0.020
191.99	21.880	21.898	-0.019
201.84	22.137	22.145	-0.008
211.70	22.385	22.392	-0.007
221.57	22.633	22.639	-0.006
231.46	22.901	22.886	0.015
241.35	23.139	23.134	0.005
251.26	23.397	23.382	0.015
261.18	23.675	23.631	0.045
271.12	23.933	23.879	0.054
281.07	24.162	24.128	0.033
291.03	24.410	24.378	0.032
301.00	24.658	24.627	0.031
310.99	24.907	24.877	0.029
320.99	25.135	25.128	0.008
331.00	25.354	25.378	-0.025
341.02	25.612	25.629	-0.017
351.06	25.831	25.880	-0.050
361.11	26.069	26.132	-0.062

T(0) = 17.093 DEG C

GRAD = 25.032 DEG/KM

STER = 0.1152 DEG/KM
95CL = 0.2411 DEG/KM

REST = 135.8 CMSECDEG/CAL

STER = 1.1 CMSECDEG/CAL
95CL = 2.3 CMSECDEG/CAL

FLUX = 1.843 MICROCAL/SQCMSEC

STER = 0.017 MICROCAL/SQCMSEC
95CL = 0.036 MICROCAL/SQCMSEC

TOPOGRAPHIC CORRECTION, 1MY CASE ANZA AN-1

UPLIFT = 2.2 KM EROSION = 1.0 KM

CORDEP	CORTEM	SMOOTH	RES
185.69	21.000	21.032	-0.032
196.97	21.250	21.271	-0.021
208.26	21.490	21.509	-0.019
219.55	21.730	21.748	-0.018
230.85	21.980	21.987	-0.008
242.16	22.220	22.226	-0.007
253.48	22.460	22.466	-0.006
264.82	22.720	22.706	0.014
276.17	22.950	22.946	0.004
287.53	23.200	23.186	0.014
298.90	23.470	23.426	0.044
310.28	23.720	23.667	0.053
321.68	23.941	23.908	0.033
333.09	24.181	24.149	0.032
344.52	24.422	24.391	0.030
355.95	24.662	24.633	0.029
367.40	24.883	24.875	0.008
378.87	25.093	25.118	-0.024
390.34	25.344	25.360	-0.016
401.83	25.555	25.603	-0.048
413.32	25.785	25.846	-0.061

T(0) = 17.105 DEG C

GRAD = 21.149 DEG/KM

STER = 0.0982 DEG/KM
95CL = 0.2055 DEG/KM

REST = 135.8 CMSECDEG/CAL

STER = 1.1 CMSECDEG/CAL
95CL = 2.3 CMSECDEG/CAL

FLUX = 1.557 MICROCAL/SQCMSEC

STER = 0.015 MICROCAL/SQCMSEC
95CL = 0.030 MICROCAL/SQCMSEC

TOPOGRAPHIC CORRECTION, 4MY CASE ANZA AN-1

UPLIFT = 2.2 KM EROSION = 1.0 KM

CORDEP	CORTEM	SMOOTH	RES
173.52	21.073	21.106	-0.033
184.04	21.328	21.349	-0.021
194.57	21.572	21.592	-0.020
205.10	21.816	21.835	-0.019
215.64	22.071	22.078	-0.008
226.19	22.315	22.322	-0.007
236.75	22.560	22.566	-0.006
247.33	22.824	22.810	0.014
257.91	23.059	23.055	0.005
268.51	23.314	23.299	0.015
279.13	23.589	23.544	0.044
289.75	23.843	23.790	0.054
300.39	24.068	24.035	0.033
311.04	24.313	24.281	0.032
321.70	24.558	24.528	0.031
332.38	24.803	24.774	0.029
343.07	25.028	25.021	0.008
353.77	25.244	25.268	-0.024
364.49	25.499	25.515	-0.017
375.21	25.714	25.763	-0.049
385.95	25.950	26.011	-0.062

T(0) = 17.099 DEG C

GRAD = 23.092 DEG/KM

STER = 0.1065 DEG/KM
95CL = 0.2228 DEG/KM

REST = 135.8 CMSECDEG/CAL

STER = 1.1 CMSECDEG/CAL
95CL = 2.3 CMSECDEG/CAL

FLUX = 1.700 MICROCAL/SQCMSEC

STER = 0.016 MICROCAL/SQCMSEC
95CL = 0.033 MICROCAL/SQCMSEC

TOPOGRAPHIC CORRECTION, 9MY CASE ANZA AN-1

UPLIFT = 2.2 KM EROSION = 1.0 KM

CORDEP	CORTEM	SMOOTH	RES
169.40	21.097	21.130	-0.033
179.66	21.353	21.374	-0.021
189.93	21.599	21.619	-0.020
200.20	21.845	21.863	-0.019
210.49	22.101	22.108	-0.008
220.78	22.347	22.353	-0.007
231.09	22.593	22.599	-0.006
241.40	22.859	22.844	0.015
251.73	23.095	23.090	0.005
262.07	23.351	23.337	0.015
272.43	23.628	23.583	0.044
282.80	23.884	23.830	0.054
293.18	24.110	24.077	0.033
303.57	24.357	24.325	0.032
313.98	24.603	24.572	0.031
324.40	24.850	24.821	0.029
334.83	25.076	25.069	0.008
345.27	25.293	25.318	-0.024
355.73	25.550	25.567	-0.017
366.20	25.767	25.816	-0.049
376.68	26.004	26.065	-0.062

T(0) = 17.096 DEG C

GRAD = 23.811 DEG/KM

STER = 0.1096 DEG/KM
95CL = 0.2293 DEG/KM

REST = 135.8 CMSECDEG/CAL

STER = 1.1 CMSECDEG/CAL
95CL = 2.3 CMSECDEG/CAL

FLUX = 1.753 MICROCAL/SQCMSEC

STER = 0.016 MICROCAL/SQCMSEC
95CL = 0.034 MICROCAL/SQCMSEC

TOPOGRAPHIC CORRECTION, 16MY CASE ANZA AN-1

UPLIFT = 2.2 KM EROSION = 1.0 KM

CORDEP	CORTEM	SMOOTH	RES
164.10	21.127	21.160	-0.033
174.02	21.384	21.406	-0.022
183.96	21.632	21.652	-0.020
193.90	21.880	21.898	-0.019
203.85	22.137	22.145	-0.008
213.82	22.385	22.392	-0.007
223.79	22.633	22.639	-0.006
233.77	22.901	22.886	0.015
243.77	23.139	23.134	0.005
253.78	23.397	23.382	0.015
263.80	23.675	23.631	0.045
273.84	23.933	23.879	0.054
283.89	24.162	24.128	0.033
293.95	24.410	24.378	0.032
304.03	24.658	24.627	0.031
314.11	24.907	24.877	0.029
324.21	25.135	25.128	0.008
334.33	25.354	25.378	-0.025
344.45	25.612	25.629	-0.017
354.59	25.831	25.880	-0.049
364.73	26.069	26.132	-0.062

T(0) = 17.093 DEG C

GRAD = 24.781 DEG/KM

STER = 0.1138 DEG/KM
95CL = 0.2383 DEG/KM

REST = 135.8 CMSECDEG/CAL

STER = 1.1 CMSECDEG/CAL
95CL = 2.3 CMSECDEG/CAL

FLUX = 1.825 MICROCAL/SQCMSEC

STER = 0.017 MICROCAL/SQCMSEC
95CL = 0.036 MICROCAL/SQCMSEC

TOPOGRAPHIC DATA, ANZA AN-2

RADII	ELDIFF
100.0	1.0
200.0	2.0
300.0	-1.0
400.0	-6.0
500.0	-12.0
700.0	-22.0
900.0	-24.0
1200.0	-22.0
1500.0	-20.0
2000.0	-15.0
2500.0	-4.0
3000.0	6.0
4000.0	19.0
5000.0	0.
7000.0	9.0
10000.0	12.0
15000.0	42.0
20000.0	-52.0
30000.0	31.0
40000.0	-0.
50000.0	-0.
70000.0	-0.
100000.0	-0.

UNCORRECTED DATA, ANZA AN-2

DEPTH	TEMP	SMOOTH	RES
100.00	18.750	18.761	-0.011
110.00	18.970	18.988	-0.018
120.00	19.190	19.214	-0.024
130.00	19.410	19.440	-0.030
140.00	19.630	19.667	-0.037
150.00	19.880	19.893	-0.013
160.00	20.130	20.119	0.011
170.00	20.370	20.346	0.024
180.00	20.590	20.572	0.018
190.00	20.820	20.798	0.022
200.00	21.050	21.025	0.025
210.00	21.280	21.251	0.029
220.00	21.520	21.477	0.043
230.00	21.740	21.704	0.036
240.00	21.960	21.930	0.030
250.00	22.180	22.156	0.024
260.00	22.390	22.383	0.007
270.00	22.600	22.609	-0.009
280.00	22.850	22.835	0.015
290.00	23.010	23.062	-0.052
300.00	23.200	23.288	-0.088

T(0) = 16.498 DEG C

GRAD = 22.634 DEG/KM

STER = 0.1221 DEG/KM
95CL = 0.2555 DEG/KM

REST = 151.7 CMSECDEG/CAL

STER = 1.6 CMSECDEG/CAL
95CL = 3.1 CMSECDEG/CAL

FLUX = 1.492 MICROCAL/SQCMSEC

STER = 0.018 MICROCAL/SQCMSEC
95CL = 0.035 MICROCAL/SQCMSEC

TOPOGRAPHIC CORRECTION, SS CASE, ANZA AN-2

CORDEP	CORTEM	SMOOTH	RES
103.08	18.764	18.768	-0.004
113.46	18.986	18.998	-0.012
123.83	19.207	19.228	-0.021
134.18	19.429	19.458	-0.029
144.53	19.650	19.687	-0.037
154.86	19.902	19.916	-0.014
165.17	20.153	20.145	0.008
175.48	20.395	20.374	0.021
185.77	20.616	20.602	0.014
196.04	20.847	20.830	0.017
206.30	21.078	21.057	0.021
216.55	21.309	21.285	0.025
226.78	21.551	21.512	0.039
237.00	21.772	21.738	0.033
247.21	21.992	21.965	0.028
257.40	22.213	22.191	0.022
267.58	22.424	22.417	0.007
277.75	22.635	22.643	-0.008
287.91	22.886	22.868	0.018
298.06	23.046	23.093	-0.047
308.20	23.237	23.318	-0.081

T(0) = 16.481 DEG C

GRAD = 22.184 DEG/KM

STER = 0.1083 DEG/KM
95CL = 0.2267 DEG/KM

REST = 151.7 CMSECDEG/CAL

STER = 1.6 CMSECDEG/CAL
95CL = 3.1 CMSECDEG/CAL

FLUX = 1.462 MICROCAL/SQCMSEC

STER = 0.017 MICROCAL/SQCMSEC
95CL = 0.033 MICROCAL/SQCMSEC

TOPOGRAPHIC CORRECTION, 1MY CASE ANZA AN-2

UPLIFT = 1.3 KM EROSION = 0.1 KM

CORDEP	CORTEM	SMOOTH	RES
104.79	18.677	18.682	-0.004
115.34	18.890	18.903	-0.013
125.88	19.103	19.124	-0.021
136.41	19.316	19.345	-0.029
146.92	19.529	19.566	-0.037
157.42	19.772	19.786	-0.014
167.91	20.015	20.006	0.008
178.38	20.247	20.226	0.021
188.84	20.460	20.446	0.014
199.29	20.683	20.665	0.018
209.72	20.905	20.884	0.021
220.14	21.128	21.103	0.025
230.54	21.360	21.321	0.039
240.93	21.572	21.539	0.033
251.31	21.785	21.757	0.028
261.68	21.997	21.974	0.022
272.03	22.199	22.192	0.007
282.37	22.401	22.409	-0.008
292.71	22.643	22.626	0.017
303.03	22.795	22.842	-0.047
313.33	22.977	23.059	-0.082

T(0) = 16.482 DEG C

GRAD = 20.989 DEG/KM

STER = 0.1073 DEG/KM
95CL = 0.2245 DEG/KM

REST = 151.7 CMSECDEG/CAL

STER = 1.6 CMSECDEG/CAL
95CL = 3.1 CMSECDEG/CAL

FLUX = 1.384 MICROCAL/SQCMSEC

STER = 0.016 MICROCAL/SQCMSEC
95CL = 0.032 MICROCAL/SQCMSEC

TOPOGRAPHIC CORRECTION, 4MY CASE ANZA AN-2

UPLIFT = 1.3 KM EROSION = 0.1 KM

CORDEP	CORTEM	SMOOTH	RES
103.94	18.721	18.725	-0.004
114.40	18.938	18.950	-0.013
124.86	19.155	19.176	-0.021
135.30	19.373	19.401	-0.029
145.73	19.590	19.627	-0.037
156.14	19.837	19.851	-0.014
166.54	20.084	20.076	0.008
176.93	20.321	20.300	0.021
187.31	20.538	20.524	0.014
197.67	20.765	20.747	0.017
208.01	20.992	20.971	0.021
218.34	21.219	21.194	0.025
228.66	21.455	21.416	0.039
238.97	21.672	21.639	0.033
249.26	21.889	21.861	0.028
259.54	22.105	22.083	0.022
269.81	22.312	22.304	0.007
280.07	22.518	22.526	-0.008
290.31	22.764	22.747	0.018
300.54	22.921	22.968	-0.047
310.77	23.107	23.188	-0.081

T(0) = 16.482 DEG C

GRAD = 21.581 DEG/KM

STER = 0.1078 DEG/KM
95CL = 0.2256 DEG/KM

REST = 151.7 CMSECDEG/CAL

STER = 1.6 CMSECDEG/CAL
95CL = 3.1 CMSECDEG/CAL

FLUX = 1.423 MICROCAL/SQCMSEC

STER = 0.017 MICROCAL/SQCMSEC
95CL = 0.033 MICROCAL/SQCMSEC

TOPOGRAPHIC CORRECTION, 9MY CASE ANZA AN-2

UPLIFT = 1.3 KM EROSION = 0.1 KM

CORDEP	CORTEM	SMOOTH	RES
103.65	18.735	18.739	-0.004
114.08	18.954	18.966	-0.012
124.51	19.173	19.193	-0.021
134.92	19.391	19.420	-0.029
145.32	19.610	19.647	-0.037
155.71	19.859	19.873	-0.014
166.08	20.107	20.099	0.008
176.44	20.346	20.324	0.021
186.78	20.564	20.550	0.014
197.11	20.792	20.775	0.017
207.43	21.021	21.000	0.021
217.73	21.249	21.224	0.025
228.02	21.487	21.448	0.039
238.30	21.705	21.672	0.033
248.56	21.923	21.896	0.028
258.81	22.141	22.119	0.022
269.05	22.349	22.342	0.007
279.28	22.557	22.565	-0.008
289.50	22.805	22.787	0.018
299.70	22.962	23.009	-0.047
309.89	23.150	23.231	-0.081

T(0) = 16.481 DEG C

GRAD = 21.782 DEG/KM

STER = 0.1080 DEG/KM
95CL = 0.2260 DEG/KM

REST = 151.7 CMSECDEG/CAL

STER = 1.6 CMSECDEG/CAL
95CL = 3.1 CMSECDEG/CAL

FLUX = 1.436 MICROCAL/SQCMSEC

STER = 0.017 MICROCAL/SQCMSEC
95CL = 0.033 MICROCAL/SQCMSEC

TOPOGRAPHIC CORRECTION, 16MY CASE ANZA AN-2

UPLIFT = 1.3 KM EROSION = 0.1 KM

CORDEP	CORTEM	SMOOTH	RES
103.30	18.753	18.757	-0.004
113.70	18.974	18.986	-0.012
124.09	19.194	19.215	-0.021
134.47	19.415	19.444	-0.029
144.83	19.635	19.672	-0.037
155.18	19.886	19.900	-0.014
165.52	20.136	20.128	0.008
175.85	20.376	20.355	0.021
186.16	20.596	20.582	0.014
196.45	20.827	20.809	0.017
206.74	21.057	21.036	0.021
217.00	21.287	21.262	0.025
227.26	21.527	21.488	0.039
237.50	21.747	21.714	0.033
247.73	21.966	21.939	0.028
257.95	22.186	22.164	0.022
268.15	22.396	22.389	0.007
278.34	22.606	22.613	-0.008
288.52	22.855	22.838	0.018
298.69	23.015	23.062	-0.047
308.85	23.204	23.286	-0.081

T(0) = 16.481 DEG C

GRAD = 22.031 DEG/KM

STER = 0.1082 DEG/KM
95CL = 0.2264 DEG/KM

REST = 151.7 CMSECDEG/CAL

STER = 1.6 CMSECDEG/CAL
95CL = 3.1 CMSECDEG/CAL

FLUX = 1.452 MICROCAL/SQCMSEC

STER = 0.017 MICROCAL/SQCMSEC
95CL = 0.033 MICROCAL/SQCMSEC

TOPOGRAPHIC DATA, ANZA AN-3

RADII	ELDIFF
100.0	3.0
200.0	-0.6
300.0	-2.0
400.0	-4.0
500.0	-9.0
700.0	-4.0
900.0	11.0
1200.0	39.0
1500.0	60.0
2000.0	84.0
2500.0	99.0
3000.0	113.0
4000.0	130.0
5000.0	159.0
7000.0	152.0
10000.0	116.0
15000.0	66.0
20000.0	170.0
30000.0	431.0
40000.0	-0.
50000.0	-0.
70000.0	-0.
100000.0	-0.

UNCORRECTED DATA, ANZA AN-3

DEPTH	TEMP	SMOOTH	RES
110.00	16.940	16.956	-0.016
120.00	17.190	17.195	-0.005
130.00	17.440	17.435	0.005
140.00	17.680	17.674	0.006
150.00	17.920	17.913	0.007
160.00	18.160	18.153	0.007
170.00	18.400	18.392	0.008
180.00	18.640	18.631	0.009
190.00	18.870	18.871	-0.001
200.00	19.100	19.110	-0.010
210.00	19.340	19.350	-0.010

T(0) = 14.323 DEG C

GRAD = 23.936 DEG/KM

STER = 0.0884 DEG/KM
95CL = 0.2000 DEG/KM

REST = 146.6 CMSECDEG/CAL

STER = 2.4 CMSECDEG/CAL
95CL = 4.9 CMSECDEG/CAL

FLUX = 1.633 MICROCAL/SQCMSEC

STER = 0.027 MICROCAL/SQCMSEC
95CL = 0.056 MICROCAL/SQCMSEC

TOPOGRAPHIC CORRECTION, SS CASE, ANZA AN-3

CORDEP	CORTEM	SMOOTH	RES
99.67	16.894	16.908	-0.014
108.85	17.140	17.145	-0.005
118.02	17.386	17.381	0.005
127.16	17.622	17.617	0.005
136.30	17.858	17.853	0.006
145.43	18.094	18.088	0.006
154.55	18.330	18.323	0.007
163.66	18.566	18.558	0.008
172.77	18.792	18.793	-0.001
181.88	19.018	19.028	-0.010
190.98	19.254	19.263	-0.008

T(0) = 14.337 DEG C

GRAD = 25.793 DEG/KM

STER = 0.0880 DEG/KM
95CL = 0.1990 DEG/KM

REST = 146.6 CMSECDEG/CAL

STER = 2.4 CMSECDEG/CAL
95CL = 4.9 CMSECDEG/CAL

FLUX = 1.759 MICROCAL/SQCMSEC

STER = 0.029 MICROCAL/SQCMSEC
95CL = 0.060 MICROCAL/SQCMSEC

TOPOGRAPHIC CORRECTION, 1MY CASE ANZA AN-3

UPLIFT = 1.3 KM EROSION = 0.1 KM

CORDEP	CORTEM	SMOOTH	RES
103.59	16.807	16.822	-0.014
113.12	17.046	17.051	-0.005
122.64	17.284	17.279	0.005
132.15	17.513	17.507	0.005
141.64	17.741	17.735	0.006
151.12	17.969	17.963	0.006
160.60	18.197	18.190	0.007
170.07	18.426	18.417	0.008
179.53	18.644	18.644	-0.001
188.99	18.862	18.872	-0.010
198.44	19.090	19.098	-0.008

T(0) = 14.336 DEG C

GRAD = 24.001 DEG/KM

STER = 0.0853 DEG/KM
95CL = 0.1930 DEG/KM

REST = 146.6 CMSECDEG/CAL

STER = 2.4 CMSECDEG/CAL
95CL = 4.9 CMSECDEG/CAL

FLUX = 1.637 MICROCAL/SQCMSEC

STER = 0.027 MICROCAL/SQCMSEC
95CL = 0.056 MICROCAL/SQCMSEC

TOPOGRAPHIC CORRECTION, 4MY CASE ANZA AN-3

UPLIFT = 1.3 KM EROSION = 0.1 KM

CORDEP	CORTEM	SMOOTH	RES
101.56	16.850	16.865	-0.014
110.92	17.093	17.097	-0.005
120.25	17.335	17.330	0.005
129.57	17.567	17.562	0.005
138.88	17.799	17.793	0.006
148.18	18.031	18.025	0.006
157.47	18.263	18.256	0.007
166.76	18.496	18.487	0.008
176.04	18.718	18.718	-0.001
185.31	18.940	18.949	-0.010
194.59	19.172	19.180	-0.008

T(0) = 14.336 DEG C

GRAD = 24.892 DEG/KM

STER = 0.0867 DEG/KM
95CL = 0.1961 DEG/KM

REST = 146.6 CMSECDEG/CAL

STER = 2.4 CMSECDEG/CAL
95CL = 4.9 CMSECDEG/CAL

FLUX = 1.698 MICROCAL/SQCMSEC

STER = 0.028 MICROCAL/SQCMSEC
95CL = 0.058 MICROCAL/SQCMSEC

TOPOGRAPHIC CORRECTION, 9MY CASE ANZA AN-3

UPLIFT = 1.3 KM EROSION = 0.1 KM

CORDEP	CORTEM	SMOOTH	RES
100.81	16.864	16.878	-0.014
110.09	17.108	17.112	-0.005
119.36	17.351	17.346	0.005
128.61	17.585	17.579	0.005
137.85	17.818	17.812	0.006
147.08	18.052	18.045	0.006
156.30	18.285	18.278	0.007
165.52	18.518	18.510	0.008
174.73	18.742	18.742	-0.001
183.94	18.965	18.974	-0.010
193.14	19.198	19.207	-0.008

T(0) = 14.337 DEG C

GRAD = 25.214 DEG/KM

STER = 0.0872 DEG/KM
95CL = 0.1973 DEG/KM

REST = 146.6 CMSECDEG/CAL

STER = 2.4 CMSECDEG/CAL
95CL = 4.9 CMSECDEG/CAL

FLUX = 1.720 MICROCAL/SQCMSEC

STER = 0.029 MICROCAL/SQCMSEC
95CL = 0.059 MICROCAL/SQCMSEC

TOPOGRAPHIC CORRECTION, 16MY CASE ANZA AN-3

UPLIFT = 1.3 KM EROSION = 0.1 KM

CORDEP	CORTEM	SMOOTH	RES
100.23	16.883	16.897	-0.014
109.46	17.128	17.133	-0.005
118.67	17.374	17.369	0.005
127.87	17.609	17.604	0.005
137.06	17.844	17.838	0.006
146.24	18.079	18.073	0.006
155.41	18.314	18.307	0.007
164.57	18.549	18.541	0.008
173.73	18.774	18.775	-0.001
182.89	18.999	19.009	-0.010
192.04	19.234	19.243	-0.008

T(0) = 14.337 DEG C

GRAD = 25.547 DEG/KM

STER = 0.0876 DEG/KM
95CL = 0.1982 DEG/KM

REST = 146.6 CMSECDEG/CAL

STER = 2.4 CMSECDEG/CAL
95CL = 4.9 CMSECDEG/CAL

FLUX = 1.743 MICROCAL/SQCMSEC

STER = 0.029 MICROCAL/SQCMSEC
95CL = 0.060 MICROCAL/SQCMSEC

TOPOGRAPHIC DATA, SAN BERNARDINO SB-2

RADII	ELDIFF
100.0	-3.1
200.0	-14.6
300.0	-26.0
400.0	-41.0
500.0	-55.0
700.0	-77.0
900.0	-88.0
1200.0	-86.0
1500.0	-54.0
2000.0	-8.0
2500.0	61.0
3000.0	122.0
4000.0	186.0
5000.0	251.0
7000.0	321.0
10000.0	394.0
15000.0	440.0
20000.0	412.0
30000.0	338.0
40000.0	-0.
50000.0	-0.
70000.0	-0.
100000.0	-0.

UNCORRECTED DATA, SAN BERNARDINO SB-2

DEPTH	TEMP	SMOOTH	RES
430.00	21.717	21.705	0.012
432.03	21.754	21.755	-0.001
434.06	21.792	21.805	-0.013
436.09	21.857	21.855	0.002
438.12	21.910	21.904	0.006
440.00	21.950	21.951	-0.001
442.03	21.994	22.000	-0.006
444.06	22.052	22.050	0.002
446.09	22.100	22.100	-0.000
448.12	22.150	22.150	0.000
450.00	22.193	22.196	-0.003
452.03	22.244	22.246	-0.002
454.06	22.294	22.296	-0.002
456.09	22.341	22.346	-0.005
458.12	22.396	22.395	0.001
460.00	22.447	22.442	0.005
462.03	22.496	22.492	0.004

T(0) = 11.147 DEG C

GRAD = 24.555 DEG/KM

STER = 0.1393 DEG/KM
95CL = 0.2968 DEG/KM

REST = 164.3 CMSECDEG/CAL

STER = 4.0 CMSECDEG/CAL
95CL = 8.0 CMSECDEG/CAL

FLUX = 1.495 MICROCAL/SQCMSEC

STER = 0.037 MICROCAL/SQCMSEC
95CL = 0.075 MICROCAL/SQCMSEC

TOPOGRAPHIC CORRECTION, SS CASE, SAN BERNARDINO SB-2

CORDEP	CORTEM	SMOOTH	RES
426.88	21.703	21.691	0.012
428.70	21.739	21.740	-0.001
430.53	21.776	21.789	-0.013
432.35	21.840	21.838	0.002
434.18	21.892	21.887	0.006
435.86	21.931	21.932	-0.001
437.69	21.974	21.981	-0.007
439.51	22.032	22.030	0.002
441.33	22.079	22.079	-0.000
443.15	22.128	22.128	-0.000
444.84	22.170	22.173	-0.003
446.66	22.220	22.222	-0.002
448.48	22.269	22.271	-0.002
450.30	22.315	22.320	-0.005
452.12	22.369	22.368	0.001
453.80	22.419	22.414	0.005
455.62	22.467	22.462	0.005

T(0) = 10.230 DEG C

GRAD = 26.849 DEG/KM

STER = 0.1566 DEG/KM
95CL = 0.3338 DEG/KM

REST = 164.3 CMSECDEG/CAL

STER = 4.0 CMSECDEG/CAL
95CL = 8.0 CMSECDEG/CAL

FLUX = 1.634 MICROCAL/SQCMSEC

STER = 0.041 MICROCAL/SQCMSEC
95CL = 0.082 MICROCAL/SQCMSEC

TOPOGRAPHIC CORRECTION, 1MY CASE SAN BERNARDINO SB-2

UPLIFT = 1.7 KM EROSION = 0.1 KM

CORDEP	CORTEM	SMOOTH	RES
449.73	21.276	21.263	0.012
451.67	21.310	21.310	-0.001
453.60	21.345	21.357	-0.013
455.53	21.407	21.404	0.002
457.46	21.457	21.451	0.006
459.25	21.494	21.495	-0.001
461.18	21.535	21.542	-0.007
463.11	21.590	21.589	0.002
465.04	21.635	21.635	-0.000
466.97	21.682	21.682	-0.000
468.76	21.722	21.726	-0.003
470.69	21.771	21.773	-0.002
472.61	21.818	21.819	-0.002
474.54	21.862	21.866	-0.005
476.47	21.914	21.913	0.001
478.25	21.962	21.956	0.005
480.18	22.008	22.003	0.005

T(0) = 10.334 DEG C

GRAD = 24.303 DEG/KM

STER = 0.1478 DEG/KM
95CL = 0.3149 DEG/KM

REST = 164.3 CMSECDEG/CAL

STER = 4.0 CMSECDEG/CAL
95CL = 8.0 CMSECDEG/CAL

FLUX = 1.479 MICROCAL/SQCMSEC

STER = 0.037 MICROCAL/SQCMSEC
95CL = 0.075 MICROCAL/SQCMSEC

TOPOGRAPHIC CORRECTION, 4MY CASE SAN BERNARDINO SB-2

UPLIFT = 1.7 KM EROSION = 0.1 KM

CORDEP	CORTEM	SMOOTH	RES
437.22	21.484	21.472	0.012
439.10	21.519	21.520	-0.001
440.97	21.555	21.568	-0.013
442.84	21.619	21.616	0.002
444.72	21.670	21.664	0.006
446.45	21.708	21.708	-0.001
448.32	21.750	21.756	-0.007
450.19	21.806	21.804	0.002
452.06	21.852	21.852	-0.000
453.93	21.900	21.900	-0.000
455.67	21.941	21.944	-0.003
457.53	21.990	21.992	-0.002
459.40	22.038	22.040	-0.002
461.27	22.083	22.088	-0.005
463.14	22.136	22.136	0.001
464.87	22.185	22.180	0.005
466.73	22.232	22.228	0.005

T(0) = 10.280 DEG C

GRAD = 25.598 DEG/KM

STER = 0.1525 DEG/KM
95CL = 0.3250 DEG/KM

REST = 164.3 CMSECDEG/CAL

STER = 4.0 CMSECDEG/CAL
95CL = 8.0 CMSECDEG/CAL

FLUX = 1.558 MICROCAL/SQCMSEC

STER = 0.039 MICROCAL/SQCMSEC
95CL = 0.078 MICROCAL/SQCMSEC

TOPOGRAPHIC CORRECTION, 9MY CASE SAN BERNARDINO SB-2

UPLIFT = 1.7 KM EROSION = 0.1 KM

CORDEP	CORTEM	SMOOTH	RES
432.78	21.553	21.541	0.012
434.63	21.588	21.589	-0.001
436.48	21.624	21.637	-0.013
438.33	21.688	21.685	0.002
440.19	21.739	21.734	0.006
441.90	21.778	21.778	-0.001
443.75	21.820	21.827	-0.007
445.60	21.876	21.875	0.002
447.45	21.923	21.923	-0.000
449.30	21.971	21.971	-0.000
451.01	22.013	22.016	-0.003
452.86	22.062	22.064	-0.002
454.71	22.110	22.112	-0.002
456.56	22.156	22.160	-0.005
458.40	22.209	22.208	0.001
460.11	22.258	22.253	0.005
461.96	22.306	22.301	0.005

T(0) = 10.262 DEG C

GRAD = 26.061 DEG/KM

STER = 0.1542 DEG/KM
95CL = 0.3287 DEG/KM

REST = 164.3 CMSECDEG/CAL

STER = 4.0 CMSECDEG/CAL
95CL = 8.0 CMSECDEG/CAL

FLUX = 1.586 MICROCAL/SQCMSEC

STER = 0.040 MICROCAL/SQCMSEC
95CL = 0.080 MICROCAL/SQCMSEC

TOPOGRAPHIC CORRECTION, 16MY CASE SAN BERNARDINO SB-2

UPLIFT = 1.7 KM EROSION = 0.1 KM

CORDEP	CORTEM	SMOOTH	RES
429.87	21.650	21.638	0.012
431.71	21.686	21.687	-0.001
433.55	21.723	21.735	-0.013
435.39	21.787	21.784	0.002
437.23	21.838	21.833	0.006
438.93	21.877	21.878	-0.001
440.77	21.920	21.927	-0.007
442.61	21.977	21.975	0.002
444.44	22.024	22.024	-0.000
446.28	22.073	22.073	-0.000
447.98	22.115	22.118	-0.003
449.81	22.164	22.166	-0.002
451.65	22.213	22.215	-0.002
453.48	22.259	22.264	-0.005
455.31	22.313	22.312	0.001
457.01	22.363	22.357	0.005
458.84	22.410	22.406	0.005

T(0) = 10.244 DEG C

GRAD = 26.506 DEG/KM

STER = 0.1554 DEG/KM
95CL = 0.3312 DEG/KM

REST = 164.3 CMSECDEG/CAL

STER = 4.0 CMSECDEG/CAL
95CL = 8.0 CMSECDEG/CAL

FLUX = 1.613 MICROCAL/SQCMSEC

STER = 0.040 MICROCAL/SQCMSEC
95CL = 0.081 MICROCAL/SQCMSEC

TOPOGRAPHIC DATA, SAN BERNARDINO S8-5

RADII	ELDIFF
100.0	2.0
200.0	1.0
300.0	1.0
400.0	22.0
500.0	30.0
700.0	30.0
900.0	28.0
1200.0	20.0
1500.0	0.
2000.0	-26.0
2500.0	-20.0
3000.0	-22.0
4000.0	-35.0
5000.0	-2.0
7000.0	90.0
10000.0	168.0
15000.0	285.0
20000.0	260.0
30000.0	180.0
40000.0	-0.
50000.0	-0.
70000.0	-0.
100000.0	-0.

UNCORRECTED DATA, SAN BERNARDINO SB-5

DEPTH	TEMP	SMOOTH	RES
200.00	13.560	13.548	0.012
210.00	13.710	13.725	-0.015
220.00	13.880	13.901	-0.021
230.00	14.100	14.078	0.022
240.00	14.270	14.255	0.015
250.00	14.420	14.431	-0.011
260.00	14.610	14.608	0.002
270.00	14.780	14.784	-0.004

T(0) = 10.017 DEG C

GRAD = 17.655 DEG/KM

STER = 0.2587 DEG/KM
95CL = 0.6331 DEG/KM

REST = 168.2 CMSECDEG/CAL

STER = 4.8 CMSECDEG/CAL
95CL = 10.2 CMSECDEG/CAL

FLUX = 1.050 MICROCAL/SQCMSEC

STER = 0.034 MICROCAL/SQCMSEC
95CL = 0.074 MICROCAL/SQCMSEC

TOPOGRAPHIC CORRECTION, SS CASE, SAN BERNARDINO SB-5

CORDEP	CORTEM	SMOOTH	RES
185.55	13.495	13.484	0.011
195.10	13.643	13.658	-0.015
204.67	13.811	13.832	-0.021
214.26	14.029	14.007	0.023
223.87	14.197	14.181	0.016
233.50	14.346	14.356	-0.011
243.15	14.534	14.532	0.002
252.81	14.703	14.708	-0.005

T(0) = 10.109 DEG C

GRAD = 18.190 DEG/KM

STER = 0.2703 DEG/KM
95CL = 0.6615 DEG/KM

REST = 168.2 CMSECDEG/CAL

STER = 4.8 CMSECDEG/CAL
95CL = 10.2 CMSECDEG/CAL

FLUX = 1.081 MICROCAL/SQCMSEC

STER = 0.035 MICROCAL/SQCMSEC
95CL = 0.076 MICROCAL/SQCMSEC

TOPOGRAPHIC DATA, SAN BERNARDINO SB-10

RADII	ELDIFF
100.0	-4.6
200.0	-12.0
300.0	-23.0
400.0	-31.0
500.0	-38.0
700.0	-36.0
900.0	-18.0
1200.0	3.7
1500.0	17.3
2000.0	38.0
2500.0	88.0
3000.0	171.0
4000.0	250.0
5000.0	325.0
7000.0	377.0
10000.0	451.0
15000.0	495.0
20000.0	470.0
30000.0	392.0
40000.0	-0.
50000.0	-0.
70000.0	-0.
100000.0	-0.

UNCORRECTED DATA, SAN BERNARDINO SB-10

DEPTH	TEMP	SMOOTH	RES
300.00	17.490	17.483	0.007
310.00	17.690	17.705	-0.015
320.00	17.930	17.927	0.003
330.00	18.140	18.149	-0.009
340.00	18.370	18.370	-0.000
350.00	18.590	18.592	-0.002
360.00	18.820	18.814	0.006
370.00	19.060	19.036	0.024
380.00	19.260	19.258	0.002
390.00	19.480	19.480	0.000
400.00	19.700	19.702	-0.002
410.00	19.920	19.923	-0.003
420.00	20.130	20.145	-0.015
430.00	20.360	20.367	-0.007
440.00	20.600	20.589	0.011

T(0) = 10.827 DEG C

GRAD = 22.186 DEG/KM

STER = 0.0619 DEG/KM
95CL = 0.1337 DEG/KM

REST = 160.0 CMSECDEG/CAL

STER = 2.5 CMSECDEG/CAL
95CL = 5.0 CMSECDEG/CAL

FLUX = 1.387 MICROCAL/SQCMSEC

STER = 0.022 MICROCAL/SQCMSEC
95CL = 0.044 MICROCAL/SQCMSEC

TOPOGRAPHIC CORRECTION, SS CASE, SAN BERNARDINO SB-10

CORDEP	CORTEM	SMOOTH	RES
275.50	17.380	17.372	0.008
284.06	17.573	17.588	-0.014
292.60	17.807	17.803	0.003
301.14	18.010	18.019	-0.009
309.68	18.234	18.234	-0.001
318.21	18.447	18.450	-0.003
326.74	18.670	18.665	0.005
335.27	18.904	18.880	0.024
343.79	19.097	19.095	0.002
352.32	19.310	19.310	0.000
360.84	19.524	19.525	-0.002
369.37	19.737	19.740	-0.003
377.89	19.941	19.956	-0.015
386.42	20.164	20.171	-0.007
394.95	20.397	20.386	0.011

T(0) = 10.420 DEG C

GRAD = 25.234 DEG/KM

STER = 0.0721 DEG/KM
95CL = 0.1558 DEG/KM

REST = 160.0 CMSECDEG/CAL

STER = 2.5 CMSECDEG/CAL
95CL = 5.0 CMSECDEG/CAL

FLUX = 1.577 MICROCAL/SQCMSEC

STER = 0.025 MICROCAL/SQCMSEC
95CL = 0.050 MICROCAL/SQCMSEC

TOPOGRAPHIC CORRECTION, 1MY CASE SAN BERNARDINO SB-10

UPLIFT = 1.7 KM EROSION = 0.1 KM

CORDEP	CORTEM	SMOOTH	RES
293.58	17.091	17.083	0.008
302.74	17.275	17.290	-0.014
311.88	17.499	17.496	0.003
321.02	17.693	17.701	-0.009
330.16	17.906	17.907	-0.001
339.29	18.110	18.113	-0.003
348.42	18.324	18.318	0.005
357.54	18.548	18.524	0.024
366.67	18.731	18.730	0.002
375.79	18.935	18.935	0.000
384.91	19.139	19.140	-0.002
394.03	19.343	19.346	-0.003
403.15	19.536	19.551	-0.015
412.28	19.750	19.757	-0.007
421.40	19.974	19.962	0.011

T(0) = 10.471 DEG C

GRAD = 22.524 DEG/KM

STER = 0.0674 DEG/KM
95CL = 0.1456 DEG/KM

REST = 160.0 CMSECDEG/CAL

STER = 2.5 CMSECDEG/CAL
95CL = 5.0 CMSECDEG/CAL

FLUX = 1.408 MICROCAL/SQCMSEC

STER = 0.022 MICROCAL/SQCMSEC
95CL = 0.045 MICROCAL/SQCMSEC

TOPOGRAPHIC CORRECTION, 4MY CASE SAN BERNARDINO SB-10

UPLIFT = 1.7 KM EROSION = 0.1 KM

CORDEP	CORTEM	SMOOTH	RES
283.51	17.231	17.223	0.008
292.33	17.419	17.434	-0.015
301.15	17.648	17.645	0.003
309.95	17.846	17.855	-0.009
318.76	18.065	18.066	-0.001
327.55	18.273	18.276	-0.003
336.35	18.492	18.486	0.005
345.14	18.720	18.696	0.024
353.93	18.908	18.906	0.002
362.72	19.117	19.117	0.000
371.51	19.325	19.327	-0.002
380.30	19.534	19.537	-0.003
389.09	19.732	19.747	-0.015
397.89	19.950	19.957	-0.007
406.68	20.179	20.167	0.011

T(0) = 10.445 DEG C

GRAD = 23.906 DEG/KM

STER = 0.0699 DEG/KM
95CL = 0.1511 DEG/KM

REST = 160.0 CMSECDEG/CAL

STER = 2.5 CMSECDEG/CAL
95CL = 5.0 CMSECDEG/CAL

FLUX = 1.494 MICROCAL/SQCMSEC

STER = 0.024 MICROCAL/SQCMSEC
95CL = 0.048 MICROCAL/SQCMSEC

TOPOGRAPHIC CORRECTION, 9MY CASE SAN BERNARDINO SB-10

UPLIFT = 1.7 KM EROSION = 0.1 KM

CORDEP	CORTEM	SMOOTH	RES
280.01	17.277	17.269	0.008
288.71	17.467	17.481	-0.015
297.41	17.697	17.694	0.003
306.10	17.897	17.906	-0.009
314.79	18.117	18.118	-0.001
323.47	18.327	18.329	-0.003
332.15	18.547	18.541	0.005
340.83	18.777	18.753	0.024
349.50	18.967	18.965	0.002
358.18	19.176	19.176	0.000
366.85	19.386	19.388	-0.002
375.52	19.596	19.600	-0.003
384.20	19.796	19.811	-0.015
392.88	20.016	20.023	-0.007
401.55	20.246	20.235	0.011

T(0) = 10.436 DEG C

GRAD = 24.402 DEG/KM

STER = 0.0709 DEG/KM
95CL = 0.1531 DEG/KM

REST = 160.0 CMSECDEG/CAL

STER = 2.5 CMSECDEG/CAL
95CL = 5.0 CMSECDEG/CAL

FLUX = 1.525 MICROCAL/SQCMSEC

STER = 0.024 MICROCAL/SQCMSEC
95CL = 0.049 MICROCAL/SQCMSEC

TOPOGRAPHIC CORRECTION, 16MY CASE SAN BERNARDINO SB-10

UPLIFT = 1.7 KM EROSION = 0.1 KM

CORDEP	CORTEM	SMOOTH	RES
277.82	17.344	17.336	0.008
286.45	17.536	17.551	-0.014
295.08	17.769	17.765	0.003
303.70	17.971	17.980	-0.009
312.31	18.193	18.194	-0.001
320.92	18.405	18.408	-0.003
329.53	18.627	18.622	0.005
338.13	18.860	18.836	0.024
346.73	19.052	19.050	0.002
355.33	19.264	19.264	0.000
363.93	19.476	19.478	-0.002
372.54	19.688	19.692	-0.003
381.14	19.890	19.905	-0.015
389.74	20.113	20.119	-0.007
398.35	20.345	20.333	0.011

T(0) = 10.427 DEG C

GRAD = 24.869 DEG/KM

STER = 0.0715 DEG/KM
95CL = 0.1544 DEG/KM

REST = 160.0 CMSECDEG/CAL

STER = 2.5 CMSECDEG/CAL
95CL = 5.0 CMSECDEG/CAL

FLUX = 1.554 MICROCAL/SQCMSEC

STER = 0.025 MICROCAL/SQCMSEC
95CL = 0.050 MICROCAL/SQCMSEC

TOPOGRAPHIC DATA, LUCERNE VALLEY LV-1

RADII	ELDIFF
100.0	-1.0
200.0	-2.0
300.0	-2.0
400.0	-3.0
500.0	-4.0
700.0	-5.0
900.0	-7.0
1200.0	-10.0
1500.0	-16.0
2000.0	-25.0
2500.0	-46.0
3000.0	-67.0
4000.0	-97.0
5000.0	-135.0
7000.0	-106.0
10000.0	-106.0
15000.0	-46.0
20000.0	57.0
30000.0	205.0
40000.0	-0.
50000.0	-0.
70000.0	-0.
100000.0	-0.

UNCORRECTED DATA, LUCERNE VALLEY LV-1

DEPTH	TEMP	SMOOTH	RES
600.00	37.170	37.173	-0.003
610.00	37.470	37.465	0.005
620.00	37.760	37.758	0.002
630.00	38.040	38.051	-0.011
640.00	38.340	38.344	-0.004
650.00	38.640	38.636	0.004
660.00	38.940	38.929	0.011
670.00	39.230	39.222	0.008
680.00	39.510	39.515	-0.005
690.00	39.800	39.807	-0.007
700.00	40.100	40.100	-0.000

T(0) = 19.609 DEG C

GRAD = 29.273 DEG/KM

STER = 0.0664 DEG/KM
95CL = 0.1502 DEG/KM

REST = 173.4 CMSECDEG/CAL

STER = 2.6 CMSECDEG/CAL
95CL = 5.4 CMSECDEG/CAL

FLUX = 1.688 MICROCAL/SQCMSEC

STER = 0.026 MICROCAL/SQCMSEC
95CL = 0.053 MICROCAL/SQCMSEC

TOPOGRAPHIC CORRECTION, SS CASE, LUCERNE VALLEY LV-1

CORDEP	CORTEM	SMOOTH	RES
624.42	37.280	37.282	-0.002
634.72	37.581	37.577	0.005
645.01	37.873	37.871	0.002
655.29	38.154	38.165	-0.011
665.58	38.455	38.459	-0.004
675.86	38.756	38.753	0.003
686.14	39.058	39.047	0.011
696.42	39.349	39.341	0.008
706.69	39.630	39.635	-0.005
716.97	39.921	39.928	-0.007
727.24	40.223	40.222	0.000

T(0) = 19.427 DEG C

GRAD = 28.595 DEG/KM

STER = 0.0640 DEG/KM
95CL = 0.1448 DEG/KM

REST = 173.4 CMSECDEG/CAL

STER = 2.6 CMSECDEG/CAL
95CL = 5.4 CMSECDEG/CAL

FLUX = 1.649 MICROCAL/SQCMSEC

STER = 0.025 MICROCAL/SQCMSEC
95CL = 0.052 MICROCAL/SQCMSEC

TOPOGRAPHIC CORRECTION, 1MY CASE LUCERNE VALLEY LV-1

UPLIFT = 0. KM EROSION = 1.0 KM

CORDEP	CORTEM	SMOOTH	RES
719.40	37.707	37.710	-0.002
731.28	38.016	38.011	0.005
743.16	38.314	38.312	0.002
755.03	38.603	38.614	-0.011
766.91	38.911	38.915	-0.004
778.78	39.219	39.216	0.003
790.64	39.528	39.517	0.011
802.51	39.826	39.818	0.008
814.37	40.115	40.119	-0.005
826.23	40.413	40.420	-0.007
838.09	40.721	40.721	0.000

T(0) = 19.457 DEG C

GRAD = 25.372 DEG/KM

STER = 0.0555 DEG/KM
95CL = 0.1256 DEG/KM

REST = 173.4 CMSECDEG/CAL

STER = 2.6 CMSECDEG/CAL
95CL = 5.4 CMSECDEG/CAL

FLUX = 1.463 MICROCAL/SQCMSEC

STER = 0.022 MICROCAL/SQCMSEC
95CL = 0.046 MICROCAL/SQCMSEC

TOPOGRAPHIC CORRECTION, 4MY CASE LUCERNE VALLEY LV-1

UPLIFT = 0. KM EROSION = 1.0 KM

CORDEP	CORTEM	SMOOTH	RES
673.04	37.499	37.501	-0.002
684.15	37.804	37.799	0.005
695.25	38.099	38.097	0.002
706.35	38.384	38.395	-0.011
717.44	38.688	38.692	-0.004
728.54	38.993	38.990	0.003
739.63	39.298	39.288	0.011
750.72	39.593	39.585	0.008
761.81	39.878	39.883	-0.005
772.89	40.173	40.180	-0.007
783.97	40.478	40.477	0.000

T(0) = 19.441 DEG C

GRAD = 26.833 DEG/KM

STER = 0.0594 DEG/KM
95CL = 0.1343 DEG/KM

REST = 173.4 CMSECDEG/CAL

STER = 2.6 CMSECDEG/CAL
95CL = 5.4 CMSECDEG/CAL

FLUX = 1.547 MICROCAL/SQCMSEC

STER = 0.023 MICROCAL/SQCMSEC
95CL = 0.049 MICROCAL/SQCMSEC

TOPOGRAPHIC CORRECTION, 9MY CASE LUCERNE VALLEY LV-1

UPLIFT = 0. KM EROSION = 1.0 KM

CORDEP	CORTEM	SMOOTH	RES
657.04	37.427	37.429	-0.002
667.88	37.730	37.726	0.005
678.71	38.024	38.022	0.002
689.54	38.308	38.319	-0.011
700.37	38.612	38.616	-0.004
711.20	38.915	38.912	0.003
722.02	39.219	39.208	0.011
732.84	39.513	39.505	0.008
743.66	39.796	39.801	-0.005
754.48	40.090	40.097	-0.007
765.29	40.394	40.393	0.000

T(0) = 19.436 DEG C

GRAD = 27.385 DEG/KM

STER = 0.0608 DEG/KM
95CL = 0.1376 DEG/KM

REST = 173.4 CMSECDEG/CAL

STER = 2.6 CMSECDEG/CAL
95CL = 5.4 CMSECDEG/CAL

FLUX = 1.579 MICROCAL/SQCMSEC

STER = 0.024 MICROCAL/SQCMSEC
95CL = 0.050 MICROCAL/SQCMSEC

TOPOGRAPHIC CORRECTION, 16MY CASE LUCERNE VALLEY LV-1

UPLIFT = 0. KM EROSION = 1.0 KM

CORDEP	CORTEM	SMOOTH	RES
636.84	37.336	37.338	-0.002
647.34	37.638	37.633	0.005
657.83	37.930	37.928	0.002
668.33	38.212	38.224	-0.011
678.82	38.515	38.519	-0.004
689.31	38.817	38.814	0.003
699.80	39.119	39.108	0.011
710.28	39.411	39.403	0.008
720.76	39.693	39.698	-0.005
731.24	39.986	39.993	-0.007
741.72	40.288	40.287	0.000

T(0) = 19.430 DEG C

GRAD = 28.120 DEG/KM

STER = 0.0628 DEG/KM
95CL = 0.1420 DEG/KM

REST = 173.4 CMSECDEG/CAL

STER = 2.6 CMSECDEG/CAL
95CL = 5.4 CMSECDEG/CAL

FLUX = 1.622 MICROCAL/SQCMSEC

STER = 0.025 MICROCAL/SQCMSEC
95CL = 0.051 MICROCAL/SQCMSEC

TOPOGRAPHIC CORRECTION, 1MY CASE LUCERNE VALLEY LV-1

UPLIFT = 0. KM EROSION = 2.0 KM

CORDEP	CORTEM	SMOOTH	RES
816.12	38.143	38.145	-0.002
829.61	38.458	38.454	0.005
843.10	38.764	38.762	0.002
856.59	39.060	39.071	-0.011
870.07	39.375	39.379	-0.004
883.55	39.691	39.688	0.003
897.03	40.007	39.996	0.011
910.51	40.312	40.304	0.008
923.99	40.608	40.613	-0.005
937.46	40.914	40.921	-0.007
950.93	41.229	41.229	0.000

T(0) = 19.475 DEG C

GRAD = 22.877 DEG/KM

STER = 0.0489 DEG/KM
95CL = 0.1107 DEG/KM

REST = 173.4 CMSECDEG/CAL

STER = 2.6 CMSECDEG/CAL
95CL = 5.4 CMSECDEG/CAL

FLUX = 1.319 MICROCAL/SQCMSEC

STER = 0.020 MICROCAL/SQCMSEC
95CL = 0.042 MICROCAL/SQCMSEC

TOPOGRAPHIC CORRECTION, 4MY CASE LUCERNE VALLEY LV-1

UPLIFT = 0. KM EROSION = 2.0 KM

CORDEP	CORTEM	SMOOTH	RES
721.40	37.716	37.719	-0.002
733.31	38.025	38.020	0.005
745.22	38.323	38.322	0.002
757.13	38.612	38.623	-0.011
769.03	38.921	38.924	-0.004
780.93	39.229	39.226	0.003
792.82	39.538	39.527	0.011
804.72	39.836	39.828	0.008
816.61	40.125	40.129	-0.005
828.50	40.423	40.430	-0.007
840.39	40.732	40.731	0.000

T(0) = 19.453 DEG C

GRAD = 25.320 DEG/KM

STER = 0.0554 DEG/KM
95CL = 0.1253 DEG/KM

REST = 173.4 CMSECDEG/CAL

STER = 2.6 CMSECDEG/CAL
95CL = 5.4 CMSECDEG/CAL

FLUX = 1.460 MICROCAL/SQCMSEC

STER = 0.022 MICROCAL/SQCMSEC
95CL = 0.046 MICROCAL/SQCMSEC

TOPOGRAPHIC CORRECTION, 9MY CASE LUCERNE VALLEY LV-1

UPLIFT = 0. KM EROSION = 2.0 KM

CORDEP	CORTEM	SMOOTH	RES
689.28	37.572	37.574	-0.002
700.65	37.878	37.873	0.005
712.03	38.174	38.172	0.002
723.39	38.460	38.471	-0.011
734.76	38.766	38.770	-0.004
746.12	39.073	39.069	0.003
757.48	39.379	39.368	0.011
768.84	39.675	39.667	0.008
780.20	39.961	39.965	-0.005
791.55	40.257	40.264	-0.007
802.91	40.563	40.563	0.000

T(0) = 19.444 DEG C

GRAD = 26.302 DEG/KM

STER = 0.0580 DEG/KM
95CL = 0.1311 DEG/KM

REST = 173.4 CMSECDEG/CAL

STER = 2.6 CMSECDEG/CAL
95CL = 5.4 CMSECDEG/CAL

FLUX = 1.517 MICROCAL/SQCMSEC

STER = 0.023 MICROCAL/SQCMSEC
95CL = 0.048 MICROCAL/SQCMSEC

TOPOGRAPHIC CORRECTION, 16MY CASE LUCERNE VALLEY LV-1

UPLIFT = 0. KM EROSION = 2.0 KM

CORDEP	CORTEM	SMOOTH	RES
648.93	37.390	37.392	-0.002
659.63	37.693	37.689	0.005
670.33	37.986	37.985	0.002
681.02	38.270	38.281	-0.011
691.71	38.573	38.577	-0.004
702.41	38.876	38.872	0.003
713.09	39.179	39.168	0.011
723.78	39.472	39.464	0.008
734.46	39.755	39.760	-0.005
745.15	40.048	40.055	-0.007
755.82	40.351	40.351	0.000

T(0) = 19.434 DEG C

GRAD = 27.675 DEG/KM

STER = 0.0616 DEG/KM
95CL = 0.1393 DEG/KM

REST = 173.4 CMSECDEG/CAL

STER = 2.6 CMSECDEG/CAL
95CL = 5.4 CMSECDEG/CAL

FLUX = 1.596 MICROCAL/SQCMSEC

STER = 0.024 MICROCAL/SQCMSEC
95CL = 0.050 MICROCAL/SQCMSEC

TOPOGRAPHIC DATA, LAKE HUGHES LH-1

RADII	ELDIFF
100.0	-1.0
200.0	-7.0
300.0	-16.0
400.0	-15.0
500.0	-12.0
700.0	-6.0
900.0	0.
1200.0	5.0
1500.0	5.0
2000.0	5.0
2500.0	9.0
3000.0	20.0
4000.0	22.0
5000.0	18.0
7000.0	-4.0
10000.0	-36.0
15000.0	-67.0
20000.0	-78.0
30000.0	-0.
40000.0	-0.
50000.0	-0.
70000.0	-0.
100000.0	-0.

UNCORRECTED DATA, LAKE HUGHES LH-1

DEPTH	TEMP	SMOOTH	RES
120.00	21.560	21.558	0.002
130.00	21.840	21.835	0.005
140.00	22.110	22.112	-0.002
150.00	22.370	22.389	-0.019
160.00	22.670	22.666	0.004
170.00	22.950	22.942	0.008
180.00	23.220	23.219	0.001
190.00	23.500	23.496	0.004
200.00	23.770	23.773	-0.003
210.00	24.050	24.050	-0.000

T(0) = 18.234 DEG C

GRAD = 27.697 DEG/KM

STER = 0.0855 DEG/KM
95CL = 0.1972 DEG/KM

REST = 161.0 CMSECDEG/CAL

STER = 1.3 CMSECDEG/CAL
95CL = 2.6 CMSECDEG/CAL

FLUX = 1.720 MICROCAL/SQCMSEC

STER = 0.015 MICROCAL/SQCMSEC
95CL = 0.030 MICROCAL/SQCMSEC

TOPOGRAPHIC CORRECTION, SS CASE, LAKE HUGHES LH-1

CORDEP	CORTEM	SMOOTH	RES
126.27	21.588	21.583	0.006
136.39	21.869	21.862	0.006
146.47	22.139	22.141	-0.002
156.52	22.399	22.420	-0.020
166.54	22.699	22.697	0.002
176.54	22.979	22.974	0.006
186.53	23.249	23.250	-0.001
196.49	23.529	23.526	0.003
206.44	23.799	23.801	-0.002
216.38	24.079	24.076	0.002

T(0) = 18.088 DEG C

GRAD = 27.675 DEG/KM

STER = 0.0909 DEG/KM
95CL = 0.2095 DEG/KM

REST = 161.0 CMSECDEG/CAL

STER = 1.3 CMSECDEG/CAL
95CL = 2.6 CMSECDEG/CAL

FLUX = 1.719 MICROCAL/SQCMSEC

STER = 0.015 MICROCAL/SQCMSEC
95CL = 0.031 MICROCAL/SQCMSEC

TOPOGRAPHIC CORRECTION, 1MY CASE LAKE HUGHES LH-1

UPLIFT = 0.3 KM EROSION = 0.3 KM

CORDEP	CORTEM	SMOOTH	RES
131.74	21.587	21.581	0.005
142.31	21.867	21.861	0.006
152.84	22.137	22.140	-0.002
163.35	22.397	22.418	-0.020
173.83	22.697	22.695	0.003
184.29	22.977	22.972	0.006
194.73	23.247	23.248	-0.001
205.15	23.527	23.524	0.003
215.56	23.796	23.799	-0.002
225.95	24.076	24.074	0.002

T(0) = 18.096 DEG C

GRAD = 26.458 DEG/KM

STER = 0.0865 DEG/KM
95CL = 0.1995 DEG/KM

REST = 161.0 CMSECDEG/CAL

STER = 1.3 CMSECDEG/CAL
95CL = 2.6 CMSECDEG/CAL

FLUX = 1.643 MICROCAL/SQCMSEC

STER = 0.014 MICROCAL/SQCMSEC
95CL = 0.029 MICROCAL/SQCMSEC

TOPOGRAPHIC CORRECTION, 4MY CASE LAKE HUGHES LH-1

UPLIFT = 0.3 KM EROSION = 0.3 KM

CORDEP	CORTEM	SMOOTH	RES
129.02	21.588	21.582	0.006
139.36	21.868	21.862	0.006
149.67	22.138	22.141	-0.002
159.95	22.398	22.419	-0.020
170.20	22.699	22.696	0.002
180.44	22.978	22.973	0.006
190.65	23.248	23.249	-0.001
200.84	23.528	23.525	0.003
211.02	23.798	23.800	-0.002
221.19	24.078	24.075	0.002

T(0) = 18.092 DEG C

GRAD = 27.050 DEG/KM

STER = 0.0886 DEG/KM
95CL = 0.2044 DEG/KM

REST = 161.0 CMSECDEG/CAL

STER = 1.3 CMSECDEG/CAL
95CL = 2.6 CMSECDEG/CAL

FLUX = 1.680 MICROCAL/SQCMSEC

STER = 0.015 MICROCAL/SQCMSEC
95CL = 0.030 MICROCAL/SQCMSEC

TOPOGRAPHIC CORRECTION, 9MY CASE LAKE HUGHES LH-1

UPLIFT = 0.3 KM EROSION = 0.3 KM

CORDEP	CORTEM	SMOOTH	RES
128.12	21.588	21.582	0.006
138.39	21.868	21.862	0.006
148.62	22.139	22.141	-0.002
158.83	22.399	22.419	-0.020
169.01	22.699	22.696	0.002
179.16	22.979	22.973	0.006
189.30	23.249	23.250	-0.001
199.42	23.529	23.525	0.003
209.53	23.798	23.801	-0.002
219.62	24.078	24.076	0.002

T(0) = 18.091 DEG C

GRAD = 27.252 DEG/KM

STER = 0.0893 DEG/KM
95CL = 0.2060 DEG/KM

REST = 161.0 CMSECDEG/CAL

STER = 1.3 CMSECDEG/CAL
95CL = 2.6 CMSECDEG/CAL

FLUX = 1.693 MICROCAL/SQCMSEC

STER = 0.015 MICROCAL/SQCMSEC
95CL = 0.030 MICROCAL/SQCMSEC

TOPOGRAPHIC CORRECTION, 16MY CASE LAKE HUGHES LH-1

UPLIFT = 0.3 KM EROSION = 0.3 KM

CORDEP	CORTEM	SMOOTH	RES
126.95	21.588	21.582	0.006
137.12	21.868	21.862	0.006
147.25	22.139	22.141	-0.002
157.36	22.399	22.419	-0.020
167.44	22.699	22.697	0.002
177.50	22.979	22.973	0.006
187.54	23.249	23.250	-0.001
197.56	23.529	23.526	0.003
207.57	23.799	23.801	-0.002
217.56	24.078	24.076	0.002

T(0) = 18.089 DEG C

GRAD = 27.518 DEG/KM

STER = 0.0903 DEG/KM
95CL = 0.2082 DEG/KM

REST = 161.0 CMSECDEG/CAL

STER = 1.3 CMSECDEG/CAL
95CL = 2.6 CMSECDEG/CAL

FLUX = 1.709 MICROCAL/SQCMSEC

STER = 0.015 MICROCAL/SQCMSEC
95CL = 0.030 MICROCAL/SQCMSEC

TOPOGRAPHIC DATA, LAKE HUGHES LH-2

RADII	ELDIFF
100.0	0.3
200.0	5.0
300.0	11.0
400.0	18.0
500.0	25.0
700.0	40.0
900.0	50.0
1200.0	93.0
1500.0	110.0
2000.0	118.0
2500.0	117.0
3000.0	113.0
4000.0	110.0
5000.0	115.0
7000.0	126.0
10000.0	151.0
15000.0	213.0
20000.0	235.0
30000.0	-0.
40000.0	-0.
50000.0	-0.
70000.0	-0.
100000.0	-0.

UNCORRECTED DATA, LAKE HUGHES LH-2

DEPTH	TEMP	SMOOTH	RES
180.00	18.400	18.395	0.005
190.00	18.620	18.617	0.003
200.00	18.840	18.839	0.001
210.00	19.060	19.061	-0.001
220.00	19.280	19.283	-0.003
230.00	19.500	19.505	-0.005
240.00	19.720	19.728	-0.008
250.00	19.950	19.950	0.000
260.00	20.170	20.172	-0.002
270.00	20.400	20.394	0.006
280.00	20.620	20.616	0.004

T(0) = 14.397 DEG C

GRAD = 22.209 DEG/KM

STER = 0.0440 DEG/KM
95CL = 0.0996 DEG/KM

REST = 160.0 CMSECDEG/CAL

STER = 1.5 CMSECDEG/CAL
95CL = 5.2 CMSECDEG/CAL

FLUX = 1.388 MICROCAL/SQCMSEC

STER = 0.013 MICROCAL/SQCMSEC
95CL = 0.046 MICROCAL/SQCMSEC

TOPOGRAPHIC CORRECTION, SS CASE, LAKE HUGHES LH-2

CORDEP	CORTEM	SMOOTH	RES
145.65	18.245	18.245	0.000
154.20	18.459	18.458	0.001
162.77	18.672	18.671	0.001
171.38	18.886	18.886	0.001
180.03	19.100	19.101	-0.001
188.70	19.314	19.317	-0.002
197.40	19.528	19.533	-0.005
206.14	19.753	19.751	0.002
214.90	19.967	19.969	-0.002
223.68	20.192	20.187	0.004
232.50	20.406	20.407	-0.000

T(0) = 14.620 DEG C

GRAD = 24.889 DEG/KM

STER = 0.0280 DEG/KM
95CL = 0.0633 DEG/KM

REST = 160.0 CMSECDEG/CAL

STER = 1.5 CMSECDEG/CAL
95CL = 5.2 CMSECDEG/CAL

FLUX = 1.556 MICROCAL/SQCMSEC

STER = 0.015 MICROCAL/SQCMSEC
95CL = 0.051 MICROCAL/SQCMSEC

TOPOGRAPHIC CORRECTION, 1MY CASE LAKE HUGHES LH-2

UPLIFT = 0.3 KM EROSION = 0.3 KM

CORDEP	CORTEM	SMOOTH	RES
157.42	18.259	18.259	0.001
166.62	18.473	18.472	0.001
175.85	18.688	18.687	0.001
185.11	18.902	18.902	0.000
194.41	19.117	19.118	-0.001
203.73	19.332	19.334	-0.003
213.09	19.547	19.552	-0.005
222.47	19.772	19.770	0.002
231.88	19.987	19.988	-0.002
241.32	20.212	20.208	0.004
250.78	20.428	20.428	0.000

T(0) = 14.601 DEG C

GRAD = 23.233 DEG/KM

STER = 0.0272 DEG/KM
95CL = 0.0615 DEG/KM

REST = 160.0 CMSECDEG/CAL

STER = 1.5 CMSECDEG/CAL
95CL = 5.2 CMSECDEG/CAL

FLUX = 1.452 MICROCAL/SQCMSEC

STER = 0.014 MICROCAL/SQCMSEC
95CL = 0.047 MICROCAL/SQCMSEC

TOPOGRAPHIC CORRECTION, 4MY CASE LAKE HUGHES LH-2

UPLIFT = 0.3 KM EROSION = 0.3 KM

CORDEP	CORTEM	SMOOTH	RES
151.10	18.250	18.250	0.000
159.95	18.464	18.463	0.001
168.83	18.678	18.677	0.001
177.74	18.892	18.891	0.001
186.69	19.106	19.107	-0.001
195.67	19.320	19.323	-0.003
204.67	19.535	19.540	-0.005
213.71	19.759	19.757	0.002
222.77	19.974	19.976	-0.002
231.86	20.199	20.195	0.004
240.97	20.414	20.414	-0.000

T(0) = 14.611 DEG C

GRAD = 24.082 DEG/KM

STER = 0.0276 DEG/KM
95CL = 0.0624 DEG/KM

REST = 160.0 CMSECDEG/CAL

STER = 1.5 CMSECDEG/CAL
95CL = 5.2 CMSECDEG/CAL

FLUX = 1.505 MICROCAL/SQCMSEC

STER = 0.014 MICROCAL/SQCMSEC
95CL = 0.049 MICROCAL/SQCMSEC

TOPOGRAPHIC CORRECTION, 9MY CASE LAKE HUGHES LH-2

UPLIFT = 0.3 KM EROSION = 0.3 KM

CORDEP	CORTEM	SMOOTH	RES
149.08	18.248	18.247	0.000
157.81	18.461	18.460	0.001
166.58	18.675	18.674	0.001
175.38	18.889	18.888	0.001
184.21	19.103	19.104	-0.001
193.08	19.317	19.320	-0.002
201.97	19.531	19.536	-0.005
210.89	19.756	19.754	0.002
219.84	19.970	19.972	-0.002
228.82	20.195	20.191	0.004
237.83	20.410	20.410	-0.000

T(0) = 14.614 DEG C

GRAD = 24.371 DEG/KM

STER = 0.0277 DEG/KM
95CL = 0.0627 DEG/KM

REST = 160.0 CMSECDEG/CAL

STER = 1.5 CMSECDEG/CAL
95CL = 5.2 CMSECDEG/CAL

FLUX = 1.523 MICROCAL/SQCMSEC

STER = 0.014 MICROCAL/SQCMSEC
95CL = 0.050 MICROCAL/SQCMSEC

TOPOGRAPHIC CORRECTION, 16MY CASE LAKE HUGHES LH-2

UPLIFT = 0.3 KM EROSION = 0.3 KM

CORDEP	CORTEM	SMOOTH	RES
147.04	18.247	18.246	0.000
155.66	18.460	18.459	0.001
164.31	18.674	18.673	0.001
173.00	18.888	18.887	0.001
181.72	19.102	19.102	-0.001
190.47	19.316	19.318	-0.002
199.25	19.530	19.535	-0.005
208.06	19.754	19.752	0.002
216.90	19.969	19.970	-0.002
225.76	20.194	20.189	0.004
234.65	20.408	20.409	-0.000

T(0) = 14.618 DEG C

GRAD = 24.679 DEG/KM

STER = 0.0279 DEG/KM
95CL = 0.0631 DEG/KM

REST = 160.0 CMSECDEG/CAL

STER = 1.5 CMSECDEG/CAL
95CL = 5.2 CMSECDEG/CAL

FLUX = 1.542 MICROCAL/SQCMSEC

STER = 0.015 MICROCAL/SQCMSEC
95CL = 0.050 MICROCAL/SQCMSEC

TOPOGRAPHIC DATA, LAKE HUGHES LH-3

RADII	ELDIFF
100.0	-11.0
200.0	-26.0
300.0	-35.0
400.0	-38.0
500.0	-41.0
700.0	-60.0
900.0	-104.0
1200.0	-123.0
1500.0	-148.0
2000.0	-196.0
2500.0	-235.0
3000.0	-235.0
4000.0	-224.0
5000.0	-210.0
7000.0	-210.0
10000.0	-125.0
15000.0	-62.0
20000.0	39.0
30000.0	-0.
40000.0	-0.
50000.0	-0.
70000.0	-0.
100000.0	-0.

UNCORRECTED DATA, LAKE HUGHES LH-3

DEPTH	TEMP	SMOOTH	RES
150.00	21.020	21.004	0.016
160.00	21.350	21.332	0.018
170.00	21.650	21.660	-0.010
180.00	21.960	21.988	-0.028
190.00	22.310	22.316	-0.006
200.00	22.650	22.644	0.006
210.00	22.990	22.972	0.018
220.00	23.320	23.299	0.021
230.00	23.640	23.627	0.013
240.00	23.950	23.955	-0.005
250.00	24.220	24.283	-0.063
360.00	27.910	27.891	0.019

T(0) = 16.084 DEG C

GRAD = 32.796 DEG/KM

STER = 0.1410 DEG/KM
95CL = 0.3142 DEG/KM

REST = 171.0 CMSECDEG/CAL

STER = 2.7 CMSECDEG/CAL
95CL = 5.4 CMSECDEG/CAL

FLUX = 1.918 MICROCAL/SQCMSEC

STER = 0.031 MICROCAL/SQCMSEC
95CL = 0.063 MICROCAL/SQCMSEC

TOPOGRAPHIC CORRECTION, SS CASE, LAKE HUGHES LH-3

CORDEP	CORTEM	SMOOTH	RES
205.31	21.269	21.222	0.047
217.43	21.608	21.571	0.038
229.49	21.918	21.917	0.001
241.48	22.237	22.262	-0.025
253.42	22.595	22.605	-0.009
265.31	22.944	22.947	-0.003
277.15	23.292	23.287	0.005
288.95	23.630	23.626	0.004
300.70	23.958	23.964	-0.005
312.41	24.276	24.300	-0.024
324.08	24.553	24.636	-0.082
450.29	28.316	28.263	0.054

T(0) = 15.322 DEG C

GRAD = 28.739 DEG/KM

STER = 0.1766 DEG/KM
95CL = 0.3934 DEG/KM

REST = 171.0 CMSECDEG/CAL

STER = 2.7 CMSECDEG/CAL
95CL = 5.4 CMSECDEG/CAL

FLUX = 1.681 MICROCAL/SQCMSEC

STER = 0.028 MICROCAL/SQCMSEC
95CL = 0.058 MICROCAL/SQCMSEC

TOPOGRAPHIC CORRECTION, 1MY CASE LAKE HUGHES LH-3

UPLIFT = 1.5 KM EROSION = 0.5 KM

CORDEP	CORTEM	SMOOTH	RES
215.29	21.151	21.107	0.044
228.07	21.482	21.446	0.036
240.79	21.784	21.784	-0.000
253.46	22.095	22.120	-0.025
266.06	22.446	22.455	-0.009
278.62	22.786	22.788	-0.002
291.13	23.127	23.120	0.007
303.59	23.457	23.451	0.006
316.01	23.777	23.780	-0.004
328.39	24.087	24.109	-0.022
340.73	24.356	24.437	-0.080
474.33	28.033	27.983	0.050

T(0) = 15.393 DEG C

GRAD = 26.543 DEG/KM

STER = 0.1603 DEG/KM
95CL = 0.3572 DEG/KM

REST = 171.0 CMSECDEG/CAL

STER = 2.7 CMSECDEG/CAL
95CL = 5.4 CMSECDEG/CAL

FLUX = 1.552 MICROCAL/SQCMSEC

STER = 0.026 MICROCAL/SQCMSEC
95CL = 0.053 MICROCAL/SQCMSEC

TOPOGRAPHIC CORRECTION, 4MY CASE LAKE HUGHES LH-3

UPLIFT = 1.5 KM EROSION = 0.5 KM

CORDEP	CORTEM	SMOOTH	RES
210.79	21.212	21.167	0.045
223.27	21.548	21.511	0.037
235.69	21.853	21.853	0.000
248.05	22.168	22.193	-0.025
260.35	22.523	22.532	-0.009
272.61	22.868	22.870	-0.002
284.81	23.212	23.206	0.006
296.97	23.547	23.541	0.005
309.09	23.871	23.875	-0.004
321.17	24.185	24.208	-0.023
333.21	24.458	24.540	-0.081
463.43	28.180	28.128	0.052

T(0) = 15.359 DEG C

GRAD = 27.552 DEG/KM

STER = 0.1677 DEG/KM
95CL = 0.3737 DEG/KM

REST = 171.0 CMSECDEG/CAL

STER = 2.7 CMSECDEG/CAL
95CL = 5.4 CMSECDEG/CAL

FLUX = 1.611 MICROCAL/SQCMSEC

STER = 0.027 MICROCAL/SQCMSEC
95CL = 0.055 MICROCAL/SQCMSEC

TOPOGRAPHIC CORRECTION, 9MY CASE LAKE HUGHES LH-3

UPLIFT = 1.5 KM EROSION = 0.5 KM

CORDEP	CORTEM	SMOOTH	RES
209.13	21.232	21.186	0.046
221.50	21.569	21.531	0.037
233.81	21.875	21.875	0.000
246.06	22.192	22.217	-0.025
258.25	22.548	22.558	-0.009
270.39	22.894	22.897	-0.002
282.49	23.240	23.234	0.006
294.54	23.576	23.571	0.005
306.54	23.901	23.906	-0.005
318.51	24.216	24.240	-0.024
330.44	24.491	24.573	-0.082
459.44	28.227	28.174	0.052

T(0) = 15.347 DEG C

GRAD = 27.919 DEG/KM

STER = 0.1704 DEG/KM
95CL = 0.3797 DEG/KM

REST = 171.0 CMSECDEG/CAL

STER = 2.7 CMSECDEG/CAL
95CL = 5.4 CMSECDEG/CAL

FLUX = 1.633 MICROCAL/SQCMSEC

STER = 0.028 MICROCAL/SQCMSEC
95CL = 0.056 MICROCAL/SQCMSEC

TOPOGRAPHIC CORRECTION, 16MY CASE LAKE HUGHES LH-3

UPLIFT = 1.5 KM EROSION = 0.5 KM

CORDEP	CORTEM	SMOOTH	RES
206.72	21.255	21.209	0.046
218.93	21.593	21.556	0.038
231.08	21.902	21.901	0.001
243.17	22.220	22.245	-0.025
255.20	22.578	22.587	-0.009
267.18	22.925	22.928	-0.002
279.12	23.272	23.267	0.006
291.01	23.610	23.605	0.005
302.85	23.937	23.942	-0.005
314.66	24.253	24.277	-0.024
326.42	24.530	24.612	-0.082
453.66	28.282	28.229	0.053

T(0) = 15.331 DEG C

GRAD = 28.431 DEG/KM

STER = 0.1743 DEG/KM
95CL = 0.3883 DEG/KM

REST = 171.0 CMSECDEG/CAL

STER = 2.7 CMSECDEG/CAL
95CL = 5.4 CMSECDEG/CAL

FLUX = 1.663 MICROCAL/SQCMSEC

STER = 0.028 MICROCAL/SQCMSEC
95CL = 0.057 MICROCAL/SQCMSEC

TOPOGRAPHIC DATA, TEHACHAPI MTNS DH-14

RADII	ELDIFF
100.0	-16.8
200.0	-42.0
300.0	-60.0
400.0	-76.0
500.0	-83.0
700.0	-87.0
900.0	-94.0
1200.0	-105.0
1500.0	-110.0
2000.0	-143.0
2500.0	-133.0
3000.0	-72.0
4000.0	-2.0
5000.0	5.0
7000.0	40.0
10000.0	60.0
15000.0	180.0
20000.0	180.0
30000.0	110.0
40000.0	-0.
50000.0	-0.
70000.0	-0.
100000.0	-0.

UNCORRECTED DATA, TEHACHAPI MTNS DH-14

DEPTH	TEMP	SMOOTH	RES
150.00	18.250	18.251	-0.001
160.00	18.510	18.513	-0.003
170.00	18.780	18.775	0.005
180.00	19.040	19.038	0.002
190.00	19.300	19.300	0.000
200.00	19.560	19.562	-0.002
210.00	19.820	19.824	-0.004
220.00	20.090	20.087	0.003

T(0) = 14.317 DEG C

GRAD = 26.226 DEG/KM

STER = 0.0537 DEG/KM
95CL = 0.1314 DEG/KM

REST = 120.0 CMSECDEG/CAL

STER = 0.8 CMSECDEG/CAL
95CL = 2.2 CMSECDEG/CAL

FLUX = 2.186 MICROCAL/SQCMSEC

STER = 0.015 MICROCAL/SQCMSEC
95CL = 0.042 MICROCAL/SQCMSEC

TOPOGRAPHIC CORRECTION, SS CASE, TEHACHAPI MTNS DH-14

CORDEP	CORTEM	SMOOTH	RES
206.15	18.503	18.497	0.005
217.36	18.768	18.771	-0.002
228.46	19.043	19.041	0.002
239.48	19.308	19.309	-0.002
250.40	19.572	19.576	-0.004
261.25	19.836	19.840	-0.004
272.02	20.099	20.102	-0.003
282.73	20.372	20.363	0.009

T(0) = 13.475 DEG C

GRAD = 24.364 DEG/KM

STER = 0.0740 DEG/KM
95CL = 0.1810 DEG/KM

REST = 120.0 CMSECDEG/CAL

STER = 0.8 CMSECDEG/CAL
95CL = 2.2 CMSECDEG/CAL

FLUX = 2.030 MICROCAL/SQCMSEC

STER = 0.015 MICROCAL/SQCMSEC
95CL = 0.040 MICROCAL/SQCMSEC

TOPOGRAPHIC CORRECTION, 1MY CASE TEHACHAPI MTNS DH-14

UPLIFT = 1.5 KM EROSION = 0.3 KM

CORDEP	CORTEM	SMOOTH	RES
214.54	18.377	18.373	0.005
226.31	18.634	18.637	-0.003
237.98	18.901	18.899	0.002
249.55	19.157	19.159	-0.001
261.04	19.413	19.416	-0.003
272.45	19.668	19.673	-0.004
283.79	19.924	19.927	-0.003
295.06	20.188	20.180	0.008

T(0) = 13.556 DEG C

GRAD = 22.448 DEG/KM

STER = 0.0661 DEG/KM
95CL = 0.1618 DEG/KM

REST = 120.0 CMSECDEG/CAL

STER = 0.8 CMSECDEG/CAL
95CL = 2.2 CMSECDEG/CAL

FLUX = 1.871 MICROCAL/SQCMSEC

STER = 0.014 MICROCAL/SQCMSEC
95CL = 0.037 MICROCAL/SQCMSEC

TOPOGRAPHIC CORRECTION, 4MY CASE TEHACHAPI MTNS DH-14

UPLIFT = 1.5 KM EROSION = 0.3 KM

CORDEP	CORTEM	SMOOTH	RES
210.43	18.440	18.435	0.005
221.93	18.702	18.704	-0.003
233.32	18.972	18.970	0.002
244.62	19.233	19.235	-0.002
255.83	19.493	19.497	-0.004
266.97	19.753	19.757	-0.004
278.03	20.012	20.015	-0.003
289.02	20.281	20.272	0.009

T(0) = 13.517 DEG C

GRAD = 23.373 DEG/KM

STER = 0.0698 DEG/KM
95CL = 0.1709 DEG/KM

REST = 120.0 CMSECDEG/CAL

STER = 0.8 CMSECDEG/CAL
95CL = 2.2 CMSECDEG/CAL

FLUX = 1.948 MICROCAL/SQCMSEC

STER = 0.014 MICROCAL/SQCMSEC
95CL = 0.038 MICROCAL/SQCMSEC

TOPOGRAPHIC CORRECTION, 9MY CASE TEHACHAPI MTNS DH-14

UPLIFT = 1.5 KM EROSION = 0.3 KM

CORDEP	CORTEM	SMOOTH	RES
208.95	18.461	18.456	0.005
220.35	18.724	18.726	-0.003
231.64	18.996	18.994	0.002
242.84	19.257	19.259	-0.002
253.95	19.519	19.523	-0.004
264.99	19.780	19.784	-0.004
275.95	20.041	20.044	-0.003
286.84	20.311	20.302	0.009

T(0) = 13.503 DEG C

GRAD = 23.704 DEG/KM

STER = 0.0712 DEG/KM
95CL = 0.1743 DEG/KM

REST = 120.0 CMSECDEG/CAL

STER = 0.8 CMSECDEG/CAL
95CL = 2.2 CMSECDEG/CAL

FLUX = 1.975 MICROCAL/SQCMSEC

STER = 0.014 MICROCAL/SQCMSEC
95CL = 0.039 MICROCAL/SQCMSEC

TOPOGRAPHIC CORRECTION, 16MY CASE TEHACHAPI MTNS DH-14

UPLIFT = 1.5 KM EROSION = 0.3 KM

CORDEP	CORTEM	SMOOTH	RES
207.29	18.487	18.482	0.005
218.58	18.752	18.754	-0.003
229.76	19.026	19.024	0.002
240.85	19.289	19.291	-0.002
251.85	19.552	19.556	-0.004
262.77	19.815	19.820	-0.004
273.62	20.078	20.081	-0.003
284.41	20.350	20.341	0.009

T(0) = 13.486 DEG C

GRAD = 24.103 DEG/KM

STER = 0.0728 DEG/KM
95CL = 0.1783 DEG/KM

REST = 120.0 CMSECDEG/CAL

STER = 0.8 CMSECDEG/CAL
95CL = 2.2 CMSECDEG/CAL

FLUX = 2.009 MICROCAL/SQCMSEC

STER = 0.015 MICROCAL/SQCMSEC
95CL = 0.040 MICROCAL/SQCMSEC

TOPOGRAPHIC DATA, TEHACHAPI MTNS DH-15A

RADII	ELDIFF
100.0	14.0
200.0	45.0
300.0	58.0
400.0	38.0
500.0	17.0
700.0	0.
900.0	-10.0
1200.0	-20.0
1500.0	-22.0
2000.0	-31.0
2500.0	-53.0
3000.0	-44.0
4000.0	10.0
5000.0	27.0
7000.0	35.0
10000.0	85.0
15000.0	200.0
20000.0	200.0
30000.0	135.0
40000.0	-0.
50000.0	-0.
70000.0	-0.
100000.0	-0.

UNCORRECTED DATA, TEHACHAPI MTNS DH-15A

DEPTH	TEMP	SMOOTH	RES
150.00	17.610	17.606	0.004
160.00	17.790	17.789	0.001
170.00	17.970	17.972	-0.002
180.00	18.150	18.156	-0.006
190.00	18.340	18.339	0.001
200.00	18.520	18.523	-0.003
210.00	18.710	18.706	0.004
220.00	18.890	18.889	0.001

T(0) = 14.856 DEG C

GRAD = 18.333 DEG/KM

STER = 0.0575 DEG/KM
95CL = 0.1407 DEG/KM

REST = 119.0 CMSECDEG/CAL

STER = 2.0 CMSECDEG/CAL
95CL = 3.0 CMSECDEG/CAL

FLUX = 1.541 MICROCAL/SQCMSEC

STER = 0.026 MICROCAL/SQCMSEC
95CL = 0.041 MICROCAL/SQCMSEC

TOPOGRAPHIC CORRECTION, SS CASE, TEHACHAPI MTNS DH-15A

CORDEP	CORTEM	SMOOTH	RES
124.39	17.495	17.492	0.003
134.81	17.677	17.676	0.001
145.27	17.859	17.861	-0.002
155.77	18.041	18.046	-0.005
166.30	18.233	18.232	0.002
176.85	18.416	18.418	-0.002
187.41	18.608	18.604	0.004
197.98	18.791	18.791	-0.000

T(0) = 15.296 DEG C

GRAD = 17.654 DEG/KM

STER = 0.0459 DEG/KM
95CL = 0.1122 DEG/KM

REST = 119.0 CMSECDEG/CAL

STER = 2.0 CMSECDEG/CAL
95CL = 3.0 CMSECDEG/CAL

FLUX = 1.484 MICROCAL/SQCMSEC

STER = 0.025 MICROCAL/SQCMSEC
95CL = 0.039 MICROCAL/SQCMSEC

TOPOGRAPHIC CORRECTION, 1MY CASE TEHACHAPI MTNS DH-15A

UPLIFT = 1.5 KM EROSION = 0.3 KM

CORDEP	CORTEM	SMOOTH	RES
133.32	17.372	17.369	0.003
144.33	17.545	17.545	0.001
155.39	17.719	17.721	-0.002
166.48	17.893	17.898	-0.005
177.60	18.077	18.076	0.001
188.75	18.252	18.254	-0.002
199.91	18.436	18.432	0.004
211.07	18.610	18.610	-0.000

T(0) = 15.240 DEG C

GRAD = 15.970 DEG/KM

STER = 0.0444 DEG/KM
95CL = 0.1086 DEG/KM

REST = 119.0 CMSECDEG/CAL

STER = 2.0 CMSECDEG/CAL
95CL = 3.0 CMSECDEG/CAL

FLUX = 1.342 MICROCAL/SQCMSEC

STER = 0.023 MICROCAL/SQCMSEC
95CL = 0.035 MICROCAL/SQCMSEC

TOPOGRAPHIC CORRECTION, 4MY CASE TEHACHAPI MTNS DH-15A

UPLIFT = 1.5 KM EROSION = 0.3 KM

CORDEP	CORTEM	SMOOTH	RES
128.83	17.433	17.430	0.003
139.55	17.611	17.610	0.001
150.30	17.789	17.791	-0.002
161.10	17.967	17.972	-0.005
171.93	18.155	18.154	0.002
182.77	18.334	18.336	-0.002
193.63	18.522	18.518	0.004
204.49	18.701	18.701	-0.000

T(0) = 15.267 DEG C

GRAD = 16.791 DEG/KM

STER = 0.0451 DEG/KM
95CL = 0.1104 DEG/KM

REST = 119.0 CMSECDEG/CAL

STER = 2.0 CMSECDEG/CAL
95CL = 3.0 CMSECDEG/CAL

FLUX = 1.411 MICROCAL/SQCMSEC

STER = 0.024 MICROCAL/SQCMSEC
95CL = 0.037 MICROCAL/SQCMSEC

TOPOGRAPHIC CORRECTION, 9MY CASE TEHACHAPI MTNS DH-15A

UPLIFT = 1.5 KM EROSION = 0.3 KM

CORDEP	CORTEM	SMOOTH	RES
127.26	17.453	17.450	0.003
137.87	17.632	17.632	0.001
148.52	17.812	17.814	-0.002
159.21	17.991	17.996	-0.005
169.93	18.181	18.179	0.002
180.67	18.360	18.363	-0.002
191.43	18.550	18.546	0.004
202.19	18.730	18.730	-0.000

T(0) = 15.277 DEG C

GRAD = 17.080 DEG/KM

STER = 0.0454 DEG/KM
95CL = 0.1111 DEG/KM

REST = 119.0 CMSECDEG/CAL

STER = 2.0 CMSECDEG/CAL
95CL = 3.0 CMSECDEG/CAL

FLUX = 1.435 MICROCAL/SQCMSEC

STER = 0.024 MICROCAL/SQCMSEC
95CL = 0.037 MICROCAL/SQCMSEC

TOPOGRAPHIC CORRECTION, 16MY CASE TEHACHAPI MTNS DH-15A

UPLIFT = 1.5 KM EROSION = 0.3 KM

CORDEP	CORTEM	SMOOTH	RES
125.57	17.480	17.477	0.003
136.07	17.661	17.660	0.001
146.61	17.842	17.843	-0.002
157.19	18.023	18.028	-0.005
167.80	18.214	18.213	0.002
178.43	18.396	18.398	-0.002
189.07	18.587	18.583	0.004
199.72	18.769	18.769	-0.000

T(0) = 15.288 DEG C

GRAD = 17.428 DEG/KM

STER = 0.0457 DEG/KM
95CL = 0.1117 DEG/KM

REST = 119.0 CMSECDEG/CAL

STER = 2.0 CMSECDEG/CAL
95CL = 3.0 CMSECDEG/CAL

FLUX = 1.465 MICROCAL/SQCMSEC

STER = 0.025 MICROCAL/SQCMSEC
95CL = 0.038 MICROCAL/SQCMSEC

TOPOGRAPHIC DATA, TEHACHAPI MTNS DH-43

RADII	ELDIFF
100.0	4.6
200.0	14.3
300.0	18.3
400.0	21.0
500.0	21.0
700.0	29.0
900.0	48.0
1200.0	60.0
1500.0	62.0
2000.0	45.0
2500.0	5.0
3000.0	-12.0
4000.0	-84.0
5000.0	-123.0
7000.0	-34.0
10000.0	60.0
15000.0	107.0
20000.0	107.0
30000.0	40.0
40000.0	-0.
50000.0	-0.
70000.0	-0.
100000.0	-0.

UNCORRECTED DATA, TEHACHAPI MTNS DH-43

DEPTH	TEMP	SMOOTH	RES
170.00	20.026	20.007	0.019
175.00	20.136	20.126	0.010
180.00	20.247	20.245	0.002
185.00	20.361	20.364	-0.003
190.00	20.459	20.483	-0.024
195.00	20.592	20.602	-0.010
200.00	20.709	20.721	-0.012
205.00	20.830	20.840	-0.010
210.00	20.960	20.959	0.001
215.00	21.086	21.078	0.008
220.00	21.201	21.197	0.004
225.00	21.323	21.316	0.007
230.00	21.442	21.435	0.007

T(0) = 15.960 DEG C

GRAD = 23.805 DEG/KM

STER = 0.1773 DEG/KM
95CL = 0.3902 DEG/KM

REST = 120.8 CMSECDEG/CAL

STER = 4.0 CMSECDEG/CAL
95CL = 8.2 CMSECDEG/CAL

FLUX = 1.971 MICROCAL/SQCMSEC

STER = 0.067 MICROCAL/SQCMSEC
95CL = 0.138 MICROCAL/SQCMSEC

TOPOGRAPHIC CORRECTION, SS CASE, TEHACHAPI MTNS DH-43

CORDEP	CORTEM	SMOOTH	RES
150.43	19.938	19.920	0.018
155.23	20.047	20.037	0.010
160.04	20.157	20.155	0.002
164.86	20.270	20.273	-0.003
169.68	20.368	20.391	-0.023
174.51	20.500	20.509	-0.009
179.35	20.616	20.627	-0.011
184.19	20.736	20.746	-0.009
189.04	20.866	20.864	0.002
193.89	20.991	20.983	0.008
198.75	21.105	21.102	0.004
203.62	21.227	21.220	0.006
208.49	21.345	21.340	0.006

T(0) = 16.242 DEG C

GRAD = 24.448 DEG/KM

STER = 0.1734 DEG/KM
95CL = 0.3816 DEG/KM

REST = 120.8 CMSECDEG/CAL

STER = 4.0 CMSECDEG/CAL
95CL = 8.2 CMSECDEG/CAL

FLUX = 2.024 MICROCAL/SQCMSEC

STER = 0.069 MICROCAL/SQCMSEC
95CL = 0.141 MICROCAL/SQCMSEC

TOPOGRAPHIC CORRECTION, 1MY CASE TEHACHAPI MTNS DH-43

UPLIFT = 1.3 KM EROSION = 0.2 KM

CORDEP	CORTEM	SMOOTH	RES
156.59	19.805	19.787	0.018
161.58	19.911	19.901	0.010
166.57	20.017	20.015	0.002
171.57	20.126	20.129	-0.003
176.57	20.219	20.243	-0.023
181.59	20.348	20.357	-0.009
186.60	20.460	20.471	-0.011
191.63	20.577	20.586	-0.009
196.66	20.702	20.700	0.002
201.69	20.823	20.815	0.008
206.73	20.934	20.930	0.004
211.78	21.051	21.045	0.006
216.83	21.166	21.160	0.006

T(0) = 16.219 DEG C

GRAD = 22.789 DEG/KM

STER = 0.1679 DEG/KM
95CL = 0.3696 DEG/KM

REST = 120.8 CMSECDEG/CAL

STER = 4.0 CMSECDEG/CAL
95CL = 8.2 CMSECDEG/CAL

FLUX = 1.887 MICROCAL/SQCMSEC

STER = 0.064 MICROCAL/SQCMSEC
95CL = 0.132 MICROCAL/SQCMSEC

TOPOGRAPHIC CORRECTION, 4MY CASE TEHACHAPI MTNS DH-43

UPLIFT = 1.3 KM EROSION = 0.2 KM

CORDEP	CORTEM	SMOOTH	RES
153.50	19.872	19.854	0.018
158.39	19.979	19.969	0.010
163.29	20.087	20.085	0.002
168.20	20.198	20.201	-0.003
173.11	20.293	20.317	-0.023
178.03	20.424	20.433	-0.009
182.96	20.538	20.549	-0.011
187.89	20.656	20.666	-0.009
192.83	20.784	20.782	0.002
197.78	20.907	20.899	0.008
202.73	21.020	21.016	0.004
207.68	21.139	21.133	0.006
212.64	21.255	21.250	0.006

T(0) = 16.230 DEG C

GRAD = 23.604 DEG/KM

STER = 0.1706 DEG/KM
95CL = 0.3755 DEG/KM

REST = 120.8 CMSECDEG/CAL

STER = 4.0 CMSECDEG/CAL
95CL = 8.2 CMSECDEG/CAL

FLUX = 1.954 MICROCAL/SQCMSEC

STER = 0.066 MICROCAL/SQCMSEC
95CL = 0.136 MICROCAL/SQCMSEC

TOPOGRAPHIC CORRECTION, 9MY CASE TEHACHAPI MTNS DH-43

UPLIFT = 1.3 KM EROSION = 0.2 KM

CORDEP	CORTEM	SMOOTH	RES
152.44	19.894	19.876	0.018
157.30	20.001	19.992	0.010
162.17	20.110	20.108	0.002
167.05	20.222	20.225	-0.003
171.93	20.318	20.341	-0.023
176.82	20.449	20.458	-0.009
181.72	20.564	20.575	-0.011
186.62	20.683	20.692	-0.009
191.53	20.811	20.809	0.002
196.44	20.935	20.927	0.008
201.36	21.048	21.044	0.004
206.29	21.168	21.162	0.006
211.21	21.285	21.279	0.006

T(0) = 16.234 DEG C

GRAD = 23.886 DEG/KM

STER = 0.1716 DEG/KM
95CL = 0.3776 DEG/KM

REST = 120.8 CMSECDEG/CAL

STER = 4.0 CMSECDEG/CAL
95CL = 8.2 CMSECDEG/CAL

FLUX = 1.977 MICROCAL/SQCMSEC

STER = 0.067 MICROCAL/SQCMSEC
95CL = 0.138 MICROCAL/SQCMSEC

TOPOGRAPHIC CORRECTION, 16MY CASE TEHACHAPI MTNS DH-43

UPLIFT = 1.3 KM EROSION = 0.2 KM

CORDEP	CORTEM	SMOOTH	RES
151.23	19.921	19.904	0.018
156.06	20.030	20.021	0.010
160.89	20.140	20.138	0.002
165.73	20.252	20.255	-0.003
170.58	20.349	20.372	-0.023
175.44	20.481	20.490	-0.009
180.30	20.597	20.608	-0.011
185.16	20.717	20.726	-0.009
190.03	20.845	20.844	0.002
194.91	20.970	20.962	0.008
199.79	21.084	21.080	0.004
204.68	21.205	21.199	0.006
209.58	21.323	21.317	0.006

T(0) = 16.239 DEG C

GRAD = 24.230 DEG/KM

STER = 0.1726 DEG/KM
95CL = 0.3800 DEG/KM

REST = 120.8 CMSECDEG/CAL

STER = 4.0 CMSECDEG/CAL
95CL = 8.2 CMSECDEG/CAL

FLUX = 2.006 MICROCAL/SQCMSEC

STER = 0.068 MICROCAL/SQCMSEC
95CL = 0.140 MICROCAL/SQCMSEC

TOPOGRAPHIC DATA, TEHACHAPI MTNS DH-65

RADII	ELDIFF
100.0	6.0
200.0	32.0
300.0	72.0
400.0	99.0
500.0	116.0
700.0	113.0
900.0	109.0
1200.0	112.0
1500.0	110.0
2000.0	83.0
2500.0	128.0
3000.0	148.0
4000.0	95.0
5000.0	55.0
7000.0	0.
10000.0	-95.0
15000.0	-100.0
20000.0	-160.0
30000.0	-240.0
40000.0	-0.
50000.0	-0.
70000.0	-0.
100000.0	-0.

UNCORRECTED DATA, TEHACHAPI MTNS DH-65

DEPTH	TEMP	SMOOTH	RES
320.00	22.180	22.141	0.039
330.00	22.330	22.321	0.009
340.00	22.510	22.501	0.009
350.00	22.680	22.681	-0.001
360.00	22.830	22.861	-0.031
370.00	23.000	23.041	-0.041
380.00	23.200	23.221	-0.021
390.00	23.380	23.401	-0.021
400.00	23.570	23.581	-0.011
410.00	23.790	23.761	0.029
420.00	23.980	23.940	0.040

T(0) = 16.384 DEG C

GRAD = 17.991 DEG/KM

STER = 0.2787 DEG/KM
95CL = 0.6304 DEG/KM

REST = 145.5 CMSECDEG/CAL

STER = 3.9 CMSECDEG/CAL
95CL = 7.6 CMSECDEG/CAL

FLUX = 1.237 MICROCAL/SQCMSEC

STER = 0.038 MICROCAL/SQCMSEC
95CL = 0.078 MICROCAL/SQCMSEC

TOPOGRAPHIC CORRECTION, SS CASE, TEHACHAPI MTNS DH-65

CORDEP	CORTEM	SMOOTH	RES
240.54	21.822	21.787	0.035
250.17	21.971	21.963	0.008
259.84	22.149	22.140	0.009
269.55	22.318	22.317	0.000
279.30	22.467	22.496	-0.029
289.08	22.636	22.675	-0.039
298.89	22.835	22.854	-0.019
308.74	23.014	23.034	-0.020
318.61	23.204	23.214	-0.011
328.51	23.423	23.395	0.028
338.44	23.613	23.577	0.036

T(0) = 17.390 DEG C

GRAD = 18.281 DEG/KM

STER = 0.2647 DEG/KM
95CL = 0.5988 DEG/KM

REST = 145.5 CMSECDEG/CAL

STER = 3.9 CMSECDEG/CAL
95CL = 7.6 CMSECDEG/CAL

FLUX = 1.256 MICROCAL/SQCMSEC

STER = 0.038 MICROCAL/SQCMSEC
95CL = 0.077 MICROCAL/SQCMSEC

TOPOGRAPHIC CORRECTION, 1MY CASE TEHACHAPI MTNS DH-65

UPLIFT = 1.1 KM EROSION = 0.3 KM

CORDEP	CORTEM	SMOOTH	RES
253.97	21.628	21.592	0.036
264.01	21.770	21.762	0.008
274.10	21.942	21.933	0.009
284.23	22.105	22.104	0.000
294.39	22.247	22.277	-0.029
304.59	22.410	22.449	-0.039
314.82	22.603	22.623	-0.019
325.08	22.777	22.796	-0.020
335.36	22.960	22.971	-0.011
345.68	23.173	23.145	0.028
356.02	23.357	23.320	0.037

T(0) = 17.290 DEG C

GRAD = 16.938 DEG/KM

STER = 0.2559 DEG/KM
95CL = 0.5789 DEG/KM

REST = 145.5 CMSECDEG/CAL

STER = 3.9 CMSECDEG/CAL
95CL = 7.6 CMSECDEG/CAL

FLUX = 1.164 MICROCAL/SQCMSEC

STER = 0.036 MICROCAL/SQCMSEC
95CL = 0.073 MICROCAL/SQCMSEC

TOPOGRAPHIC CORRECTION, 4MY CASE TEHACHAPI MTNS DH-65

UPLIFT = 1.1 KM EROSION = 0.3 KM

CORDEP	CORTEM	SMOOTH	RES
246.81	21.723	21.688	0.035
256.63	21.868	21.861	0.008
266.50	22.044	22.034	0.009
276.40	22.209	22.209	0.000
286.34	22.355	22.384	-0.029
296.32	22.521	22.560	-0.039
306.33	22.717	22.736	-0.019
316.37	22.893	22.913	-0.020
326.44	23.079	23.090	-0.011
336.53	23.296	23.268	0.028
346.65	23.482	23.446	0.036

T(0) = 17.341 DEG C

GRAD = 17.612 DEG/KM

STER = 0.2605 DEG/KM
95CL = 0.5893 DEG/KM

REST = 145.5 CMSECDEG/CAL

STER = 3.9 CMSECDEG/CAL
95CL = 7.6 CMSECDEG/CAL

FLUX = 1.210 MICROCAL/SQCMSEC

STER = 0.037 MICROCAL/SQCMSEC
95CL = 0.075 MICROCAL/SQCMSEC

TOPOGRAPHIC CORRECTION, 9MY CASE TEHACHAPI MTNS DH-65

UPLIFT = 1.1 KM EROSION = 0.3 KM

CORDEP	CORTEM	SMOOTH	RES
244.79	21.756	21.721	0.035
254.55	21.903	21.895	0.008
264.35	22.079	22.070	0.009
274.20	22.246	22.245	0.000
284.08	22.393	22.422	-0.029
293.99	22.560	22.598	-0.039
303.94	22.757	22.776	-0.019
313.92	22.934	22.954	-0.020
323.92	23.121	23.132	-0.011
333.95	23.339	23.311	0.028
344.01	23.526	23.490	0.036

T(0) = 17.357 DEG C

GRAD = 17.829 DEG/KM

STER = 0.2618 DEG/KM
95CL = 0.5923 DEG/KM

REST = 145.5 CMSECDEG/CAL

STER = 3.9 CMSECDEG/CAL
95CL = 7.6 CMSECDEG/CAL

FLUX = 1.225 MICROCAL/SQCMSEC

STER = 0.037 MICROCAL/SQCMSEC
95CL = 0.076 MICROCAL/SQCMSEC

TOPOGRAPHIC CORRECTION, 16MY CASE TEHACHAPI MTNS DH-65

UPLIFT = 1.1 KM EROSION = 0.3 KM

CORDEP	CORTEM	SMOOTH	RES
241.89	21.797	21.761	0.035
251.56	21.944	21.937	0.008
261.27	22.122	22.113	0.009
271.02	22.290	22.289	0.000
280.81	22.438	22.467	-0.029
290.64	22.606	22.645	-0.039
300.49	22.804	22.823	-0.019
310.38	22.983	23.002	-0.020
320.29	23.171	23.182	-0.011
330.24	23.390	23.362	0.028
340.20	23.579	23.543	0.036

T(0) = 17.378 DEG C

GRAD = 18.121 DEG/KM

STER = 0.2638 DEG/KM
95CL = 0.5968 DEG/KM

REST = 145.5 CMSECDEG/CAL

STER = 3.9 CMSECDEG/CAL
95CL = 7.6 CMSECDEG/CAL

FLUX = 1.245 MICROCAL/SQCMSEC

STER = 0.038 MICROCAL/SQCMSEC
95CL = 0.077 MICROCAL/SQCMSEC

TOPOGRAPHIC DATA, TEHACHAPI MTNS DH-67

RADII	ELDIFF
100.0	10.0
200.0	22.0
300.0	38.0
400.0	55.0
500.0	62.0
700.0	63.0
900.0	70.0
1200.0	75.0
1500.0	77.0
2000.0	110.0
2500.0	174.0
3000.0	199.0
4000.0	151.0
5000.0	157.0
7000.0	106.0
10000.0	8.0
15000.0	4.0
20000.0	-57.0
30000.0	-136.0
40000.0	-0.
50000.0	-0.
70000.0	-0.
100000.0	-0.

UNCORRECTED DATA, TEHACHAPI MTNS DH-67

DEPTH	TEMP	SMOOTH	RES
320.00	20.990	20.971	0.019
330.00	21.150	21.153	-0.003
340.00	21.330	21.335	-0.005
350.00	21.530	21.518	0.012
360.00	21.680	21.700	-0.020
370.00	21.860	21.882	-0.022
380.00	22.030	22.064	-0.034
390.00	22.300	22.247	0.053

T(0) = 15.138 DEG C

GRAD = 18.227 DEG/KM

STER = 0.4660 DEG/KM
95CL = 1.1403 DEG/KM

REST = 144.7 CMSECDEG/CAL

STER = 3.9 CMSECDEG/CAL
95CL = 7.7 CMSECDEG/CAL

FLUX = 1.260 MICROCAL/SQCMSEC

STER = 0.047 MICROCAL/SQCMSEC
95CL = 0.103 MICROCAL/SQCMSEC

TOPOGRAPHIC CORRECTION, SS CASE, TEHACHAPI MTNS DH-67

CORDEP	CORTEM	SMOOTH	RES
255.98	20.702	20.684	0.018
265.24	20.859	20.862	-0.003
274.52	21.035	21.040	-0.005
283.83	21.232	21.219	0.013
293.16	21.379	21.398	-0.019
302.52	21.556	21.578	-0.022
311.89	21.723	21.758	-0.035
321.28	21.991	21.939	0.052

T(0) = 15.765 DEG C

GRAD = 19.215 DEG/KM

STER = 0.4912 DEG/KM
95CL = 1.2019 DEG/KM

REST = 144.7 CMSECDEG/CAL

STER = 3.9 CMSECDEG/CAL
95CL = 7.7 CMSECDEG/CAL

FLUX = 1.328 MICROCAL/SQCMSEC

STER = 0.049 MICROCAL/SQCMSEC
95CL = 0.109 MICROCAL/SQCMSEC

TOPOGRAPHIC CORRECTION, 1MY CASE TEHACHAPI MTNS DH-67

UPLIFT = 1.2 KM EROSION = 0.3 KM

CORDEP	CORTEM	SMOOTH	RES
272.79	20.499	20.481	0.018
282.57	20.649	20.652	-0.003
292.38	20.820	20.825	-0.005
302.21	21.010	20.997	0.013
312.06	21.151	21.170	-0.019
321.93	21.322	21.343	-0.022
331.82	21.482	21.517	-0.035
341.74	21.743	21.691	0.052

T(0) = 15.693 DEG C

GRAD = 17.553 DEG/KM

STER = 0.4662 DEG/KM
95CL = 1.1407 DEG/KM

REST = 144.7 CMSECDEG/CAL

STER = 3.9 CMSECDEG/CAL
95CL = 7.7 CMSECDEG/CAL

FLUX = 1.213 MICROCAL/SQCMSEC

STER = 0.046 MICROCAL/SQCMSEC
95CL = 0.102 MICROCAL/SQCMSEC

TOPOGRAPHIC CORRECTION, 4MY CASE TEHACHAPI MTNS DH-67

UPLIFT = 1.2 KM EROSION = 0.3 KM

CORDEP	CORTEM	SMOOTH	RES
263.69	20.597	20.579	0.018
273.19	20.751	20.754	-0.003
282.71	20.924	20.929	-0.005
292.26	21.118	21.105	0.013
301.83	21.262	21.281	-0.019
311.43	21.435	21.457	-0.022
321.04	21.599	21.634	-0.035
330.67	21.863	21.811	0.052

T(0) = 15.730 DEG C

GRAD = 18.391 DEG/KM

STER = 0.4793 DEG/KM
95CL = 1.1728 DEG/KM

REST = 144.7 CMSECDEG/CAL

STER = 3.9 CMSECDEG/CAL
95CL = 7.7 CMSECDEG/CAL

FLUX = 1.271 MICROCAL/SQCMSEC

STER = 0.048 MICROCAL/SQCMSEC
95CL = 0.106 MICROCAL/SQCMSEC

TOPOGRAPHIC CORRECTION, 9MY CASE TEHACHAPI MTNS DH-67

UPLIFT = 1.2 KM EROSION = 0.3 KM

CORDEP	CORTEM	SMOOTH	RES
260.97	20.632	20.613	0.018
270.39	20.786	20.789	-0.003
279.83	20.961	20.965	-0.005
289.29	21.155	21.142	0.013
298.78	21.300	21.319	-0.019
308.28	21.475	21.497	-0.022
317.81	21.640	21.675	-0.035
327.36	21.905	21.853	0.052

T(0) = 15.742 DEG C

GRAD = 18.668 DEG/KM

STER = 0.4834 DEG/KM
95CL = 1.1829 DEG/KM

REST = 144.7 CMSECDEG/CAL

STER = 3.9 CMSECDEG/CAL
95CL = 7.7 CMSECDEG/CAL

FLUX = 1.290 MICROCAL/SQCMSEC

STER = 0.048 MICROCAL/SQCMSEC
95CL = 0.107 MICROCAL/SQCMSEC

TOPOGRAPHIC CORRECTION, 16MY CASE TEHACHAPI MTNS DH-67

UPLIFT = 1.2 KM EROSION = 0.3 KM

CORDEP	CORTEM	SMOOTH	RES
257.76	20.675	20.657	0.018
267.08	20.831	20.834	-0.003
276.42	21.007	21.012	-0.005
285.78	21.203	21.190	0.013
295.17	21.349	21.368	-0.019
304.58	21.525	21.547	-0.022
314.01	21.692	21.726	-0.035
323.45	21.958	21.906	0.052

T(0) = 15.756 DEG C

GRAD = 19.012 DEG/KM

STER = 0.4884 DEG/KM
95CL = 1.1950 DEG/KM

REST = 144.7 CMSECDEG/CAL

STER = 3.9 CMSECDEG/CAL
95CL = 7.7 CMSECDEG/CAL

FLUX = 1.314 MICROCAL/SQCMSEC

STER = 0.049 MICROCAL/SQCMSEC
95CL = 0.108 MICROCAL/SQCMSEC

TOPOGRAPHIC DATA, TEHACHAPI MTNS DH-70

RADII	ELDIFF
100.0	2.0
200.0	19.0
300.0	37.0
400.0	54.0
500.0	68.0
700.0	89.0
900.0	128.0
1200.0	150.0
1500.0	158.0
2000.0	187.0
2500.0	209.0
3000.0	221.0
4000.0	241.0
5000.0	295.0
7000.0	295.0
10000.0	385.0
15000.0	460.0
20000.0	460.0
30000.0	395.0
40000.0	-0.
50000.0	-0.
70000.0	-0.
100000.0	-0.

UNCORRECTED DATA, TEHACHAPI MTNS DH-70

DEPTH	TEMP	SMOOTH	RES
210.00	14.233	14.241	-0.008
220.00	14.450	14.453	-0.003
230.00	14.667	14.665	0.002
240.00	14.882	14.878	0.004
250.00	15.094	15.090	0.004
260.00	15.306	15.302	0.004
270.00	15.516	15.514	0.002
280.00	15.730	15.726	0.004
290.00	15.940	15.939	0.001
300.00	16.148	16.151	-0.003
310.00	16.360	16.363	-0.003
320.00	16.571	16.575	-0.004

T(0) = 9.785 DEG C

GRAD = 21.218 DEG/KM

STER = 0.0357 DEG/KM
95CL = 0.0796 DEG/KM

REST = 118.9 CMSECDEG/CAL

STER = 0.6 CMSECDEG/CAL
95CL = 1.3 CMSECDEG/CAL

FLUX = 1.785 MICROCAL/SQCMSEC

STER = 0.009 MICROCAL/SQCMSEC
95CL = 0.021 MICROCAL/SQCMSEC

TOPOGRAPHIC CORRECTION, SS CASE, TEHACHAPI MTNS DH-70

CORDEP	CORTEM	SMOOTH	RES
125.27	13.852	13.872	-0.020
132.63	14.057	14.065	-0.009
140.06	14.262	14.261	0.002
147.56	14.466	14.458	0.008
155.13	14.667	14.657	0.010
162.75	14.868	14.857	0.011
170.44	15.068	15.059	0.009
178.18	15.272	15.262	0.010
185.98	15.472	15.467	0.005
193.82	15.670	15.673	-0.003
201.72	15.873	15.881	-0.008
209.66	16.074	16.089	-0.015

T(0) = 10.581 DEG C

GRAD = 26.274 DEG/KM

STER = 0.1239 DEG/KM
95CL = 0.2760 DEG/KM

REST = 118.9 CMSECDEG/CAL

STER = 0.6 CMSECDEG/CAL
95CL = 1.3 CMSECDEG/CAL

FLUX = 2.210 MICROCAL/SQCMSEC

STER = 0.015 MICROCAL/SQCMSEC
95CL = 0.034 MICROCAL/SQCMSEC

TOPOGRAPHIC CORRECTION, 1MY CASE TEHACHAPI MTNS DH-70

UPLIFT = 1.5 KM EROSION = 0. KM

CORDEP	CORTEM	SMOOTH	RES
134.34	13.664	13.683	-0.019
142.13	13.860	13.868	-0.008
149.99	14.057	14.055	0.002
157.92	14.252	14.244	0.008
165.92	14.444	14.434	0.010
173.97	14.636	14.625	0.011
182.08	14.827	14.818	0.008
190.25	15.021	15.013	0.009
198.47	15.213	15.208	0.004
206.74	15.402	15.405	-0.003
215.06	15.595	15.603	-0.007
223.43	15.788	15.802	-0.014

T(0) = 10.488 DEG C

GRAD = 23.785 DEG/KM

STER = 0.1083 DEG/KM
95CL = 0.2413 DEG/KM

REST = 118.9 CMSECDEG/CAL

STER = 0.6 CMSECDEG/CAL
95CL = 1.3 CMSECDEG/CAL

FLUX = 2.000 MICROCAL/SQCMSEC

STER = 0.014 MICROCAL/SQCMSEC
95CL = 0.030 MICROCAL/SQCMSEC

TOPOGRAPHIC CORRECTION, 4MY CASE TEHACHAPI MTNS DH-70

UPLIFT = 1.5 KM EROSION = 0. KM

CORDEP	CORTEM	SMOOTH	RES
128.99	13.754	13.774	-0.020
136.53	13.955	13.963	-0.008
144.14	14.155	14.154	0.002
151.81	14.355	14.347	0.008
159.56	14.551	14.541	0.010
167.36	14.748	14.737	0.011
175.22	14.943	14.934	0.009
183.14	15.142	15.133	0.009
191.11	15.337	15.333	0.005
199.13	15.531	15.534	-0.003
207.21	15.729	15.737	-0.008
215.32	15.926	15.940	-0.014

T(0) = 10.537 DEG C

GRAD = 25.093 DEG/KM

STER = 0.1168 DEG/KM
95CL = 0.2603 DEG/KM

REST = 118.9 CMSECDEG/CAL

STER = 0.6 CMSECDEG/CAL
95CL = 1.3 CMSECDEG/CAL

FLUX = 2.110 MICROCAL/SQCMSEC

STER = 0.014 MICROCAL/SQCMSEC
95CL = 0.032 MICROCAL/SQCMSEC

TOPOGRAPHIC CORRECTION, 9MY CASE TEHACHAPI MTNS DH-70

UPLIFT = 1.5 KM EROSION = 0. KM

CORDEP	CORTEM	SMOOTH	RES
127.17	13.784	13.804	-0.020
134.63	13.986	13.994	-0.008
142.15	14.188	14.187	0.002
149.74	14.389	14.381	0.008
157.40	14.587	14.576	0.010
165.11	14.785	14.774	0.011
172.89	14.981	14.972	0.009
180.72	15.182	15.172	0.009
188.61	15.379	15.374	0.005
196.54	15.574	15.577	-0.003
204.53	15.773	15.781	-0.008
212.56	15.971	15.986	-0.015

T(0) = 10.554 DEG C

GRAD = 25.554 DEG/KM

STER = 0.1198 DEG/KM
95CL = 0.2670 DEG/KM

REST = 118.9 CMSECDEG/CAL

STER = 0.6 CMSECDEG/CAL
95CL = 1.3 CMSECDEG/CAL

FLUX = 2.149 MICROCAL/SQCMSEC

STER = 0.015 MICROCAL/SQCMSEC
95CL = 0.033 MICROCAL/SQCMSEC

TOPOGRAPHIC CORRECTION, 16MY CASE TEHACHAPI MTNS DH-70

UPLIFT = 1.5 KM EROSION = 0. KM

CORDEP	CORTEM	SMOOTH	RES
126.40	13.828	13.848	-0.020
133.82	14.032	14.041	-0.009
141.30	14.237	14.235	0.002
148.86	14.439	14.431	0.008
156.47	14.639	14.629	0.010
164.16	14.839	14.828	0.011
171.90	15.038	15.029	0.009
179.69	15.241	15.231	0.009
187.54	15.439	15.435	0.005
195.44	15.637	15.640	-0.003
203.39	15.838	15.846	-0.008
211.39	16.039	16.054	-0.015

T(0) = 10.569 DEG C

GRAD = 25.947 DEG/KM

STER = 0.1218 DEG/KM
95CL = 0.2714 DEG/KM

REST = 118.9 CMSECDEG/CAL

STER = 0.6 CMSECDEG/CAL
95CL = 1.3 CMSECDEG/CAL

FLUX = 2.182 MICROCAL/SQCMSEC

STER = 0.015 MICROCAL/SQCMSEC
95CL = 0.033 MICROCAL/SQCMSEC

TOPOGRAPHIC DATA, HOLLISTER HO-1

RADII	ELDIFF
100.0	-12.0
200.0	-44.0
300.0	-73.0
400.0	-92.0
500.0	-111.0
700.0	-143.0
900.0	-160.0
1200.0	-235.0
1500.0	-235.0
2000.0	-260.0
2500.0	-280.0
3000.0	-280.0
4000.0	-257.0
5000.0	-211.0
7000.0	-155.0
10000.0	-90.0
15000.0	-0.
20000.0	-0.
30000.0	-0.
40000.0	-0.
50000.0	-0.
70000.0	-0.
100000.0	-0.

UNCORRECTED DATA, HOLLISTER HO-1

DEPTH	TEMP	SMOOTH	RES
278.00	25.143	25.144	-0.001
280.00	25.205	25.205	0.000
282.00	25.265	25.265	-0.000
284.00	25.326	25.326	0.000
286.00	25.388	25.386	0.002
288.00	25.446	25.447	-0.001
290.00	25.508	25.507	0.001
292.00	25.567	25.568	-0.001
294.00	25.630	25.628	0.002
296.00	25.690	25.688	0.002
298.00	25.748	25.749	-0.001
300.00	25.807	25.809	-0.002

T(0) = 16.742 DEG C

GRAD = 30.224 DEG/KM

STER = 0.0586 DEG/KM
95CL = 0.1305 DEG/KM

REST = 152.0 CMSECDEG/CAL

STER = 0.9 CMSECDEG/CAL
95CL = 1.8 CMSECDEG/CAL

FLUX = 1.988 MICROCAL/SQCMSEC

STER = 0.012 MICROCAL/SQCMSEC
95CL = 0.025 MICROCAL/SQCMSEC

TOPOGRAPHIC CORRECTION, SS CASE, HOLLISTER HO-1

CORDEP	CORTEM	SMOOTH	RES
405.18	25.715	25.716	-0.001
407.59	25.779	25.779	0.000
409.99	25.841	25.841	-0.000
412.39	25.904	25.904	0.000
414.79	25.968	25.966	0.001
417.19	26.027	26.028	-0.001
419.58	26.091	26.091	0.001
421.97	26.152	26.153	-0.001
424.36	26.217	26.215	0.002
426.74	26.278	26.277	0.002
429.13	26.338	26.339	-0.001
431.50	26.399	26.401	-0.002

T(0) = 15.182 DEG C

GRAD = 25.998 DEG/KM

STER = 0.0423 DEG/KM
95CL = 0.0942 DEG/KM

REST = 152.0 CMSECDEG/CAL

STER = 0.9 CMSECDEG/CAL
95CL = 1.8 CMSECDEG/CAL

FLUX = 1.710 MICROCAL/SQCMSEC

STER = 0.011 MICROCAL/SQCMSEC
95CL = 0.021 MICROCAL/SQCMSEC